
UNIVERSITY OF BIRMINGHAM

# Multi-Point Forming Utilising Novel Elastic Cushion Designs

by

**Abror Tolipov**

A-thesis-submitted-to

T. The-University-of-Birmingham.

E for-the-degree-of.

**QDOCTOR-OF-PHILOSOPHYs.**

School-of-Mechanical-Engineering's.

College-of-Engineering-and-Physical-Sciences.

University-of-Birmingham's.

June-2019.

# ABSTRACT

Currently, there is an increased need for flexible manufacturing methods, which can meet the rapidly changing customer requirements. Reconfigurable dyes can be readily changed to create several shapes with a flexible sheet metal forming technique, which is known as Multi-point forming (MPF). While MPF methods are comprised of unique height-adjustable punches, the overall process has a few geometrical defects. These include wrinkling, maximum deviation along with thickness variation. Wrinkling may occur due to the discrete punch elements, which may result in defective products. Maximum deviation is a measure of the geometrical accuracy where the deviation from the target shape is measured. It takes place between the formed part and the target shape. Thickness variation is also a representation of the quality of the formed part. Elastic cushions can be inserted amid the multi-point die and the metal sheet to avoid such issues.

Earlier works have focused on optimising the process parameters, such as cushion thickness, the coefficient of friction, radius of curvature of the workpiece and pin size. The MPF process makes use of a matrix of multi-point pins, which assist in the creation of the die surface. However, very little attempts were made to develop and modify the process to eliminate the geometrical defects. This thesis is aimed on investigating two different optimisation processes; new mesh-type elastic cushion and hole-type elastic punch through experimental work and numerical simulations.

In this work, an MPF stamping process utilising a new model mesh-type elastic cushion was studied along with exploring about its influence on wrinkling, maximum deviation, thickness variation and the forming force. This research aims to investigate the effect of the hole types (circular and square) and sizes of the new mesh-type cushion. This was done as using holes on a sheet is a better idea than using a pure solid, where holes facilitate

the formability process. ABAQUS/Explicit FE software and response surface method are used in this investigation to explore the influence of the process variables on wrinkling, maximum deviation, thickness variation, and forming force. Achieved results were matched with the outcomes of the numerical simulations of the MPF for hemispherical shape using a solid cushion. It was revealed that the use of a new model mesh-type cushion could lead to a reduction in wrinkling, maximum deviation, thickness variation and forming load. All numerical results were validated by the experimental results and a fairly reasonable agreement was observed.

In terms of the elastic cushion thickness, it was found that this parameter had no influence on the wrinkling and thickness variation. This study also made use of the Design of Experiments (DoE) approach to derive a process for the relevant process variables, which was then used to pick the most relevant variables. A hole-type elastic punch was developed instead of the MPF punch for reducing the adjustment times and tool costs. It was revealed that this new approach saves half the tool cost and time along with providing the desired results. With the help of the experimental results and numerical simulations, a suitable hole-type (circular) and forming compression (of about 70%) was chosen.

# ACKNOWLEDGEMENTS

I wish to thank my supervisors Dr Khamis Essa and Professor Dun Pham for their continuous support and guidance throughout this thesis work. For me, I believe it was a privilege to study at the University of Birmingham under an excellent supervision.

I also thank my colleagues and other staff members at the university who have always supported me and provided a good company throughout this PhD journey.

Special thanks to my loving mother and father who have always provided me with their constant love and support. I am, indeed, very grateful to the rest of my family for all the affection and care they have given me throughout the last few years.

# PUBLICATIONS

**Some of the material presented in this thesis has already been published and below is the list of these publications.**

1. Tolipov, A.A., Elghawail, A., Shushing, S., Pham, D. and Essa, K., 2017, September. Experimental research and numerical optimisation of multi-point sheet metal forming implementation using a solid elastic cushion system. In Journal of Physics: (Vol. 896, No. 1, p. 012120). IOP Publishing.
2. Tolipov, A., A. Elghawail, M. Abosaf, D. Pham, H. Hassanin, and K. Essa. "Multipoint forming using mesh-type elastic cushion: modelling and experimentation." The International Journal of Advanced Manufacturing Technology (2019): 1-12.
3. Abosaf, M., Essa, K., Alghawail, A., Tolipov, A., Su, S. and Pham, D., 2017. Optimisation of multi-point forming process parameters. The International Journal of Advanced Manufacturing Technology, 92(5-8), pp.1849-1859.
4. Elghawail, A., Essa, K., Abosaf, M., Tolipov, A., Su, S. and Pham, D., 2018. Low-cost metal-forming process using an elastic punch and a reconfigurable multi-pin die. International Journal of Material Forming, pp.1-11.
5. Elghawail, A., Essa, K., Abosaf, M., Tolipov, A., Su, S. and Pham, D., 2017. Prediction of springback in multi-point forming. Cogent Engineering, 4(1), p.1400507.

# POSTERS

Tolipov, A.A., Elghawail, A., Shushing, S., Pham, D. and Essa, K., 2017, September. Finite Element Modeling of Multi Point Forming tools. College of Engineering Physical Sciences, University of Birmingham.

# TABLE OF CONTENTS

# LIST OF FIGURES

# LIST OF TABLES

# ABBREVIATIONS

| | |
|---|---|
| FEA | Finite Element Analysis |
| SB | Spring-back |
| DOE | Design of Experiments |
| RSM | Response Surface Method |
| ANOVA | Analysis of Variance |
| CCD | Central Composite Design |
| DA | Displacement Adjustment |
| SF | Spring Forward |
| CAD | Computer Aided Design |
| FBG | Fibre Bragg Grating |
| MPDD | Multi-point Deep Drawing |
| BHF | Blank Holder Force |
| LE | Logarithmic Strain |
| MPF | Multi-point Forming |
| FEM | Finite Element Modeling |
| LR | Literature Review |
| SHMF | Sheet Metal Forming |

# NOMENCLATURE

$P^{(K)}$ The form of the working surface and $(k)$number of correction iterations.

$\Delta S$ −Shape error of the formed parts

$\overline{\sigma}$ −Effective Von Mises stress

$\sigma_y$ −Yield stress

$\boldsymbol{\alpha}$ −Back stress tensor

$l_0$ −Original length of a line segment

$l_m$ −Length of a line segment at the midsurface

$\varepsilon_\theta$ −Circumferential true strain

$\varepsilon_a$ −True strain in the midplane

$\varepsilon_b$ −Bending true strain

$\varepsilon_m$ −Membrane engineering strain

$\varepsilon_\theta^p$ −Plastic strain

$\sigma_\theta^p$ −Circumferential stress

$T^e$ −Force produced by the elastic stresses

$T_T^p$ −Tensile force produced by the plastic stresses

$T_c^p$ −The compressive forces produced by the plastic stresses

$M^e$ −Elastic bending moment

$M_T^p$ −Plastic part of the total bending moment in the tension area

$M_c^p$ −Plastic part of the total bending moment in the compression

$A_0$ −Original area of the specimen

$r_a$ —Plastic anisotropy

$\varepsilon_{2\ +}\varepsilon_3$ —Width and thickness strain of the specimen

$\lambda_B$ —The Bragg wavelength

$n_{eff}$ —Effective refractive index

$\alpha_t$ —Thermal expansion

$\alpha_n$ —Thermo − optic coefficient

$p_e$ —Photo − elasticity coefficient,

# CHAPTER 1 INTRODUCTION

## 1.1 General background –

Today, society expects excellence in both, products and product delivery systems and, in particular, this has meant that formed metal panels are in use almost everywhere. Using sustainable and renewable manufacturing resources, and modern know-how in all manufacturing sectors can enhance processing efficiency and save costs. Sheet-metal forming (SHMF) is a vital component of the current industry. SHMF is a process that enables the production of high quality, complex geometry products at relatively low cost. Metal forming processes which, according to Zhongyi and Mingzhe, include "stamping, deep drawing, bending, hydroforming, rubber forming, and incremental single forming" [1] are used extensively in, for example, aircraft, ship and vehicle production, and domestic appliance manufacturing. SHMF can be used with a large number of metals but has been particularly useful with aluminium, copper, nickel, steel and tin. With SHMF, it is possible to fabricate an extensive variety of parts, ranging from large structural elements such as an aircraft fuel usage down to a retractor for use in hospitals. Most of these products have a sufficiently high finish hence there is no need for any additional machining [1].

Chung and Richmond [2] in a report published in 1992, investigated what were the optimum initial and intermediate configurations when using sheet metal forming to produce a defined final form, where optimum was defined as the process following the minimum work path and producing a final shape where the distribution of the limited deformations were optimally close to the required form. The emphasis of this work was on the forming of sheet materials under plane stresses. Chung and Richmond also used numerical methods for modelling these processes. It was reported that the results obtained

showed that the mathematical analysis and model, based on ideal forming theory, can predict optimum process parameters [3]. Here the optimal form is the desired form produced by plastic deformation without the necessity of any further machining. It is usual for the elastic deformation that occurs during SHMF to produce wrinkling and dimpling on the final form, and sheet-springback which occurs after forming is complete.

## 1.2 Background to reconfigurable die-

The use of reconfigurable dies with separated pins for 3-D SHMF is not new. Many articles have reported the use of SHMF in opposite punch processing. SHMF using a multi-point die (MPF) is a flexible manufacturing method suitable for the 3-D forming of diverse large sheets. In the multi-point die, the forming surface is the envelope formed by tips of the pins. Reconfigurable dies can be used to produce many of the basic shapes normally obtained using MPF, without wrinkling and spring-back Reconfigurable dies are those which can be used to produce different final forms because the location of each pin forming the die can be varied in a controlled manner, independently of the others. MPF based on step-by-step forming, can be used to form a large sheet with a small machine providing flexibility in the application of MPF technology [4].

Chapter 3 (three) will further explain in a step-by-step process about the changes in pin position with each step on MPF tooling. An optimisation mesh-type elastic cushion constative model is recognised to describe the stress and strain relation of steel and aluminium sheets, and it is process parameters are obtained based on the analysis of the experimental data [5].

Moving the pins to adjust their relative positions is an easy way to change the geometrical envelope that is the forming surface. This capacity of MPF to modify the geometric shapes of the products provides substantial saving in both time and money

when compared to SMF using traditional solid dies which would require re-tooling. Naturally, the larger the die/product the greater the savings.

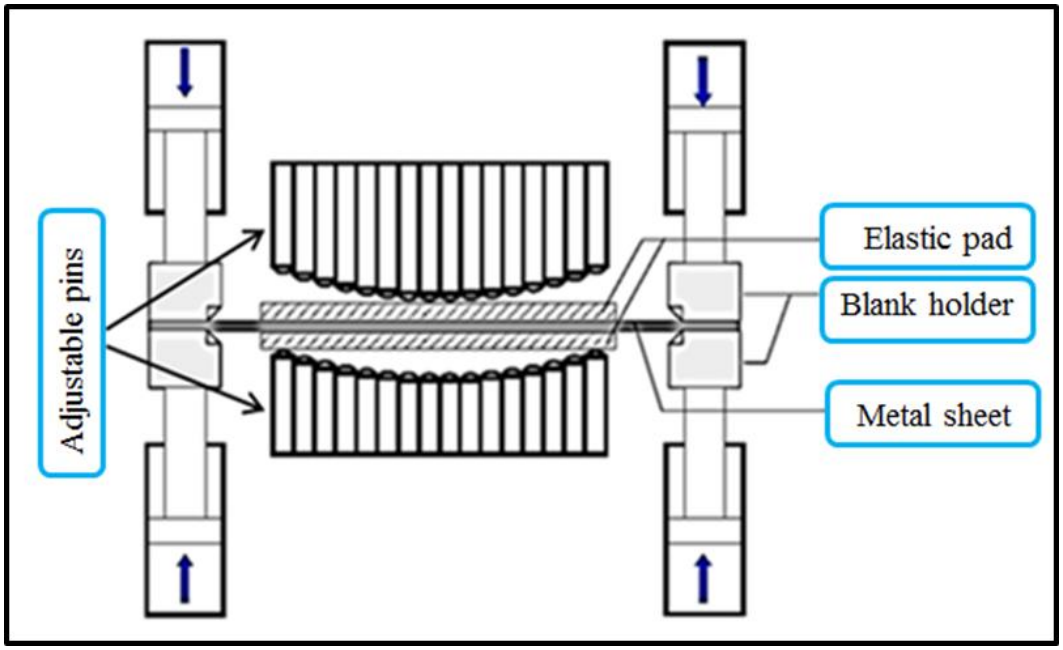


Figure 1.1 Schematic diagram of the flexible multi-point tooling [93]

MPF has another enormous advantage. If the forming surface can have its shape changed during the process itself, then the deforming path of the metal sheet being formed can be changed as well. It should be possible by moving a group (or groups) of pins in real time to confirm the process follows the optimal forming path and produce a final form with minimum risk of wrinkling, thickness variation or spring-back other faults.

## 1.3 Research aim, objectives and contribution to knowledge-

The motivation for this research work is to provide an integrated prototype system obtained by applying a different geometry which is mesh-type elastic cushion and hole type elastic punch to MPF die tooling. Relevant process parameters have been developed in this research, which include the thickness of the sheet, elastic cushion hole size, elastic cushion thickness, radius of curvature and forming force on the MPF tool. Overall, in reality, building tools for reducing issues such as wrinkling in a sheet metal is a very

expensive option. However, this study has developed a tool which can reduce wrinkling for the sheet metal at a cheaper cost along with leading to potential savings in time. This was found to be the main contribution of this research to the existing knowledge on the relevant topic.

The other more important contributions, which are also the objectives of this research include:

a) Design and construction of a MPF die, considering: pin tooling surface and size, machine working setup, upper and lower dies, hole-type elastic-punch tool geometry and forming force measuring model.

b) Optimization of a software package, which will be directed at the generation of a package for square pin adjustment of a 3-D die surface CAD model.

c) Optimization of a package for numerical simulations of MPF adjustment centred on ABAQUS/Explicit.

d) The recognition of basic methods for the improvement of surface quality of the FARO Arm/CMM instruments.

e) A contribution to the academic community by intending to produce a patent in the near future along with two conference papers and three journals papers already published. (AUTOMAN LTD PROJECT).

Flexible MPF dies are gaining attention as an advanced manufacturing method for 3-D sheet materials. This thesis will seek to fill gaps in existing knowledge regarding MPF. In particular it will provide information that should improve the shapes of forming surfaces which should, in turn improve the quality of the formed products. The project will use numerical methods to model and study deformation of the sheet surface and

process characteristics for three SMF processes: i) Traditional solid die, ii) Flexible multi-point forming and iii) A new hole-type elastic punch geometry with MPF of sheet metal.

## 1.4 Summary

This thesis contains seven chapters. A brief general introduction is given in the first chapter. The second chapter provides definitions and a comprehensive review of the relevant literature. Next, the third chapter provides details of the experimental setup for the MPF assembly and elastic cushion. The fourth chapter presents an optimisation of the MPF using numerical analysis and FEM (Finite Element Modelling). The fifth chapter presents the discussion on Design of Experiments (DOE), the MPF process parameters, and the mesh-type and forming processes for the numerical examination, to explore the forming force, thickness variation shear strains with radius of curvature and experimental validation of the work. The sixth chapter discusses process development and optimization using a mesh-type elastic cushion with validation, and DoE strategies to improve precision in elastic punch forming with MPF die processes. The conclusions from this work and suggestions for further research are provided in the final chapter.

The main objective of this work was to perform multi-point forming, which is a flexible manufacturing technique where a user-defined material model is implemented in Abaqus/Explicit against the commercial forming multi-point forming. It was considered to be an important step in order to understand the capabilities and limitations of the state-of-the-art commercial codes, as these are more widely accepted in the industry.

However, there were concerns that the performed numerical simulations may not provide the flexibility required to model the current wrinkling problem. Whilst previous researches published in the literature typically predicted the forming behaviour for individual thin pins of the same orientation, the novelty of this work lies in studying

hemispherical shape and how they perform with potentially different material behaviour in elastic cushion sheet metal forming. The Abaqus/Explicit model is known to be computationally efficient, adopting the elastic material model to simulate the forming behaviour of curvature performance, containing the elastic cushion. In addition, this study also analysed experimental data in terms of the tensile testing performed for the elastic cushion and steel as well as aluminium sheet metals. The data achieved was used for verifying and validating the numerical simulations.

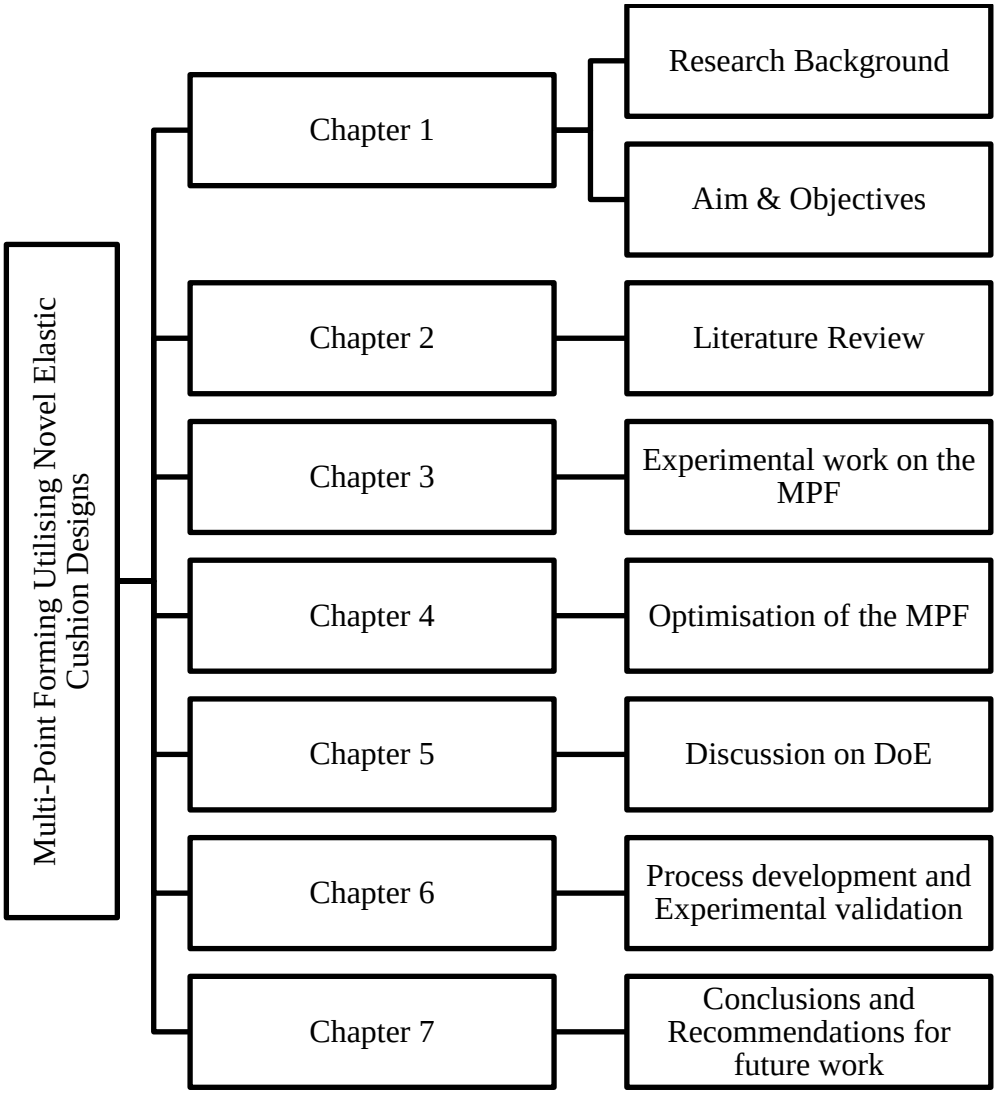


Figure 1.2 Thesis structure

# CHAPTER 2 LITERATURE-REVIEW

## 2.1 -Preamble

This article scrutinizes a schematic analysis of integrated Literature Review (LR) sections drawn from research articles across two disciplines. The analysis mainly focuses on the schematic structure, namely the constituent moves and steps. The economic pressures for efficient and environmentally friendly industrial processes has meant that research into tools that are reconfigurable is now a necessity, but such optimization is complex because it requires the integration of many different aspects of a multi-faceted system, including design, assembly, process planning and manufacture. Figure 2-1 is a schematic diagram of this literature review, which shows the four elements of MPF of metal sheets; pin design, methods for tools surface contour adjustment and forming defects:

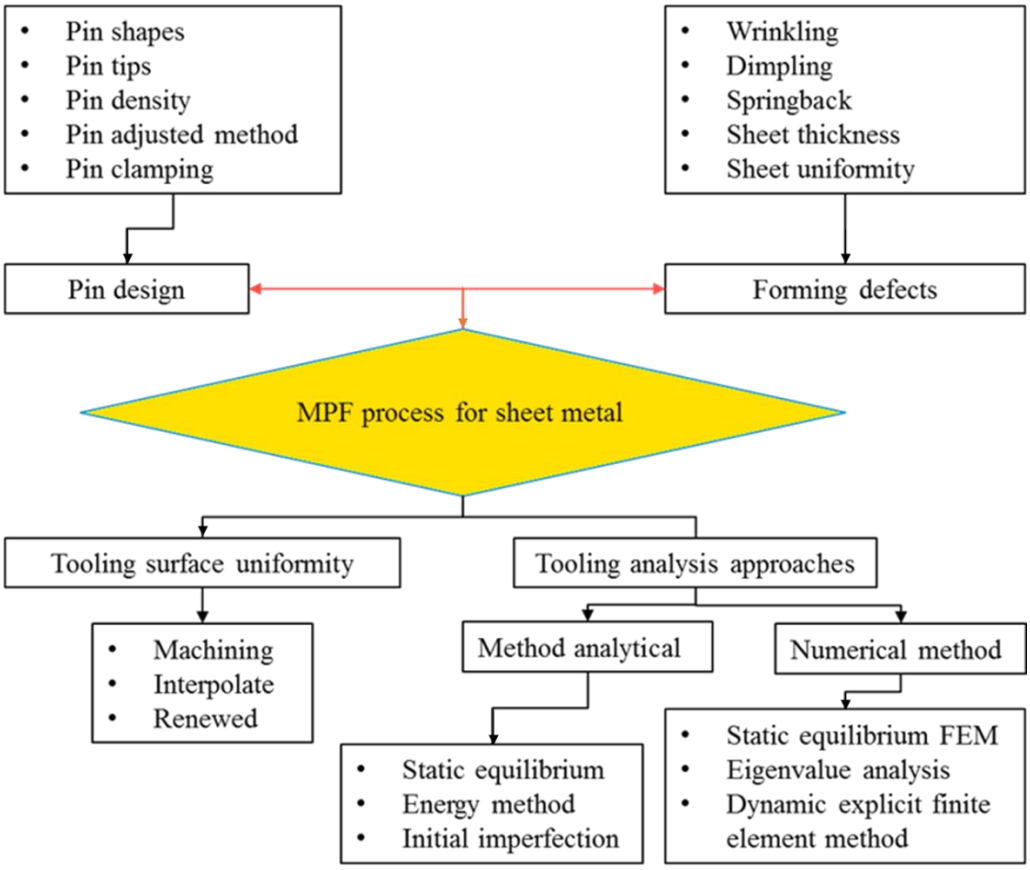


Figure 2.1 Schematic persanted of literature review in the research structure

## 2.2 -Multi-Point-Forming pin design-

Multi-point sheet metal forming refers to a process whereby metal sheets are formed into 3D shapes, usually by pressing the sheet between a punch (upper surface) and die (lower surface), see Figure 2-2. This chapter reviews the relevant previous research works and is limited to three areas:

- Flexible MPF with and without a blank-holder.
- Sheet forming with a multi-point die with elastic cushion.
- Development forming curvature should be simply clamped into a rigid tool.

There are several number of research publications available in the literature relating to these topics. This is mainly due to the MPF approach attracting a huge amount of interest, as it appears to be a flexible technique that can reduce manufacturing costs. This chapter intends to provide a literature review on the following topics [13]: Plasticity in MPF; Classifications of MPF; Advantages and applications of MPF; Analysis of MPF die system. In addition, a summary is also presented, which briefly highlights possible research topics, identified from the review. Square and hexagonal pins can be assembled into a matched matrix with no gaps amid the adjacent pins. However, there will be some minute gaps between the round pins and the threaded pins. Next, the round pins are made into a hydraulic or pneumatic cylinder. This allows these pins to be independently activated in the closed pack.

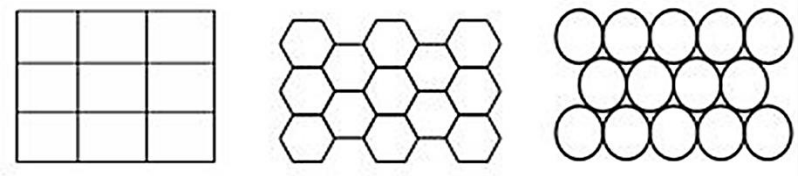

A) Square pin B) Hexagonal pin C) Circular pin

Figure 2.2 Schematic type of the pin shapes [12]

## 2.3 Plasticity-

The plasticity of the metal being formed is one of the most important parameter to be considered with MPF because the material hardness is important for reducing the wrinkling and dimpling of the sheet surface. Here the processes that will considered are the use of a multi-point punch with pinheads and a hemispherical punch for all-purpose sheet metal pressing. Theoretically, the simplest problems to be analysed are those with stable deformation, the most difficult, and usually the most interesting, are those where some form of failure occurs, such as wrinkling of the metal sheet due to tensile instability.

For the manufacturing industry, the load needed for any procedure can be easily obtained with a good enough accuracy through a straightforward approximation and analysis. However, with an in-depth investigation, the strain required and its relationship with the experimentally measured strain can be predicted. Such a method refers to the finite element (FE) method for ensuring that the suitable yield criteria is met along with confirming that the related flow rule has been chosen. It is not possible to overlook anisotropy, which although describes the distortion of the MPF of steel very well but appears to be sub-standard for several other materials. Especially, when the plastic strain ratio, the *r*-value, is lesser than unity, other yield criterion must be considered along with flow rules for describing the plastic flow of the relevant materials [6].

It is relevant to assess the influence of macroscopic plasticity on applied sheet material forming. Up to now, this is not answered properly and it seems that it will not have a direct application anytime soon [6]. In MPF the presence of a non-uniform fracture strain after necking can be important. To predict necking and associated fractures with some accuracy a plasticity model has been introduced into the FE analysis of the tensile tests [6]. In [6], localized necking behaviour of DC05 Steel along with aluminium 5251-O was analysed

including plasticity in the FE analysis to produce forming limit diagrams up to necking and fracture.

When considering plasticity in sheet metals using FE analysis, stress concentrations at the boundaries can initiate local deformations. Analysis was carried out for obtaining the form limit illustrations for several strain paths. The results were compared with the experimental work. Another study [7] used a modified Cockcroft Latham damage model in the analysis of necking. In the study it was assumed that damage was related to the shear strain because the plastic deformation mechanism is based on slip planes and is calculated by Equation (2-1) [8]:

$$dD = \mathrm{f(x)} = \begin{cases} \frac{\gamma d\bar{\varepsilon}}{\gamma_{cr} \cdot \Delta\bar{\varepsilon}_{cr}} & for\ \gamma \geq \gamma_{cr}\ and\ d\varepsilon_1 \geq 0, \\ 0 & for\ \gamma < \gamma_{cr}\ or\ d\varepsilon_1 < 0 \end{cases} \tag{2-1}$$

In Equation (2-1), $\gamma$ is the shear strain, $\gamma_{cr}$ is the critical shear strain beyond which damage begins to accumulate, and $\Delta\bar{\varepsilon}_{cr}$ is the amount of plastic strain from damage initiation to fracture. If $\gamma < \gamma_{cr}$, deformation is compressive and the damage increment is 0 (zero). Parameters $\gamma_{cr}$ and $\Delta\bar{\varepsilon}_{cr}$ need to be determined.

$$D = \int dD \tag{2-2}$$

In Equation (2-2) the values of $\gamma_{cr}$ and $\Delta\bar{\varepsilon}_{cr}$ have been found to be as 0.233 and 0.08, respectively (8). The commercial software package ABAQUS has been used to implement the plasticity model. This is done via user-defined subroutines. For computation effectiveness, analyses of the tensile test are usually performed for only a part of any tensile sample as shown Figure 2.3.

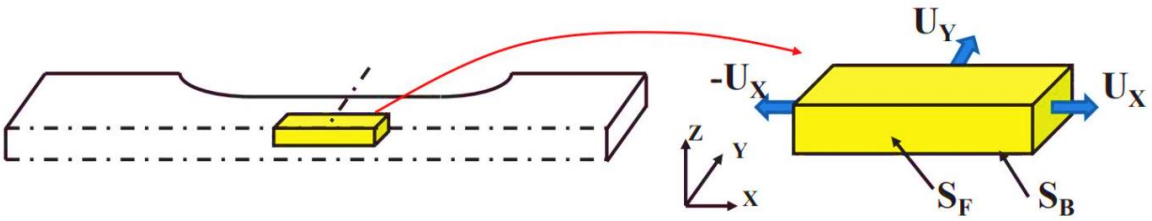


Figure 2.3 Boundary condition for forming limit diagram of the tensile test [8]

The front and bottom surfaces ($S_F$ and $S_B$) in Figure 2.3 are considered as planes of symmetry. $U_X$ and - $U_X$ were imposed on the left and right surfaces, respectively, and $U_Y$ in the Y direction in the continuing domain next to the surface paths.

### 2.3.1 Classification of metal forming-

Metal forming is usually divided in three general processes: a) bulk forming which includes rolling, drawing and extrusion, b) sheet metal forming (SHMF) which includes deep drawing and stretch forming and c) hybrid forming which combines different processes, for example, deep drawing and electromagnetic forming where SHMF represents a highly significant group of industrial processes [9]. SHMF can be divided into cold and hot forming. In the cold forming of a metal, the plastic deformation itself generates strain hardening, but because ductility is limited, so is the extent of any change of shape [10]. Hot working occurs at a temperature, which is above the re-crystallisation temperature, where plastic deformation does not generate work hardening and the metal has a lower yield strength. Despite these differences the broad principles that determine SMF are much the same for both hot and cold forming, and design of tools, for example, is not determined by the temperature of the operation but on the specified geometries of the inputs and outputs, the material to be processed and required rate of production.

In SHMF a blank sheet is deformed into a complex 3-D shape. This is usually undertaken with the intention of preserving the sheet thickness and surface finish. Sheet metal forming operation are usually performed as cold working processes, at a temperature, which is less than the re-crystallization temperature of the material being formed. However, some sheet forming operation are conducted at elevated temperatures, for example, warm forming of aluminium, steel, or titanium alloy sheets or hot stamping of special steel to obtain specific properties. Within metal forming processes, the work-piece may be a billet, rod or sheet, and the bulk deformation is usually characterized by a substantial change in shape with a large

increase in the ratio of surface area to the volume of the formed part. Also, for bulk forming (but not sheet forming) the process is such that elastic recovery in the work-piece being plastically deformed is usually not a problem [10]. Note that a single forming step may not be sufficient to produce the required final form and several operations are necessary. With SMF the blanks undergo plastic deformation into complex 3-D shapes without any appreciable modification of the thickness of the sheet, nor of its surface characteristics, so the ratio of surface area to volume does not undergo any substantial change which is a useful means of differentiating bulk deformation from SHMF. This also means that with SHMF, the elastic recovery (springbuck) can be a significant problem.

## 2.4 Advantages and applications-

A new and effective method of SHMF has attracted attention because it can produce shapes which other processes such as solid dies cannot easily produce. SHMF is used in many industries, in particular automobile production, the aerospace industries and even the construction industry. Such industries require that the dimensions of the parts produced conform closely with the designed shape, and these requirements are becoming increasingly stringent [11]. At the same time, the drive to reduce costs means that materials with lower plasticity and less formability need to be formed. Sheet metal forming (SMF) uses complex solid dies that are robust and well-suited for mass production but are extremely expensive to produce in regards to the development design time and cost of fabrication. However, they are not economical for producing a single item or for small batches. The block of a forming die with an adjustable contour has long been an attractive idea and could be the means of cutting the costs of die design, as a single block could be relative quickly and cheaply adjusted to produce final forms of different shapes [12]. [13, 14] have developed the concept of SHMF based on variable contour discrete dies that can be modified to produce different shaped parts, and which are cost-effective for small batch production. Figure 2-4 shows examples of

conventional forming of sheet metals and SHMF, in each case with and without a blank-holder.

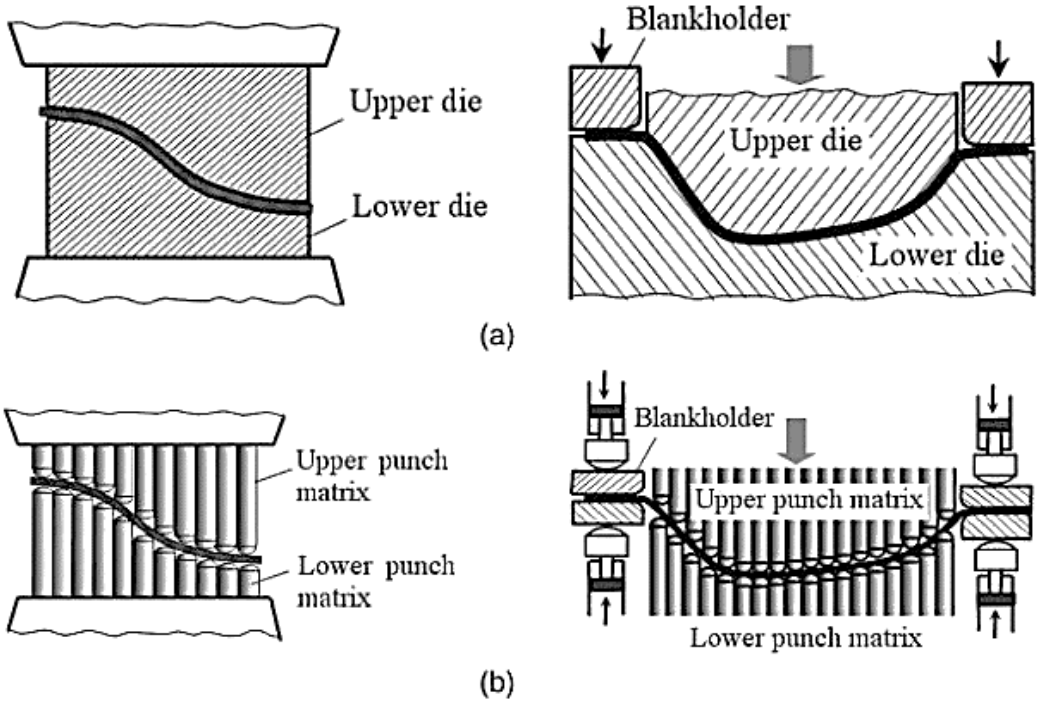


Figure 2.4 Schematic diagram of a) conventional forming of the sheet metal with and without a blank-holder and b) SHMF also with and without a blank-holder [12]

### 2.4.1 Pin-configuration and cross-sectional-shape-

An FE method has been developed by [13] to model multi-point sheet metal forming (SHMF) for a die consisting of two matrices of pins (upper punch and lower die), a metal sheet and an elastic cushion. The basic concept of MPF is to use a matrix of elements (punch heads or pins) to describe the required surface shape, as would be seen in a traditional or conventional die. Today such dies can be computer controlled so that the contours of the surface can be changed almost at will, by movement of the individual pins, and can be linked to, for example, a CNC machine. If the pinheads are flat, see Figure 2-5 (b), then initially, at least the pins will be in almost complete contact with the work-piece. However, if the shape to be formed is not flat then, as the punch moves down, see Figure 2-5 (b), the pin faces will

be at an angle to the forming shape and possibly, only the edges will be in contact. Such an arrangement can cause severe defects to occur, in particular dimpling. On the other hand, if the pinheads are rounded as in Figure 2-5 (a) then the overall shape of the formed surface is likely to be more accurate. Some researchers claim that it is relatively easy to determine the desired pin positions and then to actively control their movement to produce the desired deformation of the metal sheet [11].

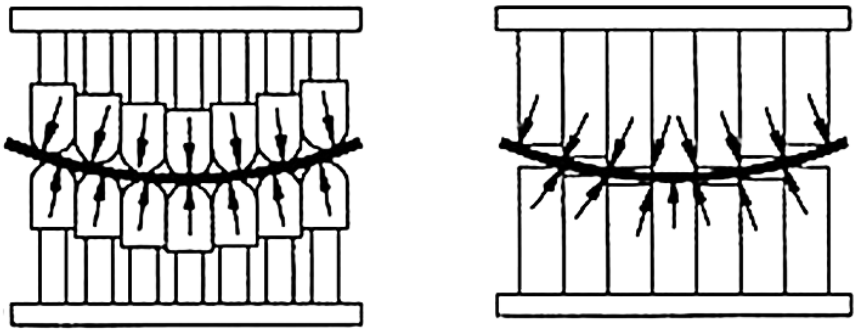


Figure 2.5 SHMF contours a) Hemispherical pins, b) Flat circular pins ( [12])

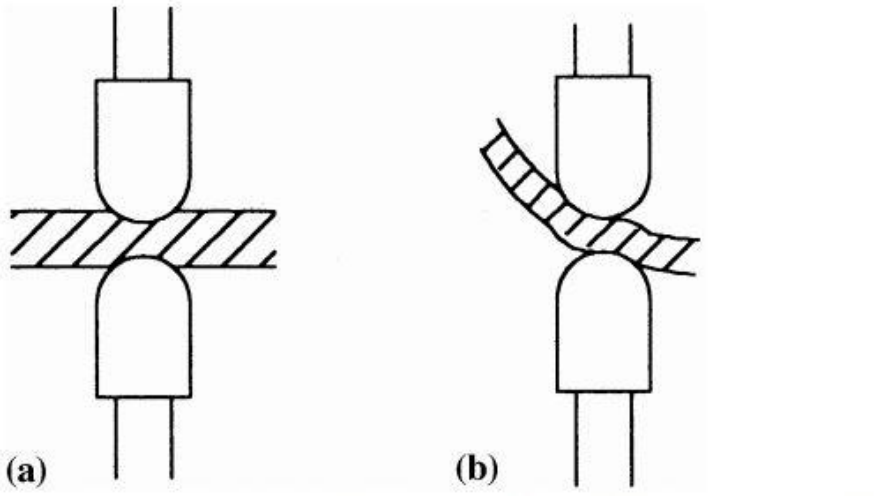


Figure 2.6 MPF dimpling of metal sheet: a) aligned: b) disarranged [12]

However, there is a problem with the use of hemispherical pins. It can be seen that the area of the pin in contact with the sheet metal is not large and it is found that such an arrangement

can give rise to dimpling of the surface, as demonstrated in Figure 2.6. When the pins are aligned the strength of the sheet is not seriously adversely affected because the relative area of the dimpling is less as compared to the sheet area [12]. But when the pins are, "disarranged", the dimpled area is substantially increased and this may not be acceptable [12]. This is a problem with MPF but, fortunately is relatively easily resolved.

The vertical position of the upper punch is designated as being in the z-direction, with the hemisphere forming the pin surface determining the z-coordinate. The punch surfaces and die (the punch matrices) are, of course, coincident with the lower and upper faces of the part being formed when the die is closed and the tips of the hemispheric pins are in contact with the metal sheet being formed, see Figure 2-7. It is apparent that the target surface is a distance ($r_p + t/2$) from both the upper and lower isometric surfaces.

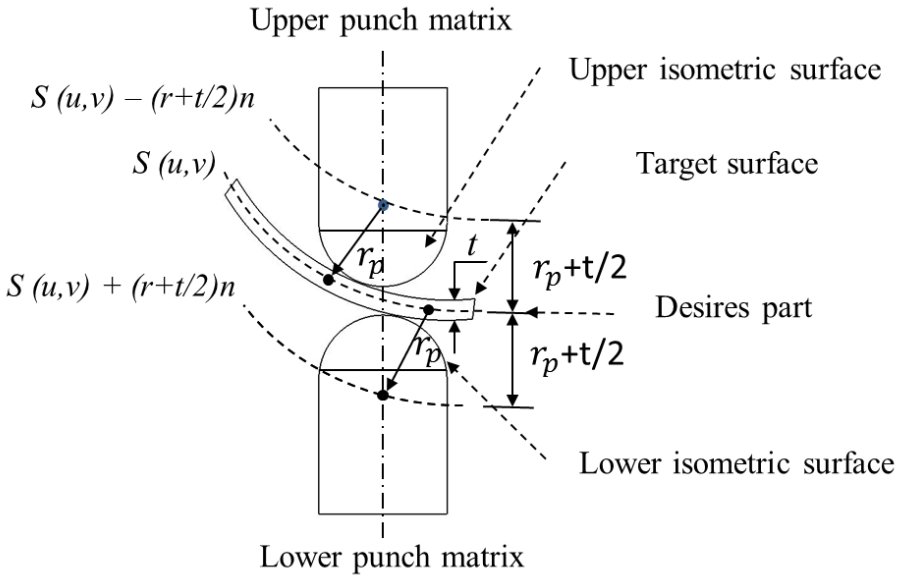


Figure 2.7 Schematic of lower and upper

Where punches with hemispherical pins and metal sheet to be formed, showing the system parameters including the desired shape of the formed surface, *S(u, v)* is the design surface of the formed part, see Figure 2-7, and *n* - is unit vector normal to the surface *S*(*u*, *v*) in an outward direction. Note that Equation 2-3 is in fact a non-linear system of equations.

Assuming $r_p$ is the radius of curvature of the hemispherical end of the pin, and t the thickness of the metal sheet being formed then the equations representing matrices forming the upper punch and lower die can be written as [13]:

$$\begin{cases} S(u,v) - (r_p + t\ /2)\boldsymbol{n} \ \text{(upper isometric surface)} \\ S(u,v) + (r_p + t\ /2)\boldsymbol{n} \ \text{(lower isometric surface)} \end{cases} \quad (2\text{-}3)$$

Implicit in Equation 2-3 are three unknowns, $u_T, v_T$ and $z_c$, where $u_T$ and $v_T$ are the $u-$ and $v-$ coordinates of the point of contact of the spherical surface of radius $r_p + t\ /2$, and the target shape $S(u, v)$. $z_c$ is the $z$- coordinate of the centre of the radius of curvature of the hemispherical pin. If we now describe the target shape using Cartesian rectilinear coordinates of the form z = $S(x, y)$, then Equation (2-3) may be written as [15]:

$$\begin{cases} \partial S\ (x,y)\ /\ \partial x\ + (x - x_c^k)/d_k = 0 \\ \partial S\ (x,y)/\partial S + (y - y_c^k)/d_k = 0.. \\ z_c^k = S(x_t, y_T) + \ d_k(X_T, y_T) \ldots\ldots \end{cases} \quad (2\text{-}4)$$

Where $x_c^k$ and $y_c^k$ are the Cartesian coordinates of the centre of the hemisphere forming the tip of the kth pin, where $d_k\ =\ \lambda\sqrt{r_p + t/2)^2\ - (x - x_c^k)^2}$

Where $\lambda$ = + 1 for pins in the upper matrix (punch) and $\lambda = -1$for a pin in the lower matrix (die). The coordinates, $(x_T,\ y_T)$, of the point of contact with the metal sheet can be found from Equation 2-4, using the two equations containing $\partial S\ (x, y)$. $z_c$ the $z$-coordinate found from the remaining equation in Equation 2-4 [15].

## 2.5 Effect of multi-point forming pin configuration

Some authors [65] have published studies on the performance of square pins and their corresponding effects. Another previous work [16] has also investigated numerical modelling of MPF dies, where the system consisted of a metal sheet, upper and lower pin matrices, and the presence of two elastic cushions which were included for reducing dimpling and wrinkling. In a study by [22], the researchers examined the influence of including elastic

cushions on surface quality using micro MPF. These researchers all considered the cushion thickness, material and coefficient of friction, and all found that an appropriate choice of elastic cushion could substantially reduce dimpling and wrinkling [22]. In this investigation the mathematical model was restricted to only one quarter of the die. It was assumed that the symmetry of the system made this acceptable, and it reduced computational time substantially. Note that the condition of symmetry applied to punch matrices, the blank sheet and the elastic cushion.

The pins studied were all of square cross-section with a hemispherical tip. Three tip radii of curvature were investigated: 10 mm, 15 mm and 20 mm, see Figure 2-8.

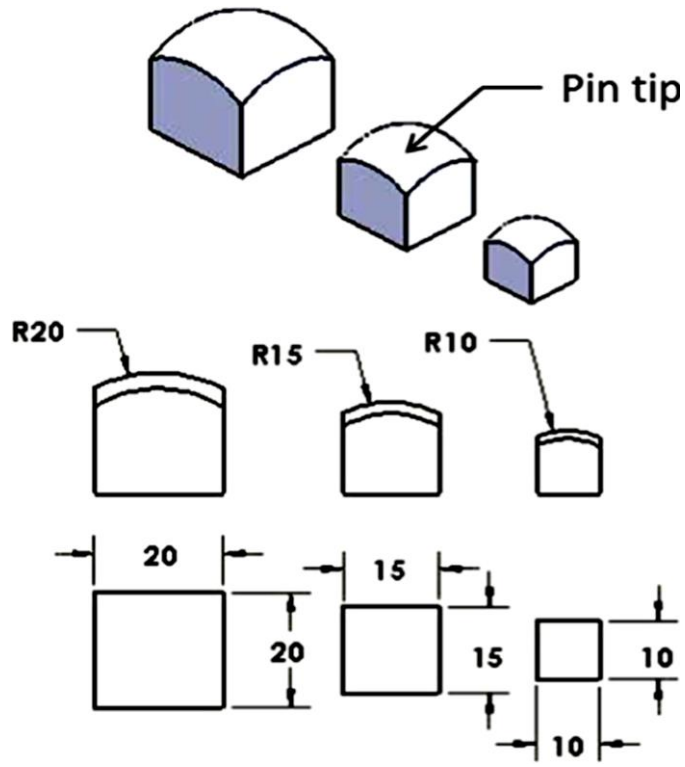


Figure 2.8 Commonly used matrix pin shapes and dimensions [14, 15, 16, 21]

The blank metal sheet considered in the simulations was 1 mm thick medium strength non-alloy steel grade CD05, as demonstrated in Table 2-8. It was assumed that the steel was isotropic, which means that its mechanical properties are the same in all directions, and that

an elastoplastic model could be utilised. For denoting the flow stresses in steel, Equation 2-5 is adopted, which is the power law relation.

$$\sigma = k.\varepsilon^{n} \qquad (2\text{-}5)$$

Over here, $\sigma$ represents the true stress, $k$ denotes the coefficient of strength, $\varepsilon$ denotes true strain and $n$ denotes the strain hardening exponent [17].

The FE model, see Figure 2-9, consisted of upper and lower pin matrices, a blank metal sheet with a layer of elastic cushion either side. The validation was performed for three pin arrangements with matrix configurations of a) $5\ \text{pins} \times 5\ \text{pins}$ with 20 mm radius of curvature for the pins; b) $6\ \text{pins} \times 6\ \text{pins}$ with 15 mm radius of curvature and c) $10\ \text{pins} \times 10\ \text{pins}$ with 10 mm radius of curvature. The use of too large a pin (increased size pins) can increase pin offset and generate a non-uniform stress distribution. This will be particularly noticeable at the sheet edges where wrinkling would be likely to occur.

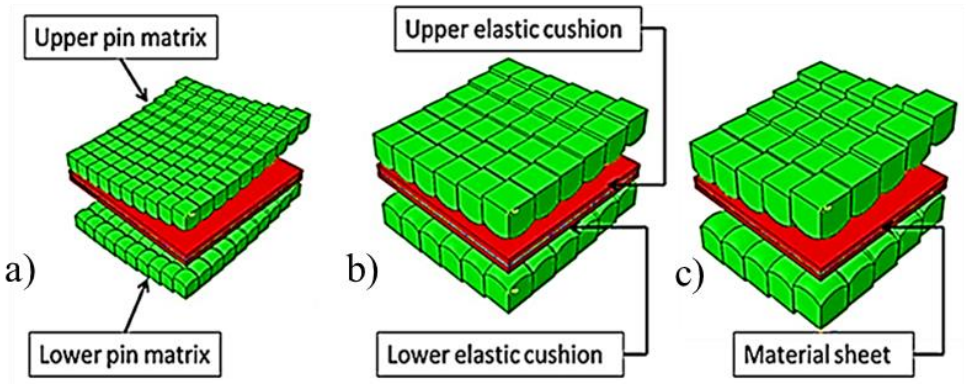


Figure 2.9 Illustration of three different pin matrix configurations, [65]

The presence of the elastic cushion was to test system performance with a protective layer to shield the sheet metal from dimpling. The work done in [65] tested various materials for suitability as an elastic cushion. Hardness was an important characteristic and this was measured using a Zwinch tensile test machine. The material selected was, in all cases, polyurethane A90.

It was consistently found that minimum wrinkling occurred with large radii of curvature and medium sized pins. Figure 2.10 shows comparison of forming shape with target shape using a curvature radius of 800 mm and pins of 10 mm [18].

Minimum spring-back occurs with small radii of curvature of the formed shape combined with large BHF (blank-holder force).

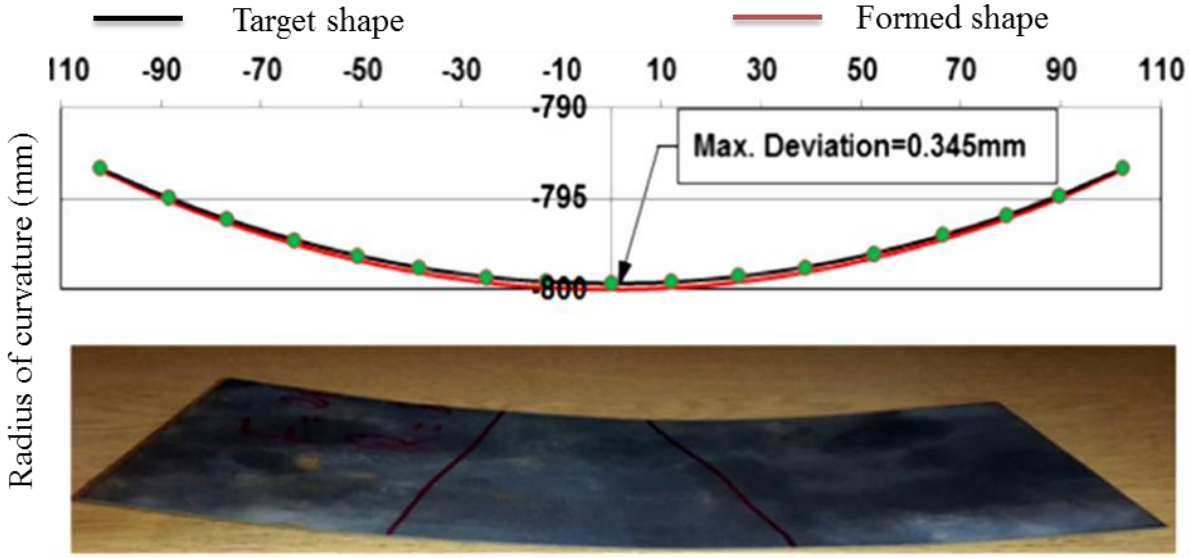


Figure 2.10 Comparison of target and formed shapes on R800 curvature, [11, 18]

## 2.6 Multi-point forming application

MPF presses have been developed for thick blank sheets of large size with large deformations. However, single step forming can introduce defects such as wrinkling, dimpling and spring-back. When forming metal sheets into complex 3-D shapes it is often found that the in-plane compressive stresses generated can lead to wrinkling of the edges of the sheet. With conventional forming as in Figure 2-4 (a) wrinkling can be reduced or even suppressed by the use of a blank-holder. Similarly, with MPF [39].

If there are numerous pins forming the matrices in an MPF punch and die it could take some time to set-up the desired contour. To minimise this time the pins should be set simultaneously. This is best done using a CAD 3-D modelling program though, of course, this will require

linkage to a programmable CNC toolpath. The aim of this system is for the product to be designed using CAD and the "drawings" analysed to generate a control programme for the MPF punch, see Figure 2-11. This is intended to be an iterative process whereby the two stages feed into each other to optimise the production process while preserving the essential characteristics of the design. Such software can save considerable time.

a) 3D is called CAD files that CNC machines can accept.

b) CNC machines tool

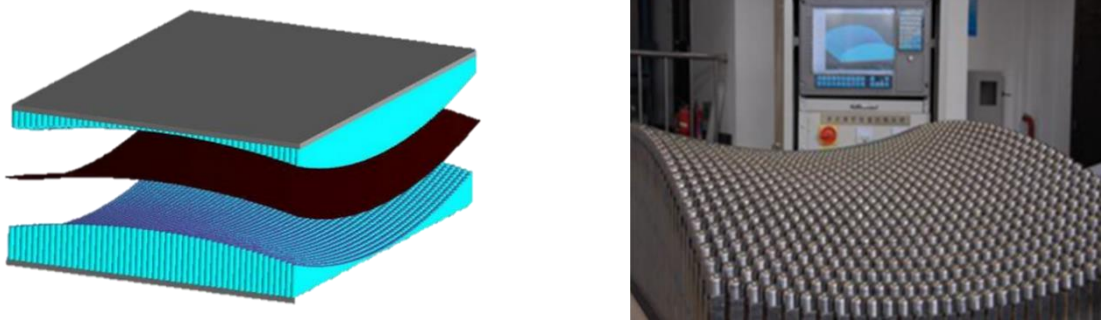

Figure 2.11 MPF matrices computer controlled by a CNC unit (after, [13])

Figure 2-12 shows a unit where each pin is individually controlled by a microprocessor, a mini-motor and a driving mechanism, and b) is a spherical end part formed using this MPF system [15]. With MPF, a relatively simple tool should be able to produce complex 3-D shapes without using a blank holder by moving the individual pins of the punch matrix along pre-determined controlled paths. Some researchers [19] were amongst the first to create dies that were modifiable to accommodate changes to the final form.

c) MP stamp forming tooling system

d) Industrial application

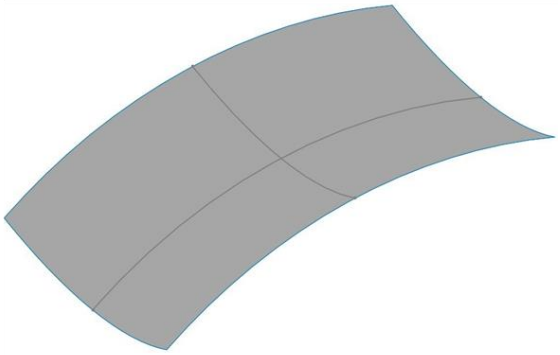

Figure 2.12 Correction insert a) and b), instead of c) and d)

(a) MPF of a spherical shape using multi-point matrix, (b) spherical part formed by CAD controlled MPF, [19].

### 2.6.1 Equipment-for-MPF

Commonly, SHMF requires four components: a blank sheet to be formed, a forming tool, a mechanism for powering the tool and a blank-holder. Design and manufacturing excellence are key factors in the quality of the sheet deformation processes. The efficiency and reliability of MPF equipment are important considerations in determining suitability of a given machine and process for a particular application. Good quality work-pieces with MPF almost always requires the use of a blank-holder; a continuous frame that will rigidly clamp the perimeter of the work-piece, see Figure 2-13. Today. the design of forming tools tends to use “virtual prototyping” [20], which includes computer aided engineering (CAE) and computer aided design (CAD) using numerical simulation. The use of sensors for process monitoring and control, assists in improving and maintaining quality of the formed part. Achieving the flexibility potential of MPF is important because of the increasing variability of products and smaller batch runs. MPF allows the manufacture of different (but similar) product geometries in one tool, representing today’s preferred strategy [18]. MPF are used

when material flow needs to be restrained more than can be provided by a flat blank-holder plate using blank-holder pressure only, see Figure 2-13. Punch and die radii are other important variables affecting the flow and stretch of sheet materials.

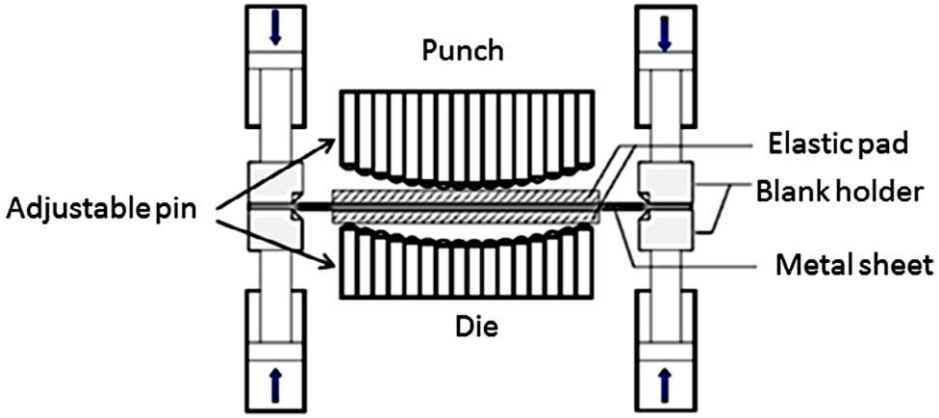


Figure 2.13 Diagram of the MPF process with blank-holder force (BHF) at changed positions, [18]

A variable blank holder in MPF is relatively new, [22], where combining a variable blank holder with variable BHF (Blank Holder Force) was extremely effective in eliminating wrinkling when forming spherical shapes [21]. In this process, the blank holder is divided into separate blocks, each of which can have a variable force applied to it.

Choice of machine suitable for use with a variable BHF for a particular process will depend primarily on the time taken to complete the process, the quality of the finished form and the forces required to complete the process. However, other considerations for optimum selection will include the physical dimensions of the machine, any environmental impact, cost and complexity of maintenance procedures, and any specific requirements for the required process.

### 2.6.2 Implementation-assembly-positioning

The implementation of the variable BHF technique with a MPF system requires change in BHF with location of the punch stroke. However this is not widely used in current

production because it is difficult to estimate the BHF that should be applied by each of the blocks forming the blank holder [21]. MPF employs adjustable punches and dies in matrix form, where each individual pin forming the matrices is actuated separately to change its vertical position. This means a separate, discrete contour can be generated by the hemispherical tips of the pins, see Figure 2-14. MPF technology is suitable for rapid stamp-stretch forming and flexible assembly of large radius of curvature metal sheets. Figure 2-14 shows the principle of MPF geometry of curved panels where A) is stamping forming, B) is stretch forming, and C) is assembly positioning.

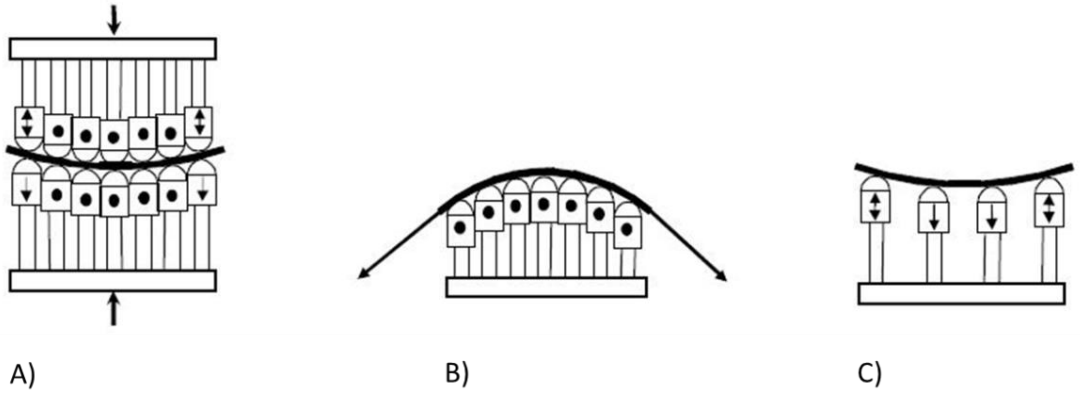


Figure 2.14 MPF used for A) stamping forming, B) stretch forming, and C) assembly positioning [21]

Using the same arrangement, a variety of subsidiary operations can be performed. For example, the edge of the formed part could be the blank holder. Figure 2-15 presents a typical MPF procedure.

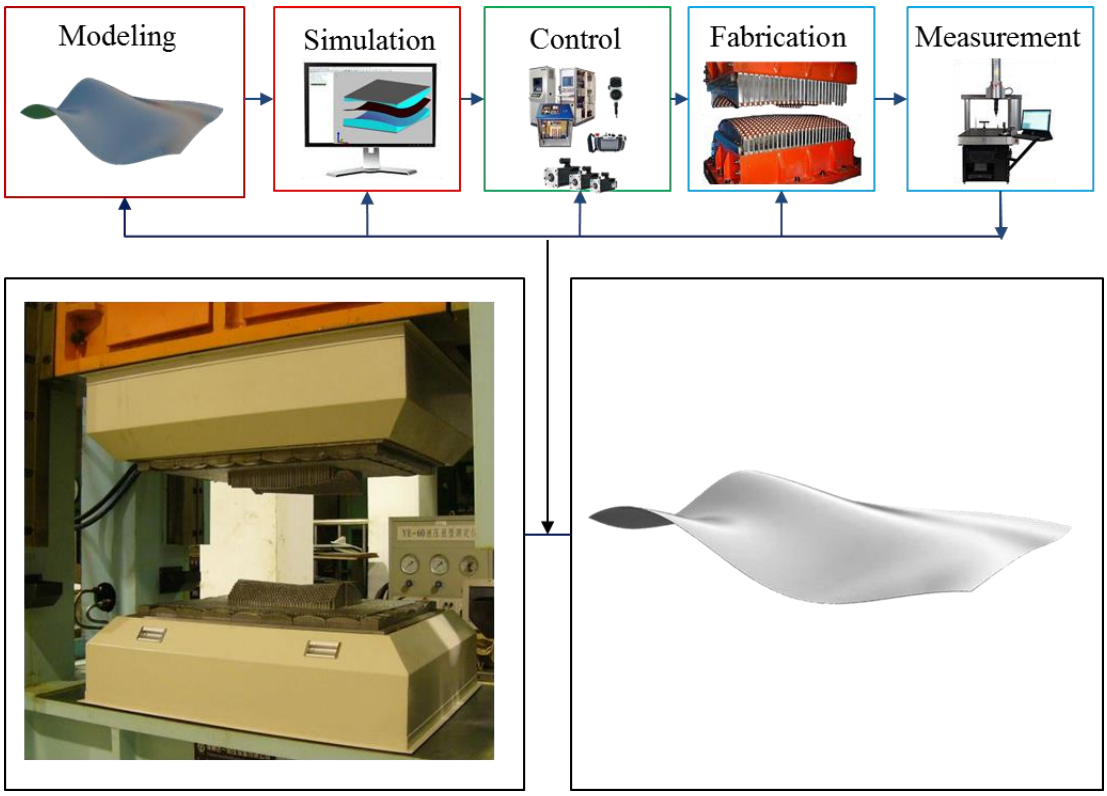


Figure 2.15 Experimental flexible SHMF manufacturing system [11]

Figure 2.16 shows typical formed panels obtained with a MPF tooling system [11]. However, this particular system was not economically efficient because productivity was lowered. This was due to the processes being derived entirely from the knowledge and expertise of individual researchers [11].

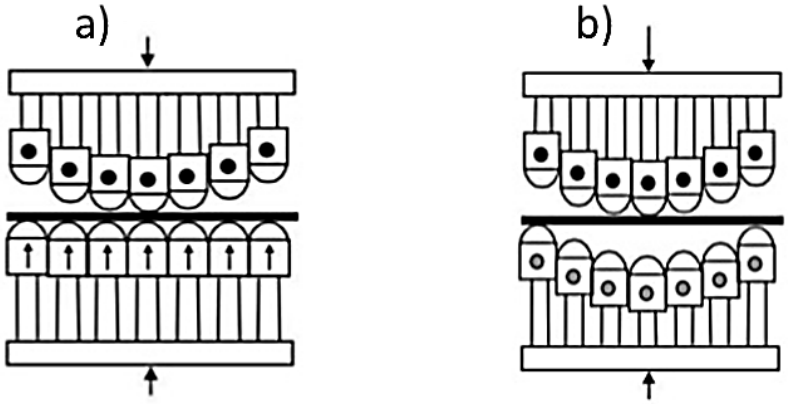


Mobile multipoint press forming method  Flexed multipoint press forming method

Figure 2.16 Industrial applications of flexible SHMF [11].

### 2.6.3 Investigative-approaches-in-MPF-product

Investigations using numerical simulation and analytical method have attempted to measure relevant process features and assess the workings of SHMF. The experimental investigation of flexible MPF processes reported here is concerned with producing curved surfaces with the contour of the punch and die made up of a multiplicity of pins; as demonstrated in Figure 2.17a, which is a diagrammatic presentation of mobile MPF and flexible MPF methods.

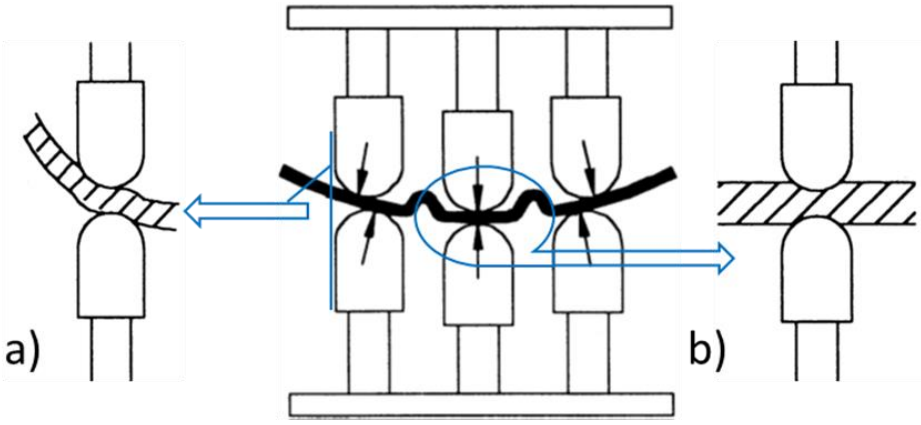


Figure 2.17a Pad wrinkling a) disarranged and b) aligned [24]

The basis of computer controlled MPF is to have each element forming the surface contours of the punch and die (the pins) controlled by some form of computer which enables the surface contour - which is what, forms the work piece to be altered throughout the forming technique [25]. This method can either be pre-programmed following earlier FE analysis or based on feedback control. Both dimpling and wrinkling are inherent problems with MPF due to the relatively small area of contact between the pinheads and the metal sheet being formed [11]. The occurrence of both faults can be minimised by inserting a pad or layer of hard, elastic material, which will have the effect of increasing contact area.

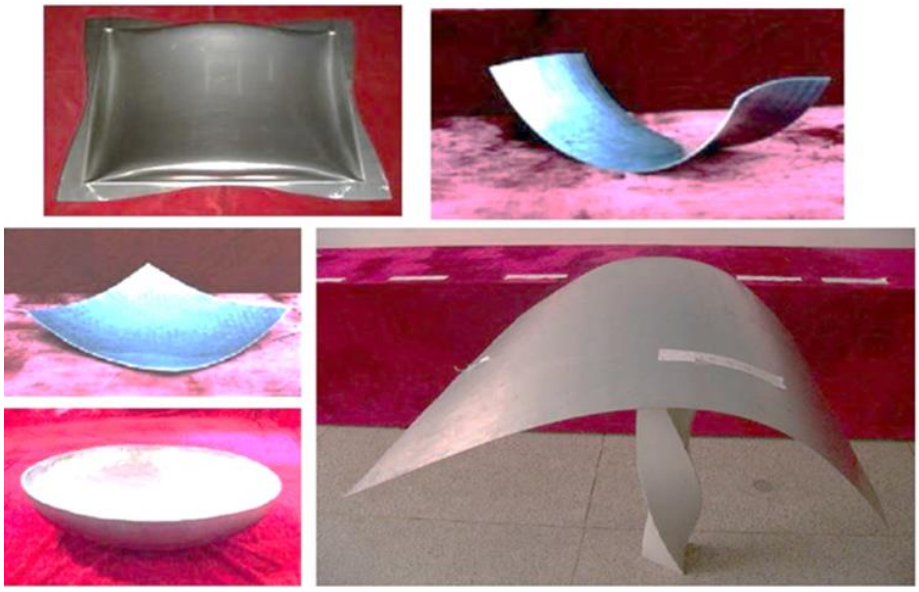

Figure 2.17b Flexible tooling in sheet metal forming (24)

It is plausible to control and calculate the required movement of the pins so that the surface contour formed produced a shape of the desired radius of curvature, as demonstrated in Table 2-1 for methods of adjusting the pins.

Table 2.1 Adjusting method on-MPF

| Type of pins | Mark | Adjusting method | Forming force (kN) control |
|---|---|---|---|
| Passive | 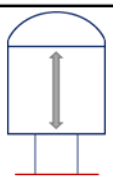 | Be made to move in process | None |
| Active | 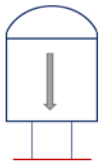 | Freely controlled in process | Large |
| Fixed | 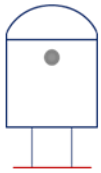 | Before forming | Small |

With sheet metal, during the application of the compressive forces, wrinkling can happen in regions close to the blank-holder. The less the sheet thickness and the greater the yield strength, the more likely wrinkling is to occur. But these are desirable properties and thus wrinkling is an increasing problem for sheet metal forming [26]. Many analyses of wrinkling in sheet metal are based on the work of [26], which used a criteria based on what Hutchinson described as: “post-bifurcation and imperfection-sensitivity”. Two researchers considered thin shells of double-curvature and recommend the concept of a buckling limit curve, or yield surface. In case the applied stress remains within the curve (or surface), then the sheet remains elastic. However, in case the applied stress goes beyond the limit, then wrinkling can occur. Essentially this is the application of the J2 deformation theory to thin sheets [25].

FE simulation is also being widely used to assess the likelihood of wrinkling [28]. Generally the analysis follow one of two paths; either introducing some imperfection at the start of the process, such as in the mesh representing the metal sheet to be formed, or having wrinkle indicators in the FE code [26]. Another work [27] has extended bifurcation analysis to the

study of wrinkle formation in doubly curved sheets of materials exhibiting planar anisotropy and compared predictions with experimental findings.

### 2.6.3.1 Wrinkling-criterion in sheet metal-forming

The examination of wrinkling developed here uses criteria developed by Hutchinson [28] and later extended by [29]. This defined in the ($\omega_1$ , $\omega_2$,$k_{1,}$) axes as:

$$\acute{u}1 = Btsin\left[\frac{\lambda}{l}\,\omega_1\right], \qquad \acute{u}_2 = 0, \qquad \acute{u}_3 = At\,cos\left[\frac{\lambda}{l}\,\omega_1\right] \qquad 2-6$$

Where : ú1, $\acute{u}_2$ and $\acute{u}_3$ are wrinkling criterion in sheet metal forming [29].

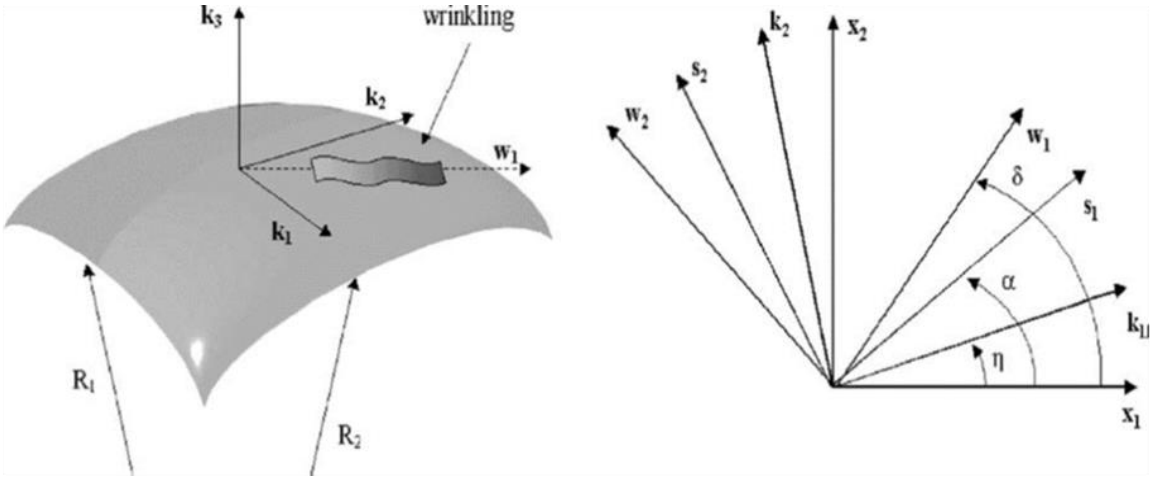


Figure 2.18 Axes and angles used in wrinkling analysis, [30].

The axes and angles used in this analysis are shown in Figure 2-18. An example yield surface in the principle stress plane ( $\sigma_1, \sigma_2$) is shown in Figure 2-19, for different angles $\alpha$, where $\alpha$ is the angle between principal orthotropic and stress axes, i.e. between the orthotropic axes ($x_1, x_2$).

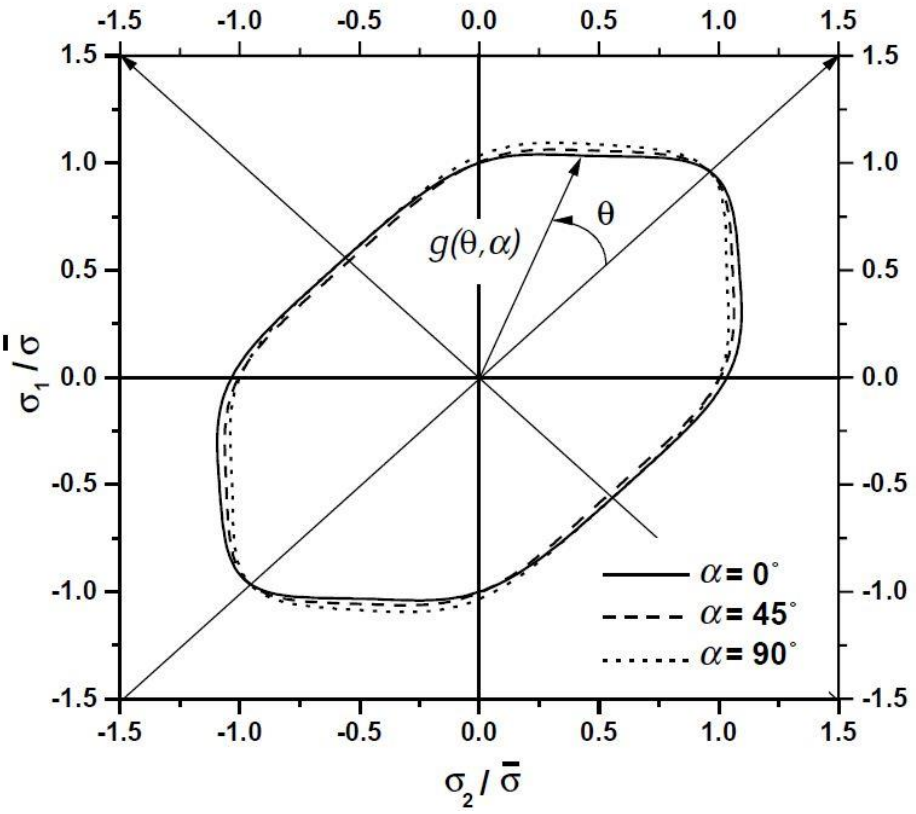


Figure 2.19 Yield surface in principle stress plane [31]

The plane stress yield surfaces $(\sigma_1, \sigma_2)$ are normalised by dividing by the effective stress recognised as the equal-axial yield stress [31]. For the normal anisotropy, the function g($\theta$) is known by:

$$(1-k)\, g(\theta)^{-6} = (cos^2\theta + A\sin^2\theta)^3 - k\, cos^2\theta - Bsin^2\theta)^2 \qquad 2\text{-}7$$

Here $A, B$ and $k$ are dimensionless constants for the material. Inserting values of $A$ = 3 and $B$ = 9 into Equation 2-7, the quadratic expression for Hill's yield criterion (see Equation 2-9) can be obtained in the particular case of $k$ = 0 and $A$=1+2$r$, where r is the coefficient for normal anisotropy [32].

### 2.6.3.2 Analytical-predictions-of-wrinkling

The material to be considered is modelled as planer isotropic with planar anisotropy coefficient, *R*. The parameter, R, is described as the ratio of the in-plane plastic strain of the sheet being formed, to the plastic strain normal to the plane of the sheet. R can be found using a simple tension test.

Hills 1948 expression for quadratic strain, $\bar{\varepsilon}$, is given in [32] as.

$$\overline{\sigma} = \frac{\sqrt{(\sigma_1 - \sigma_2)^2 + (\sigma_2 - \sigma_3)^2 + R(\sigma_1 - \sigma_3)^2}}{\sqrt{(1 + R)}}, \qquad 2-9$$

$$\bar{\varepsilon} = \frac{\sqrt{1+R}}{1 + 2R}(\varepsilon_1^2 + \varepsilon_3^2). \qquad 2-10$$

The Swifts equation for describing the strain hardening behaviour is: [74].

$$\overline{\sigma} = K(\varepsilon_0 + \bar{\varepsilon})^n, \qquad 2-11$$

Here *K* is a constant representing the strength of the material, *n* is an exponent determined by the work hardening behaviour, and $\varepsilon_0$ is the strain. With a flat plate and edge displacement $u_x/L$, (see Figure 2-20) the corresponding strain distribution $\varepsilon_{1_0}$ can be obtained as [74]:

$$\varepsilon_{1_0}\, 1n\left(1 - 2_{u_x}/L\right), \qquad 2-12$$

$$\varepsilon_{2_0} = \frac{1 + \alpha}{1 + R - \alpha R}\varepsilon_{1_0}. \qquad 2-13$$

$$\varepsilon_{3_0} = \frac{(1 + R)\alpha - R}{1 + R - \alpha R}\varepsilon_{1_0}. \qquad 2-14$$

If there is no transverse tension, $\alpha = O$ and it is possible to determine $\Delta\varepsilon_3$, the strain difference as:

$$\Delta\varepsilon_3 = \varepsilon_{3_0} - \varepsilon_{3_0}/\alpha = 0 = \frac{\propto (1 + 2R)}{(1 + R - \alpha R)(1 + R)}\varepsilon_{1_0} \qquad 2-15$$

Substituting the Equations 2-13 and 2-14 in Equation 2-12, the effective strain for a flat plate is obtained as $\bar{\varepsilon}_0 = c_1\varepsilon_{1_0,}$ where:

$$c_1 = -\sqrt{\frac{1 + R}{1 + 2R}\left(1 + \frac{R(1+\alpha)^2 + (\alpha + \alpha R - R)^2}{(1 + R - \alpha R)^2}\right)}. \qquad 2-16$$

It follows that the strain energy per unit width of a uniform flat sheet, $E_{0,}$ under edge compression and transverse tension can be shown to be:

$$E_w = \frac{1}{w}\iint \overline{\sigma}\, \mathrm{d}\bar{\varepsilon}\, \mathrm{d}V = \frac{KL_t}{n+1}(\varepsilon_0 + c_1\varepsilon_{1_0})^{n+1}. \qquad 2\text{-}17$$

However, for a buckled plate, see Figure 2-10, we can obtain the strain energy per unit width, $E_w$, as follows. An assumption is made that for edge displacement $u_x/L$, the mode shape of the buckled plate, is sinusoidal in form:

$$y = \delta(1 + \cos(mx)), \qquad 2-18$$

Where x is the lateral distance, *m* is the angular frequency of the mode in radians, and [33]:

$$m = 2\pi x/(L - 2_{u_x}). \qquad 2-19$$

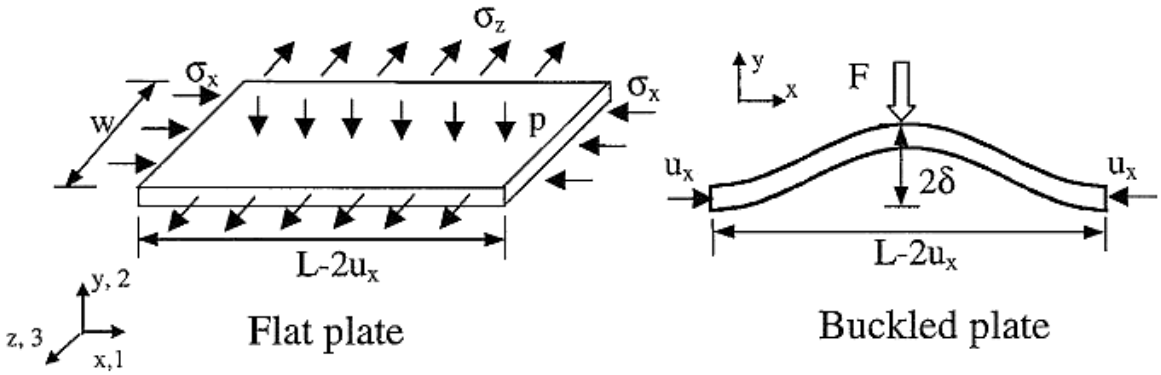


Figure 2.20 Schematic of a wrinkling sheet being suppressed by the BHF [34]

Assuming that the metal is incompressible and suffers no significant variation in thickness, one can easily derive an expression for volume per unit width as:

$$V = L_t = (1 + \Delta\varepsilon_3) \int t\mathrm{ds} = 2t(1 + \Delta\varepsilon_3) \int_0^{L/2-u_x} (1 + m^2\delta^2 \sin^2(mx))^{\frac{1}{2}} dx. \qquad 2-20$$

Simplifying using Taylor's expansion, it is possible to derive the amplitude of the modal deflection as:

$$\delta = \frac{1}{\sqrt{2\pi}} \sqrt{\sqrt{\left(\frac{L}{1 + \Delta\varepsilon_3}\right)^2 - (L - 2u_x)^2}}. \qquad 2-21$$

This simple model predicts that for a given edge compression, the strain energy contained in a flat sheet, $E_{0,}$ is greater than that contained in a wrinkled sheet, $E_{w,}$ provided both sheets are free of any normally applied constraint. The difference between $E_0$ and $E_w$ for any edge displacement $u_x$ corresponds to the external work, $W_{n,}$ executed by the normally applied force

F to suppress the wrinkling ($\int_0^{2\delta} F du_{y,}$). It follows that wrinkling can be presented in terms of the principle of conservation of energy [33]:

$$W_n = E_0 - E_w = \int_0^{2\delta} F du_{y,} \qquad 2-22$$

Where $u_y$ is the wrinkling deflection, $\delta$ is maximum height of the wrinkle for edge displacement $u_{x.}$. More than one mode is possible. The simplest is as shown in Figure 2-20. This is the first the wrinkling mode, half a sinusoid, and $m = 2\pi/(L - 2_{u_x})$. The second wrinkling mode is a full sinusoid, $m = 2\ x\ 2\pi/(L - 2_{u_x})$ see Figure 2-21, and L/2 denotes the wrinkling wavelength [35]. The general expression for m is $n\ x\ 2\pi/(L - 2_{u_x})$ which represents the $n^{th}$ mode.

Assuming $F = F_{max} - F_{max}\ (u_{y/\delta} - 1)^2$, the critical pressure, corresponding to the least force on the edge of the sheet of material being formed necessary to overcome any wrinkling of the $n^{th}$ mode for a normalized displacement $u_x/L$, can be expressed as a relationship between the calculated critical pressures $p_1$ and $p_2$, for the first and second nodes, respectively, as functions of edge compression $u_x$/L from Equation 2-23 [33].

$$p_n = \frac{F_{max}}{L_w} = \frac{3(E_0 - E_{wn})}{4\delta_n\ Lw} \ . \qquad 2-23$$

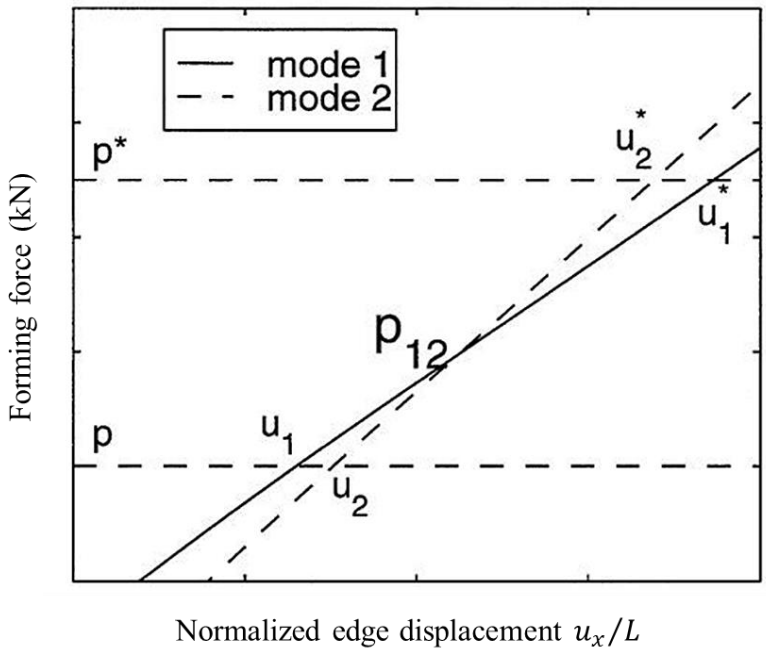


Figure 2.21 The forming force as function of edge displacement for wrinkle modes 1 and mode 2 to demonstrate the wrinkling idea [34]

[36] investigated the bifurcation of double curved metal sheets using shallow shell theory but restricted their investigation to areas of the work-piece free of any surface contact, which meant the blank-holder was excluded. [37] investigated wrinkling in a sheet by modelling the effect of the stiffness of the blank holder, which was treated as an annulus with an elasticity that could be modelled as a simple elastic spring. The investigation was to determine critical stress corresponding to the inception of wrinkling and the extent and degree of the wrinkling. As might be expected, their results were found to compare favourably with results previously obtained without a blank-holder, but there was no assessment of similar cases subject to normal blank-holder constraints.

#### 2.6.3.3 Modelling and simulation

The spring-back observed with sheet metals subject to forming are sometimes modelled as Chaboche non-linear materials. Innovative models using advanced plasticity

invariably require stress-strain curves to be experimentally determined. Such models have been found to provide good agreement between measured and calculated spring-back [38].

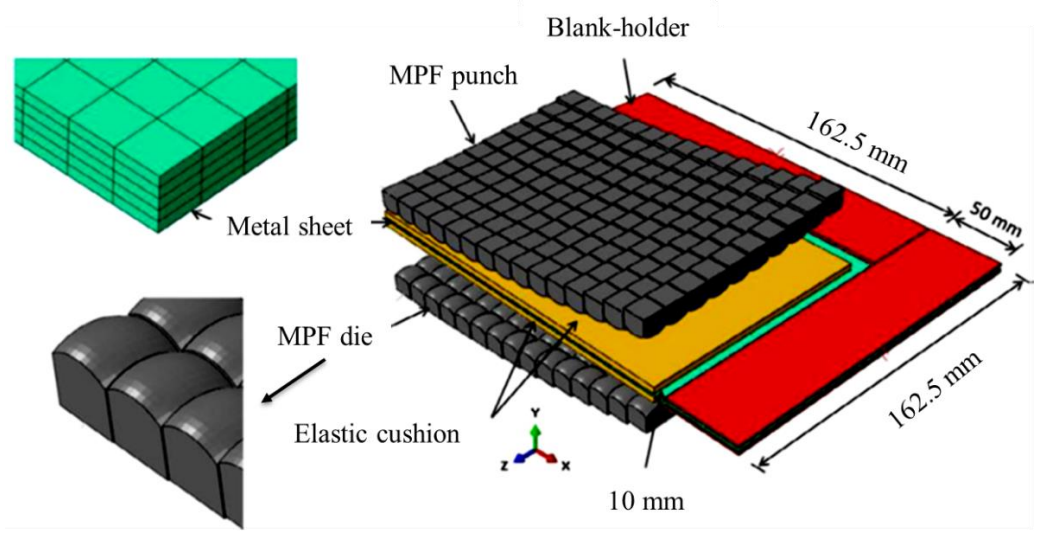


Figure 2.22 Finite-element-model [18].

The researchers [18] reported numerical modelling of MPF using FEM. This model replicated two pin matrices forming the upper punch and lower die, the blank-holder, two sheets of an elastic cushion and the metal sheet to be formed, see Figure 2-22. The yield behaviour of the metal was considered isotropic. Also, the plastic performance was modelled using Ludwig's Equation [39]:

$$\sigma = \sigma_0 + \mathrm{K} \cdot \varepsilon^n \qquad 2-24$$

Where $\sigma$ is the true stress, $\sigma_0$ the yield stress, $K$ the coefficient of hardness, n is the exponent of hardening (typically, 0 < n < 1) and $\varepsilon$ is the true strain. Figure 2-23 shows the strain-stress curve for the tested material [20].

The work-piece was aluminium 5251-0 alloy, 1.2 mm thick. A Zwick-Roell testing machine was employed to determine the tensile characteristics of the aluminium alloy in two different directions, 45$^o$ and 90$^o$, with respect to the rolling direction [8]. Relevant properties of the aluminium are shown the Table 2-2. In the constitutive model, the per volume strain, energy of the sheet to the formed may be determined from Equation 2-25 as:

$$U = C_{10}(\bar{I}_1 - 3) + C_{01}(\bar{I}_2 - 3) \qquad 2-25$$

Where $U$ is the strain energy reference volume, $C_{10}$ and $C_{01}$ are constants for the material but are temperature dependent. The values of $C_{10}(0.861)$ and $C_{01}(0.354)$ correspond respectively to $\bar{I}_1$ and $\bar{I}_2$, which are the first and second invariants of the strain tensor in the material model [40]. In typical sheet forming processes, such as MPF various stresses will be present in the work-piece at some distance from the pin point during the forming operation.

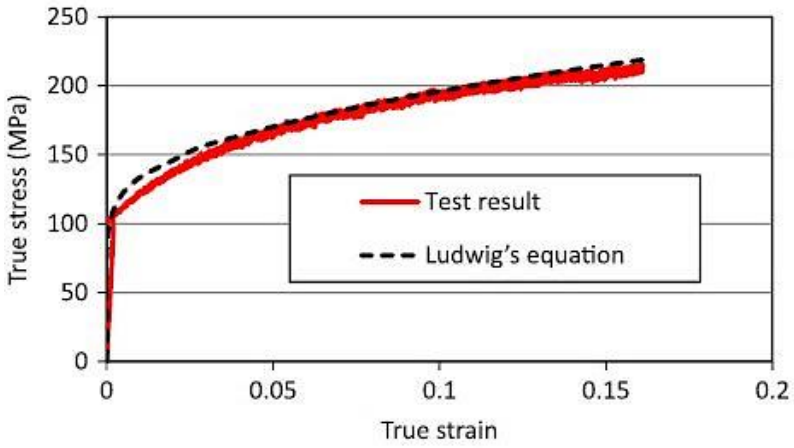


Figure 2.23 Results of stress-strain test for aluminium 5251-O alloy [18]

Table 2.2 Mechanical characteristics of aluminium 5251-O alloy [18]

| Properties | Values |
|---|---|
| Density (ρ) 2,700 kg/m3 | 2,700 kg/m3 |
| Modulus of elasticity (E) | 65 GPa |
| Yield stress (σ0) | 100.2 MPa |
| Poisson's ratio (v) | 0.33 |
| Strength coefficient (k) | 270 MPa |
| Hardening exponent (n) | 0.45 |

In general, at a point in the material, the internal forces (kN) can be completely described by stress components acting in three orthogonal planes (X, Y, Z) passing through the point [4].

Figure 2.24 shows the MPF formed sheet with spring back as a 3-D representation.

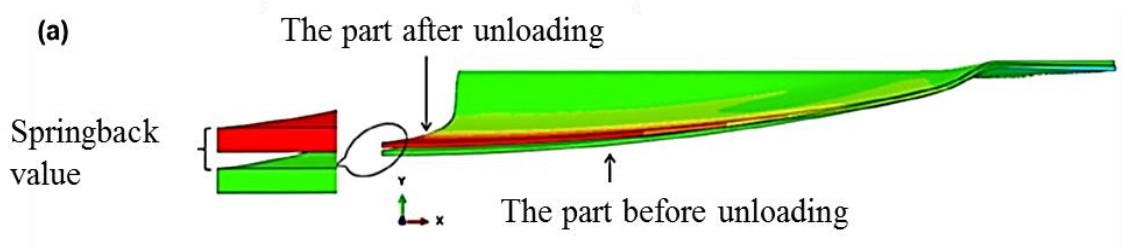


Figure 2.24 MPF formed sheet with spring back: a) 3-D representation

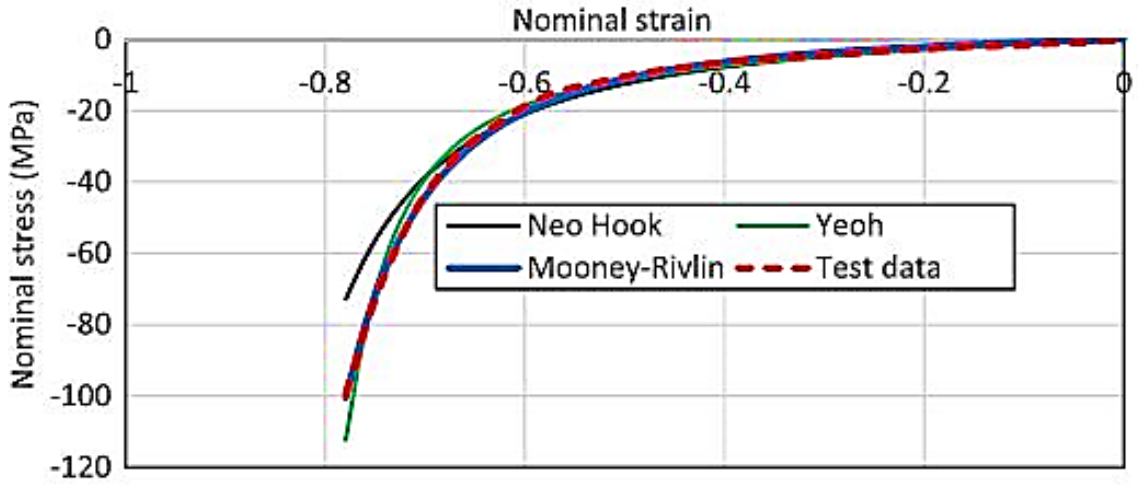


Figure 2.25 Comparison of hyper-elasticity results for A90 elastic cushion obtained using Abacus with three standard models [18]

## 2.7 Results of analysis of MPF die system

Figure 2-26 shows the results obtained by Elghawali for spring-back of metal sheets subject to MPF to form spherical surfaces [18]. Figure 2-26 (a) is a 3-D representation of the formed shape before and after being unloaded from the press. Figure 2-26 (b) shows how the spring-back was quantified.

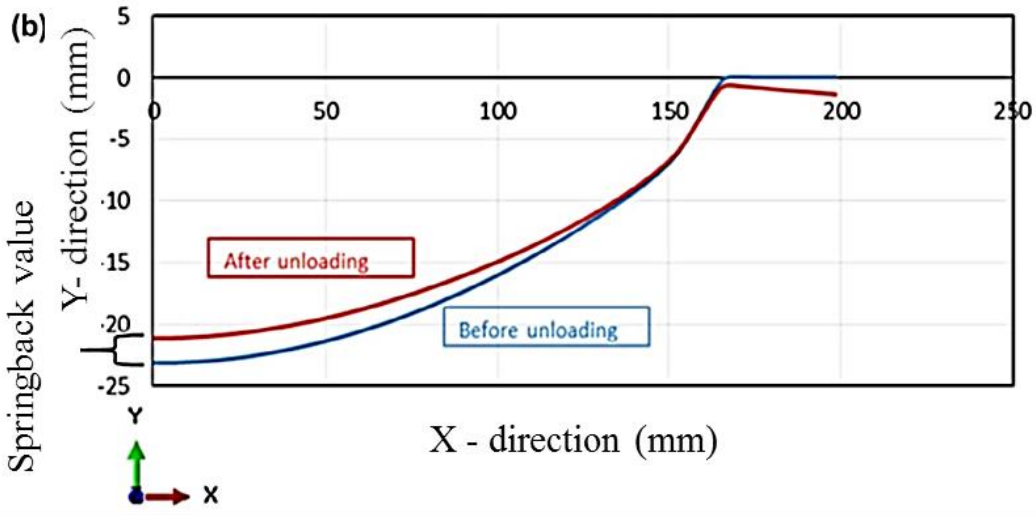


Figure 2.26 MPF formed sheet with spring back: b) how spring back was evaluated, [18]

Figure 2.26 shows a multipoint forming on R800 curvature of the process for correcting the elastic return.

In order to produce an innovative operating surface for the digitsed matrix [20], the numerical simulations are considered of the preceding forming cycle. Next, the object geometry of the part is related to the geometry of the deformed part. This helps in obtaining form errors, which are then analysed for further assistance in the production of an operating surface.

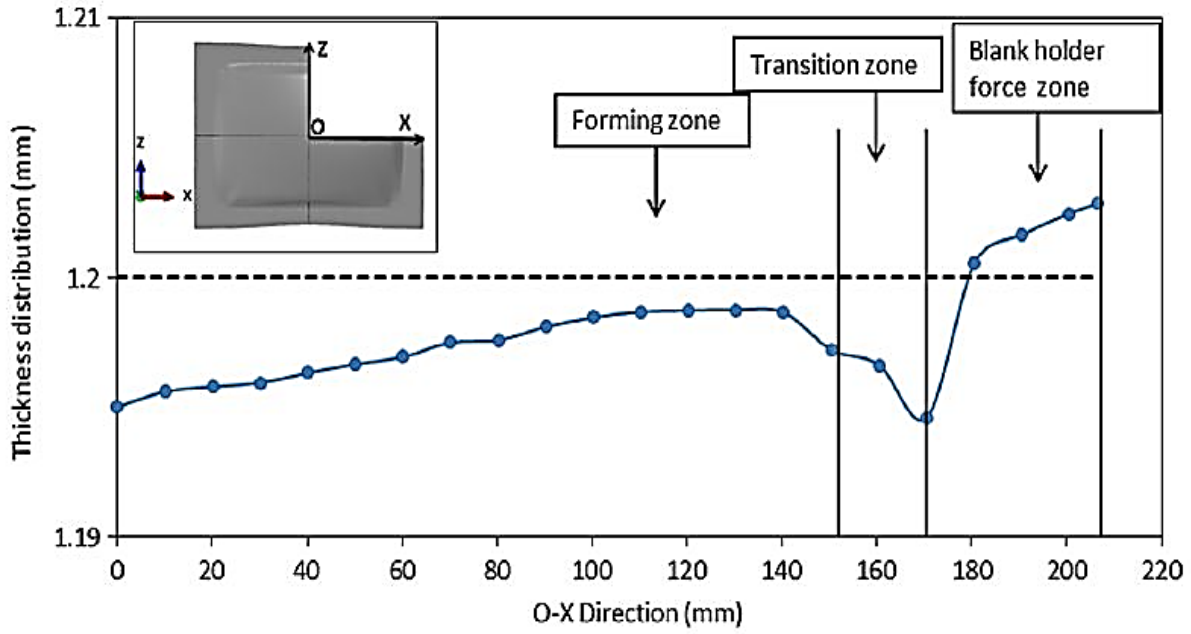


Figure 2.27 Predicted thickness distribution of formed sheet along O-X, [18]

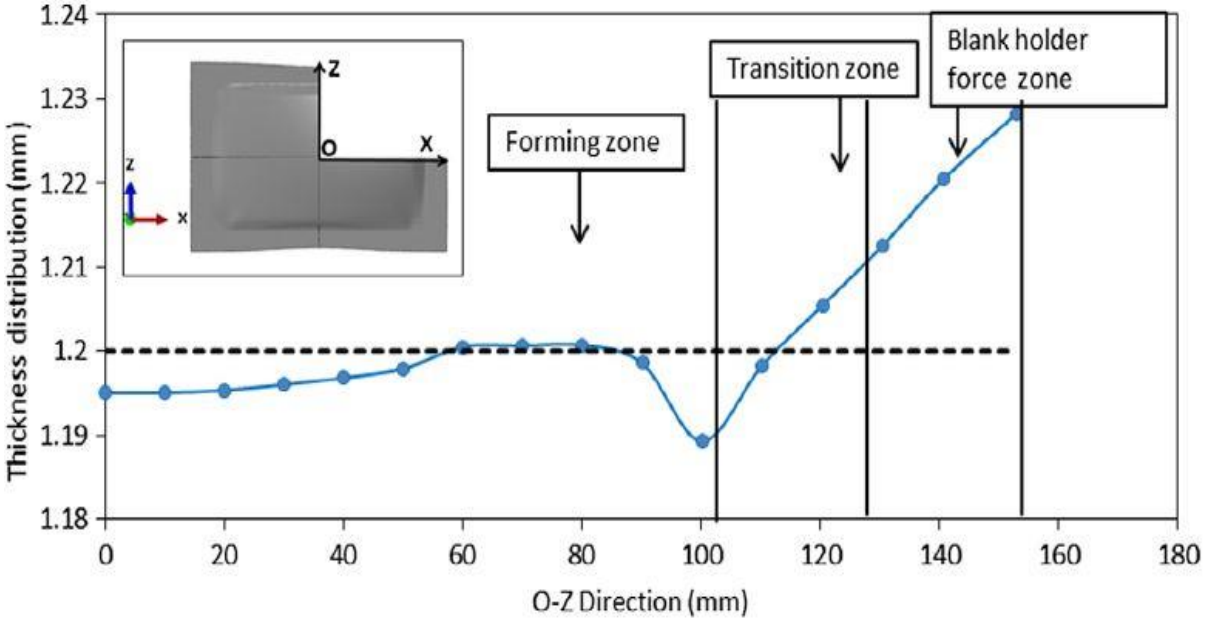


Figure 2.28 Predicted thickness distribution of formed sheet along O-Z, [18]

It can be seen from Figures 2-27 and 2-28 that thickening of the sheet was predicted because of the forming procedure, particularly close to the blank holder.

Table 2.3 Experimental validation best factor and corresponding values, [18]

| Significant factors | Response factors | |
|---|---|---|
| | Springback | Thickness variation |
| Radius of forming curve (A) | 0.0001 | 0.0001 |
| Blank holder force (B) | 0.0165 | 0.0001 |
| Elastic cushion thickness (C) | 0.139 | 0.3147 |
| Parameter interactions | (AB) = 0.3911 | (AB) = 0.3338 |
| | (AC) = 0.0502 | (AC) = 0.1273 |
| | (BC) = 0.0549 | (B × C) 0.0067 |

Where is comparison with predicted values. The likely spring-back that would occur as a result of MPF was studied using ABAQUS, with the aim of reducing wrinkling and spring-back by determining the optimum time for the formed sheet to be retained within the punch. The study also sought to determine the radius of curvature for which spring-back was least. This included using the MPF model developed with elastic cushions of different hardness.

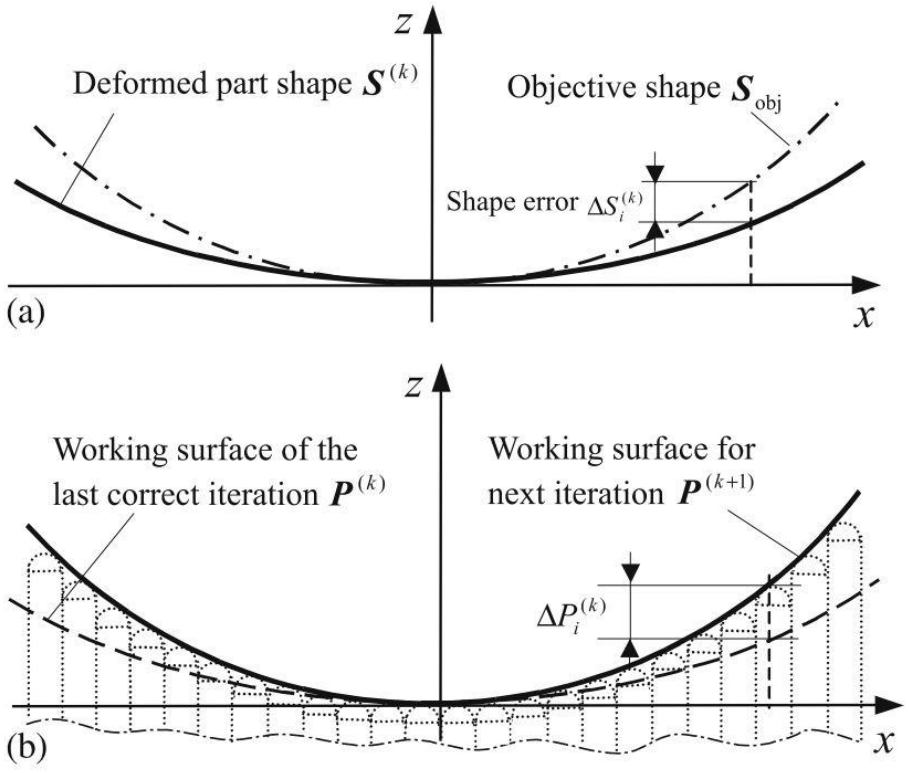


Figure 2.29 Spring-back modifying the operating surface of digitized die, [41]

Figure 2.29 illustrates a result diagram of the process for correcting the elastic return. In order to produce an innovative operating surface for the digitsed matrix, the numerical simulations are considered of the preceding forming cycle. The object geometry of the part is related to the geometry of the deformed part. This helps in obtaining form errors, which are then analysed for further assistance in the production of an operating surface.

## 2.8 Summary and Conclusions

The potential of SHMF as a manufacturing tool that can be used to fabricate an extensive variety of products is now firmly established. A number of significant publications appear in the literature reflecting on the great amount of experiments, analyses and numerical work, which has been undertaken regarding the traditional solid die and MPF. A review of such literature shows that several areas are in need of further research study, such as reducing the costs of elastic punch on MPF die. The forming force in MPF has received considerable attention regarding shear displacement. However, the effect of using different shaped punches and dies in subsequent passes on stress-strain distribution has not yet been the topic of much study. Surprisingly, advanced statistical methods such as ANOVA (Analysis of Variance) and modern experimental approaches such as DOE (Design of Experiment) which can be combined into an extremely powerful approach for identifying the working parameters that most critically affect the quality of the formed part are not widely used. Such an approach could be further developed to optimise the parameters for the best quality of the finished parts. It is seen that the combination of DOE and ANOVA has great potential for SHMF and could be used to optimise large plastic deformations of metal blanks via stretching the sheet but minimising thinning and avoiding thickening. Such an approach could also be an important factor in minimising spring-back and wrinkling.

# CHAPTER 3 EXPERIMENTAL SETUP AND ACQUISITION OF MECHANICAL PROPERTIES

## 3.1 Introduction

A process for developing multi-point forming processes is described within this chapter. Design and manufacture of process tools are essential factors in determining their level of performance of deformation processes. The major factor to successful deformation is tooling design, which is discussed here with a review of the main experimental processes and equipment used in the project. The alternative options considered during the design, as well as the reasons for the final selection, and details of the project and equipment are described. The experiments were performed in the University of Birmingham with the use of a Zwick/Roell tensile test machine located in the Elastoplastic Laboratory at the School of Metallurgy and Materials. To identify relevant properties of the materials of the test sheets, two classes of specimen were sliced at varying angles to the rolling direction (0°, 45° and 90°) and sets of tension-uniaxial and compression-tension tests were carried out on them. Metals can be divided into two main groups - ferrous metals that consist of iron and non-ferrous metals that do not consist of iron. The four sheets of materials utilised were obtained by Automated Manufacturing Process Integrated with Intelligent Tooling Systems (AUTOMAN), UK. Both, high strength and low strength steel as well as aluminium were used in the following manner:

- It is known that typically, any steel with 210 to 550 MPa of yield strength is referred to as the “high-strength” and something tougher is referred to as “advanced high-strength”.
- A low modulus refers to a structure, which is flexible while a high modulus is a structure that will be stiff and also inflexible.
- DC05 high strength steel, thickness of 1.0 mm.

- DC04 low strength steel, thickness of 1.0 mm.
- Al 5052 high strength aluminium alloy, thickness 1.1 mm.
- Al 5251 Low strength aluminium alloy, thickness 1.1 mm.

The thesis required knowing the mechanical properties of the material used, which may be affected by the proposed thesis activity (multipoint forming (MPF)). Information about the various parameters such as punch-movement, forming force and radius of curvature (used to compare the achieved shape with the design) are listed and described below. This thesis used digitally controlled tooling of multi-point sheet metal forming for the manufacture of automobile panels. The main focus of attention is the development and use of tooling with digital control using multi-point technology for the formation of 3D sheet metal body panels for an automobile. The goal is for the MPF process to provide faster, more flexible and economical formation of the panels using digitally controlled multi-point equipment. It is expected that the cost of tooling will be reduced by up to 65%, and installation time by 45%. It should also reduce the processing time compared to traditional utilisation of the tool. The key activities of the projects are to match the geometry of the produced moulded part with the preferred design geometry of the structure and assess the requirements for hardness of the processed material. Furthermore, it is important to take into consideration the storage requirements and the significant increase in the use of the tools. Finite Element Methods (FEM) will be used to investigate the key technological problems associated with adjustable multi-point tooling. This will be used mainly for modelling flexible multi-point tools composed of perforated matrices to replace the traditional hard snap. The thesis will also consider design of integrated CAD software and robotic closed-loop control devices for a modular structure. This will lead to innovative analysis and process optimization, automatic control of punches and quick adaptation to changes in the design of the element.

## 3.2 Acquisition of mechanical properties

As is known, various metals along with alloys have varying mechanical and technological characteristics. These can largely predict the excellence of the machine parts along with the machinability of the metals. Mechanical properties are characteristics of the material and determine its behaviour under the action of applied external mechanical forces. These are determined by testing specimens. For the characterisation of the material used for the Y- the yield unloading the specimen and U- ultimate tensile strength, models of the selected sheet materials along with suitable shapes were sliced at varying angles to the rolling direction [0°, 45° and 90°]. The specimens and their dimension are shown in Figure 3.1.

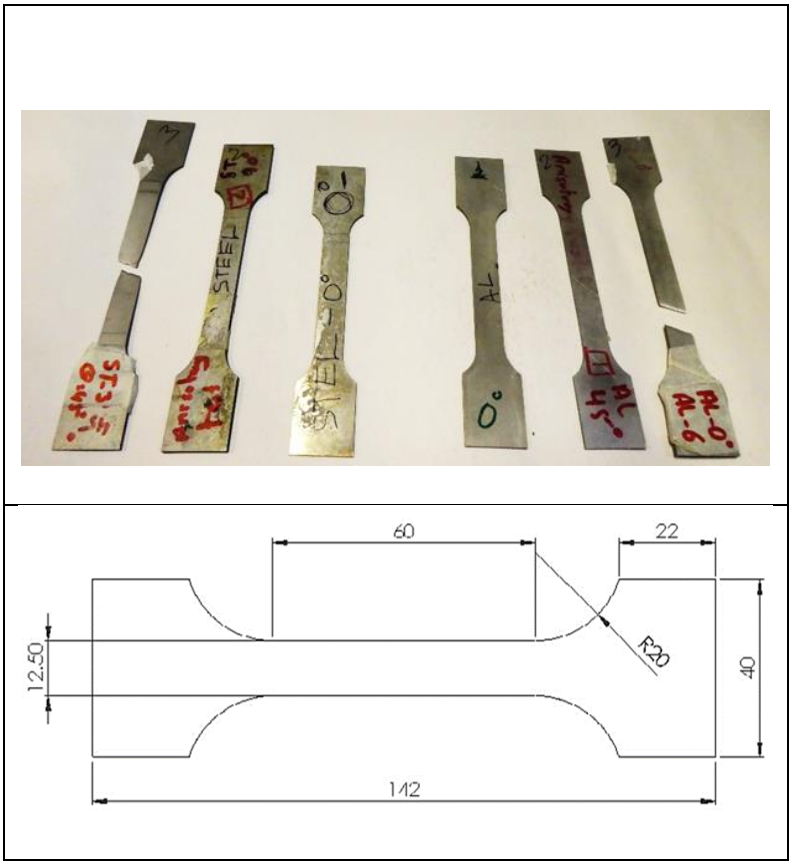


Figure 3.1 Tensile specimens is usually a standardized sample

The specimens were produced by wire cutting standardized test piece in a tensile test machine. A continuous uni-axial load was applied until the occurrence of failure. Both, the load (stress) and the test piece extension (strain) are measured. The obtained results are utilised

to plot a stress-strain curve. The total number of samples required for both classes of specimen at 0°, 3 samples at 45° and one other at 90° to the rolling direction of the specimen. Tests of mechanical properties were carried out under different types of loads - static, dynamic and cyclic. Static loads increased slowly from zero to the maximum value; Dynamic loads increased rapidly, in fractions of seconds; cyclic loads are characterized by a sinusoidal form with multiple changes in direction and magnitude. The tests are distinguished in accordance with the nature of the existing loads, static, dynamic and fatigue last versions of the software. Cartesian axes are used to present the results obtained, the abscissa represents the degree of deformation, (ε - relative decrease in area cross-section), and the ordinate axis represents stress ($\sigma = P / S$, force acting per unit area of the transverse pattern of the sample).

### 3.2.1 Tensile testing of steel and aluminium sheets

The Zwick / Roell tensile testing machine, which was used in the experimental work, is illustrated in Figure 3.2. The machine consists of a load capacity of 75 kN. The crosshead velocity can be changed from 0.0005 to 1000 mm/min within ± 0.1 %. The standard test programs, enabled the researcher to find the appropriate test program with accurate and two-sided E modulus determination to International Standard Organisation (ISO) registration number 6892-1, /2016 Metallic materials - Tensile testing, and TENSTAND WP4 [16]. The data is collected from a specified computer, which consists of the required package for controlling the machine. Hence, upon deformation of the structure, the effect of hardening shall also diminish. Nevertheless, the Young's Modulus tends to decrease with an increase in the orientation angle. Moreover, it is known that the maximum force and stress are a result of the 90° orientation.

The properties of the metal blank of steel DC05 were derived from an applied tensile test on a standard specimen (manufactured by wire-cutting) at varying angles to the rolling direction by using Zwick / Roell machine. This was according to the results of [65].

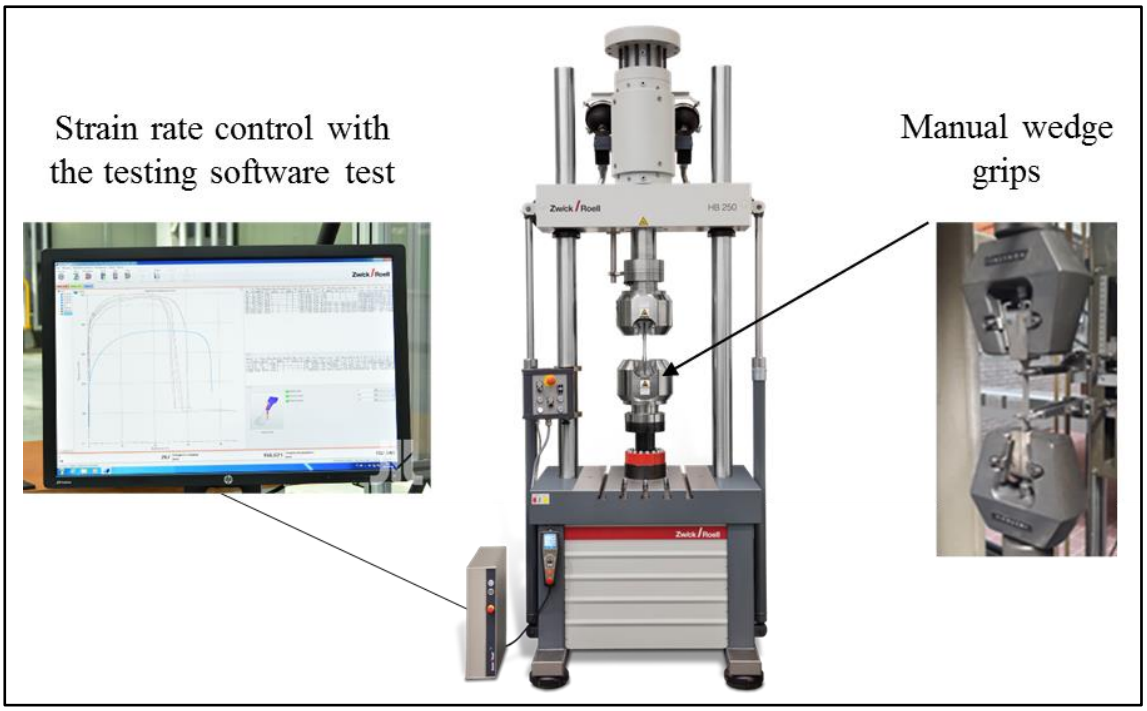


Figure 3.2 Zwick / Roell tensile test machine employed in this study

During a material properties and characterization tensile test, these formability properties can be determined automatically using The Zwick / Roell Universal software at University of Birmingham . To determine n-value, axial strain needs to be measured after yield and determined at or between strain values. More traditional contacting extensometers are designed to be removed during the test and may be limited in total travel. Using the latest technology, such as the releases in installation Guides, strain can be measured throughout the test while ensuring the highest accuracy of results. To determine R-value, the transverse strain must also be measured, traditionally done using an additional extensometer. With either of these devices, axial and transverse strain can be measured at the same time.

The uni-axial tensile test was carried out on two samples taken in parallel: (0°), transverse (45°) and diagonal (90°) to the rolling direction. Upon clamping of the sample, an extensometer was used for carrying out the strain measurements. This is shown in Figure 3.3. A tensile load was applied to the specimen with a continuous cross-head velocity of 0.5

mm/min. This application was seized when the ultimate stress was reached resulting in the subsequent failure.

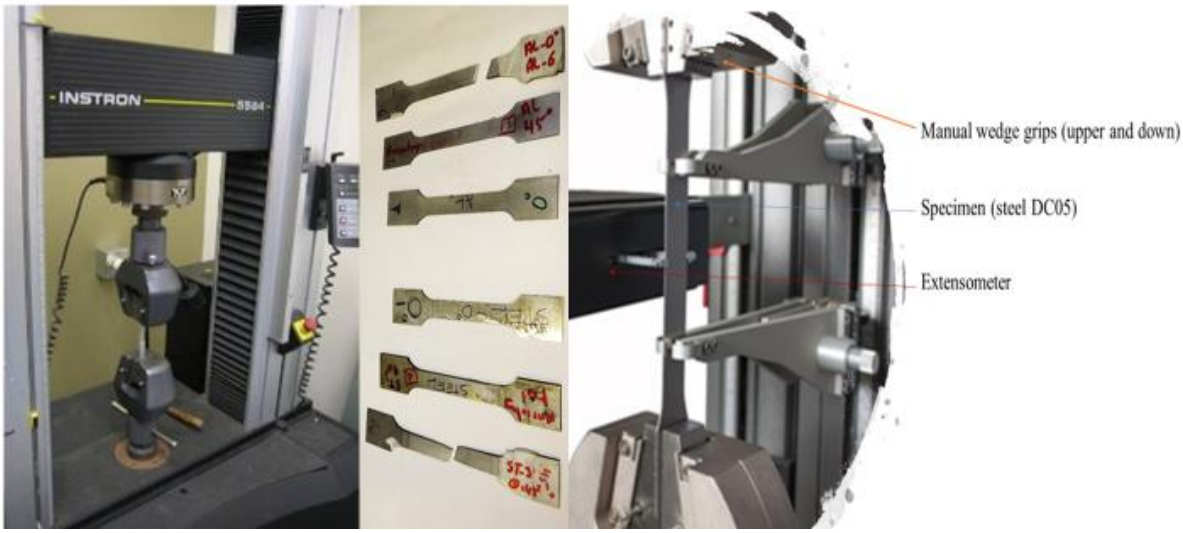


Figure 3.3 Clamped specimen for conducting strain measurement with extensometer

The tests were carried out for two samples for each of the cuts: $0^0$, $45^0$ and $90^0$ to the rolling direction. This was done to evaluate the stress-strain curves for the material for different directions. The results were used to define the stress-strain relationship with the help of Equations 3.1 and 3.2 [42]:

$$\sigma_{eng} = \frac{P}{A_0} \tag{3.1}$$

$$\varepsilon_{eng} = \frac{\Delta L}{L_0} \tag{3.2}$$

Where, P and $A_0$ refer to the instant tensile load and the original specimen's cross sectional area, respectively. $\Delta L$ and $L_0$ signify the assumed displacement and the length during plastic deformation. The true stress-strain were evaluated using Equation 3.3 and 3.4:

Anisotropy coefficient $$\sigma_T = \sigma_{eng}(1 + \varepsilon_{eng}) \tag{3.3}$$

The normal anisotropy coefficient is obtained using:

$$\varepsilon_T = \ln(1 + \varepsilon_{eng}) \quad (3.4)$$

Information was introduced to the computer, which was linked with the test machine, and the stress-strain curve was plotted for the steel DC05 for the three directions, using the above equations. The standard procedures for performing static tensile tests, as a rule, limit the rate of deformation or the rate of application of the load. The ASTM E-8 standard limits the rate of deformation to 0.03-0.07 mm / min. The blank sheet panels used in the numerical simulations were steel DC05 with thickness 1 mm. The t Young's modulus was calculated as the slope of the stress and strain curve in the elastic region. This was based on the ASTM E-8, which is the relevant standard for tensile tests in metal subjects [42].

### 3.2.2 Results of tensile testing

The stress-strain curves obtained for the DC05 steel are illustrated in Figure 3.4, for all three angles to the direction of rolling, the stress-strain curves are almost identical for all three orientations there were no significant changes between the results. The FE simulation of sheet metal forming, mechanical properties of the blank should be accurate enough to obtain robust result that can be trusting to start production. The tensile behaviours of the DC05 specimen tested in terms of the angles is shown in Figure 3.7. The subsequent tensile characteristics are listed in Table 3.1. Based on previous works, it is predicted that the 0° orientation will result in an increased strength. This will be in the case that it is adequately heated and aged. Also, it seems that the force and tensile stress tend to increase with an increase in the orientation angle. The 45° angle appears to provide the highest strain along with the work-hardening results. The rationale behind this is that increased stress levels are directly dependent on the alteration of plastic deformation. Nevertheless, strain hardening can only take place in the initial steps of the plastic deformation. Hence, upon the structural deformation and break down, the effect

of work-hardening shall also diminish. On the contrary, the Young's Modulus tends to decrease with an increase in the orientation. The study tells that the highest force and stress are a result of the 90° orientation. The properties of the metal blank of steel DC05 were obtained from a tensile test carried out on a standard specimen (manufactured by wire-cutting) at varying angles to the rolling direction by using Zwick / Roell machine. This was according to the results of [65]. The tensile tests were performed on a standardised specimen, as illustrated in Figure 3.6 .

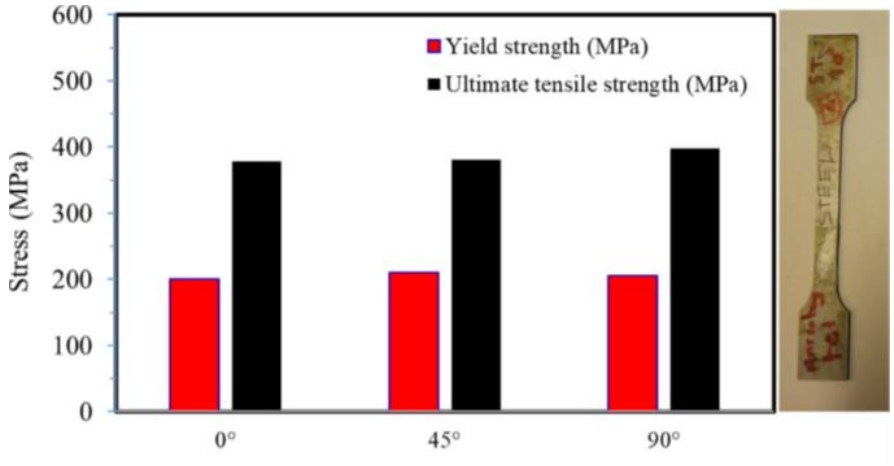


Figure 3.4 Ultimate and yield stress as a function of direction in which the steel DC05 specimens were sliced in relation with the roll path.

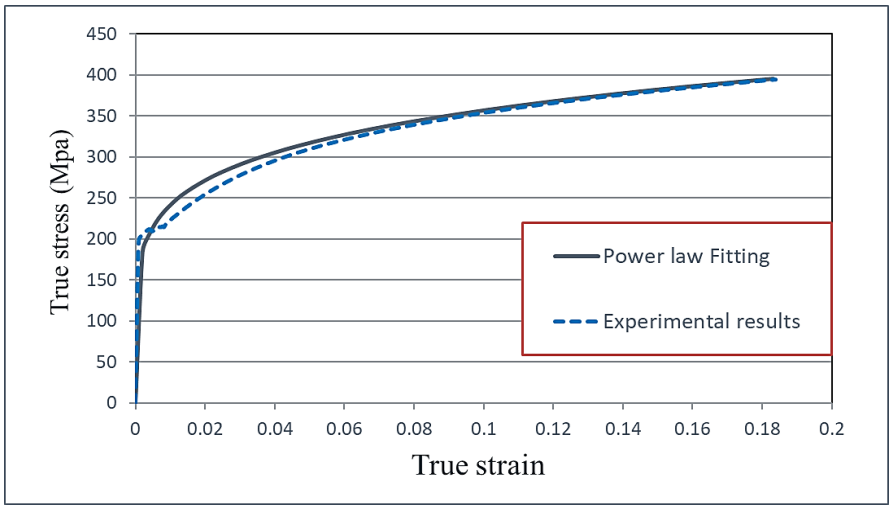


Figure 3.5 The mechanical stress-strain curves for steel DC05

However, from Figure 3.5, which shows yield and ultimate stresses, that the sample cut at $0^0$ to the rolling direction had maximum yield along with the ultimate stresses of 401.5 and 391.8 MPa, respectively. Minimum values for maximum yield along with ultimate stresses were obtained for the samples cut at $90^0$ to the rolling direction; 369.7 and 645.5 MPa respectively. The elastic/plastic behaviour of the steel sheet was simulated utilizing ABAQUS/Explicit, with isotropic elasticity, utilising the anisotropic characteristics. The experimental results for the true stress and strain tensile tests for the DC05 steel are illustrated in Figure 3.4 and Figure 3.5, whilst Table 3.1 shows the properties of the blank material. It should be noted that plastic and brittle materials will differ the destructive mechanisms.

Table 3.1 Mechanical characteristics of the DC05 steel blank material

| Degree to Rolling. | Maximum. | Ultimate Tensile. | Fracture. | Elasticity, E (GPa) Modulus of | Work Hardening, w |
|---|---|---|---|---|---|
| | Force. | Strength, UTS. | Stress. | | |
| Direction. | Fmax (kN) | (MPa) | (MPa) | | |
| 0° | 20.63 | 671.8 | 421.8 | 220 GPa | 0.17 |
| 45° | 20.16 | 669.7 | 401.5 | 218 GPa | |
| 90° | 20.83 | 645.9 | 391.8 | 215 GPa | |

DC05 are particularly suitable due to their excellent deformation behaviour. The choice of the right steel grade should be in line with the predicted forming stress. This can allow for the use of steel in different drawn parts. In contrast to this, grades with a high R-value behave more favourably in MPF in terms of the limiting forming ratio. This is very much the case with higher-strength DC05 steel. Plastic materials form an appreciable neck before rupturing, and fracture occurs at an angle of approximately at $0^0, 45^0, 90^0$ to the extension axis (the latter is clearly seen on flat samples, Figure 3.1). Fragile materials tend to break almost without neck formation along the plane, the normal axis of stretching. Mechanical characteristics are divided into three groups: Strength characteristics, plasticity characteristics and viscous

characteristics. Strength characteristics measure the forces within the solids, produced as a reaction to the effect of external loads of Aluminum-5251-O material density. This reaction is not constant during the loading process, and several characteristic zones can be clearly traced in the loading diagram. The following Table 3.2 provides the aluminium alloy's R values at the three orientations of the roll. Based on predictions, at orientation 187, the magnitude of $ra$ is maximum and this magnitude is minimum at orientation of 181.9. Experimental measurement of stress/strain for aluminium samples cut $0^0, 45^0$ and $90^0$to the direction of rolling at as shown in the results of Figure 3.6.

Table 3.2 $\boldsymbol{Ra}$ for $45^0$and $90^0$ orientations of the Aluminum-5251-O material

| Orientation | No. of samples | $\boldsymbol{ra}$ | average | $\boldsymbol{Ra}$ |
|---|---|---|---|---|
| $0^0$ | 1<br>2 | 0.605<br>0.573 | 0.589 | 0.570 |
| $45^0$ | 1<br>2 | 0.522<br>0.535 | 0.528 | |
| $90^0$ | 1<br>2 | 0.604<br>0.667 | 0.635 | |

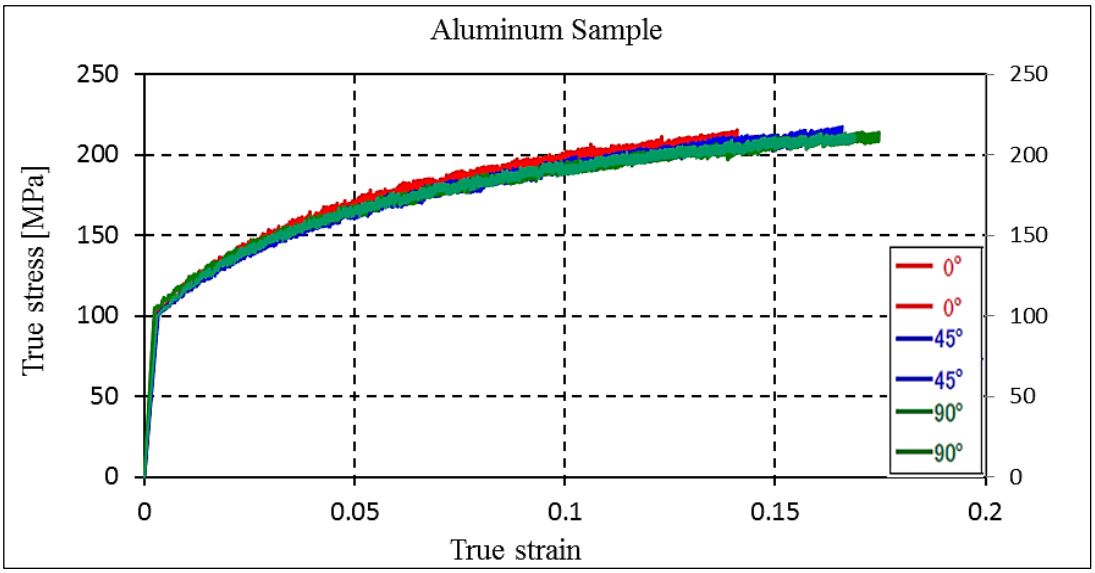


Figure 3.6 Experimental measurement of stress/strain for aluminium samples cut at $0^0, 45^0$ and $90^0$to the direction of rolling

### 3.2.3 Compression testing of polyurethane material

Polyurethane materials, which have a mix of the toughness and hardiness of metals along with the elasticity of rubber are utilised in MPF because their cushioning effect can be useful. In FE analysis, polyurethanes are explained as hyper elastic material which when exposed to increased amounts of strains can experience elastic deformation. This deformation stands for the momentary distortion of the material. The material is then able to return to its original state after the release of the directed force. In general, such an elastic deformation can be explained as a linear relationship of the stress and strain in materials such as metals. However, with rubbery materials, the elastic deformation may be highly non-linear. Hence, for such a case an exceptional correlation is needed for describing the stress strain properties of the material. The ABAQUS software is equipped with various models which can be used for describing the strain energy potentials along with the elastic cushioning materials. These numerical models include the "Arruda-Boyce, Ogden, van der Waals, Marlow, neo-Hookean and Mooney-Rivlin".

Figure 3.7 shows the information obtained for the polyurethane from the experiments where the hardness of the shore was A90 and the information was achieved using an uniaxial compression test. This test was used due to its relevance to the deformation that occurs through the MPF procedure. Circular shapes with diameters of 28.6 ± 0.1 mm and thickness of 12.5 ± 0.5 mm are required for polyurethane samples. This is based on the ASTM D575 standard [37]. This is detailed in Figure 3.7. Lengthened rods of polyurethane with the right diameters were cut to achieve the test pieces. Next, three samples were scrutinised in this work and the obtained results were averaged with the aim of reducing any experimental uncertainties, which might arise due to the cutting step. The testing procedure along with the compression testing were performed for achieving a deflection equivalent to the 70% of the maximum compression

ratio, utilised in the current study. Afterwards, 10 mm/min of compression rate was achieved with the application of the force. In order to prevent any side slipping which can take place amid the testing machine and the specimen, a sandpaper with satisfactory properties was positioned between the surface of the tool and rubber polyurethane. This was in accordance with the ASTM D575-91 (2012).


Figure 3.7 Compression test system for A90 polyurethane specimens

The experimental performance of the elastic cushion was associated with three material models, namely, Neo-Hooke, Yeoh, and Mooney–Rivlin. Figure 3.8 shows the hyperplastic model of Mooney–Rivlin, which best defines the hyperplastic performance of polyurethane (A90), as detailed in Equation 3.4. This was chosen in this investigation as it is commonly used in MPF in ABAQUS. Hoverer, FE simulation predict issues during the process:

Test different tool design, optimise the process, help in the material choice, save time and money innovate.

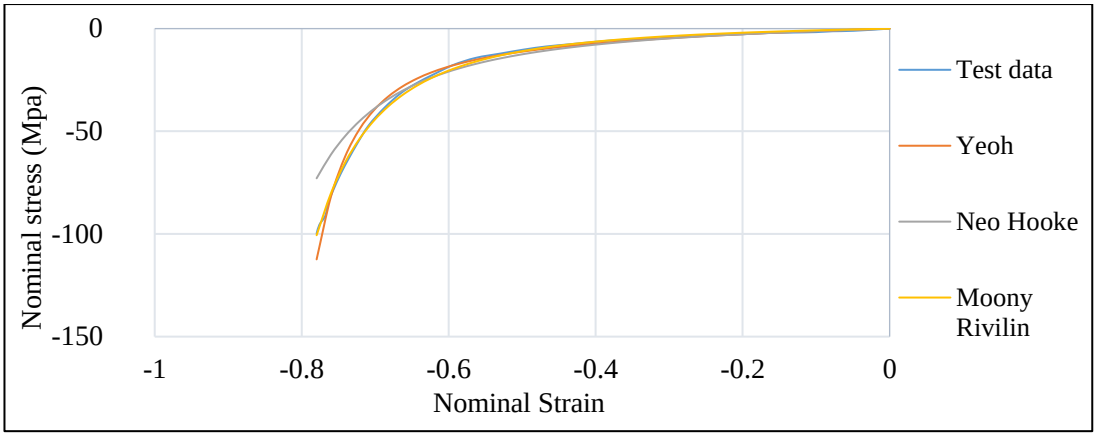


Figure 3.8 Nominal compressive stress/strain deformation for elastic-cushion material predicted by ABAQUS software compared to experimentally determined results

Table 3.3 Experimental compressive test material parameter of the elastic cushion [39]

| Method | Material/ Hardness | Abaqus Model | Material thickness | Model elasticity (E) | Poisson's ratio (υ) |
|---|---|---|---|---|---|
| Zwick / Roell tensile test machine | Poluyurathane A90 | Mooney–Rivlin | 3 mm | 2.87 MPa | 0.499 |

$$U = C_{10}(I_1 - 3) + C_{01}(I_2 - 3)\ [39] \qquad (3.4)$$

Where U is the strain energy per unit volume; ($I_1$) and ($I_2$) are the first and second invariants of the deviatory strain tensor; and ( $C_{10}$ ) and ( $C_{01}$ ) are temperature dependent sheet metal material characteristics achieved from a uniaxial compression test performed using polyurathene with a Shore hardness of A90. The values of ($C_{10}$) and ($C_{01}$ ) are 0.861 and 0.354 respectively. The material was considered isotropic and the elastic-plastic model was utilised. Ludwig's equation was chosen for representing the flow stress in the material, as shown in

Equation 3.4 [17]. Figure 3.9 demonstrates the load vs compression plots obtained with compression testing.

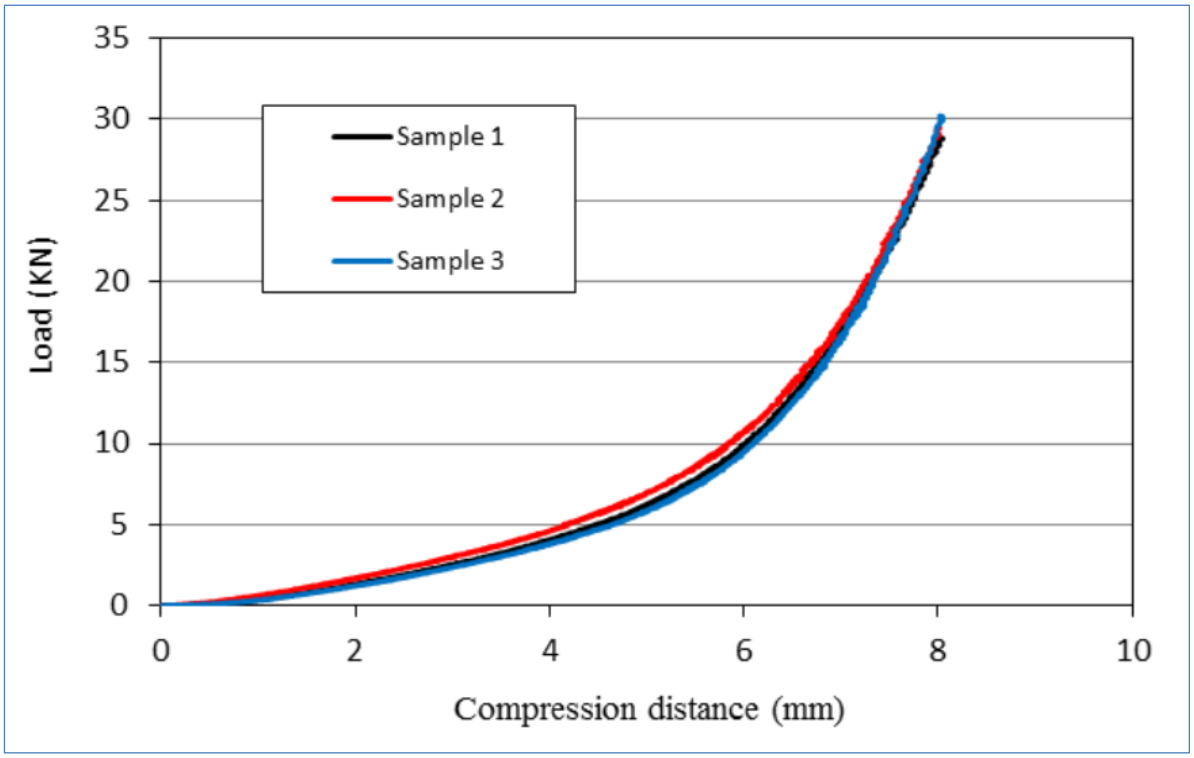


Figure 3.9 Analysis of load displacement relations for polyurethane with Shore hardness A90 for three samples

## 3.3 Background to machine setup for the MPF

Tooling setup is complicated work and requires specific know-how. The testing rig was gathered on a Mackey Bowley 200 tonne hydraulic press, based in the Mechanical Engineering Workshop. This is a four column down stroke digitally controlled hydraulic press (T-200 / serial number 10994-99). For a schematic of the hydraulic press, see Figure 3.10, and for a photograph see Figure 3.11.

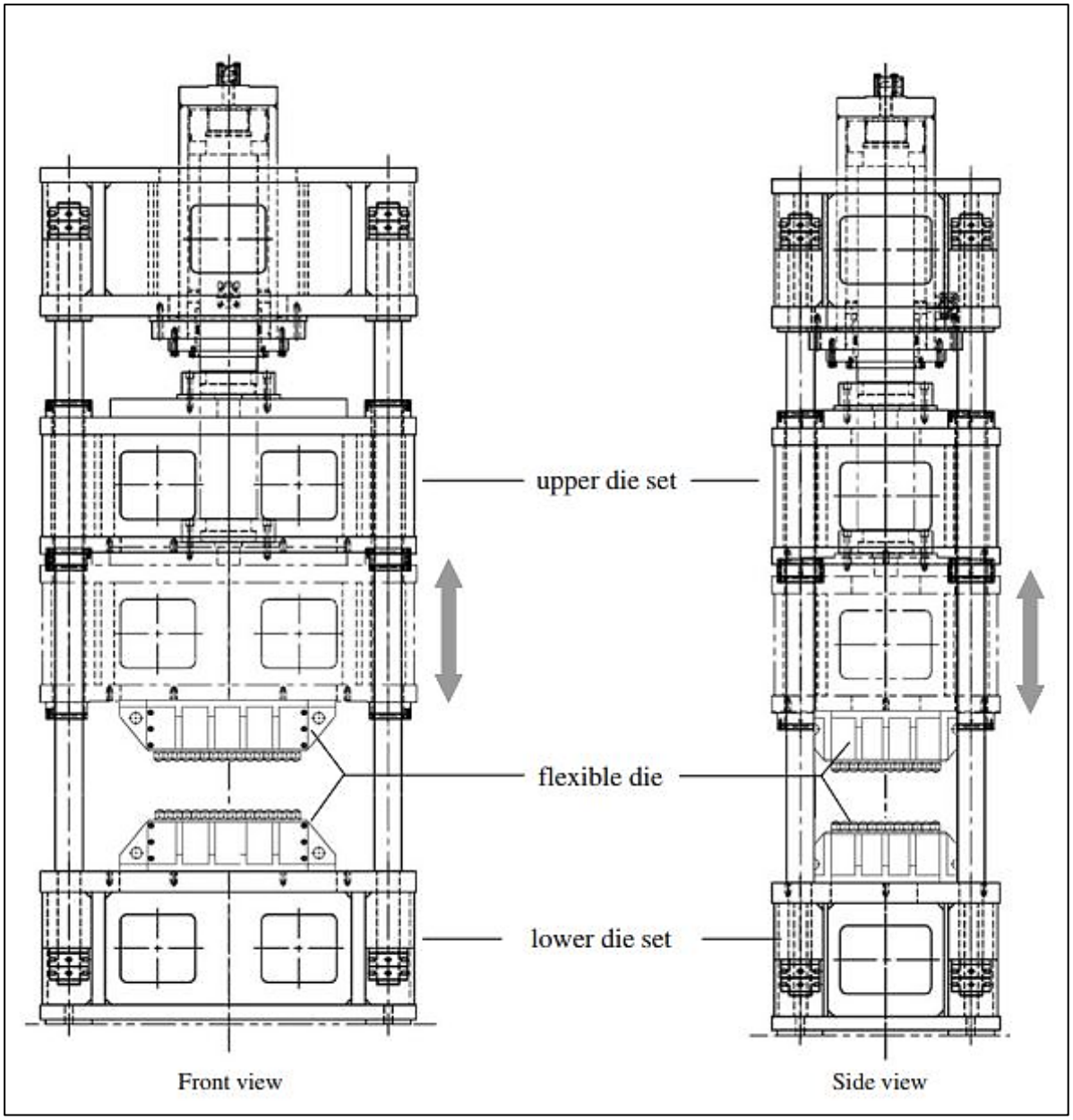


Figure 3.10 Schematic of Mackey Bowley T-200 hydraulic press [42]

Hydraulic presses are more versatile then mechanical presses, because the forming force and stroke can be controlled more easily. These presses are mainly load restricted facilities. Hence, their competence for performing a forming press is restricted, mainly by the highest available load [43].

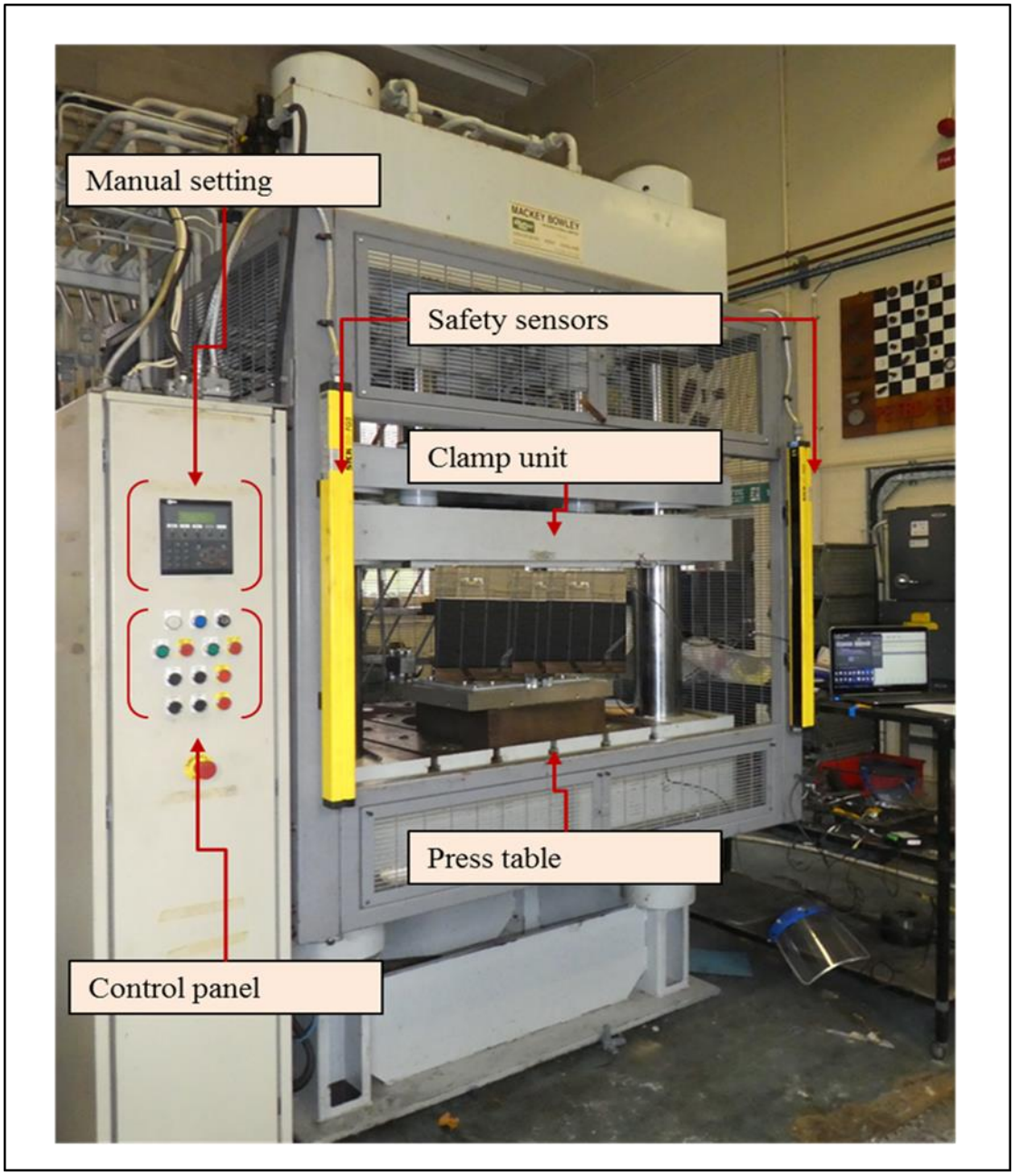


Figure 3.11 Mackey Bowley hydraulic press

Finite element methods, can enable a background study of the relative importance of the design parameters when using MPF tools to produce, double curved sheet metal forms. The parameters, investigated here, are forming load, elastic cushion (as detailed in literature review) and curvature radius for the designed geometry. Typical component parts for MPF are demonstrated in Figure 3.12.


Figure 3.12 Multipoint forming tooling

Components for the flexible tooling:

1) Punch Load cell
2) MPF upper die
3) MPF lower die
4) Distance sensor fixing
5) Saddle-type sheet plate and elastic cushion (sandwich method)
6) MPF punch springs

As illustrated by Figure 3.12, in the multi-point forming tool the pins are the major factor for the determination of the geometry of the formed part and should be of a material that can withstand the necessary load while being small enough to follow the design contour. Here the pins used in the test programme had cross-sections of 10x10 mm with a tip of radius 10 mm,

see Figure 3.13. Experimental MPF has commonly used pins with a square cross-section and a hemispherical tip [44]. There is substantial research and study of the processes of numerical control of an instrument using the MPF methodology for formation and fabrication. These should lead to the realization of the formation and precise manufacture of panels in the automotive, shipbuilding and aircraft industry using a multipoint tooling.

The goal of a robotic or CNC machine is to perfect digital processing and its application to manufacturing procedures with the goal of rapid alterations of multipoint tools during production that could lead to novel procedures and instant response when manufacturing panels. Such developments could: Reduce surface-area measurements, make more efficient use of labour, and Produce more consistent and accurate panels. As illustrated in Figure 3.13 and Figure 3.14 set up time for CNC machines is composed mainly of setting up the shape to be punched out by the square pins. The adjusting time is dependent on the number of pins and method of adjustment, though this is usually done by screwing the pins into place. The larger the number of screw pins, the longer the set-up time, but the more accurate the finished product. Figure 3.15 and Figure 3.16 show the continuous forming surface of a reconfigurable MPF tool. The size of the finished form and the machine bed size determine the number of square pins in the tool.

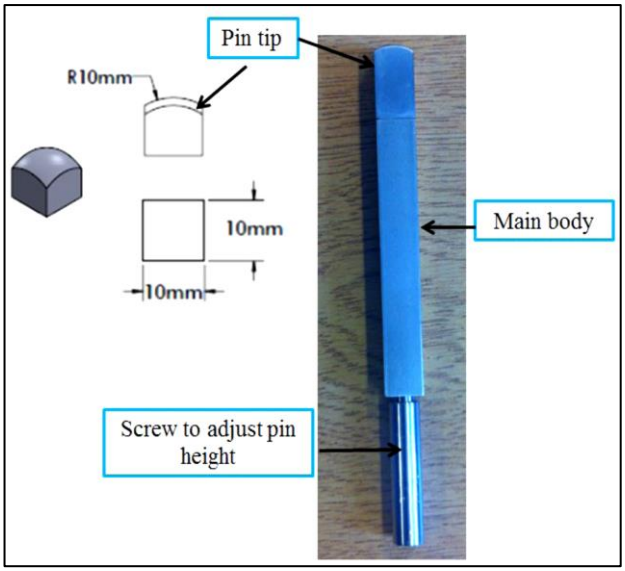


Figure 3.13 MPF pin design with dimension

Figure 3.16 Square pin tips

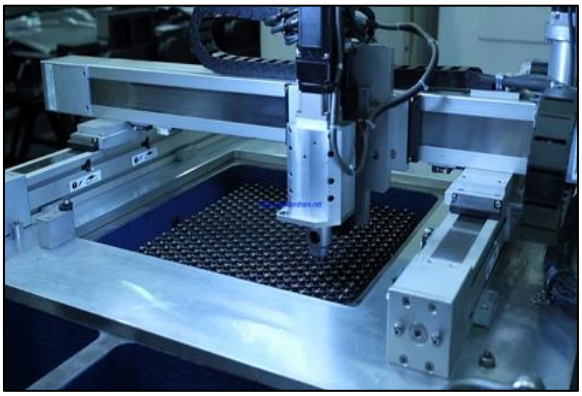

Figure 3.15 CAD/CAM packages developed for CNC machine tools

Figure 3.17 MPF tooling (punch and die)

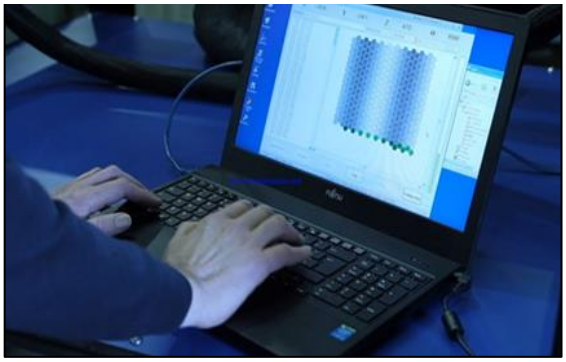

Figure 3.14 CNC-CAM software setup

The key advantages of CNC are that it is fast, versatile, economical and flexible, compared to existing rigid tools for sheet metal forming and sheet metal production. This thesis will study the methodology of numerical MPF and the possibilities of using flexible technology for forming automobile panels. A theoretical analysis of the MPF mechanism will be carried out for dispersion-free applications. For this research, all square pins used for tooling will have the same size, because the most accuracy is for R400 curve. To elaborate, in the presence of a systemic error, an increase in the sample size will lead to an increase in the accuracy but will not enhance the pin precision. FEM will also be used to explore in detail the use of adjustable multi-point attachments for connection procedures measurement of assembled automotive panels, in particular surface positioning procedures and non-contact measurements. The surfaces produced by MPF tend to show such geometric defects as; deformation, sheet plate wrinkles and dimpling which cause serious problems for surface quality [44]. This research investigates the influence of varying the hardness of the elastic cushion, the force on the blank-holder, the friction coefficient, the thickness of the cushion the radius of curvature of the formed parts, the quality of the parts formed by a flexible multiplier, the point punching central point [39]. The main contributions of the study are:

- The optimisation of the MPF and the corresponding process parameters for the numerical analysis of multipoint tooling in the FE simulation, for example, boundary conditions and time.
- Study the effects of utilising new blank holder design on wrinkling and necking
- Development of the effects of elastic cushion thickness on the force and thickness strain in the MPF process modelling.
- Validation by experiment of the numerical analysis model for the MPF with the given number, shape and size of pins.

- Investigate optimisation of MPF using three different radius of curvature for the formed part (R = 400, 600, and 800 mm).

### 3.3.1 Square pin tooling parameters

A MPF tool was designed to produce double curvy parts, with varying radii of curvature, 400, 600 or 800 mm. The 10 mm square pin described above is the main factor in the construction of the reconfigurable tool and was assessed as being able to withstand the applied external load necessary to produce a form of the required shape and size. The MPF punch along with the die were each formed of $30 \times 20$ pins. Also, $300\ \text{mm} \times 200\ \text{mm}$ was the size of the active blank. As shown in Figure 3.18, the pins were combined in a uniform matrix manner. This was done to achieve a continuous formed surface. Thereafter, the use of an active mechanical technique allows for modifying the reconfigurable pin tools. This means that the pin heights can be modified just by the rotation of the lead screw, which is positioned at the base of the pins. This is illustrated in Figure 3.12.

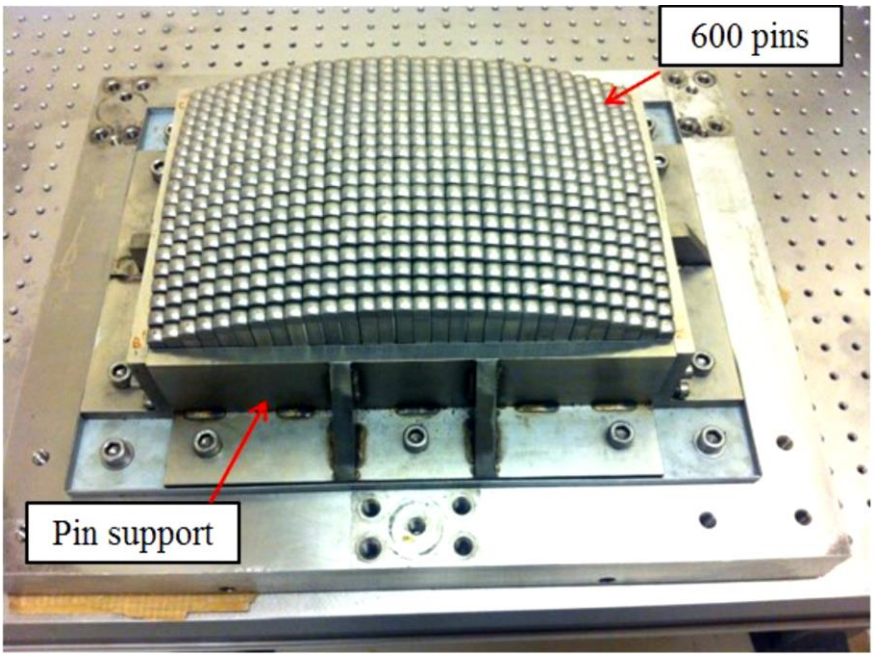


Figure 3.18 Reconfigurable MPF punch

Subsequent to constructing the square pin array pattern, it is vital to form the square pin container parametrically. The square pin-cross section was $10 \times 10$ mm with a 10 mm tip radius and with 0.25 mm gap between adjacent pins. Then, the blank could not be 300 x 200 mm. It would have to be 307.25 x 204.75 mm.

### 3.3.2 Blank-holder system in MPF press

The Blank Holder Force (BHF) has a key part in the MPF study. It aids in controlling the material flow into the die cavity. This is also illustrated in Figure 3.19. In this chapter, a design procedure is projected for determining the BHF exerted by springs of a known stiffness on the bolts holding the upper plate of the BH. Rotating the nuts compressed the springs and increased the BHF. The nuts are screwed until the BHF attains the required value.

A study of the effect of the BHF was performed to determine whether it could be used to avoid both wrinkling and tearing. The evidence supplied by the manufacturer of the springs was authenticated using a compress equipment. The results showed that a force of 260 N was created by each unit mm compression of the spring. Each spring needed screwing by 8 mm for clamping the sheet with 20 kN force. During the forming procedure, it was needed that the metal sheet has a uniform pressure distribution while being clamped. Hence, the blank-holder and the springs' position was studied for confirmation.

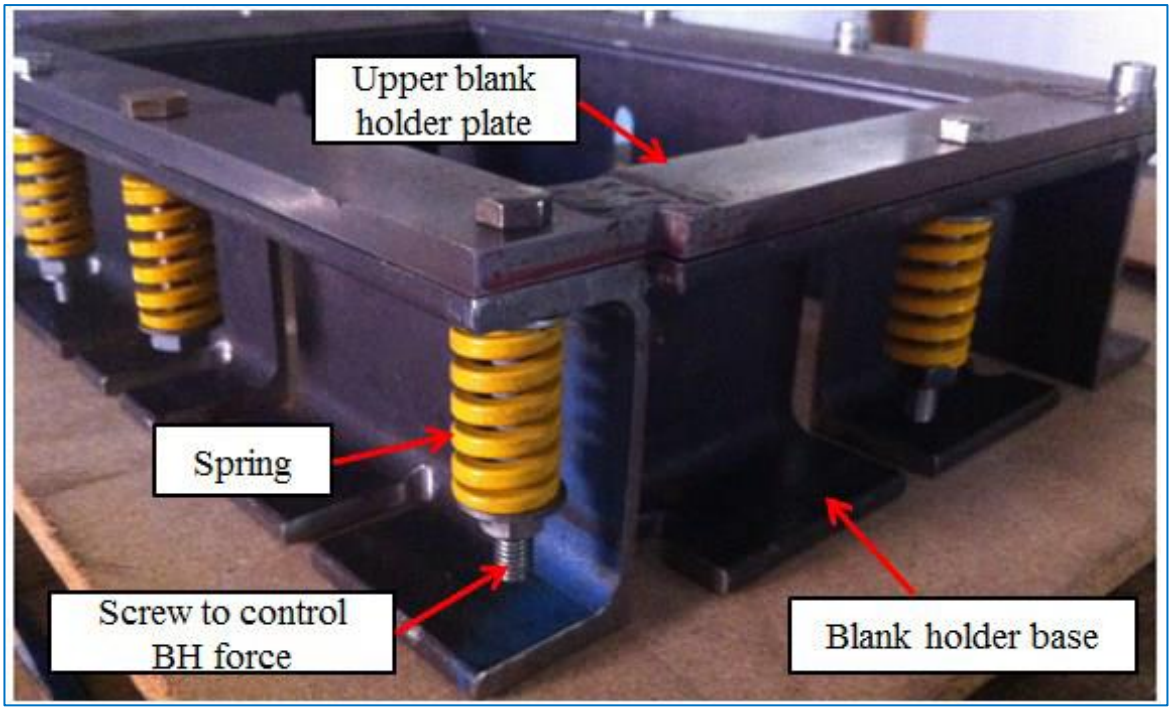


Figure 3.19 Experimental blank-holder

## 3.4 Acquisition of forming force

Load cells are a type of transducers, which are used for converting the force into a quantifiable electrical signal. Different load cells will operate according to different principles; detecting the force by bending, shearing, tension and compression, etc. With the exception of some

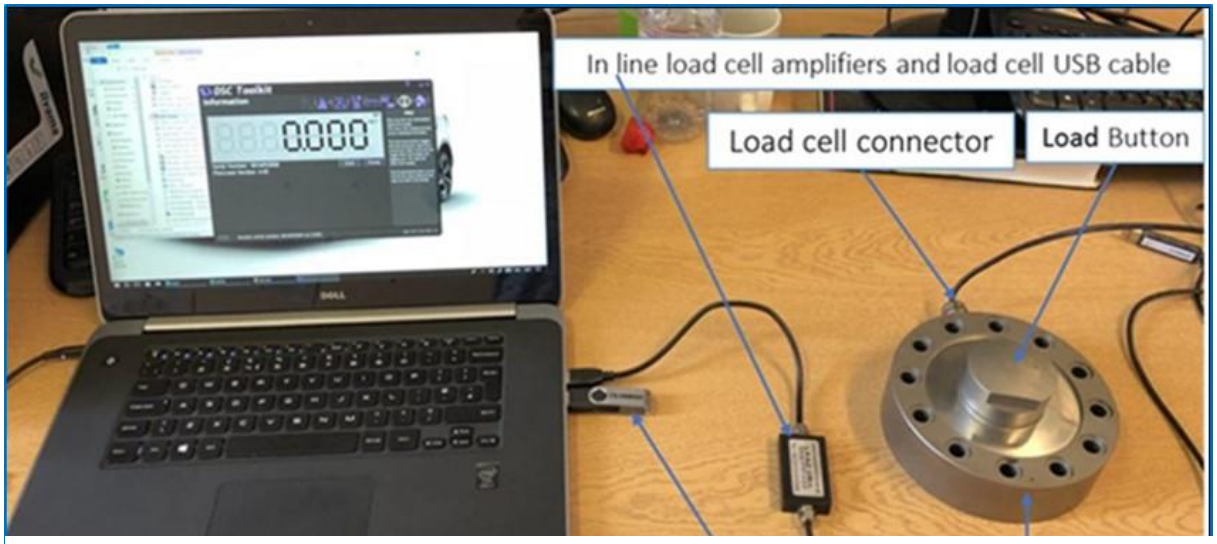


Figure 3.20 Low Profile Load Cell with 100 kN

facilities which accurate mechanical balances are used, the strain gauge load cells tend to govern the weighing manufacturing. These cells provide accuracies of 0.03% in full scale. Hence, these are appropriate choice for about all industries. The selected load cell was a Richmond Industries machine, 100-series low-profile with the choice for being connected straight to a computer using the USB ports. This is illustrated in Figure 3.20 [45]. This particular load cell was developed to suit a large variety of applications. Next, chosen forces were applied to the load cell and resulting readings were noted. This was done to confirm the accuracy of the equipment. Achieved results confirmed the accuracy of the cell, which gave confidence in the results obtained.

### 3.4.1 Microsonic-distance sensor

This section also defines an ultrasonic sensor, which can quantify the distance from a reference point to selected points on the punch. The microsonic (M-30) sensor is shown in Figure 3.21. A constrained optimisation approach was used to achieve reflected ultrasonic pulses. These are effortlessly obvious with a threshold comparator [46]. Experimental tests, for working ranges from 30 mm to 250 mm were used to detect the location of the multi-point punch [47]. The M-30 sensor was linked to a data logger (Omega) and data recorder, monitored with a PC, that allowed the user to view the position and velocity of the reference point on the punch. The software can demonstrate data in real-time directly onto the screen of the PC/Laptop.

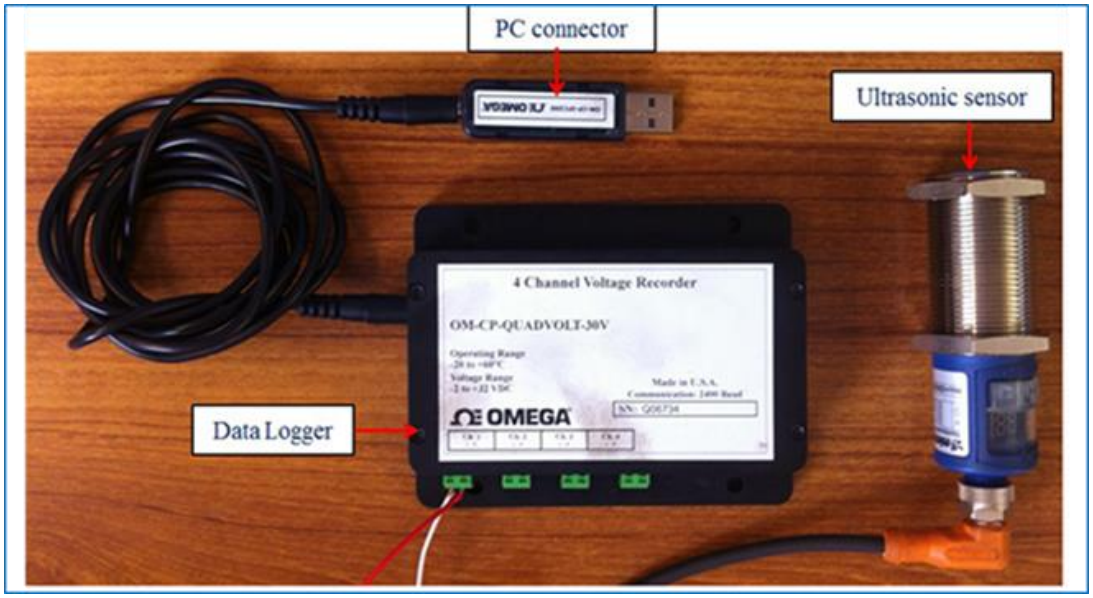


Figure 3.21 Microsonic-distance M30 sensor with connecter to data logger

### 3.4.2 Geometrical and dimensional measurements

The flexibility of portable inspection arms, such as the FARO scan arm, when combined with CAD files such as STEP. STL and IGES makes for an ideal system for measurement, inspection and evaluation of body parts with a view to their re-design [48]. The FARO arm can be used with a laser system for non-contact inspection or with ball probes for contact measurement. The formed component can be scanned to produce a 3D image that can be compared to the CAD file, and differences between design shape and formed part caused, for example, by indentations due to the individual pins can be identified.

A series of steps are required to ensure the design and formed part are properly aligned, these include scan registration, and analysis and comparison of place measurements, e.t.c. Figure 3.21 shows the MPF prototype die being scanned with a resolution and precision of ± 25 μm. The scanner offers fast data point assembly, which can be stored on an appropriate cloud, at a scan rate of 580,000 points/sec. Such detail can be necessary when comparing the CAD design files with measured data, to compare the formed part with the design to determine the presence of wrinkling or unwanted variation in formed thickness [49].

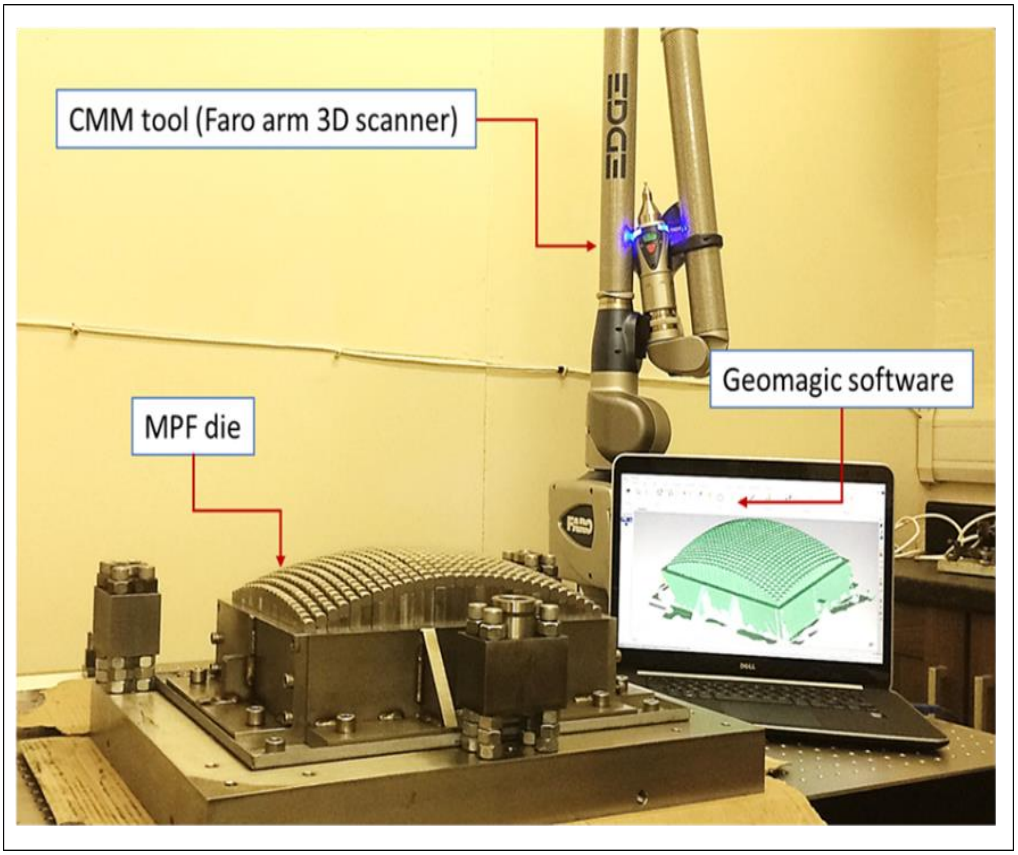


Figure 3.22 University of Birmingham Metrology is an approved supplier of Geomagic software for the Faro Arm scanner

## 3.5 Summary and Conclusions

In this chapter, the research amenities available to attain the mechanical characteristics required for modelling the performance of the samples utilising FEM are described. The stress-strain curves for all of the tested samples were plotted for the Steel DC05 material hardness, and elastic cushion polyurethane A90. The Steel DC05 material had a serrated stress-strain curve because of the Profile Load Cell effect.

An overview on the MPF tools is provided with the correlated apparatus utilised to finalise the validation of the numerical simulations [50].

The Microsonic-distance measuring system (M30) was used to measure the movement of the punch. This included ultrasonic sensor, interrogator unit, and the processing unit which converted the period required for the signal to reach the reflector and back again, into distance and speed of movement.

# CHAPTER 4 FINITE ELEMENT MODEL-ANALYSIS-AND-OPTIMIZATION OF-MULTI-POINT-FORMING

The methodology and results described in this chapter have been published in: [39]

## 4.1 Introduction

A multipoint forming (MPF) project using digital-controlled tooling for the manufacture of automobile panels focuses on the analysis and augmentation of MPF components with digital adjustment for manufacturing automobile panels. One of the key focuses of this paper involves analysis of developing tools with digital control using multi-point technology for the formation of 3D sheet metal fuselage and wing covers in automobile. As part of this research, the researcher requires MPF to provide a fast, flexible and economical formation of skin panels, which can be used on automobiles. The associated pins are controlled through the multi-point equipment with following the industrial and scientific breakthrough objectives. In this thesis, it is also aimed to improve the multi-point equipment and digital processing techniques in the automotive and sheet metal products. This will reduce the cost of tooling by 65%, which will decrease the installation time by 45% while also decreasing the time required for the traditional use of the tool.

In addition, it is necessary to take into account the need to equip the storage facility and significantly increase the use of tools. There are some FEM key technological problems of adjustable multi-point tooling. This will mainly be for implementing flexible multi-point tools that compose perforation matrices to replace the traditional solid stamp. Proper designing of an integrated CAD software and robotic closed-loop control devices for modular structures will lead to innovative analysis and process optimization, automatic control of punches and quick adaptation to changes in the design of the element.

An extensive review on the processes of numerical control of an instrument using the MPF methodology for formation and fabrication will lead to the realisation in the production of skin panels while directing to the exact manufacture details of panels in the automotive, shipbuilding and aircraft industries with the use of a multipoint tooling. The goal of a robotic or CNC machine is to enable digital processing of tooling by an impeccable application on its manufacturing procedure for the automotive industry. In addition, it is aimed that the need for rapid improvement of multipoint tools in production will lead to novel procedures and instant manufacturing exploration. The key advantages of CNC are that it is fast, versatile and economical with high flexibility as compared to existing rigid tools for sheet metal forming and sheet metal production. This highlights a study on numerical methodology of MPF while further exploring the possibilities of flexible technology for automobile panels. A theoretical analysis of the MPF mechanism will be carried out for dispersion-free applications. FEM will also explore in detail the use of adjustable multi-point attachments for connection procedures, measurement of assembly automotive panels, in particular surface positioning procedures and non-contact measurements. The surface of developed MPF, after the same geometric defects as deformation, sheet-wrinkles and damping, was found to be seriously affected in terms of surface quality [44]. This research investigates the effect of the implementation of the structure such as the hardness of the elastic cushion, friction coefficient, force of the blank-holder, thickness of the cushion and radius of curvature, characteristics of the formed parts by the flexible multiplier along with the punching point [39]. The main contributions of the study described at this point are as follows, based on the changes in material density, the technique and boundary condition:

- The optimisation of the MPF and the corresponding process parameters for the numerical analysis of multipoint tooling in the FE simulation

- Exploration of the effects of using a new blank-holder design on wrinkling and necking.
- Optimisation on the effects from the elastic cushion thickness on the force and strain due to thickness.
- An experimental analysis followed by the validation of numerical investigation of the model on the MPF; a pins combination.
- An optimisation of the multipoint forming on the effects of using three different radii of curvatures (R400, R600, R800).

## 4.2 Numerical-Modelling of-MPF-processes

FE model to be investigated for the 3D-numerical simulation of multipoint tooling processes was parameter-analysis and utilised the ABAQUS FEA software with the simplified boundary and suitable anisotropic properties of material conditions. The finite element (FE) results are similar to the results obtained from experimental work thus allowing for quality validation. Reducing the material hardness can be done by reducing the thickness of the sheet plate wall and maintaining sufficient strength so that the sheet forming can serve its purpose without the blank-holder.

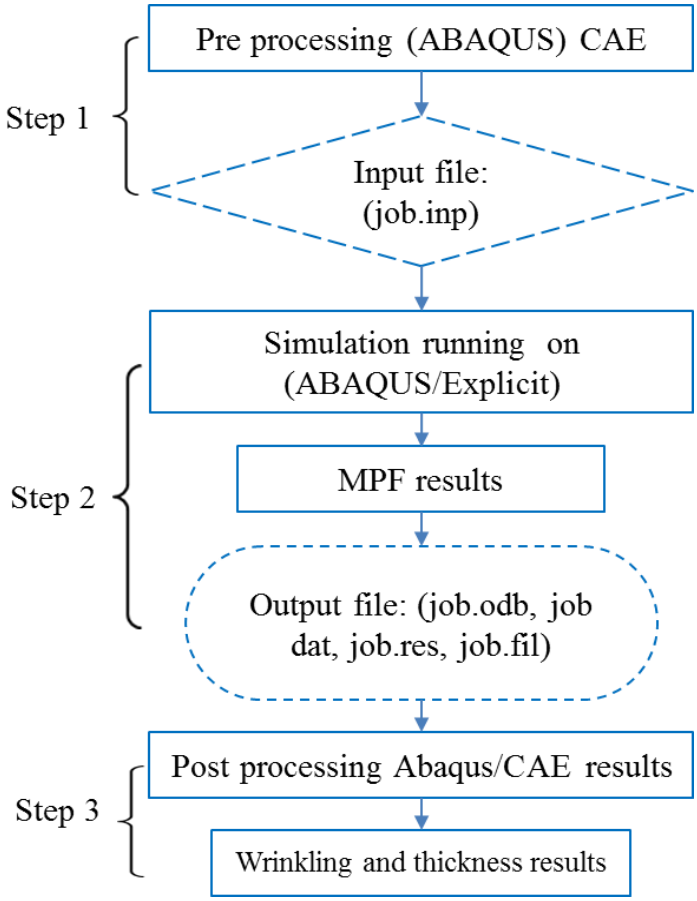


Figure 4.1 The method of ABAQUS simulation, [39]

The geometry of the model must meet expectations listed in Figure 4.1 while also ensuring that requirements and properties of the material is suitable for packaging food or beverages are satisfied. Traditionally, this process, as well as most methods of metal forming, have been tested experimentally using the trial and error methods along with the empirical methods, which are costly and time consuming approaches, due to production of stamps, empty holders and punches. Polyurethane of two types with the hardness of Shore A90 and A85 were tested. The MPF process model is used with a lower and upper group. In both groups, the punches are moving simultaneously towards both the surfaces [39].

## 4.3 Development-of Finite-Element-Model

One application of FEM simulation involves the placement of the elastic cushion on both sides of the blank and using an elastic cushion with variable thicknesses between the matrices and

the blank holder. The second application is decreasing the thickness by increasing hardness. Elastic cushion of 3mm is used and plastic deformation occurs at the location where all the pins are connected. The pin tip, blank holder, elastic cushion and the radius of curvature were all considered in this study. To conduct and obtain accurate results, the mesh density is allocated [40]. Symmetric boundary conditions were applied to the sheet metal (DC05) and a hardness of Shore A90 is applied to the polyurethane as only a quarter of the FEA model is considered. Quadratic element was used, and both the elastic and cushion were considered as deformable bodies in the ABAQUS/Explicit software C3D8R [39]. Figure 4.2 shows the hydraulic blank-holder tooling. This is also called a viscous pressure bulge test. In this test, the sheet metal is clamped at the edges and is stretched against a circular multipoint die using old as a working fluid.

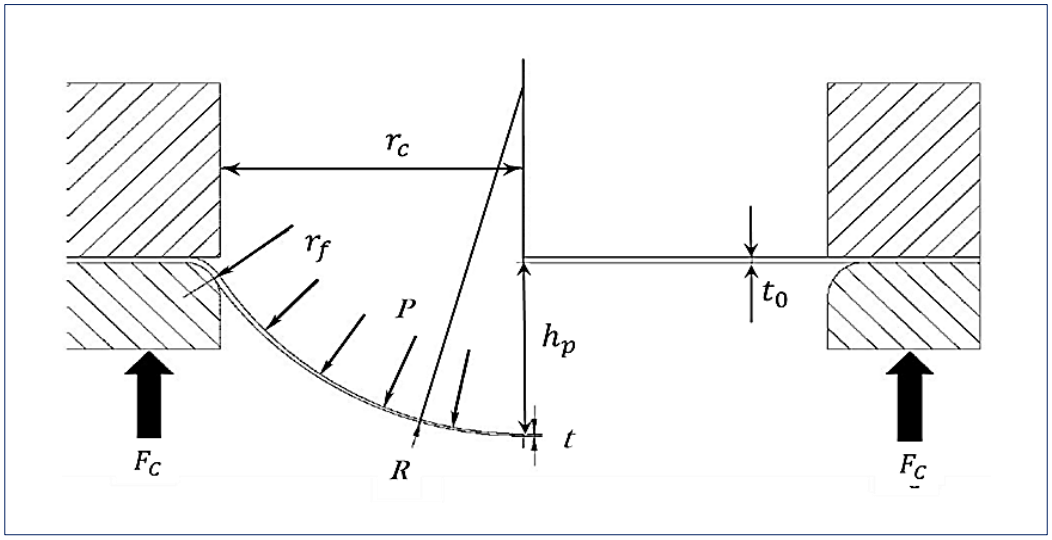


Figure 4.2 Schematic of sheet panel bulge test (to = original sheet metal thickness, P=MPF pressure, r = blank-holder radius, h =Tooling height, R = MPF radius of curvature, [51]

Metal sheet of industrial quality and uniform thickness of 1mm was used. As mentioned earlier, polyurethanes of Shore A hardness of 90 A and 85 A are considered for the elastic cushion. FEM simulations performed for the two applications establish an elastic cushion on

work piece on both sides, along with use of an elastic pad, which has a different thickness between the dies and the workpiece holder. By adjusting the hardness of the elastic cushion, the thickness can be adjusted. The pins have a square cross section with a hemispherical tip. All pins are in contact at this location and undergo plastic deformation with the 3mm elastic cushion. The exerted force increase quickly as the plastic deforms because of strain hardening. Only a quarter of the MPF crystal was modelled by FEM justified by the symmetry to save computational costs, as shown in Figure 4.3 [39].

## 4.4 Process-Parameters, Boundary-Conditions, -Material-models

The prediction of stress levels determines the accuracy of wrinkling investigation during the final stages of stamping and sheet wrinkling. Advanced models have more parameters for testing and require more advanced mathematical methods to determine these factors and hence have limited applications [53]. Isotropic hardening and kinematic hardening material are two different models in MPF, which are employed to predict the wrinkling more accurately [54].

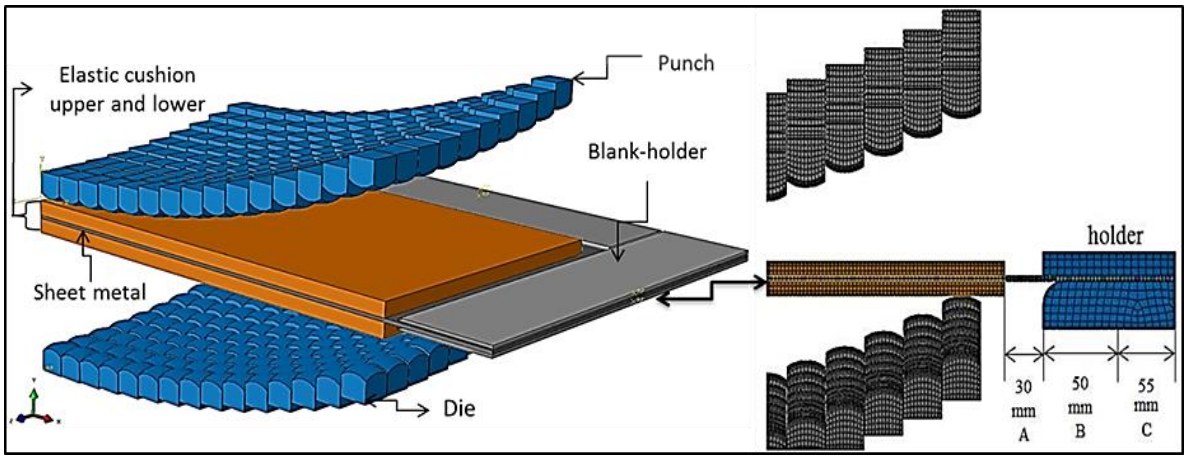


Figure 4.3 Development of FEM for using quarter model multipoint forming, [39]

Table 4.1 MP tooling basic geometric parameters

| Process parameter | Parts dimension in mm |
|---|---|
| Reduce of curvature (punch and die) | 400 |
| MP tool pin numbers (quarter model) | 15 × 10 |
| MP tool pins size (PS) | 10 |
| MP tool pins shoulder hemispherical tip and square cross section | 1 |
| Elastic cushion size (upper and lower) | 100 × 150 |
| Elastic cushion thickness | 3 |
| Sheet metal size | 100 × 150 |
| Sheet metal thickness | 1 |
| Blank-holder size radius | 10 |
| Blank-holder thickness upper | 10 |
| Blank-holder thickness upper | 20 |

With symmetry, the FE simulation of multipoint tooling process was achieved with the use of a quarter of the three-dimensional numerical model to reduce the tuning time. The numerical model is shown in figure 4.1. In a discrete rigid model, the multipoint equipment of the stamp, punch and holder was used. MPF instrument and trigger holder in which the element is placed (R3D4) are also employed. Then, only 300 × 200 mm sheet metal with a reduction of 1 mm with a reduced shell element of type S4R was deformed [55]. ABAQUS simulations are able to run solid models or shell elements. Shell elements lead to increased accuracy and the total time of the simulation is faster. However, it is very difficult to measure thickness variation with shell elements. Thus, it is better to use solid elements in the numerical simulations using individual nodes.

### 4.4.1 Isotropic-hardening-material-model-for the MP-sheet-metal-forming

Hardening parts of the material behaviour obeys Holloman law in the isotropic hardening model, Equation 1, and obeys Hills with the plasticity law [54]. The yield surface maintains the same shape but increases in size due to plastic straining in isotropic hardening.

$$\sigma = k\,\varepsilon^{n} \tag{4-1}$$

$\boldsymbol{k}$ is the strength coefficient, $\boldsymbol{\varepsilon_p}$ is the effective plastic strain, $\boldsymbol{\sigma_y}$ is the yield stress and $\boldsymbol{n}$ is the work hardening [54, 56].

### 4.4.2 Kinematic-hardening-material-model

Yoshida Uomuri (YU) is a two-surface model, which assumes kinetic hardening of the yield surface $\boldsymbol{f_o}$, back-stress $\boldsymbol{\alpha}$ within the bonding surface $\boldsymbol{F}$ with back stress $\boldsymbol{\beta}$ hardening of mixed isotropic kinematic hardening**,** the centre of the yield surface $\boldsymbol{f}$ is moving with the back stress **α.** Bounding expanding occurs due to plastic strain hardening that is represented as B+R. B is the bounding surface, F is the initial size and R is the isotropic hardening component [16].

$$f_O = \varphi(\sigma - \alpha) - Y = O \tag{4-2}$$

$$\mathrm{F} = \varphi(\sigma - \beta) - (B + R) = O \tag{4-3}$$

### 4.4.3 Boundary conditions

As stated before, due to the FE model's symmetry, only one-quarter of it was utilised. For the metal sheet as well as the elastic cushion, symmetric boundary conditions are used. The minor part and die are blocked from movements in the X-Y, Z directions. The MPF punch and the upper part of the blank-holder are positioned in only two directions, X-Z. These components are allowed to move along in the vertical direction, O-Y. Punch force is varied and directed for holding the sheet metal in Y-direction. Figure 4.4 presents the applied finite element model with boundary conditions.

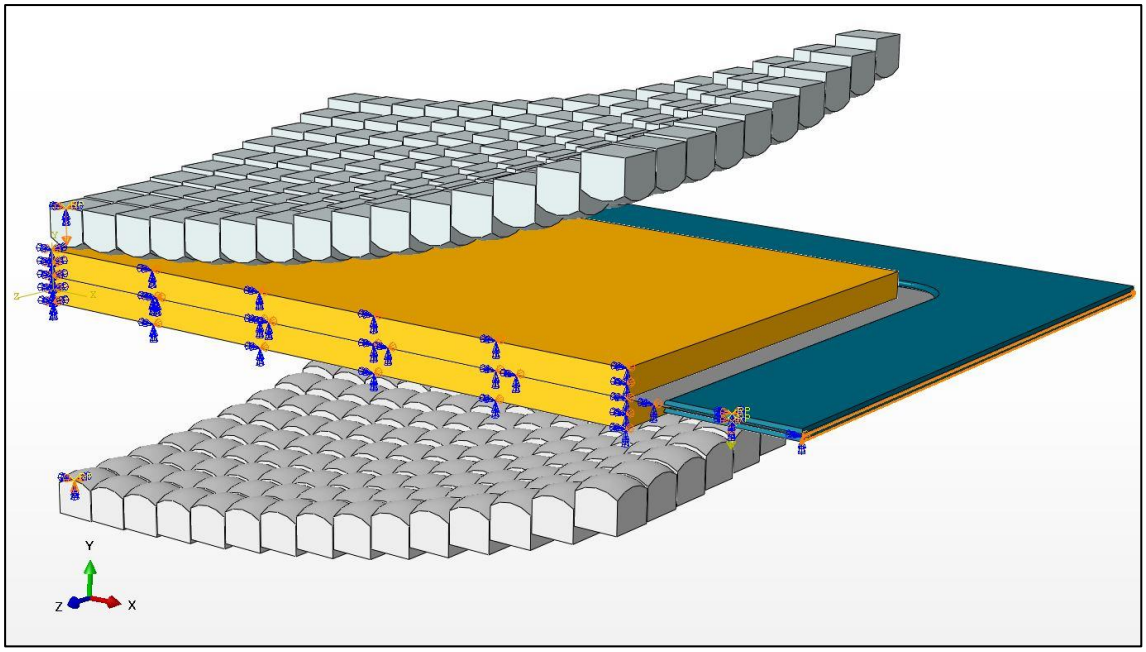


Figure 4.4 Model simulation and affected boundary condition of FEM

The cold sheet metal forming uses Steel-DC05. The properties of steel DC05 sheet due to different thicknesses under uniaxial tension was investigated. The thickness of the steel-DC05 is reduced in the range of 1mm using chemical etching (to reduce sheet thickness). This was done so that the dimensions can be adjusted without having to change the microstructure and grain size. In addition, the effect of mesh size was determined by FE calculations performing using FE code, as shown by Figure 4.5 with applied boundary conditions.

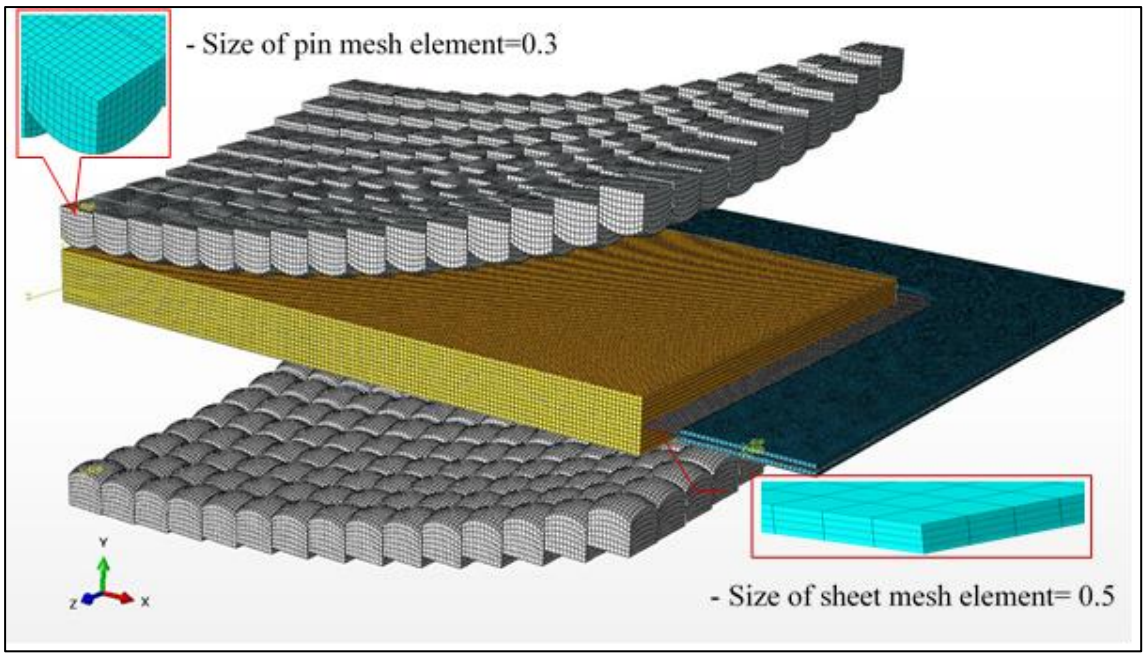


Figure 4.5 FEM element with a hexahedron mesh type and two different mesh element sizes

Computational solutions of partial differential equations require a 10 by 10 matrix with a mesh size of 0.5mm and 10mm pin tip representing a discrete mesh. A mesh partitions a volume into elements over which equations can be approximated. Mesh zone boundaries can be used to create ideal mesh-shaped zones for computational performance, or they can be assigned fixed boundaries to represent internal/external conditions within a model.

Meshes are also used extensively in the analysis of geographical and cartographic data. A radius of 400mm is applied to the curvature of the saddle shape on the quarter MPF used in FEM. FE mesh has been used first, with equivalent plastic strain-on surface at contact points. The material sheet was steel DC05 with 1 mm thickness. The dynamic analysis method in the ABAQUS/explicit is founded on the application of the explicit integration rule combined with diagonal or lumped element mass matrices [58]. The equations of equilibrium governing the linear explicit procedure have the following form:

$$R = M\ddot{U} + C\dot{U} + KU \qquad (4\text{-}4)$$

Where $M$, $C$, and $K$ are the mass, damping, and stiffness matrices respectively. $R$ is the vector denoting externally applied forces. $U, \dot{U}$, and $\ddot{U}$ are the displacement, velocity and acceleration vectors, respectively. The equations of motion (4-5) and (4-6) for the body is integrated using the explicit central difference integration method:

$$U^{(i+1)} = U^{(i)} + \Delta t^{(i+1)}\, \dot{U}^{(i+1)} \qquad (4\text{-}5)$$

$$U^{(i+1/2)} = \dot{U}^{(i-1/2)} + 1/2(\Delta t^{(i+1)} + \Delta t^{(i)})\ddot{U}^{(i)} \qquad (4\text{-}6)$$

where $\dot{U}$ is the velocity and $\ddot{U}$ is the acceleration, i refers to the increment number and (i - 1/2) and ( i + 1/2) refer to mid-increment numbers [58].

## 4.5 -Material-models for the sheet and solid-cushion

Finite element modelling was investigated for MPF die consisting of a pair of pin matrices, sheet panels and two elastic cushions. As discussed in Chapter 3, the mechanical characteristics of the sheet metal were obtained with the Zwich-Roell testing equipment on the specimens at $0^o, 45^o, 90^o$ orientation angles relative to the roll directions. ABAQUS/explicit was chosen for simulating the forming processes [57]. The pin is 10 mm and has a hemispherical tip and a square cross-section. The length for the square cross-sectional area is equivalent to the radius, as shown in Figures 4.4 and 4.5; the pin shape and conditions.

Table-4.2 explains the characteristics of the tested material.

Table 4.2 Mechanical-characteristics of the sheet-panel

| Properties | Values |
|---|---|
| Poisson ratio ($\boldsymbol{v}$) | 0.3 |
| Yield stress ($\boldsymbol{\sigma}$) | 202.8 Mpa |
| Density ($\boldsymbol{p}$) | 7870 kg/m3 |
| Modulus of elasticity (E) | 220 Gpa |

As depicted by Figure 4.6, the strain-stress curve of steel hardness DC05 is experimentally obtained from the tensile test using the Zwick tensile testing machine.

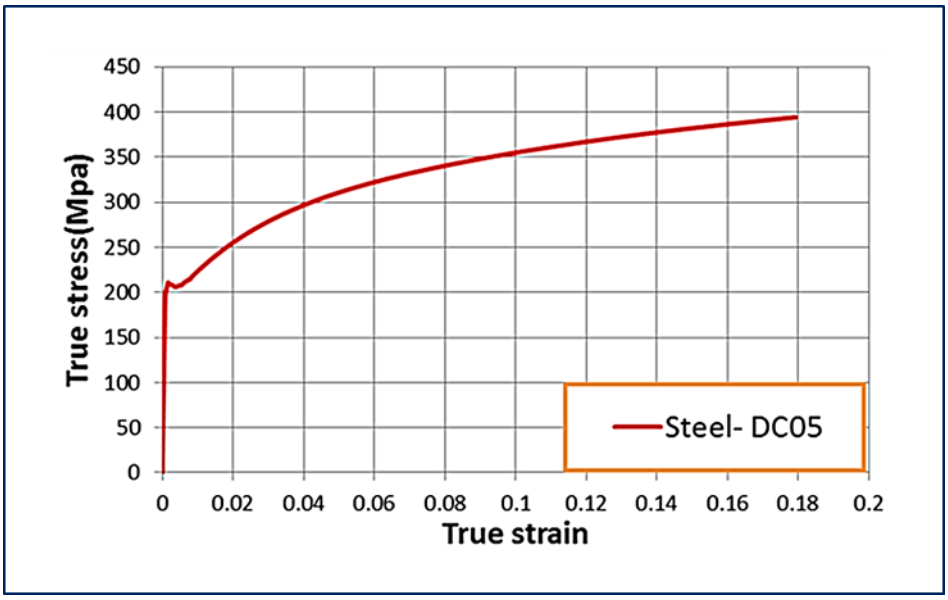


Figure 4.6 Experimentally obtained stress strain curve of sheet DC05

Elastic-cushion material hardness is a requirement in the MPF to protect the pin damage and sheet panel dimpling defect [16]. A study on the selected material, polyurethane A90, is performed as it is usually used in this research process [59]. Hyper-elastic model was selected to represent the hyper-plastic conduct, which is expressed as:

$$w = C_{01}(I_2 - 3) + C_{10}(I_1 - 3) \tag{4-7}$$

Over here, w represents the strain energy per unit of volume. $C_{10}$ and $C_{01}$ are the temperature coefficients, which depend upon the material characteristics attained from uniaxial compression tests. $I_1$ and $I_2$ are the first and second invariants for the deviatoric strain tensor. The material has a rating of A90.

Figures 4.7 and 4.8 show the experimental and numerical results of the nominal strain vs nominal stress curves for polyurethane A90. Experimental results were obtained with the use of the Zwick testing machine. Similar findings were also achieved in [60].

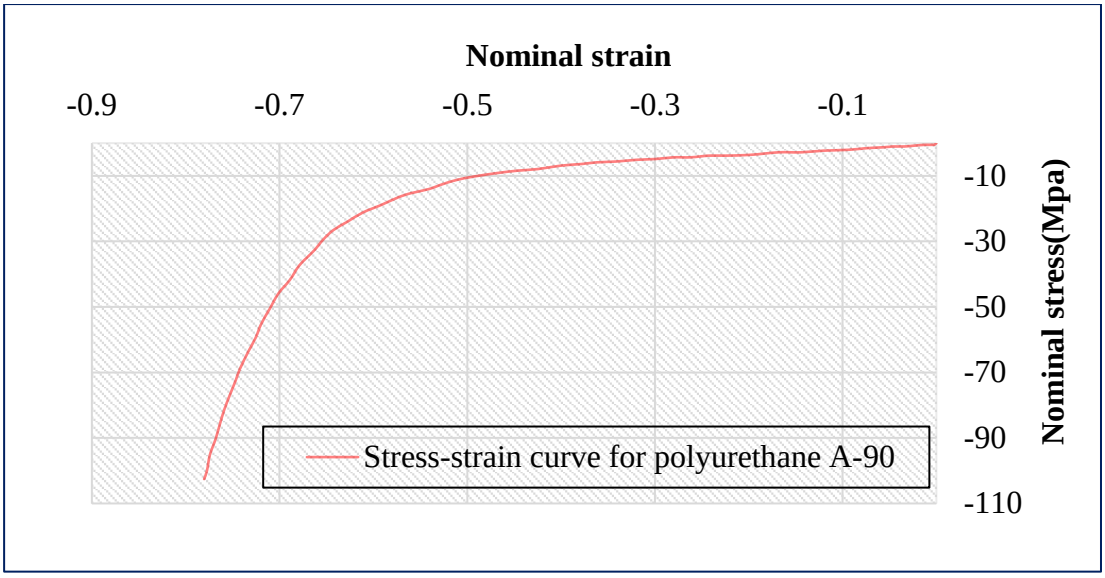


Figure 4.7 Experimental nominal compression stress-strain relationship of polyurethane A90

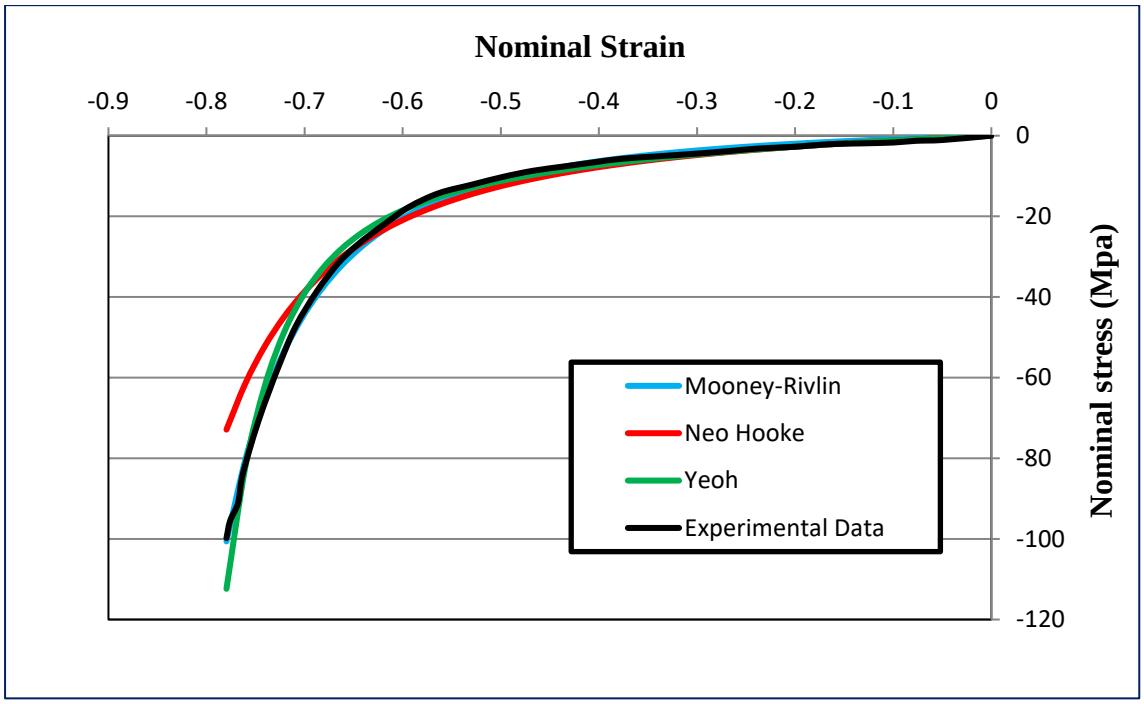


Figure 4.8 Numerically achieved nominal compression of the strain-stress relationship for A90 polyurethane with Moony-Rivlin, Neo Hooke and Yeoh model

## 4.6 Validation-of the-Finite-Element-Model- (FEM)

The sheet metal along with the elastic cushion were modeled as deformable figures with the use of ABAQUS C3-D8 R quadratic-type [57]. The 1 mm thickness number of meshing cells for a unit mm thickness sheet plate and the 3 mm elastic cushion were 9,258 and 298,300. Total elements generated for the abovementioned elastic cushion were 9258 elements and 298300 elements for the metal sheet. Upper and lower dies are modeled as firm structures with a R3D4 element type. ABAQUS offered the evolution function to test experiment data while analysing the hyperplastic material against different forms for the strain energy potentials [61]. The total elements for the upper die and the lower die were equal in all three models, i.e. they were 59,400, 46,080 and 53,550 elements for dies with pin sizes of 10 mm, 15 mm, and 20 mm, respectively. Symmetric boundary conditions were applied as only the quarter model is considered for the elastic cushion and the sheet. To position the lower die in the X, Y and Z directions, displacement boundary conditions on the model were applied. On the contrary, the upper die was fixed in the X-Z direction and punch displaced in the Y direction. Figure 4.9 illustrates the finite element mesh along with the boundary conditions.

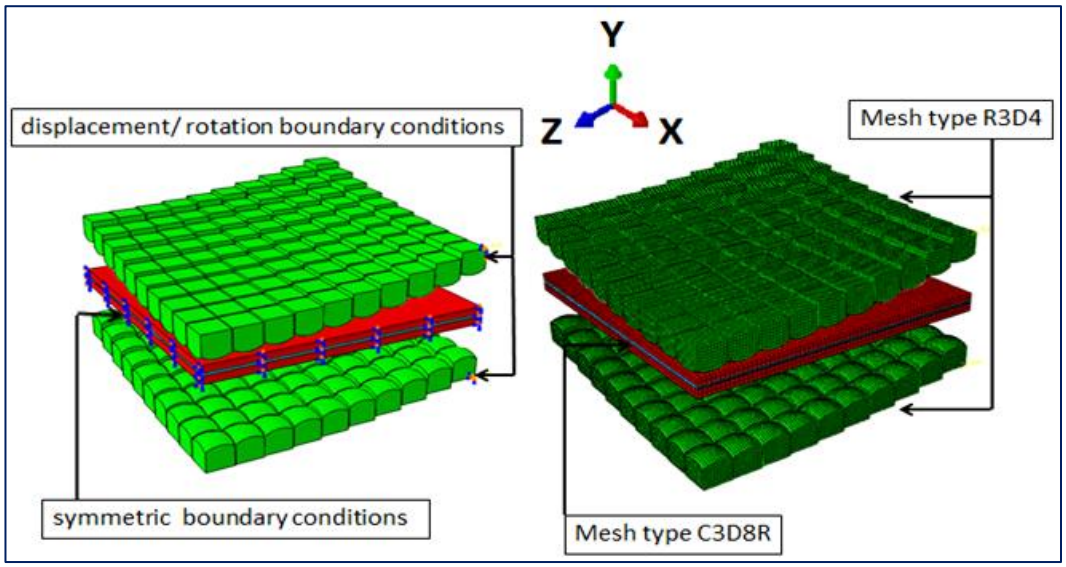


Figure 4.9 MPF meshing element in addition to the boundary conditions applied along with

the rigid fixed blank holder

### 4.6.1 Distribution of thickness

The numerical and experimental analysis of the process and therefore a comparison between the present works against the values which have been recorded with 1 mm thickness for sheet metal of the multipoint forming in to blank-holder were used to validate the shape model characteristic and thickness variations of the quarter on 3D shape model blank. Figures 4.10 and 4.11 show the difference between the steel DC05 and aluminium 5151-0 thickness measurement locations on the MPF sheet metal for the model validation. The thickness measurement was made for the sheet blank at 12 location points located from Z to X direction.

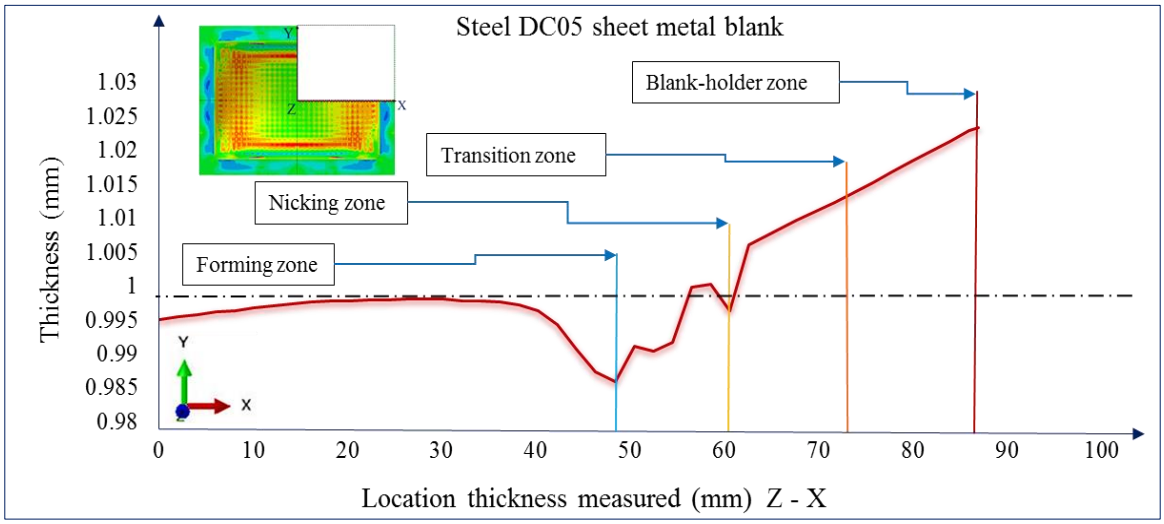


Figure 4.10 Numerical resultant thickness values measured at points located from Z to X for the MPF model validation

The thickness variation along the Z to X direction for numerical simulation on MPF are presented. The specimen for mechanical test was DC05 steel and aluminium 5151-0 with 1 mm thickness. After that the expected wrinkling for the finite element simulation was 0.97 mm which happened to be the best case amongst totally simulated environments. The numerical modeling involved the use of a 1 mm thick steel sheet metal with the radius of

curvature being R-400 mm, and the blank-holder force being 11 kN. This is shown in Figures 3.7 and 3.8, where it is apparent that the average thickness distribution in the blank-holder of the present finite element modeling (FEM) is more close to the average obtained from the reference results [93].

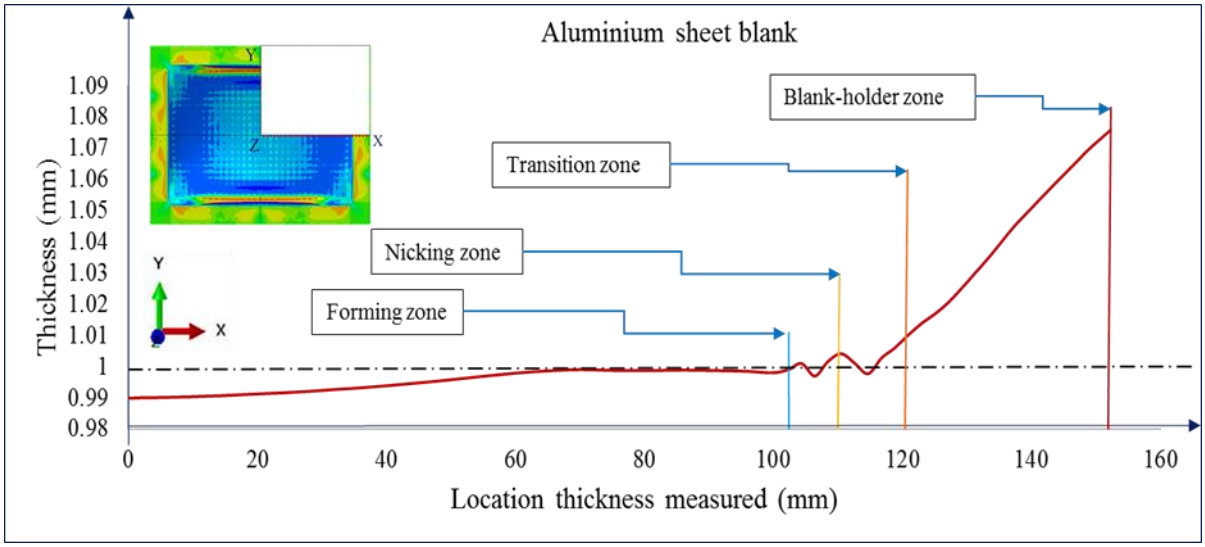


Figure 4.11 . Numerical resultant thickness values measured at points located from Z to X for the MPF model validation

The presented results are very close to the ones obtained numerically with differences not exceeding an average of 3.1%. However, the thinning and nicking was fully quartered along the Z to X direction and no sheet thickenings were made in the sheet forming zone except under the blank-holder. The selection of aluminum 5151-0 as the sheet blank of deformation in the case of R400 reduces the curvature in combination with high sheet blank clamping forming force, which leads to a reduction in thickness in the complete sheet metal forming part. Also, the thickness was a quarter of the FEM simulaton model. The sheet blank curved steel DC05 blank sheet was used for identifying variables which had an influence on wrinkling, thickness, and maximum deviation. The higher the force of the blank-holder

device, the better the deformation will be over the surface of the multi-point punch tooling, since the process is incomplete by deformation of the side wall [62].

Table 4.3 The specific levels and process variables examined, [39]

| Process variables | Units | Levels | | |
|---|---|---|---|---|
| | | Low | Medium | High |
| A) Curvature radius | mm | 400× 400 | 600× 600 | 800× 800 |
| B) Force of the blank holder | kN | 10 | 15 | 20 |
| C) Thickness of the elastic cushion | mm | 3 | 6 | 9 |

### 4.6.2 Influence-of-blank-holder-force on wrinkling and sheet-thickness

Numerical modelling was carried out showing the influence of controlling the force of the shutter on the fault and crushing in a multipoint formation (MPF) of a hemispherical shape. In these FEM models, DC05 sheet steel preforms were formed with a thickness of 1 mm using the radius of curvature, R-400. The initial FEM was performed using the constant beam fixation forces (BHF) of 11kN. With an empty holder of 15 kN, a slight wrinkling occurred at 32 mm. At 15 kN, there was an insignificant wrinkle. Therefore, to prevent wrinkles and fractures at the same time, the strength of the empty holder was high initially, when wrinkles were more critical. Then, it was reduced until the finish of the stroking, to facilitate metal movement and for avoiding destruction.

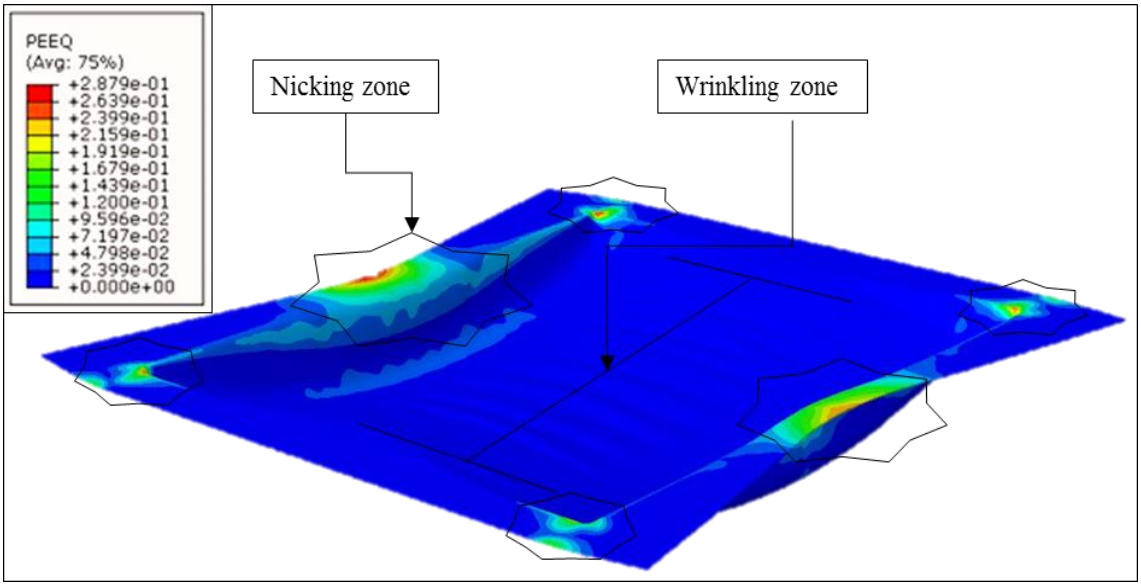


Figure 4.12 MPF deformed sheet metal shape along with signficant wrinkling projected by FE analysis simulation of process with a blank holder force

Numerical and experimental results demonstrate the various effects of major wrinkling and deformation, as illustrated in Figure 4.16. The results potray the effects of the pin shape which leads to the deformation of the sheet metal along with the influence of the elastic cushion.

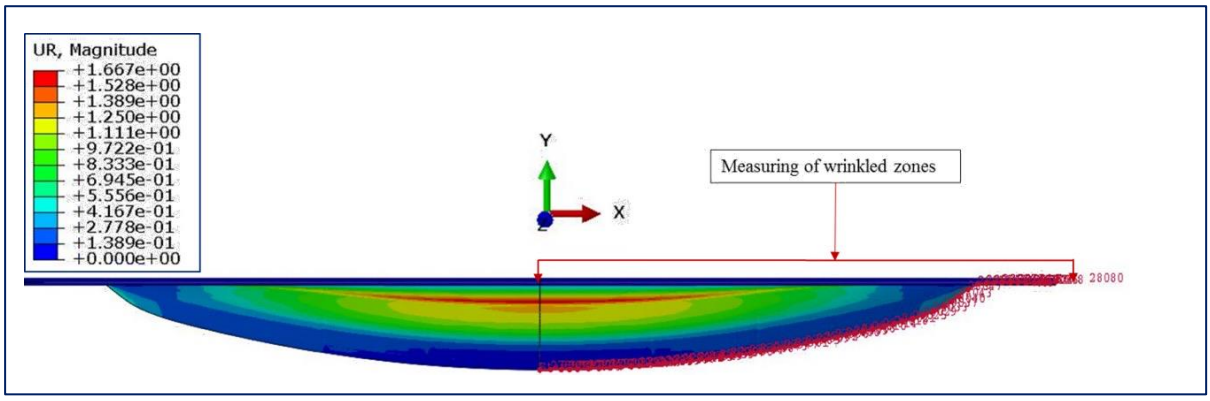


Figure 4.13 Wrinkling and fracture bounds for hemispherical MPF after varying blank geometries

The effect of BH geometry on wrinkling is shown in Figure 4.13, where a quarter MP punch travels 50 mm, with surface wrinkling amplitude dimensions on the line format to 150 mm depth under a 15 kN blank-holder force used. Due to the hemispherical shape in the tooling, the amplitude of the wrinkle measurements varied at central positions on the multipoint forming Figure 3.10. The fracture limits for wrinkles of hemispherical shape produced by the varying blank geometries are illustrated in Figure 4.14. Such bounds are evaluated for a wrinkling amplitude of 0.68 mm. In addition, in the process simulations which used FEA, there was an apparent wrinkling present. The deformed multipoint geometry with several wrinkling points was projected by the FEM simulation with the use of a BH force of 10 kN.

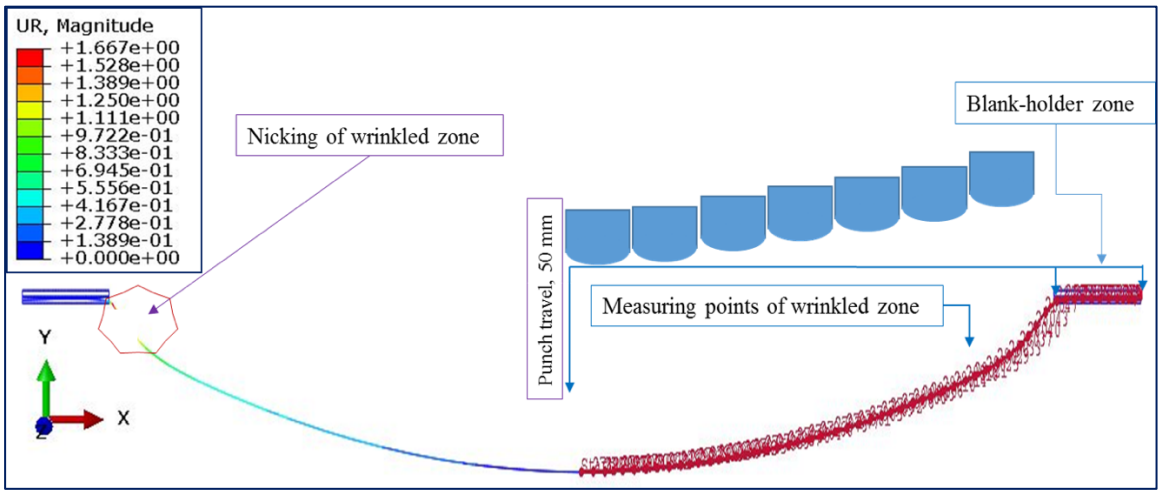


Figure 4.14 Punch travelling 50 mm, with blank-holder forces

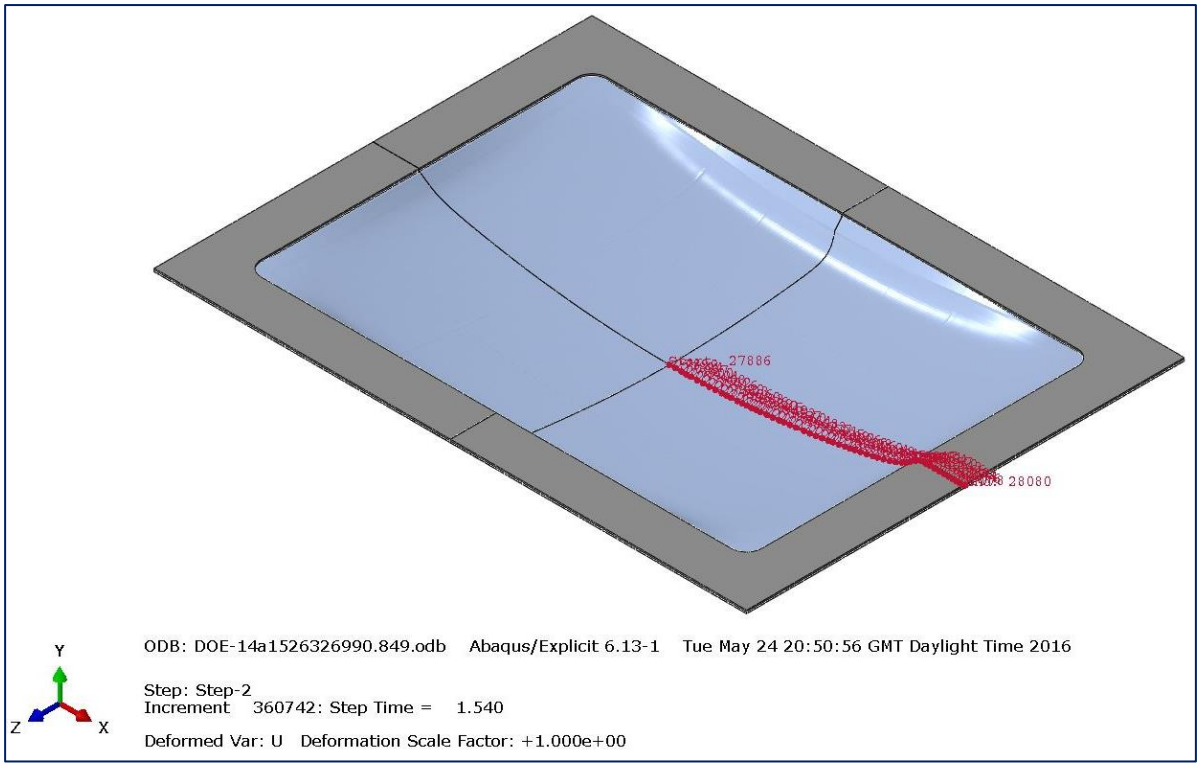


Figure 4.15 MPF deformed sheet metal shape with significant wrinkling projected by FE analysis simulation utilising a different BH geometry

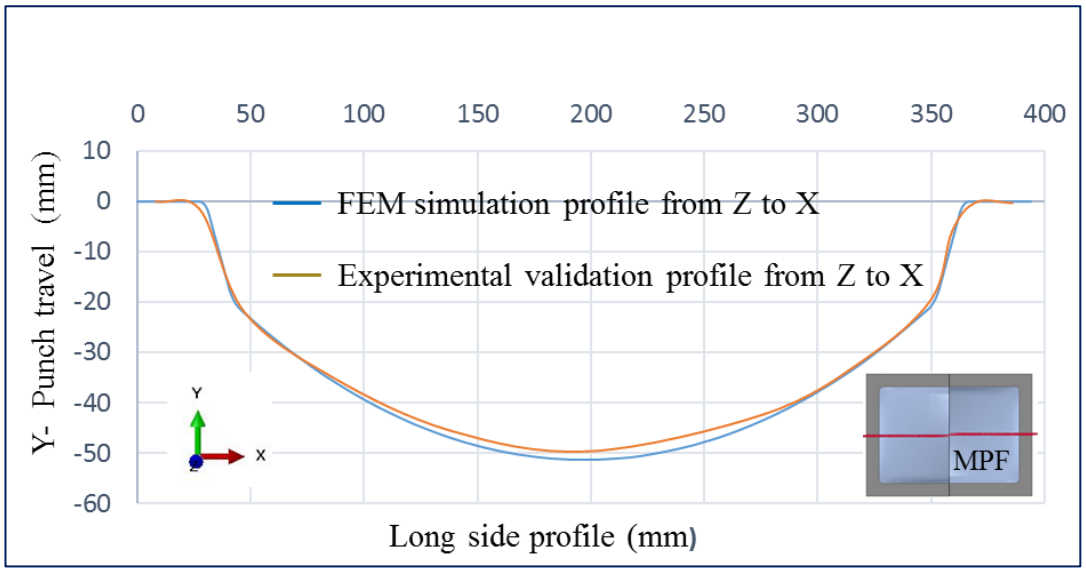


Figure 4.16 The wrinkling measurements on experimental validation and FEA profile line under a BH force of 15 kN

The numerical along with experimental validation results show the influence of thickness variation and wrinkling. The results revealed the effect of the shape of the pin on the deformation of the sheet along with the influence of the elastic cushion. Both curves start from the forming load value of 62 kN, as illustrated in Figure 4.17, which shows the validation of the forming force using experimental results.

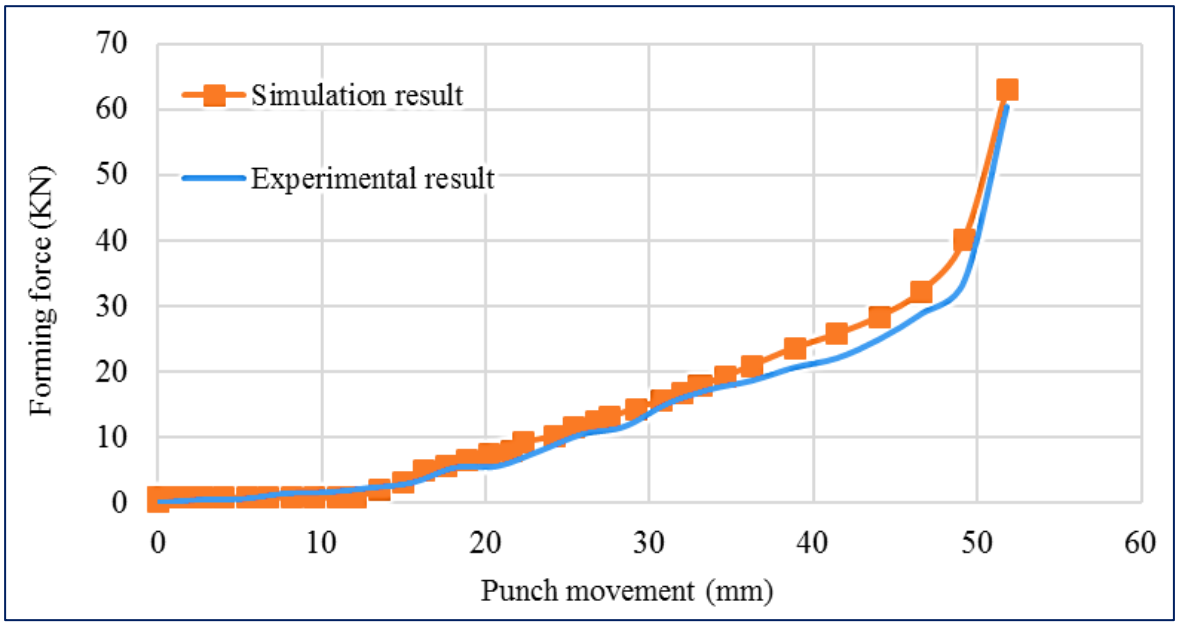


Figure 4.17 Validation forming force (kN)

In the current study, when a similar whole validation model was created, the FEM results showed a lower force in terms of the effects of the pin shape on the sheet metal deformation. MPF load slowly increases to 53.84 kN, which relates to the 40 mm of the upper die displacement. All pins were in an interaction with the elastic cushion and plastic deformation commenced. Next, the force tends to quickly increase with plastic deformation because of the material's strain hardening [39]. The highest projected force is around 55.98 kN, with the upper and lower dies being secured. Figure 4.18 demonstrates the contrast of the expected metal of the finite element and the measured experimental results of the concluding geometry

by the use of a FARO 3D scanner. There was a satisfactory agreement in the forecasted and investigational results, at a distance of 1.85 mm, close to the profile's center.

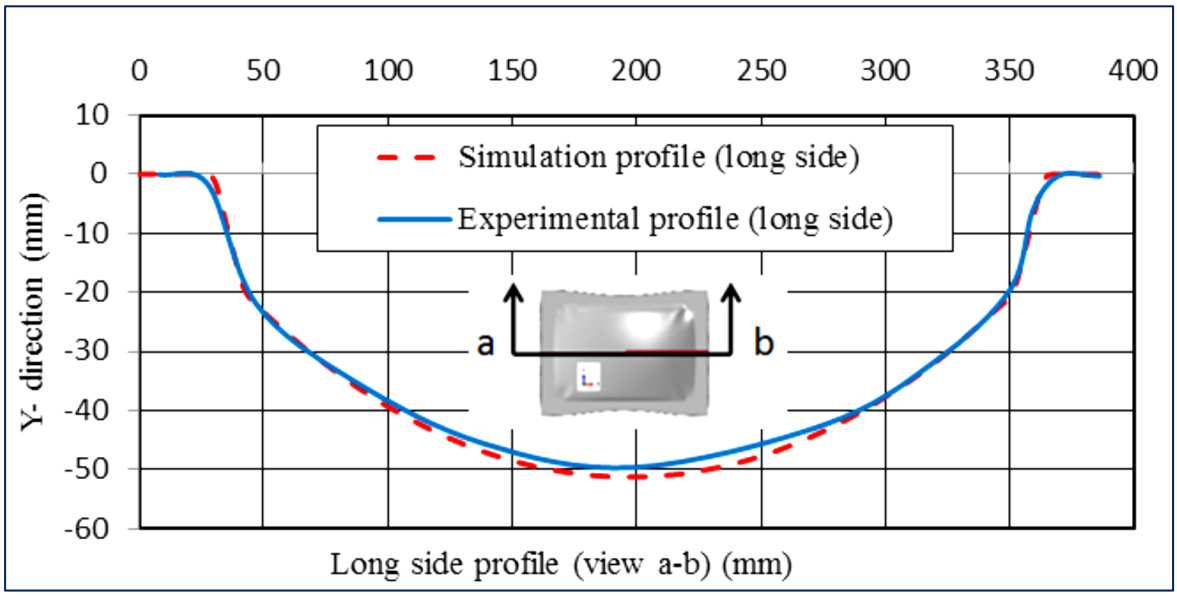


Figure 4.18. Final profile validated experimentally

### 4.5.3 Effect of forming curvature's radius

For differential geometries, the radius of curvature, R, is usually the reciprocal of the curvature. In terms of a curve, this is equivalent to the circular arc's radius. This also is able to approximate the nature of the curve at that location. In regards of surfaces, the curvature's radius is expressed as the circle's radius which fits best a normal section or a combination of sections. The effect of forming curvature had levels R400-R600 and R800. It was found that if the radius is small, resulting wrinkling will also be less following the unloading stage. Wrinkling rises from 2.30 mm to 4.50 mm as the radius increases from 400 mm to 800 mm. It must be noted that this is because of the elastic and plastic deformation ratio which are larger for the lowest radius. Also, due to the increased sheet springback value, which occurs at the sheet edges of the forming sheet, thus reducing wrinkling value in the produced sheet, as depicted by Figure 4.19.

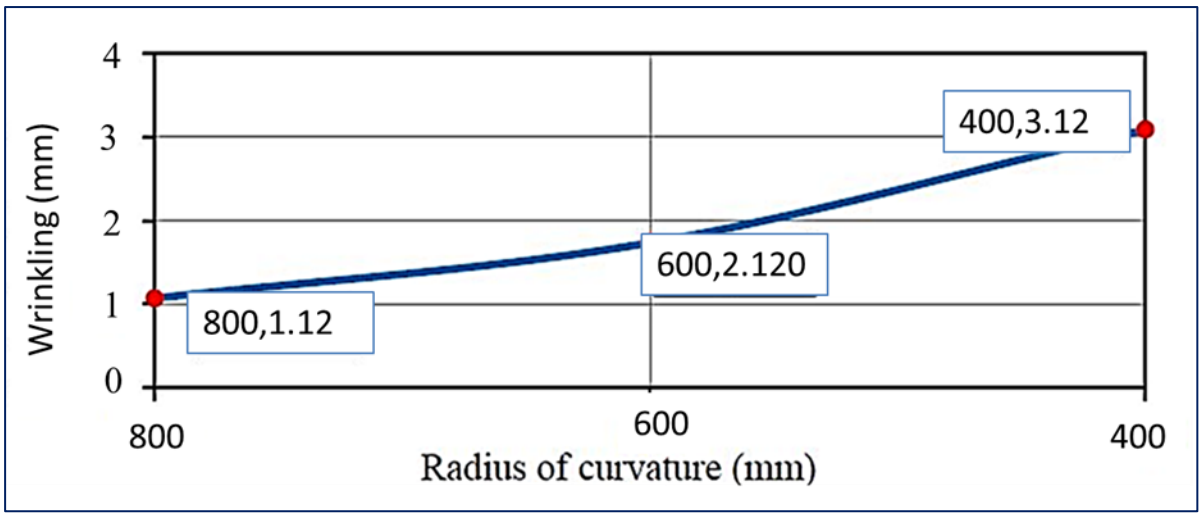


Figure 4.19. The influence of the multi-point forming curvature on sheet surface wrinkling

Figure 4.20 shows A) R400, B) R600 and C) R800 radius of curvatures where the corresponding plastic strain distribution of forming sheet for varying radii is shown. Maximum plastic strain occurrs in the produced sheet with the use of the lowest radii, i.e. A) R400 mm.

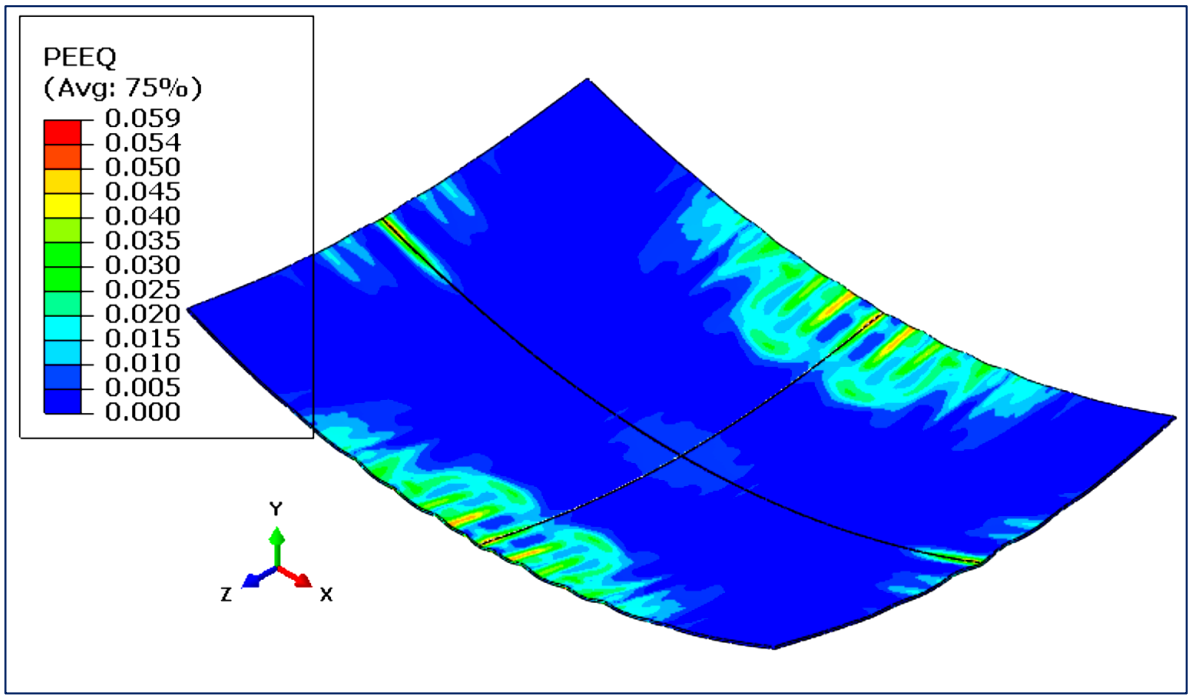


A) Curvature's radius effect on R400 mm

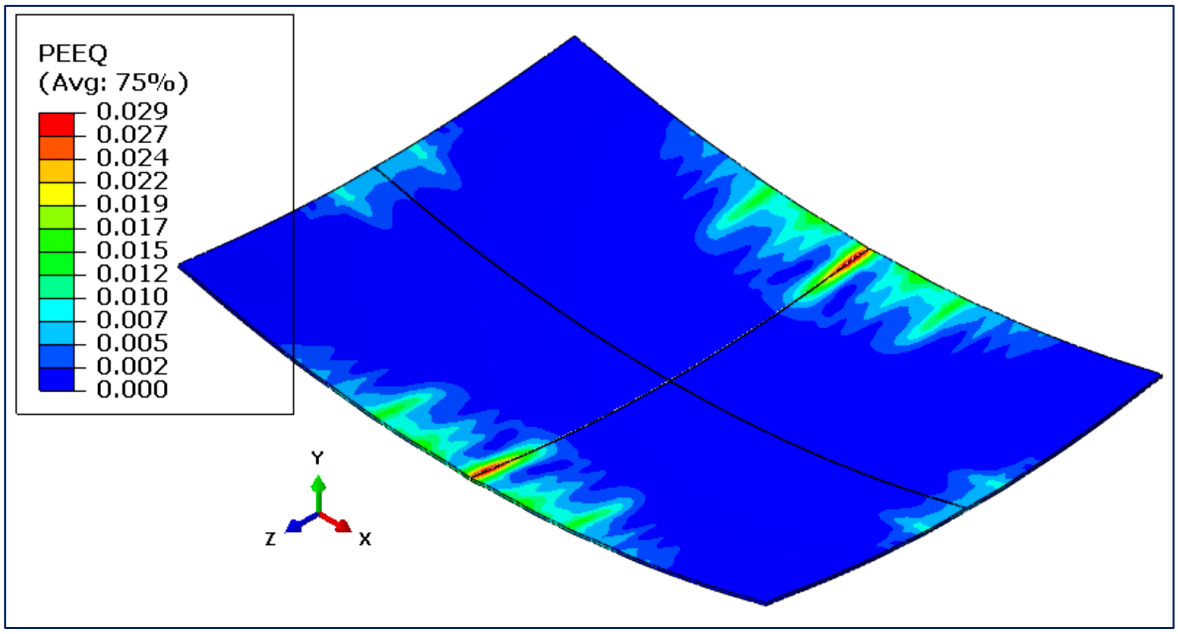


B) Curvature's radius effect on R600 mm

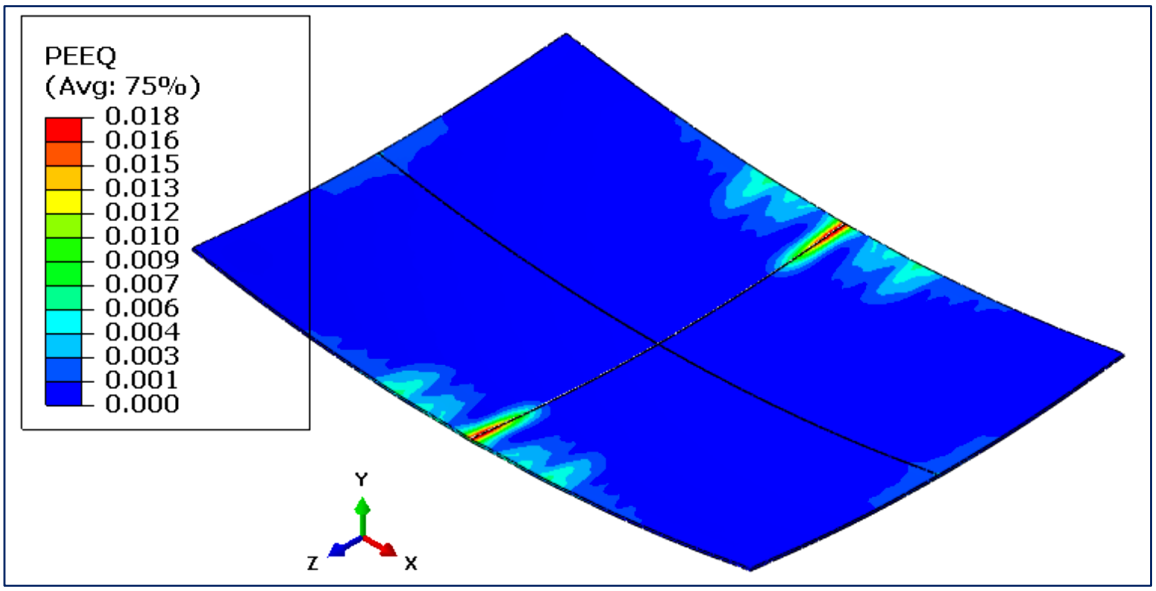


C) Curvature's radius effect on R800 mm

Figure 4.20. MPF plastic strain distribution for three varying radii

### 4.5.4. Influence of elastic cushion thickness

In order to reduce wrinkling on the formed parts, the layers of the elastic cushions were used in the MPF procedure. This section discusses and investigates the influence of the hardness of the elastic cushions and thickness on wrinkling. As shown by Figure 4.19, the simulated stress distribution and wrinkling vary with the elastic cushion for three different shore hardness levels. These are (a) A65, (b) A85 and (c) A90. Shore A90 hardness for the polyurethane sheet was utilised in the simulations which had a forming curvature radius of 800 mm. From Figure 4.24, it is apparent that wrinkling reduces with an increase in the hardness of the elastic cushion. This takes place because of the increase in the metal sheet's stress distribution, which is uniform. Hence, it is now known that the any elastic sheet which is to be utilised in a MPF procedure must be hard enough and must have a suitable thickness [23].

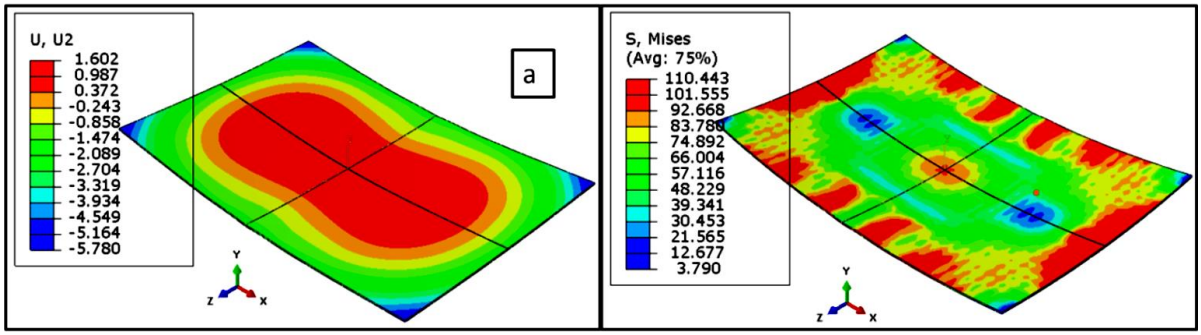


Figure 4.21. Effect of the numerical simulation of Shore hardness (a) A65 on MPF

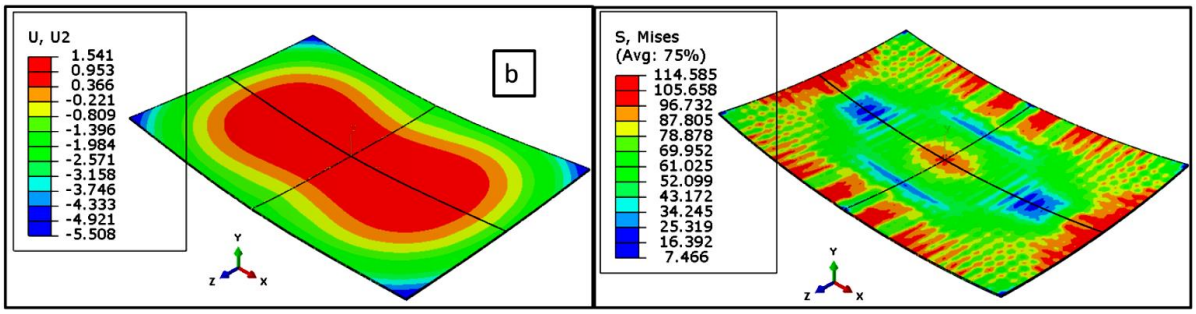


Figure 4.22. Effect of the numerical simulation of Shore hardness (b) A85 on MPF

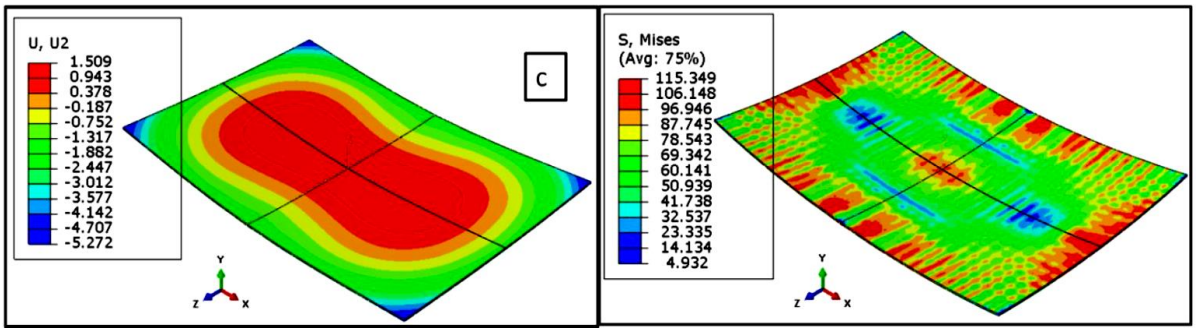


Figure 4.23. Effect of the numerical simulation of Shore hardness (c) A90 on MPF

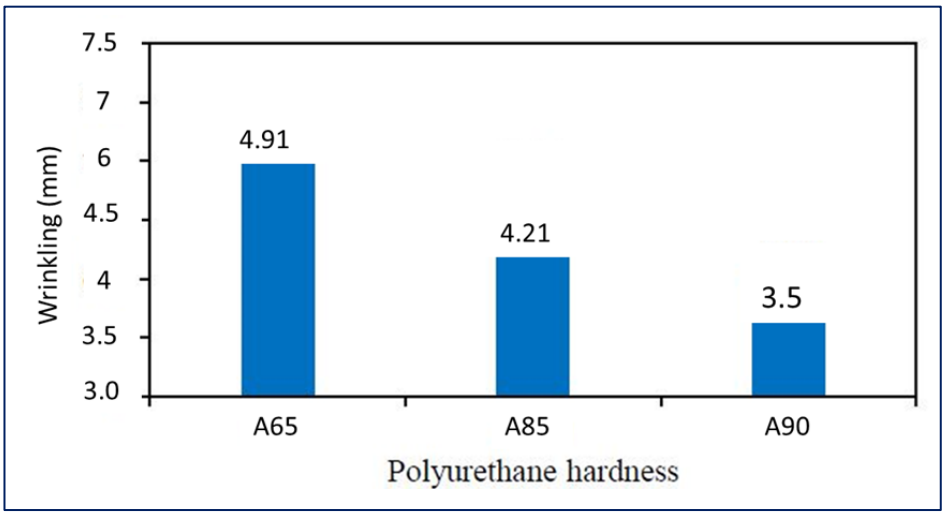


Figure 4.24. Numerical simulation on an elastic cushion of 3 mm thickness with three varying hardness materials to determine the respective sheet surface wrinkling

The forming curvature's radius of 800 mm was investigated numerically along with thickness of (a) 3.5, (b) 4 and (c) 6.2 mm of the elastic cushion with the shore hardness of A90. It is apparent that wrinkling reduces with a rise in the elastic cushion thickness, as depicted by Figure 4.20, and thus will have an influence on the shape precision [63]. Results of the wrinkling simulations in terms of the thickness of the elastic cushion are shown in Figure 4.21.

## 4.7 Summary and Conclusions

The FE modelling in the MPF procedure was established and discussed in-depth. The characterisitcs of the materials used in this work; the sheet metal along with the elastic cushion, were attained from mechanical testing. The FE modelling outcomes were verified with the experimental results; where the forming force against punch displacement curves agreed well with the simulations and the formed part's profiles at final stage.

The influence of the thickness of the elastic cushion, coefficient of friction, the blank holder force and the curvature radius on the sheet surface wrinkling were studied for understanding the significance of these variable. Findings showed that the forming curvature's radius had a significant outcome on sheet metal wrinkling in the MPF procedure.

The purpose of the research work is successful simulation of the process of multi-point forming and confirming the results, by comparing them with those already published earlier in the literature [18]. The validation contains both experimental and numerical results that are consistent with each other and therefore are established as a reference for comparison purposes.

# CHAPTER 5 MULTI-POINT FORMING USING MESH-TYPE ELASTIC CUSHION MODELLING AND EXPERIMENTATION

This chapter introduces a detailed numerical approach for predicting wrinkling in MPF technology. FE models were established for the simulation of MPF of doubly curved panels in stainless steel DO5. The Response Surface Method (RSM) along with the Analysis of Variance (ANOVA) was used to recognise the substantial procedure factors along with the determination of appropriate combinations to ehance the formed part quality. The effect of the abovementioned factors on thickness variation through the formed panel and the succeeding influence of those deviations on the amount of wrinkling was examined. The influence of blank clamping force and punch dimensions on the formed part were considered in a study [64]. The authors of this study determined that smaller pin sizes lead to an improved quality of the formed surface. In another study [65], the researchers mentioned that the pin dimensions (i.e. the sizes and radii of the formed part) have a substantial influence on the overall shape accurateness in MP forming. One study [40] confirmed that elastic cushions are a crucial part in multi-point deep drawing (MPDD) and are known to have a major influence on the precision of the formed product. In [66] it was disovered that the use of a flexible blank holder enhanced the forming limit while elminiating wrinkling in a thin sheet. In the past, Several methods were used and designed for compensating or decreasing the wrinkling effect in MPF. Further, [67] suggested that a reduction in wrinking could take place at the completion of a forming procedure if the sheets were preloaded initially Also, [68] recommended that over-forming can help in the compensation of wrinkling. [69] showed in their study that the effect of various parameters on a known shape decreases with the use of new proposed methodology for determining the formability limits by wrinkling.

[70] explored the effects of the blank holder force and material characteristics on wrinkling in a deep drawing for which MP forming tools could be employed. The outcomes of the work demonstrated that the yield strength of the work piece has a major influence on the geometrical precision with materials of yield strength. These include materials for instance, steel, which experiences increased levels of wrinkling. The study also revelaed that fastening the work piece was important in decreasing the sheet thickness. [62] used a MP forming tool for deep drawing and determined that using elastic pads with the least probable thickness and increased hardness decreased wrinkling. In addition, the use of small pins also reduced dimpling and significantly; greater forces are necessary in forming.

FE analysis is an economical technique to understand the effects of process variables on wrinkling and geometric precision [71]. FE analysis was employed here for the simulation of the MPF of doubly curved sheets panel. At industrial levels, the Design of Experiments (DOE) and ANOVA are commonly adopted [72] and thus, will be used in this work as well, to examine the influence of process variables . The RSM was utilised to understand the influence of the process parameters on the wrinkling in Multi-Point Die Forming (MPDF), i.e. part geometry. The total amount of sheet wrinkling, thickness variation, and maximum deviation across the MPF tools was explored and the correlation between thickness distribution and sheet metal wrinkling was determined. As an existing Multi-Point Die Forming (MPDF) tool [65] was utilised for the validation of the numerical solutions, the size of the pin was maintained with a square of 10 x 10 mm cross section together with a tip whose radius of curvature was 10 mm.

## 5.1. Design-of-experiment

Both, DOE as well as ANOVA are the commonly used procedures for examining the influence of process variables in the formation of sheet metal [65, 73]. In the current study, the main design process variables which were considered were: radi of forming curvatures, the elastic

cushion's thickness and force of the blank holder [64, 65, 74, 75]. The objective function is to use the best optimum parameter, for example, elastic cushion thickness, cushion hole-size, forming force and radius of curvature. The use of approximated response surface (Central Composite) helped in predicting expected wrinkling at points in the design space that exist amid the chosen ones for which simulated outcomes were attained. Finally, for determining the optimal variables which provide the minimum response variation (minimum springback and minimum thickness variation), the optimum case variables were used at the last-step exploration for validating the results. RSM offers a correlation in terms of the objective function (Y) and the inputs of other variables ($x_i$). The model generally utilised here is a quadratic equation, which is a 2$^{nd}$-order polynomial ( Equation 5-1) to form an experiential model which is able to describe the experiment results in Table 5-2. The values $x_1$ to $x_9$ are the coefficients of the empirical model which are obtained by using a regression analysis. A Genetic Algorithm (GA) was then used to find the optimal setting of the process parameters which agree with the objective function's mean. Figure 5.1 shows the series of steps used in a DOE.

$$y = a_0 + \sum_{i=1}^{n} a_i\, x_i + \sum_{i-1}^{n} \sum_{j=1}^{n} a_{ij}\, x_i\, x_j + \varepsilon \qquad (5\text{-}1)$$

Over here, $a_0$, $a_i$ and $a_{ij}$ represent the model coefficients.

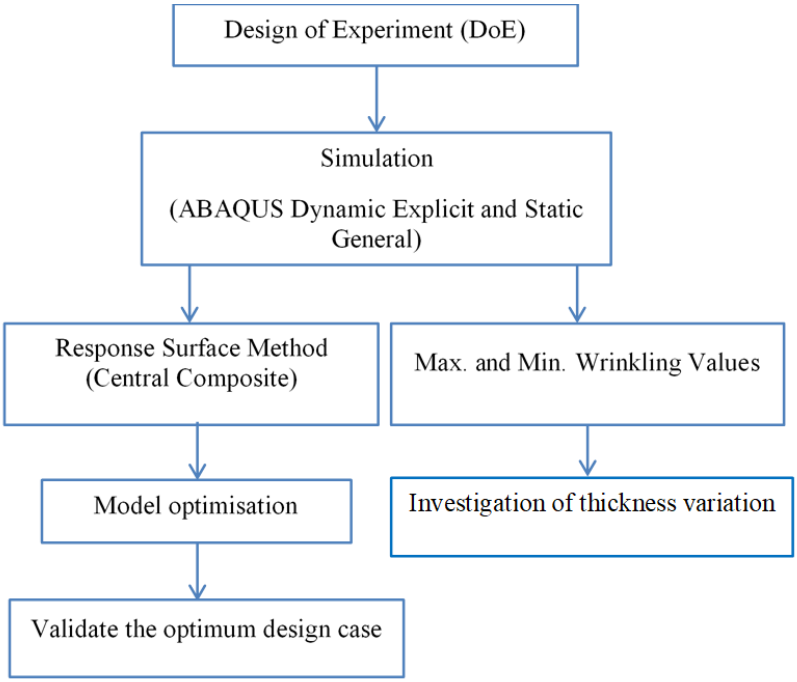


Figure 5.1 Sequences used in DOE and optimisation steps

### 5.1.1. Process parameters

During MP forming procedures, the selected factors that affect the part quality were considered in the DOE. Each factor had three values, which offered an acceptable range (low, medium and high). The process variables studied are: holes-size of the mesh-type cushion, the type of holes whether they are as squares or are circular, and the cushion thickness. The levels are: low, medium and high, as depicted by Table 5.1.

Table 5.1 Levels and values of the DOE parameters, [65]

| Process parameters | Units | Levels | | |
|---|---|---|---|---|
| | | Low | Medium | High |
| Elastic-cushion-hole-size (A) | mm | 2*2 | 3*3 | 4*4 |
| Elastic-cushion-thickness (B) | kN | 3 | 6 | 9 |
| Elastic-Cushion-hole-type (C) | mm | - | -Square/Circular | - |

For an MPF process with 10 mm pins, a 46.0 kN die force and a 400 mm radius of curvature, the best process parameters to achieve minimised wrinkling and thickness variation are: an elastic cushion with a hole-size of 3.5 mm and thickness of 3.0 mm.

### 5.1.2. Optimisation-of response-parameters

The model was investigated to form double curve shapes with different type model was used mesh-type elastic cushion with two different holes (square A and circular B), as shown in Figure 5.2. The metal sheet along with the elastic cushion were modeled as deformable bodies, and ABAQUS was employed. Pin size was 10 mm as recommended by [65]. Hence, each punch and die comprise of 300×200 pins while every pin had a cross section of 10 ×10 mm, and the 10 mm tip radius. The blank sheet as well as the elastic cushion is described as several C3D8R solid elements. This type is eight-node linear brick, reduced integration, hourglass control element. Measurement of the sheet is 153 mm×102 mm×1mm. The sheet is divided into five layers through thickness in the finite element model (FEM) as recommended by [57], dimension of initial FEM elemental is 1mm×1mm in the sheet plane and 0.24 mm in thickness direction. The aspect ratio element l: t was set to 1:5 where l and t are the element length and thickness respectively and this in the range of aspect ratio. Around 182250 mesh elements were utilised in the meshing of one quarter of the sheet. The initial elastic cushion dimension is 153.5mm×102.25mm with thickness 3 mm and a total of 49140 elements were utilised for the elastic cushion. The punch group of MPF tool modelled with R3D4 elements. By using SolidWorks Software, the location of the pins was evaluated based on the acquired CAD profile. Symmetric boundary conditions were applied to the sheet and elastic cushion. The die and as well as the lower part of the blank sheet are fixed in X-Y-Z direction while the punch and the upper part of the blank sheet are fixed in X and Z directions only and are free to move 50 mm in Y-axis [77].

### 5.1.3. Optimisation of shape and thickness considering stress response

To measure the quality of the final product, a particular criterion, or a mixture of criteria, could be considered. Here, wrinkling and thickness uniformity were implemented for determining the value of the produced part. To characterise wrinkling in the produced part, the shift in the path of the thickness (Y) beyond the unloading stage was demonstrated by ABAQUS [76]. In addition, to evaluate variations in the thickness of the resulting part, the correlation used was:

$$\text{Thickness variation} = \sqrt{\frac{1}{N}\sum_{i=1}^{N}(x_i - \bar{x})^2} \qquad (5\text{-}2)$$

Over here, N signifies the entire points where thickness was recorded, $x_i$ denotes the thickness measure at point $i$ and $\bar{x}$ denotes the mean of thickness of all measured points. For this study, larger wrinkling size and higher thickness variation refers to lower part quality and, obviously, the opposite applies. Figure 5.2 presents the boundary condition in terms of thickness of 3 mm of the quadratic geometry. In addition, the effects of the deformed sheet using square and circular mesh-type cushion are shown in Figure 5.3a and Figure 5.3b, respectively.

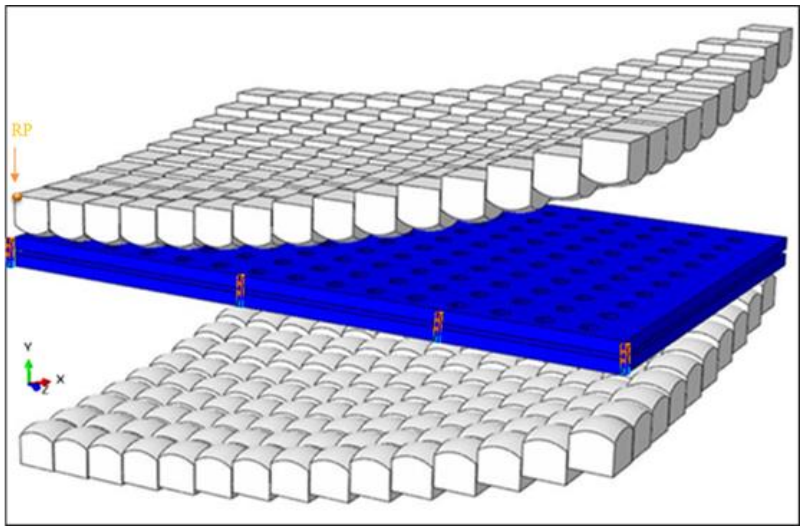


Figure 5.2 Boundary conditions of the 3D model of mesh-type elastic cushion

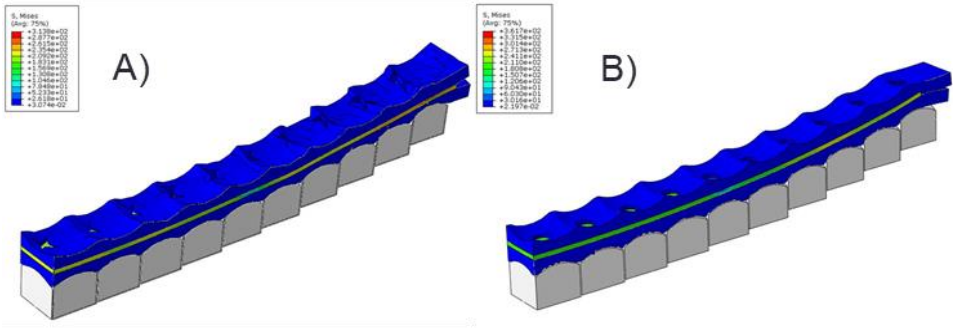


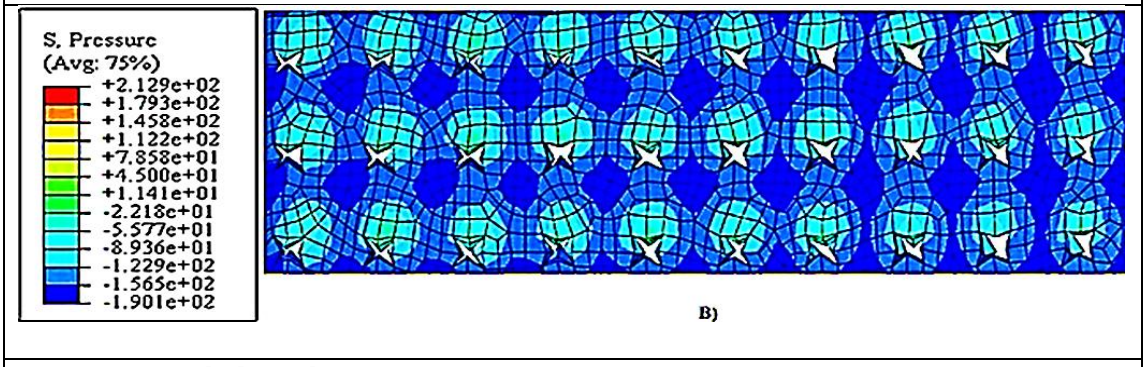


A) Square hole with 3 mm

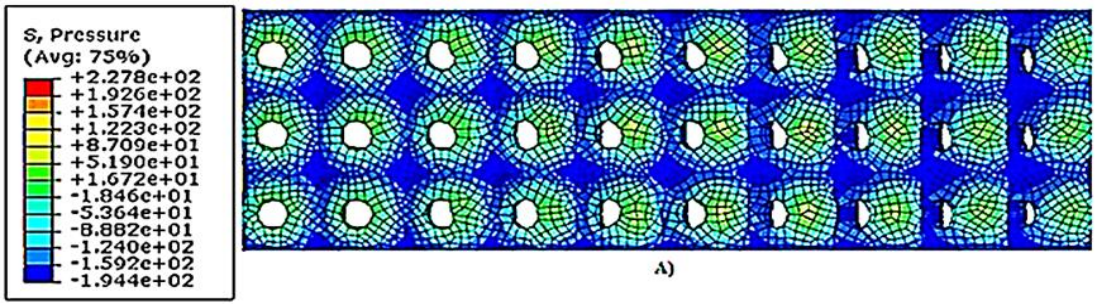


B) Circular hole with 3 mm

Figure 5.3 Effect of the deformed sheet using square and circular mesh-type cushion

### 5.1.4. Analysis and Discussion

Table 5.2. displays the overall conditions for the experiments along with the subsequent measurements of wrinkling thickness variation and press forming force. It is worth mentioning that the solutions of the numerical simulations went through a statistical analysis with the use of Design Expert, 7.0 [65, 77]. ANOVA was used for identifying the crucial process variables.

Null hypothesis for this study was that variables examined had no significant influence on outcome. A significance level of 7% was used which means that the higher the *P*-value falls below 0.05 the more important is the factor [65, 78]. Table 5.3. shows the *P*-values for the main factors and interactions. The ANOVA results indicate that the force of the blank holder as well as the forming curvature's radius affects wrinkling significantly, but this is not mainly due to the forming force. The difference in thickness is mainly under the effect of the radius of forming curvature, press forming force and also due to the interactions which take place between the blank holder force and the thickness of the elastic cushion thickness. This is further demonstrated in Table 5.3.

Table 5.2 Strategy for the experiments and numerical simulations

| Exp. Run | Factor 1 | Factor 2 | Factor 3 | Response 1 | Response 2 | Response 3 | Response 4 |
|---|---|---|---|---|---|---|---|
| | A: Hole size | B:Cushion thickness | C:Hole-type | Wrinkling | Sheet metal Thickness | Thickness Variation | Maximum Deviation |
| 1 | 2.29 | 3.88 | Square | 1 | 1 | 0.003217 | 1.32 |
| 2 | 4 | 6 | Circular | 1.65 | 0.99 | 0.005451 | 0.56 |
| 3 | 3.71 | 3.88 | Circular | 1.5 | 1 | 0.003266 | 1.34 |
| 4 | 3.71 | 3.88 | Square | 1.5 | 1 | 0.003883 | 1.36 |
| 5 | 3 | 9 | Circular | 0.81 | 1 | 0.009041 | 0.89 |
| 6 | 3 | 6 | Circular | 0.79 | 1 | 0.003817 | 0.79 |
| 7 | 2 | 6 | Square | 1.15 | 1 | 0.006134 | 1.08 |
| 8 | 3 | 3 | Square | 0.65 | 1 | 0.00164 | 0.35 |
| 9 | 3 | 6 | Square | 0.79 | 1 | 0.007452 | 0.65 |
| 10 | 3 | 9 | Square | 0.34 | 1 | 0.009041 | 1.03 |
| 11 | 3.71 | 8.12 | Circular | 1.11 | 1 | 0.008974 | 2.11 |
| 12 | 2.29 | 8.12 | Circular | 1.45 | 1 | 0.007974 | 0.74 |
| 13 | 3.71 | 8.12 | Square | 0.5 | 1 | 0.007208 | 0.72 |
| 14 | 3 | 3 | Circular | 1 | 1 | 0.001983 | 0.68 |
| 15 | 2.29 | 3.88 | Circular | 1.5 | 1 | 0.003217 | 1.32 |
| 16 | 4 | 6 | Square | 1.65 | 1 | 0.007451 | 0.56 |
| 17 | 3 | 6 | Circular | 0.79 | 1 | 0.007817 | 0.78 |
| 18 | 2.29 | 8.12 | Square | 0.27 | 0.89 | 0.008356 | 0.06 |

Table 5.3 Factors and resulting P-values, [65]

| Response factors / Significant factors | Wrinkling | Thickness variation | Maximum Deviation |
|---|---|---|---|
| Cushion hole size (A) | 0.0001 | 0.0001 | 0.0001 |
| Cushion thickness (B) | 0.0021 | 0.0001 | 0.0001 |
| Cushion hole-type (C) | 0.139 | 0.3147 | 0.6715 |
| Parameter interactions | (AB)=0.3811<br>(AC)=0.0502<br>(BC)=0.0559 | (AB)=0.3538<br>(AC)=0.1273<br>(B×C) 0.0057 | (AB)=0.6338<br>(AC)=0.4373<br>(BC)=0.5472 |

## 5.2. Wrinkling

In MP forming, geometric inaccuracies could be split as two types. While the first error takes place prior to unloading (dimpling and wrinkling), the second occurs after unloading (thickness variation) [79]. Wrinkling effect of the two different hole-size with cushion thickness increases as the elastic cushion of a circular hole is used. This is demonstrated by Figure 5.4, which shows that wrinkling increases as the elastic cushion hole-size increases and the cushion thickness decreases.

In this case, the elastic cushion hole-size is much larger than the deformed cushion resulting in areas with direct contact between the pins and the sheet, which further resulted in areas with high developed pressure which increased wrinkling. The minimum wrinkling of 1.71 mm was achieved at an elastic cushion hole-size of 3.5 mm and a cushion thickness of 3 mm.

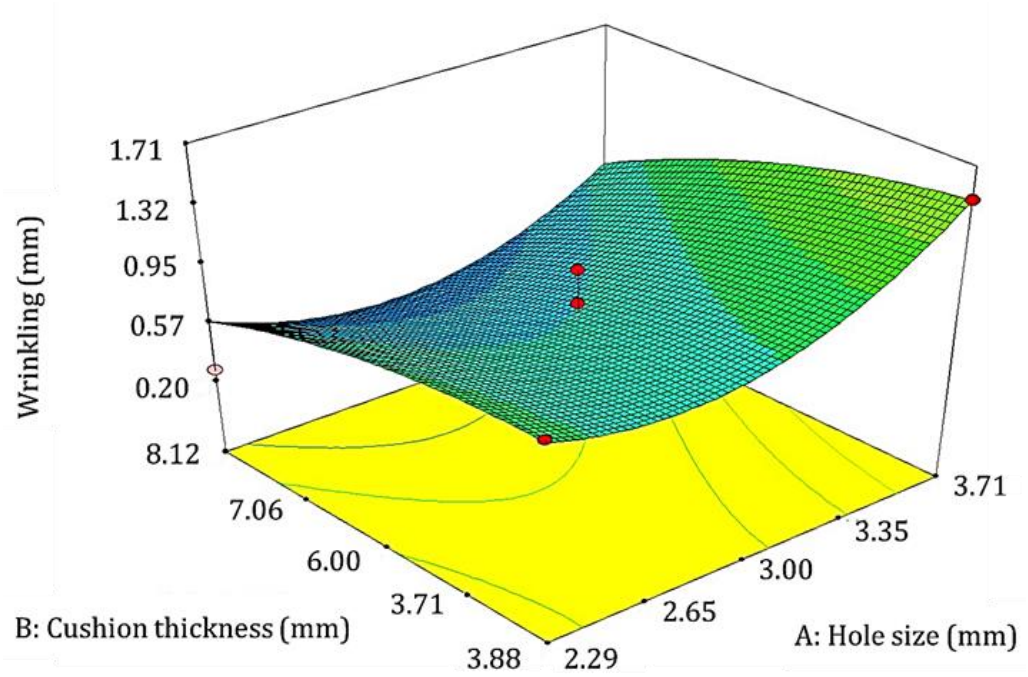


Figure 5.4 Effect of hole-size and elastic cushion thickness on wrinkling

### 5.2.1. Effects of Thickness Variation

Figure 5.5. demonstrates the influence of hole-size and cushion thickness on the thickness variation. It can be observed that the thickness variation increases as the cushion thickness increases while being slightly affected by the hole size. From the figure, it can also be noted that an increase in the radius of the curvature can have a major impact on the reduction of the thickness variation. This further indicates the improved thickness uniformity in the produced part. Moreover, the use of a larger radius of curvature, such as R400 mm, could mean that the workpiece shape is in connection with a greater number of pins at the start of the deformation procedure. This can lead to stress uniformity while reducing changes in the thickness.

Similar findings were also mentioned in earlier works [65, 76]. A minimum thickness variation of 0.017 mm was achieved at a hole size of 3.5 mm and cushion thickness of 3 mm. The use of a large hole-size elastic cushion can lead to an increased stretching deformation around the work piece, which can then further cause an increased change in the thickness.

Thus, the least change in the thickness variation can be achieved with the use of a large elastic cushion thickness with optimum hole-size and a reduced blank holder force.

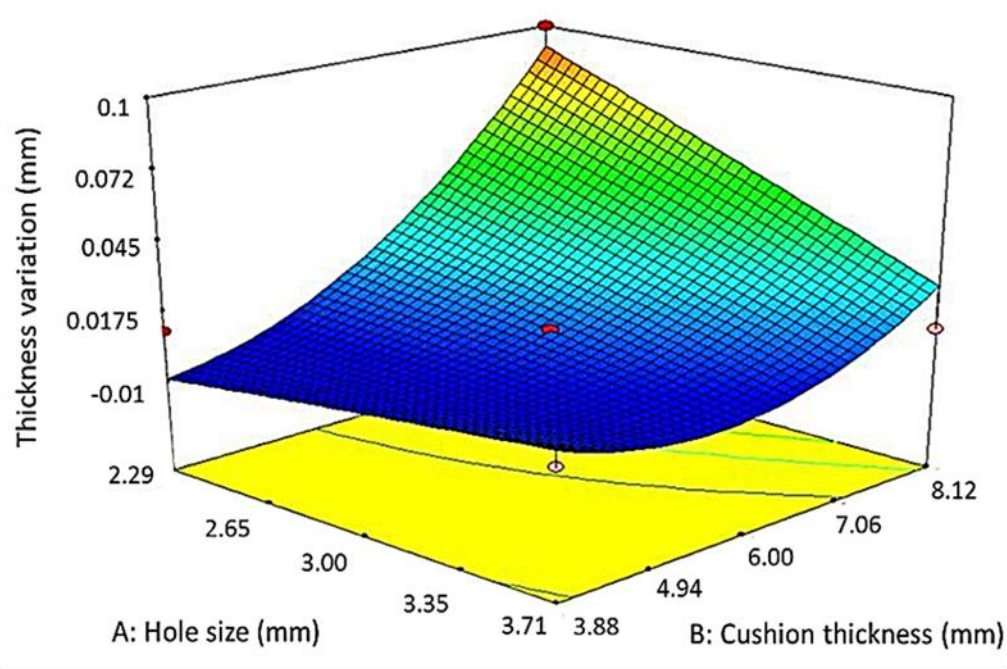


Figure 5.5 Effect of hole-size and cushion thickness on the thickness variation

### 5.2.2. Maximum deviation

Figure 5.6 demonstrates the influence of elastic cushion thickness and hole-size on maximum deviation of the deformed sheet. It must be noted that in such an event, any trivial change in the elastic cushion thicknesses can impact the local sheet thinning, therefore affecting the change in the thickness. With the use of thin elastic cushions, the local deformation occurring by each pin is observable. A minimum maximum deviation of 0.60 mm was achieved at a hole-size of 3.88 mm and cushion thickness of 3.01 mm.

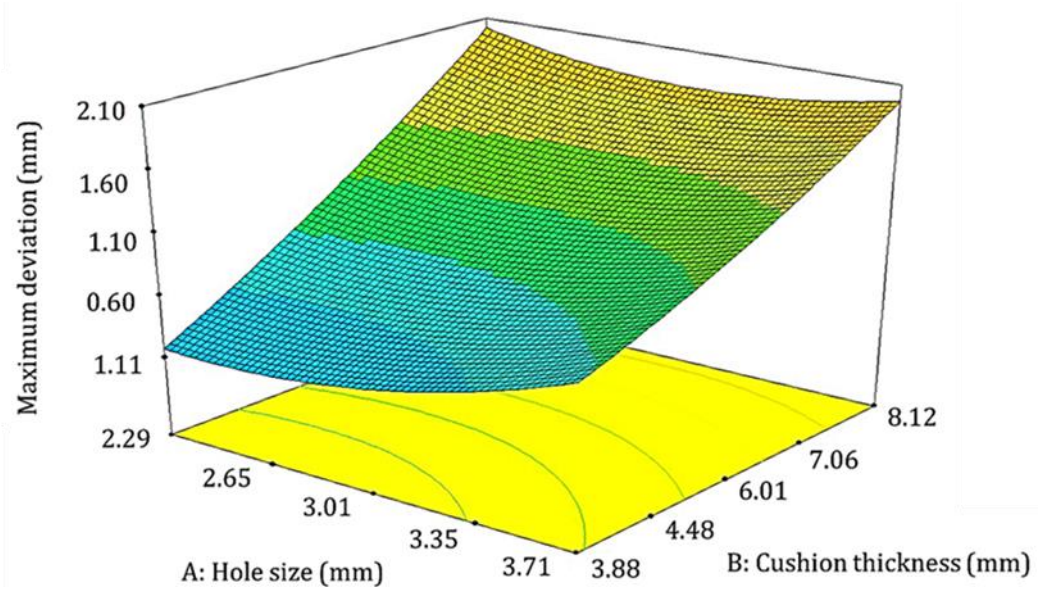


Figure 5.6 Effect of elastic cushion thickness and hole-size on maximum deviation

The use of a thick elastic cushion implies that the local deformation is marginal while the stress levels on the surface of the sheet lead to more uniformity. Also, the distribution of the mesh-type elastic cushion is improved around the work piece. On the contrary, the use of a thinner elastic cushion leads to the local deformity through each pin becoming obvious. This further causes a decrease in the uniformity of the stress distribution. At such a stage, any changes, regardless of the magnitude, in the force of the blank holder can infuence on the performance of the local sheet, therefore having an affect on the change in thickness [71].

### 5.2.3. Response factors

A theoretical equation was set to present the response surfaces (the wrinkling, thickness variation and the maximum deviation) as a function of hole-size and cushion thickness using Equation 5-3. This correlation was developed to base on the three process variables, as listed in Table 5.2. Table 5.4 lists the coefficient $x_1$ to $x_9$ for these varying process variables.

Response = b0 + b1A + b2B + b3C + b4AB + b5AC + b6BC + b7A2 + b8B2+ b9B2 (5-3)

In the above equation, X corresponds to a constant for a known response factor. A represents the hole size, B denotes the elastic cushion thickness and C symbolises the hole-type. Further,

x1 – x9 represent the model coefficients, as mentioned in Table 5.4. This type of correlation aids in predicting wrinkling and changes in the thickness variation upon any given arrangements of process controls.

Table 5.4 The value of each coefficient for objective functions, [65]

| Coefficient | Wrinkling (mm) | Thickness variation (mm) | Maximum deviation (mm) |
|---|---|---|---|
| Constant (X) | 1.84755 | 3.60633 | -0.02307 |
| x1 | -3.10900×10-3 | 1.16540×10-3 | -0.021315 |
| x2 | -0.13927 | 5.97254×10-3 | -0.022133 |
| x3 | 0.37777 | 0.56882 | -0.019781 |
| x4 | 3.00000×10-5 | 2.65000×10-5 | 0.010012 |
| x5 | -1.938E-004 | 1.763E-004 | 0.047207 |
| x6 | 4.000E-003 | -0.0143 | -0.018003 |
| x7 | 5.715E-006 | -3.201E-006 | 0.124241 |
| x8 | 3.144E-003 | 5.059E-003 | 0.383021 |
| X9 | -0.024222 | +4.54510E-003 | 0.0184457 |

## 5.3. Optimum parameters on multi-point forming

The use of response surface parameters aids in finding the optimal settings of the procedure variables where it is aimed to minimise the variations in sheet thickness, wrinkling along with maximum deviation, simultaneously. In order to achieve the abovementioned aim, the best possible setting for the process variables was obtained numerically by resolving the empirical correlation, Equation 5.3. The optimisation aimed to reduce wrinkling along with the changes

in the thickness. The model was further validated with the scanned geometry of the deformed part at the optimum process parameters. As shown in Table 5-5, the optimal simulation settings were: An MPF die with 10 mm pins size and with three optimum process parameters (DOE) restricted to within the preselected ranges. For experimental validation, the three-dimensional point cloud image of the formed part was captured using a FARO Edge 3D scanner [77]. In order to demonstrate the magnitude of deviation, as depicted by Figure 5-5, the structure measurements in the MPF tooling of the R400 curvature for the surface of the chosen part were carried out along with measuring the deviation in Y-direction. To measure the thickness at different points, a micro metre with a resolution of 0.01 mm was used at the centre of the formed part, in the X-direction, as demonstrated by Figure 5.5. The calculation of mean and standard deviations aided in representing the varying thickness, as demonstrated by Equation 5-4. The experiment was carried out using an A 90 solid cushion and a mesh-type elastic cushion, where the punch movement was 40 mm and the cushion compressor was operated at 40%. This is further detailed in Table 5-5. Based on the achieved results, it can be observed that model results agree well with the practical measurements.

Table 5.5 Optimum parameters achieved from computational simulations for the validation of experiments

| Parameter results | Hole type | Hole size | Cushion thickness | Wrinkling (mm) | Max. deviation (mm) | Thickness variation (mm) |
|---|---|---|---|---|---|---|
| Solid cushion | solid | solid | 3 | 3.1858 | 0.0358 | 0.019320 |
| Mesh-type cushion | square | 3.5 | 3 | 1.0741 | 1.7848 | 0.09850 |

$$\text{Thickness variation} = \sqrt{\frac{1}{N}\sum_{i=1}^{n}(x_i - \bar{x})^2} \quad = 0.01932 \qquad (5\text{-}4)$$

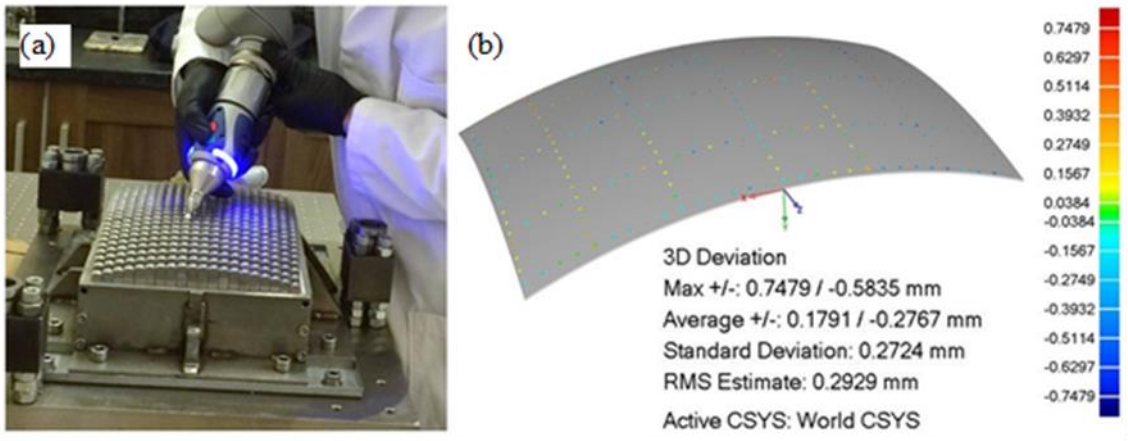


Figure 5.7 Curvature measurements for formed area on MPF tools

## 5.4. Thickness distribution and local strain on formed part

A FEA model was employed for studying the MPF procedure with mesh-type elastic cushion. The model consists of a pair of pins matrices, which form the die along with the punch, a blank sheet, and two sheets of mesh-type elastic cushion. Also, the pins of the die and punch are square shaped with hemispherical tips [78]. Figure 5.7 represents the FEA model and its components. SolidWorks was used to construct the model while the numerical simulations were carried out using ABAQUS Explicit.

As the model is symmetric, only one quarter of the model was used for simulations in order to speed up the computational time. ABAQUS, C3D8R quadratic element type was used in the simulation. The elastic cushion and blank sheet were modelled as deformable bodies while the lower and upper dies were simulated as rigid bodies using R3D4 as an element with the upper die moving along the Y-direction. The dimensions of the metal sheet were 155 mm × 100 mm × 1 mm while the elastic cushion was 155 mm × 105 mm × 3 mm. A maximum thinning was noticed at the midpoint of the sheet, which basically was the first point of contact with the pins [65]. Also, maximum thinning was noted at the transitional zone, which was in

the middle of the sheet middle and the starting of the forming area, as shown by Figure 5-7. The sheet in this area was open to increased expanding because of the clinching by the blank holder along with the punch pressing the sheeting into the die. Conversely, at the shorter side, O-Z, the thinning of the sheet occurs at the start of the forming area as this is the first point of contact for the punch and the sheet. This is further demonstrated by Figure 5.8 Consequently, thinning is observed at the centre of the formed part due to local stress levels [65]. Nevertheless, a slight thickening of the sheet occurred near the starting point of the forming area. As suggested by literature, [80], thickening occurs because of the compressive stresses which act perpendicularly to the drawn-in direction. This can be further based on the suppression of the movement of the material due to the blank holder, from the middle to the edges that were pressurised by the punch. In addition, the sides of the sheet were not lengthy neither the part height (400 mm) was enough for accommodating the movement of the material, thus resulting in thickening of the sheet.

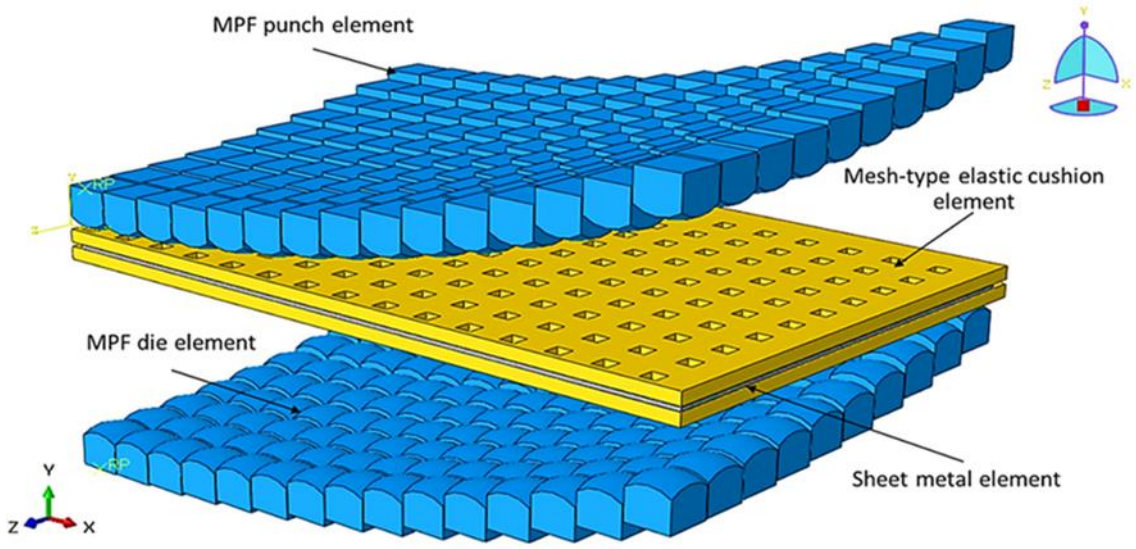


Figure 5.8 Simulation 3D model of MPF process with mesh-type layered polyurethane

To study the local strain distribution on formed part for two previous cases, the next step involved obtaining the local deformation measurements on certain elements to present the

deformation along selected paths O-X and O-Z. This step was essential to be carried out at the end of the loading step.

a). The sheet metal was divided into 5 layers and modelled by C3D8R eight-node brick FE C3D8R.

b). After FE simulation, the strain tensor $\boldsymbol{\varepsilon}$ in global coordinate system *x*-*y*-*z* at each integrating point was provided by ABAQUS directly and the strain, $\boldsymbol{\varepsilon}'$, in the local coordinate system, *x'*-*y'*-*z'*, was then obtained by:

$$\boldsymbol{\varepsilon}' = \boldsymbol{\beta}\boldsymbol{\varepsilon}\boldsymbol{\beta}^T \tag{5-5}$$

where, $\begin{Bmatrix} x' \\ y' \\ z' \end{Bmatrix} = \boldsymbol{\beta} \begin{Bmatrix} x \\ y \\ z \end{Bmatrix}$, and *y'* is in the normal direction (thickness direction), *x'* is in the tangential direction, as explained in Figure 5.13 and 5.14. Maximum thickening of the sheet occurring due to the blank holder area could be based on the material accumulating because of the holding force. This further restricts the flow of the metal at various angles, based on the magnitude of the clamping force. Figure 5.9 shows the boundary conditions and the meshing models. An explicit solver was employed in the simulation to avoid convergence problems because of the large number of elements used.

A) Boundary conditions B) Mesh model

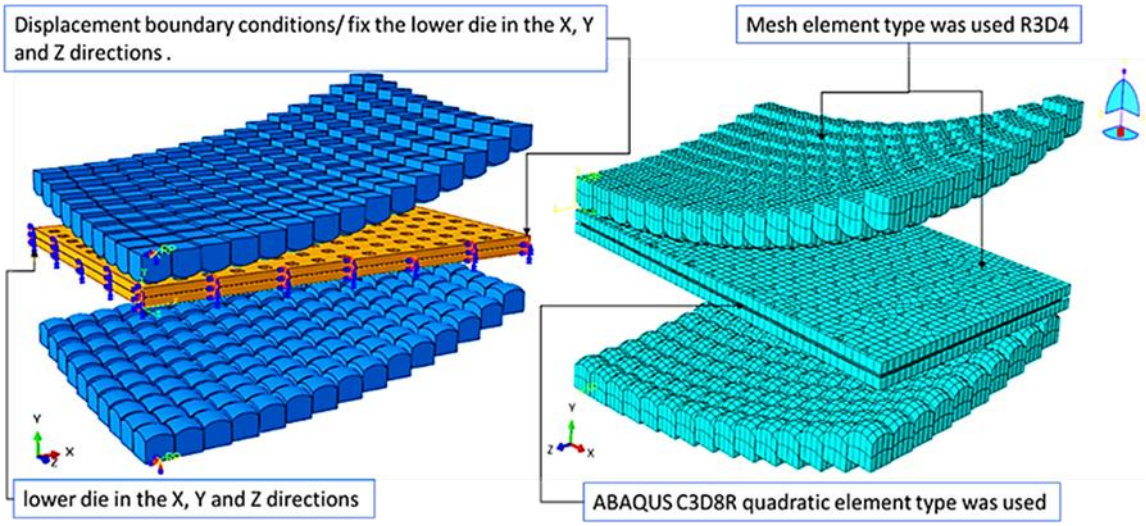


Figure 5.9 Boundary conditions and mesh of the MPF model

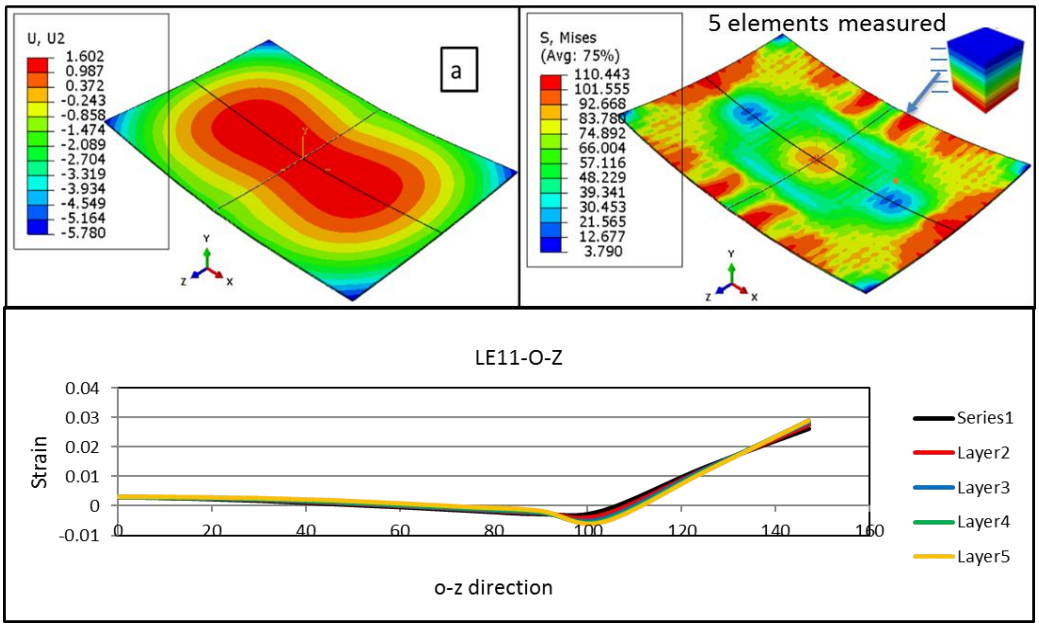


Figure 5.10 Curve deformation constant in the direction of O-Z

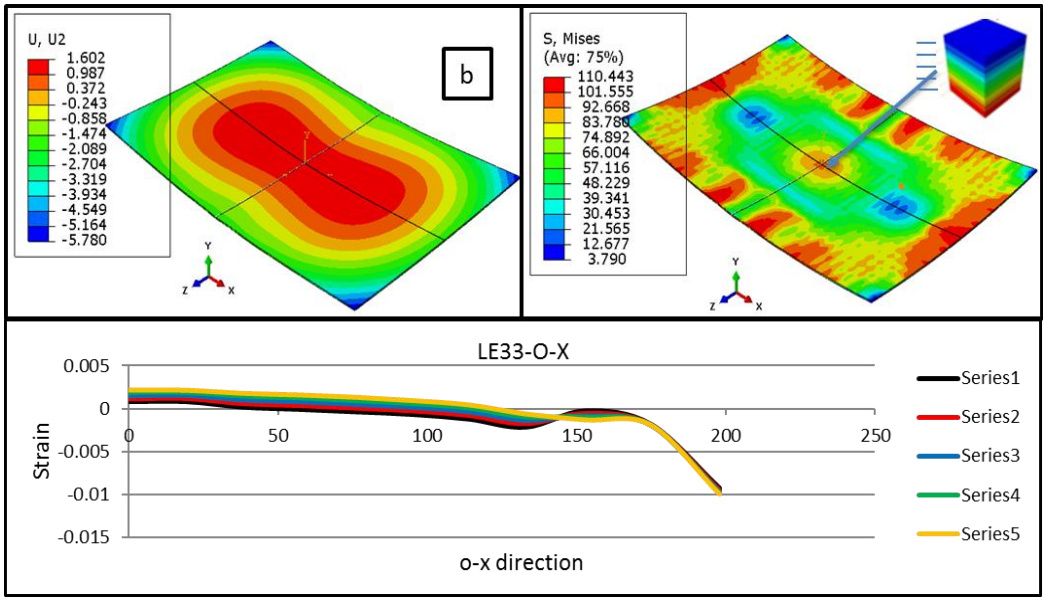


Figure 5.11 Curve deformation constant in the direction of O-X

The material in the transitional zone was directed to a tensile stress in the lower layer and compressive stress in the upper layer. This was because of the reverse bending effect which was somewhat also found by [57]. Furthermore, the strain values of LE22 and LE33 along the path O-Z, which are demonstrated in Figures 5.10 (a) and 5.11(b) also demonstrated a similar trend along the path O-X.

The sheet path deviation was evaluated with the use of a high-resolution CAM 2-point type at 300 points, around the sheet corner from A to B and with an internal line comparison of formed shapes with the targeted shape using a solid cushion and new model mesh-type elastic cushion wrinkling, as shown in Table 5.7 and 5.8. The results show the detailed wrinkling structural study of the experimental MPF die and FE simulations. Figure 5.12 presents the major results of the study by showing the resulting sheet geometry compared to the actual draw in curve scanned from a real part. It is apparent that the inclusion of the die deformations was essential for accurate simulation results in this case.

Figure 5.13 and 5.14 shows a comparison between the scanned profiles of two different experimental blanks (steel DC05) formed using mesh-type and solid cushions. The thickness distribution along the O-X and O-Z directions for experiment are shown in Figure 5.11 and Figure 5.12. The predicted wrinkling during the experimental run was 1.2 mm. This deemed as the most feasible case amongst all other simulations on mesh type-elastic cushion. In such a case, the radius of curvature was 400 mm and the deformation depth was larger as compared to the experimental run. As a result, increased expansion took place along with an increased deformation path. Consequently, an increased sheet thinning was also observed as compared to the experimental run 14.

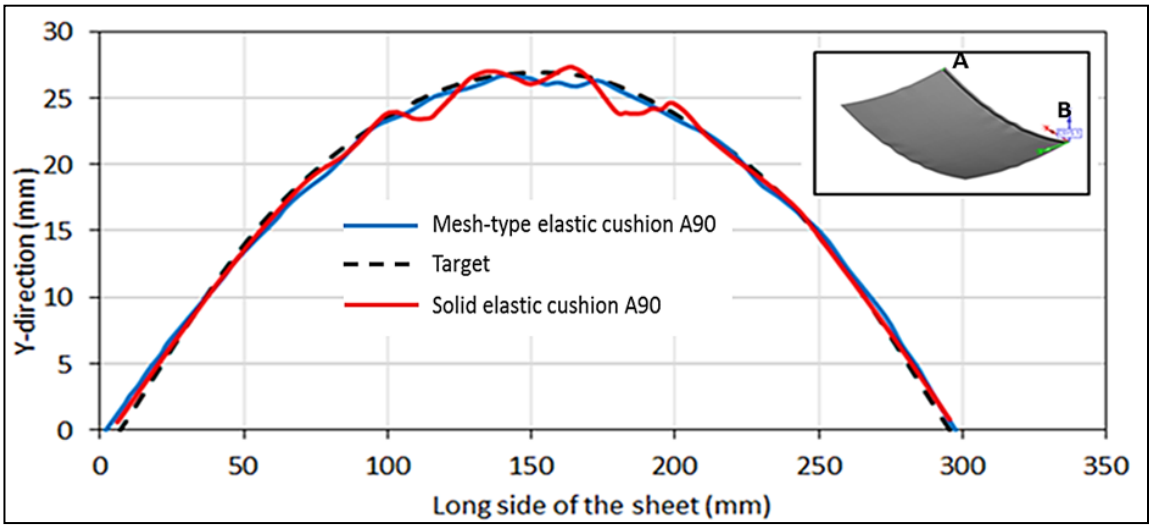


Figure 5.12 Wrinkling measurements for formed area

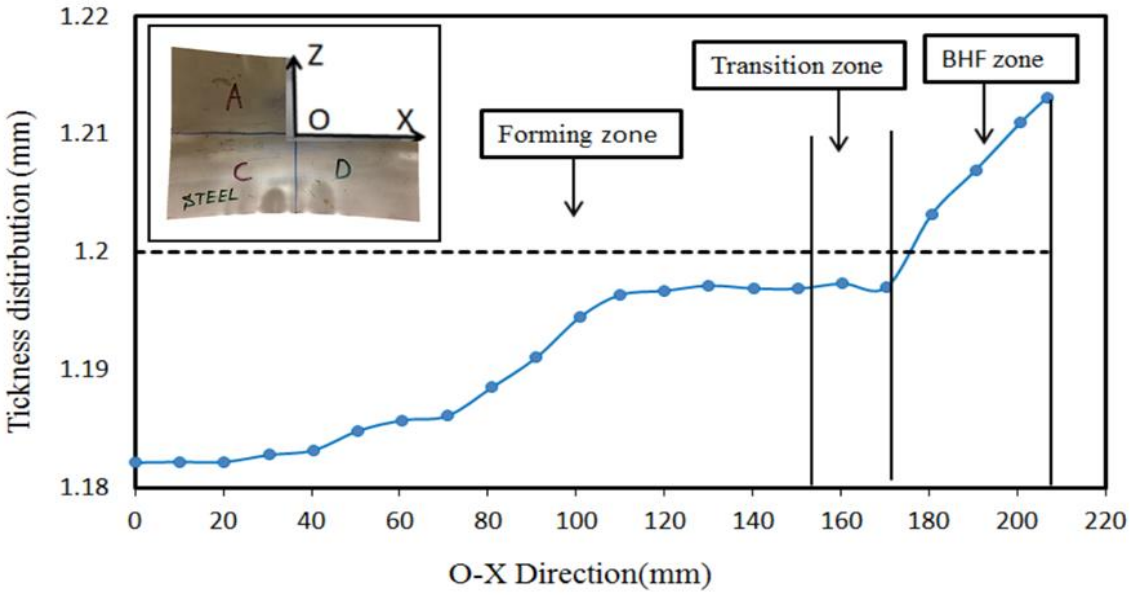


Figure 5.13 Experimentally formed shapes were measured at a thickness of 150 points on the corner and middle using a solid cushion

$$\text{Thickness variation} = \sqrt{\frac{1}{N}\sum_{i=1}^{n}(x_i - \bar{x})^2} \quad = 0.09850 \qquad (5\text{-}6)$$

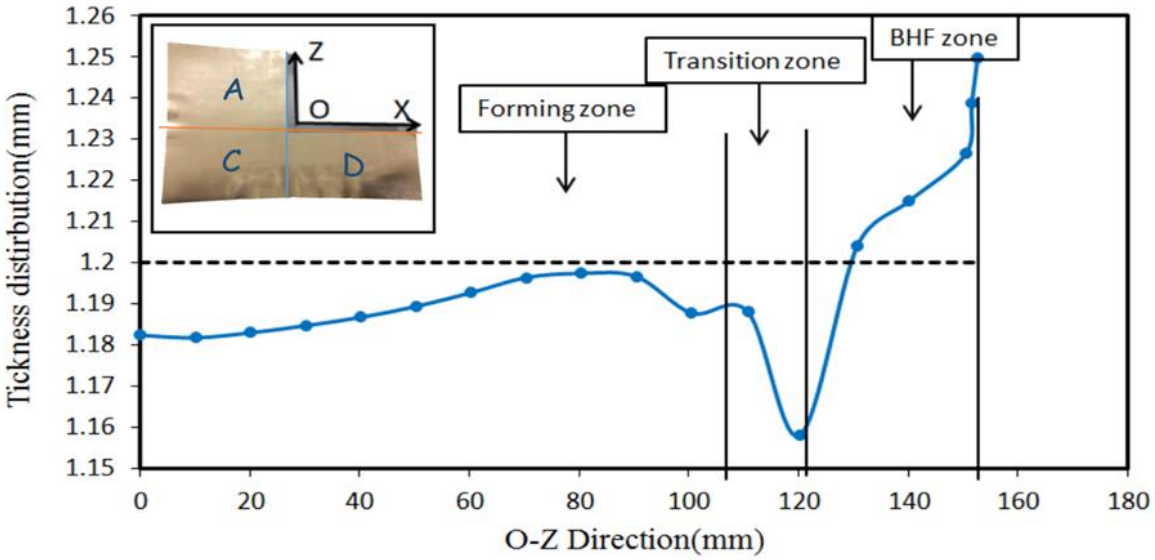


Figure 5.14 Experimentally formed shapes were measured at a thickness of 150 points on the corner and middle using a new mesh-type square hole elastic cushion

The standard for calculating thickness was:

$$\text{Thickness variation} = \sqrt{\frac{1}{N}\sum_{i=1}^{n}(x_i - \bar{x})^2} \quad = 0.01932 \qquad (5\text{-}7)$$

As shown in Table 5.7, the sheet formed using new design mesh-type elastic cushion is more in agreement with the target profile than the sheet formed using solid cushion. In addition, the thickness is clearly notable for the sheet formed using solid cushion. A schematic of the real surface calculated from the FEM simulation error is shown in equation (5-7), RMS 4.30%.

The experiments for the surface MPF with the A90 new model mesh-type indicated that the elastic cushion is effective for suppressing the local surface defects and reducing wrinkling and thickness variation, as shown by Table 5.6, where the numerical simulation results are credible.

Initial results from the experiment were successful; the 3.5 mm elastic cushion mesh hole-size is found to be the best among of the elastic cushion (square) holes methods, after testing for optimisation between the 2 mm and 3.5 mm holes.

Table 5.6 Experimentally selected polyurethane with the hardness of Shore A90, [2]

| Solid Cushion | Square hole type | Circular hole type |
|---|---|---|
| 300 × 200 mm | 300 × 200 mm | 300 × 200 mm |
|  | 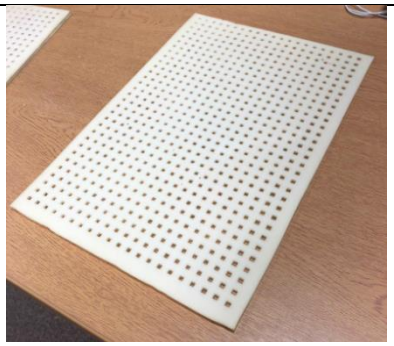 | 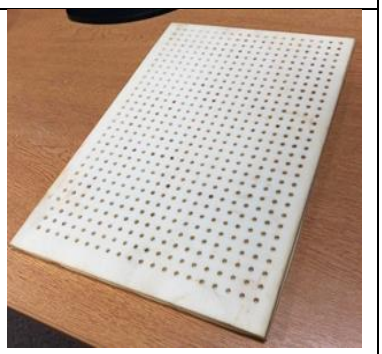 |

Table 5.7 Predicted and measured response parameters' effect of new model mesh-type suggested the use of square hole elastic cushion was better, [65]

| | Wrinkling [mm] | Max. deviation [mm] | Thickness variation [mm] |
|---|---|---|---|
| Predicted | (2.08900E-007)≈0 | 1.0267 | 0.1000 |
| Measured | 1.0741 | 0.0358 | 0.01932 |

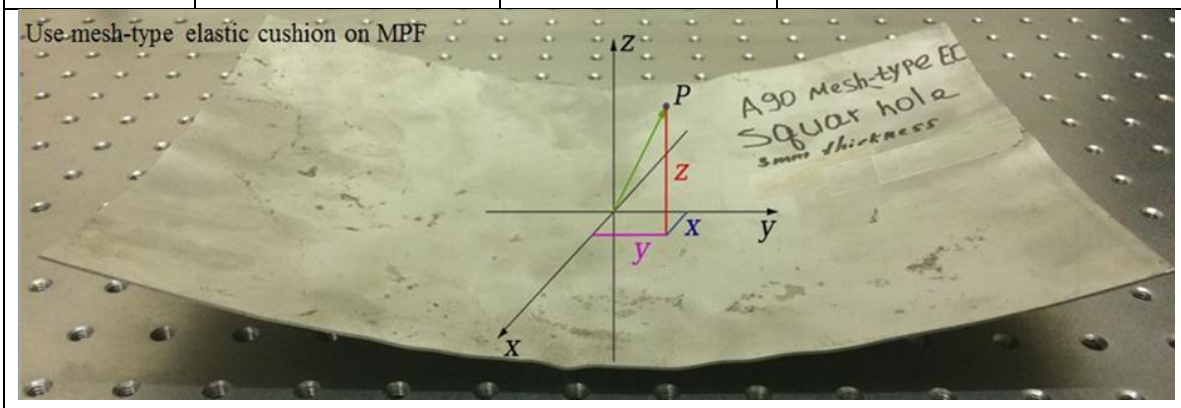


Table 5.8 Predicted and measured response parameters' effect on solid elastic cushion, [65]

| | Wrinkling [mm] | Max. deviation [mm] | Thickness variation [mm] |
|---|---|---|---|
| Predicted | (2.08900E-007)≈0 | 1.0267 | 0.1000 |
| Measured | 3.1858 | 1.7848 | 0.0985 |

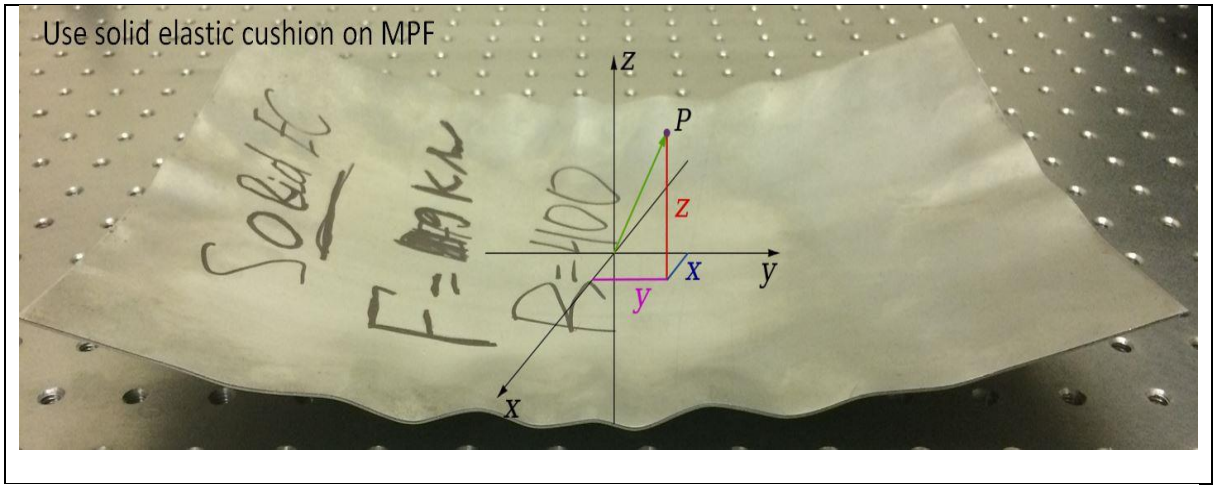


## 5.5. Summary

To conclude, the sheet metal forming was tested (best-fit alignment) and the results corresponded effectively with the finite element modelling results. Therefore, a comparison between the scanned profiles of two different experimental blanks (steel DC05) formed using mesh-type and solid cushions was made. A large difference between the estimated values of the solid cushion and the new model mesh-type elastic cushion were perceived.

Experimental and numerical results demonstrate various effects of significant wrinkling:

The most important effect of the deformed shape accuracy was on the forming curvature and sheet thickness.

The corresponding parameters of the elastic cushion such as measured hardness and thickness variation, maximum deviation and wrinkling are determinative on MPF. However, it will make the PEG (punch element group) complicated and expensive.

A FE model, which considers the size effects, has been developed to simulate the elastic cushion on the MPF sheet metal forming process. More varied elastic cushion types and conditions are currently being investigated as a part of this research and further research on the effect of MPF parameters on attenuation and accuracy of the models is ongoing. DOE is an important step in order to ensure that optimum parameters are chosen. The response

surface parameters DOE were chosen for optimum parameter cushion thickness and to optimise the dimensions of the elastic cushion holes (square 3.5mm and circular 3.5mm) as these tend to significantly affect thickness variation and maximum deviation on MPF.

# 6. CHAPTER 6 DEVELOPMENT AND OPTIMISATION OF MESH-TYPE ELASTIC PUNCH

## 6.1. Introduction

This chapter discusses a possible way to improve the production of doubly curved parts. To do so, a new formation approach has been implemented, which involves the replacement of the upper pin matrix through a rubber punch. This rubber punch is relatively thick in size and is used for the formation of a doubly curved part from a steel sheet. In order to understand the corresponding effects, the influence of the hole-type rubber punch was explored in terms of the standard of the part formed. This was achieved by investigating the overall wrinkling, thickness variations and compression ratio of the formed part (40%, 60% and 70%). In order to validate the above-mentioned approach, an experimental study was performed as well. This would also help in comparing the results achieved from the new setup with the traditional MP forming results. Further, an optimisation was performed for investigating the dimensional and compression ratio effects of the hole-type rubble punch along with the radii of the formed curved and the overall process quality, which concerns the wrinkling, thickness and maximum deviation.

Accomplishing a quality forming process with a distinctive formed sheet panels would require a deep understanding on the structures of the tools used in terms of the punch and dies and the application force in terms of the formed sheet and the blank. Failure in the adequate designing of any of these tools may result in serious problems with the dimensions. Hence, a wide variety of tooling approaches have been implemented to overcome these potential issues in achieving appropriate shape features. Recently, tooling manufactures have attempted to utilize elastic pads. These include rubbers and polyurethanes with a hardness of A90 inside a rigid container. This approach is usually adopted in the studies of aerospace engineering for relevant applications including the formation of short-runs of light-metal parts. Although there are a

few limitations associated with the use of this flexible formation approach, it has a couple of advantages as well.

The use of a rubber punch for forming of a metal sheet can improve the resulting finish of the product [82]. In addition, this reduces the tools costs. Also, the tools are easy to be altered in a newer shape without requiring any alignment or having any mismatch problems. Further, the use of rubber punch is able to reduce material thinning [83]. Interestingly, the same setup can be used for forming another material with varying thickness [84]. Along with these favourable qualities, polyurethane is an excellent material, which possesses superb physical properties as it has an elastic-like property similar to a rubber and the toughness along with durability comparable to metals [85]. Nevertheless, the use of a rubber elastic punch for forming sheet metals may have some associated drawbacks. These include the finite longevity depending on the process variables for producing final parts, which have adequate features and the punch's suitability for low production or prototype specimen [86].

[82] provides an extensive literature review on the use of flexible tools for the formation of sheet metal. Another study [87] explored the ability of flexible dies in producing defect free parts. Moreover, their study was also able to optimize the relevant process variables in order to achieve the optimum setup. [88] performed an investigative research on the flexible forming processes of steel and aluminium tubes through bending variables. These variables included the bent radii, the effect of rubber properties and roller radii.

Their study revealed that rubber hardness is a crucial property, which has an influence on the bent radii. Further, a study [89] looked into the formation of thin sheets of aluminium alloys using several flexible die shapes and materials. Their work suggested that better results may be achieved in terms of forming if rubbers with higher hardness levels were used. Another study [90] studied of the effects of process variables such as forming speed and compression ratio of the rubber in the deformed part. Their study suggested that the wrinkling change in

the rubber forming process was of a reduced amount as compared to the traditional sampling method. One study [91] shows the importance of selecting a material with adequate harness levels for the elastic punch A90, which can result in the elimination of the defects from the produced part. [92] applied a new theoretical model to study the static and kinematic functions in the elastic pads forming approach. Their study showed a good agreement between the experimental and numerical results.

## 6.2. Tooling setup of the Mesh-type Elastic Punch Multipoint Forming (Mesh-type EPMPF) approach

A Finite element model was developed to study the rubber punch MPF is a sheet metal forming approach where a mix of both, the rubber pad and multipoint forming are adopted to acquire the benefits of these two techniques. In order to confirm the significance of the hole-type rubber punch MPF die process, this study designed an experimental model.

As a first point, the time taken to set the tools for designing was much less than the time needed for setting up in conventional multipoint forming. Additionally, there was no need of the alignment method, which is used in the conventional MPF for tooling. Further, a load cell with known ability was utilised in synchrony with a distance sensor positioned on the press plate for measuring the punch movement. This design is illustrated in Figure 6.1. Optimum process variables were selected for yielding a product with a spherical shape which had nearly no signs of wrinkling and minimum shape deviation along with thickness. The FEM base features of this new method to produce a double curved panel are highlighted in Figure 6.2.

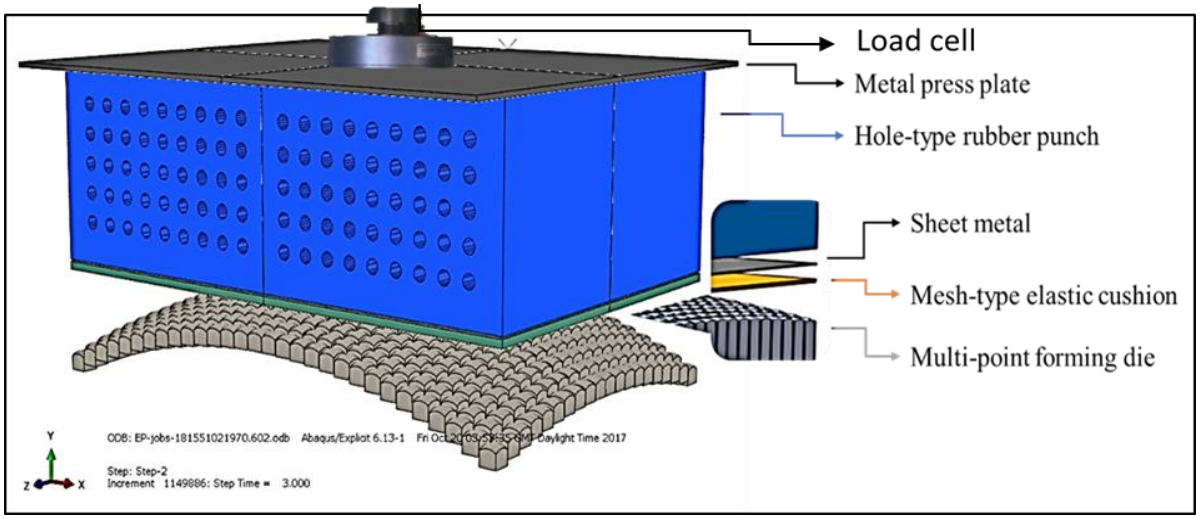


Figure 6.1 Illustration of FEM tools of the hole-type EPMPF Setup

To study wrinkling, FE simulation (ABAQUS) of 30*20. matrix of punches for spherical shape (square pin10 mm) have been carried out using elastic cushion with hardness (Shore-A95) and different thicknesses (3 ,6 and 9 mm) with high strength steel, (PD600).

- Using mesh-type elastic cushion to suppress dimpling on lover die.
- Using with container to eliminate wrinkling.
- Assessment of optimum forming parameters influencing wrinkling in MPF
- Measuring multi-point (MP) forming die, using coordinate measuring machine CMM tools.

To meet this objective of the study, the list of steps adopted for this numerical study are provided in Figure 6.1. As the model is symmetrical, only one quarter of the model was utilised to speed up the computational time. The sheet and elastic cushion were modeled as deformable bodies and C3D8R quadratic element type was used. The element size is 1-mm and a total element is 278,602 were used to mesh one quarter of the deformed sheet, while a total of elements is 87.280 were used for the elastic punch. The elastic punch thickness size of 100 mm was recommended in previous investigation [93].

## 6.3. Finite Element simulation of multipoint forming (MPF) die model development for hole-type rubber punch optimization

The FE model adopted for simulating this new approach of hole-type rubber punch MP die forming is reported in this section. Also, the investigation on the deformed part's quality with regards to the sheet metal, thickness and wrinkling is highlighted in this section. Steel-DC05 was used for the new approach in the production of the double curved parts. The hole-type rubber punch FE model utilises the MP forming die along with the metal sheet, the mesh-type elastic cushion, hole-type rubber punch without the container using the two types of elastic rubber punch materials with the hardness of Shore A65 and Shore A90 because of the increased hardness levels of polyurethane Shore A90 as well as the press plate, as demonstrated in Figure 6.3.

In order to decrease the computational times and resources, this study considered only a quarter of all the model components due to the symmetric nature of the models, which allows for scalability. The MP forming die was a compound of 300 × 200 pins with a spacing of 0.25 mm. This die is used in producing doubly curved parts with varying curve radii. Each pin of the compound consists of a cross section of 10 × 10 mm and a tip radius of 10 mm. Polyurethane (A90) is known as a hyper elastic material, which can be used for the hole-type punch as well as the mesh-type elastic cushion in the numerical simulations. To define the association between the stress and strain of the rubber, the Mooney- Rivlin model was chosen [93, 65]. Figure 6.2 demonstrates the FE modelling of EPMPF approaches.

| Using the two types of elastic punch materials with the hardness of Shore A65 and A90 | Name of parts |
|---|---|
| 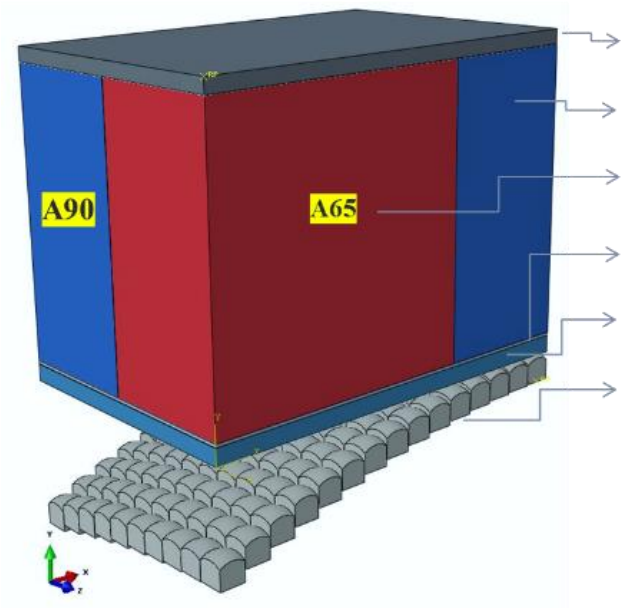 | A. Press metal plate<br>B. Elastic punch A-90<br>C. Elastic punch A-65<br>D. Metal sheet<br>E. Mesh type elastic cushion A-95<br>F. Multi-point forming die |
| Elastic Punch with hole, the hardness of Shore A90 | Name of parts |
| 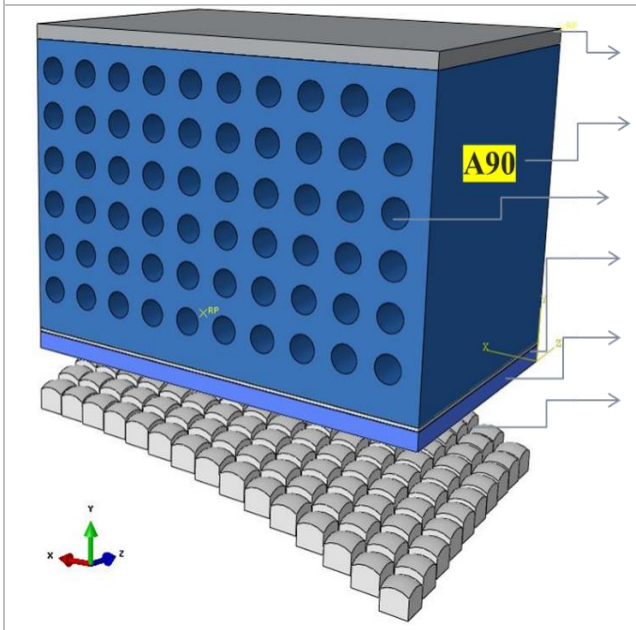 | A. Press metal plate<br>B. Elastic punch A-90<br>C. Elastic punch holes<br>D. Metal sheet<br>E. Mesh type elastic cushion A-95<br>F. Multi-point forming die |

Figure 6.2 FE modelling of EPMPF approaches

While the sheet used was 153 mm × 102 mm × 1.2 mm in size, the mesh-type elastic cushion was 153.5 mm × 102.5 mm × 6 mm in size and the rubber punch was 153 mm × 102 mm × 100 mm in size. Deformable solid cells were used to model these 3 components. A symmetry boundary condition was used for these 3 components as the assembly was assumed symmetrical. In addition, the MP forming die node at the end of the symmetry was positioned in the XYZ directions. Also, as stated earlier, the hole-type rubber punch was not fixed in a rigid box. Hence, the application of the forming load was made in the Y direction, as demonstrated in Figure. 6.3.

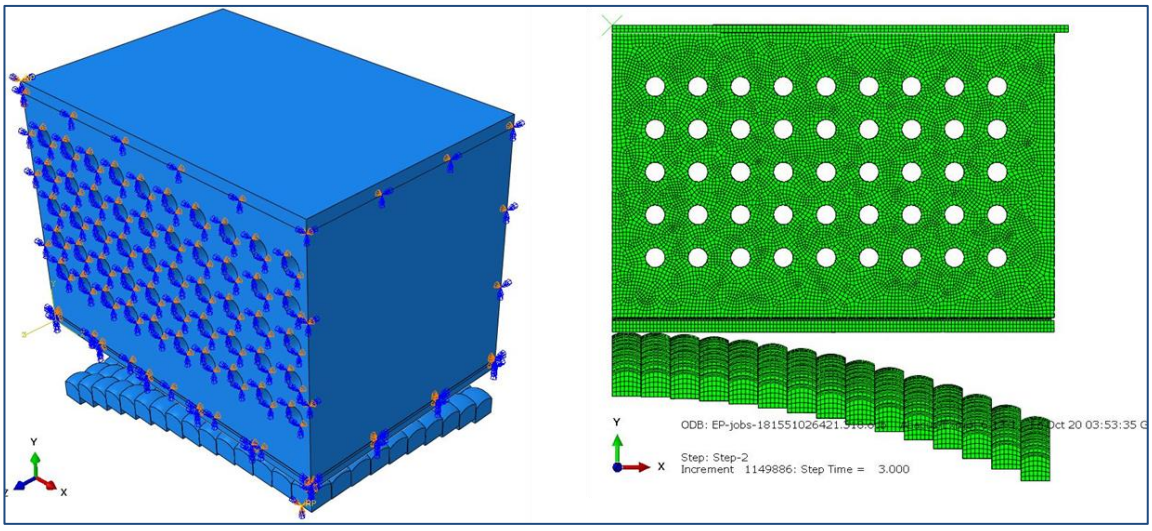


Figure 6.3 For the FE model, the hole-type rubber punch elements along with boundary conditions

## 6.4. Results and discussion

The FE model was designed for the double curved parts with a radius of 400 mm. This model was examined with the use of ABAQUS. Figure 6.4 demonstrates the achieved pressure distribution on the top and bottom surface of the sheet after the completion of the forming process. Both, mesh-type elastic cushion and hole-type rubber punch approaches are shown in the figure. Also, increased bending deformations are needed [65]. As illustrated in the figure, the stress pressure states of the formed part with the hole-type rubber punch on MPF

die technique are well-distributed as compared to the stress pressure produced using the MP forming punch.

MPF mesh-type elastic cushion

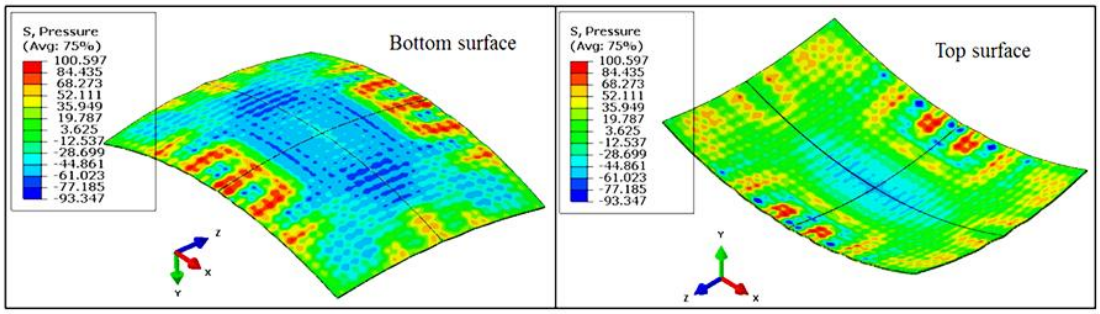


MPF hole-type elastic punch

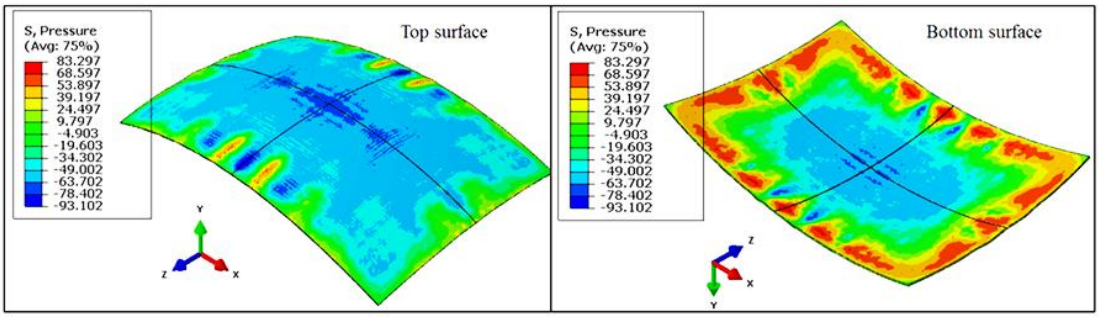


Figure 6.4 Distribution of pressure on the bottom and top surfaces of the part formed at a step prior to wrinkling through the mesh-type elastic cushion and hole-type elastic punch method for the (R=400 mm) curvature

The reason is due to the hole-type rubber punch being deformed along with the metal sheet through the process of loading. This indicates that the relative movement between the punch and the sheet was extremely small and thus the effect of friction is null. The multi-point forming punch is rigid in nature, hence the relative movement at the interface is much higher and the existence of frictional forces hinders the flow of the blank material, especially in cases which involve an increase in the friction coefficient [97]. Further, this resulted in stress instability and wrinkling [65, 76]. At the mid of the long side edge, for both cases, it is apparent

that the stresses were able to fluctuate within the minimum and maximum bounds, which mainly resulted in wrinkling [65, 76, 78].

The wrinkling waves are lesser in the case of the hole-type rubber punch as compared to the MP forming punch. In case of the greater radii of the formed curve, 400 mm, which needed less bending deformations, the results are presented in Figure 6.5. The pressure distribution is more uniform, which is the main parameter to regulate wrinkling and thickness variation, on the top and bottom surfaces of the formed part by hole-type rubber punch MPF die as compared to the the part produced by the MP forming punch.

This results in stress stability with the vanishing of wrinkling waves and decrease in wrinkling along with thickness variations in the formed part than the results of the formed part created using MP forming punch.

### 6.4.1. Modelling of two different geometries in the MP process for the accurate prediction of the wrinkling defect

The numerical outcomes of the formed part with the 400 mm radii curvature resulted by MP forming and hole-type rubber punch on MPF die demonstrate that wrinkling can be meaningfully decreased with the use of a hole-type rubber punch, which has a Shore hardness A90 [91], as demonstrated by Figure 6.5.

Wrinkling was measured as the distance amid the formed and target shapes at each wrinkling wave. This is illustrated in Figure 6.6, along with the procedure of measuring the wrinkling value between designed part and the part produced by two techniques.

The numerical value of wrinkling was determined using the root mean square error (RMSE), as shown by equation 6.1.

$$RMSE = \sqrt{\frac{1}{n}\sum_{i=1}^{n} x_i^2} \tag{6-1}$$

In equation 6.1, the number of wrinkling waves is represented by the variable n. The difference between magnitude of wrinkling wave and target curve for the $i^{th}$ wrinkle peak is denoted by$x_i$.

The value of RMSE was 0.506 mm when hole-type rubber punch was used whereas it was 1.20 mm when MP forming punch was used. This was recognised as a major decrease.

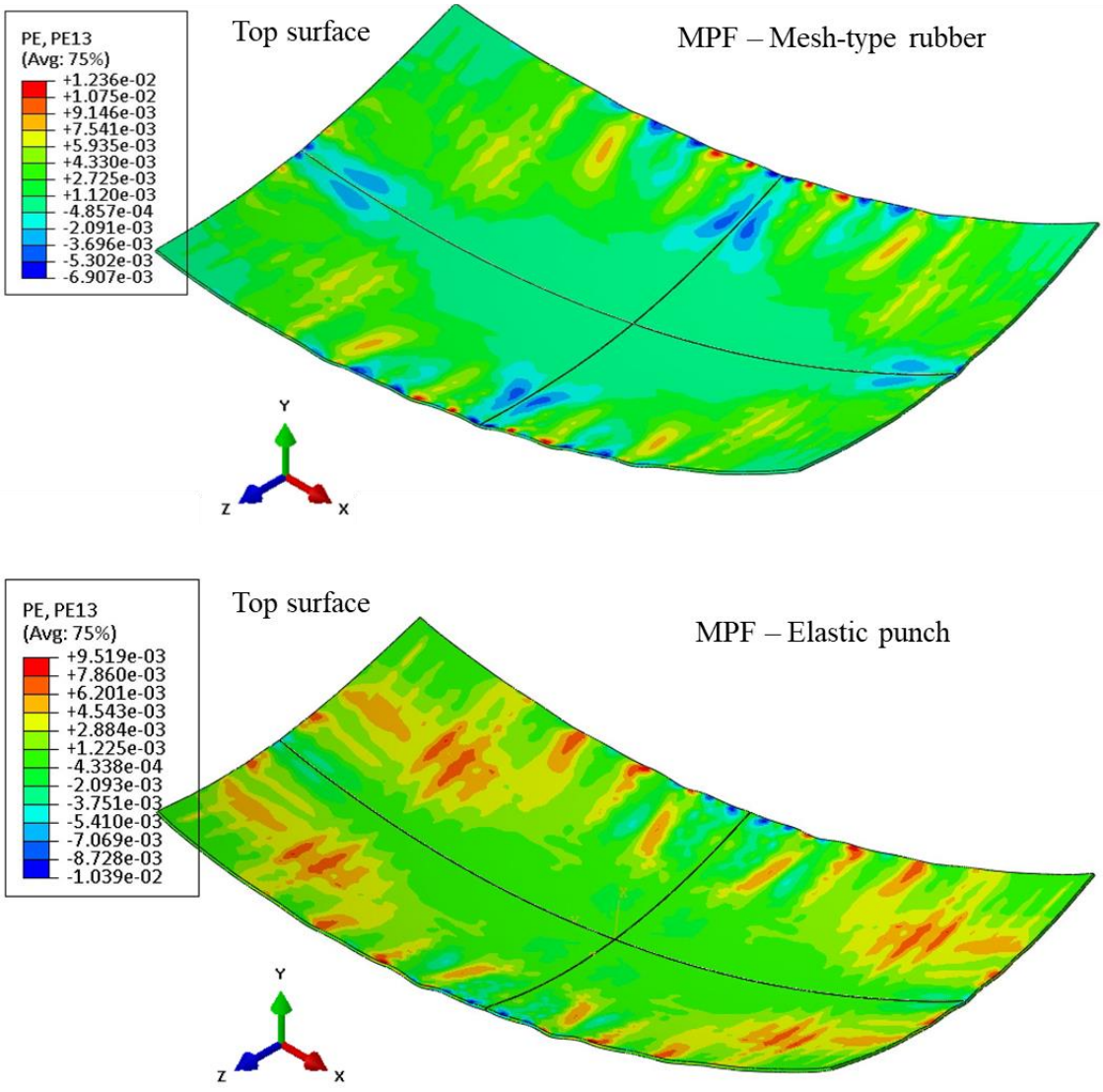


Figure 6.5 Wrinkling simulations at formed part with the use of two different techniques (R = 400 mm)

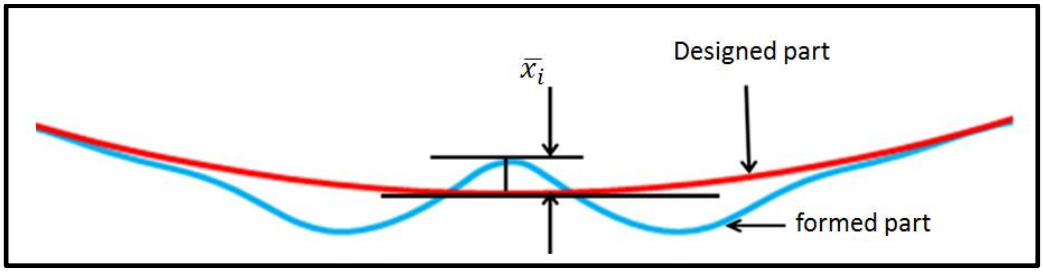


Figure 6.6 Method for measuring wrinkling with respect to target designed part

### 6.4.2. Characterisation of wrinkling in hole-type elastic punch on multi-point forming die

The deformed part with 400 mm radius was analysed using the new technique. The results obtained using the new technique were compared with MP forming punch technique. A comparison between the final part and wrinkling part was undertaken to study the effect of hole-type rubber punch. Hole-type rubber punch on MPF die and mesh-type elastic cushion MPF are shown on Figure 6.7. The figure displays the simulation results, obtained using the two techniques, for wrinkling in the part with radius of 400 mm at the curvature. The total wrinkling of 1.86 mm was noticed when simulated using MP forming die, this simulation is represented in Figure 6.5 mesh-type elastic cushion. At the same time Figure 6.5 hole-type elastic punch, illustrates the wrinkling result of 0.58 mm simulated using the hole-type rubber punch (A90). The wrinkling on the elastic punch was significantly affected.

At the tip of the pins more concertation is noticed which is influenced by the thickness of the elastic cushion and its properties. In determining the wrinkling phenomena, major importance was given to the results obtained for uniformity of stress distribution on the final formed part. It was noticed that more uniformity on the friction condition results in less thickness variation [90, 98].

Figures 6.7. shows the comparison between target shapes, simulated shape at the end of applied force (pre-wrinkling) and the shape post- maximum deviation for the two forming techniques on the FE model with compression ratio of 70%.

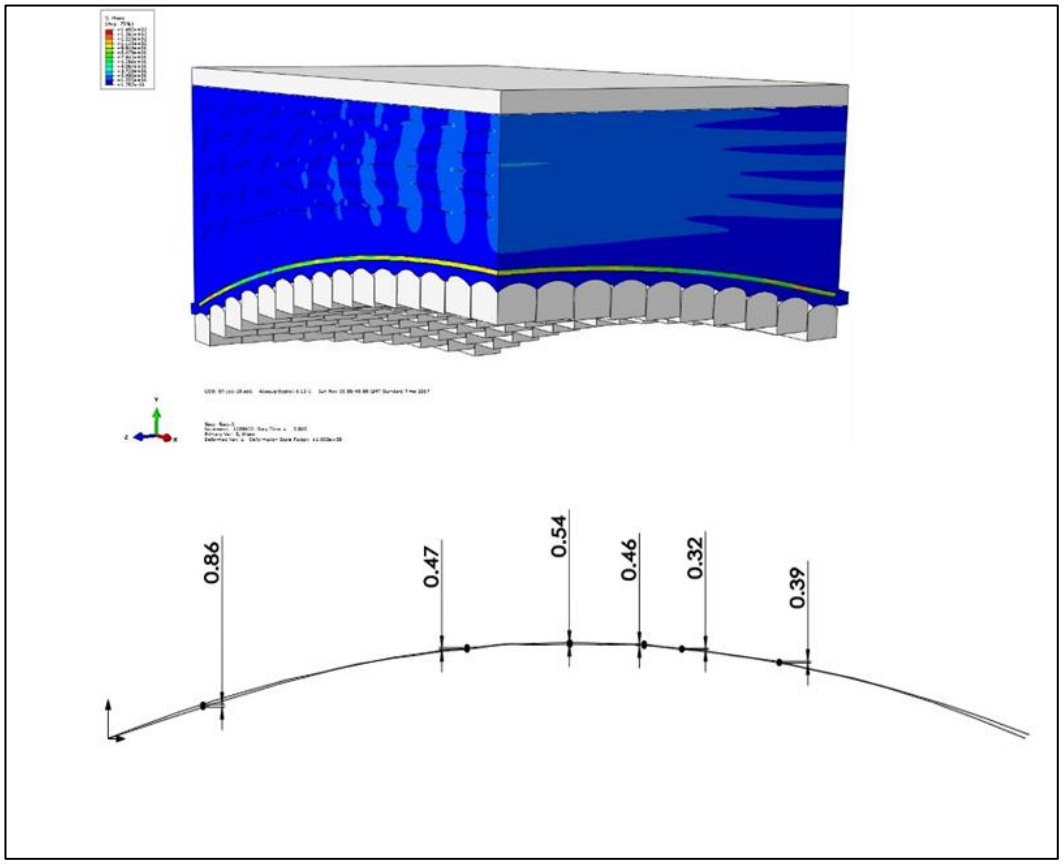


Figure 6.7 Maximum deviation of part formed by hole-type rubber punch MPF die

$$RMSE = \sqrt{\frac{1}{n}\sum_{i=1}^{n} x_i^2} = 0.506 \text{ (mm)} \qquad (6\text{-}2)$$

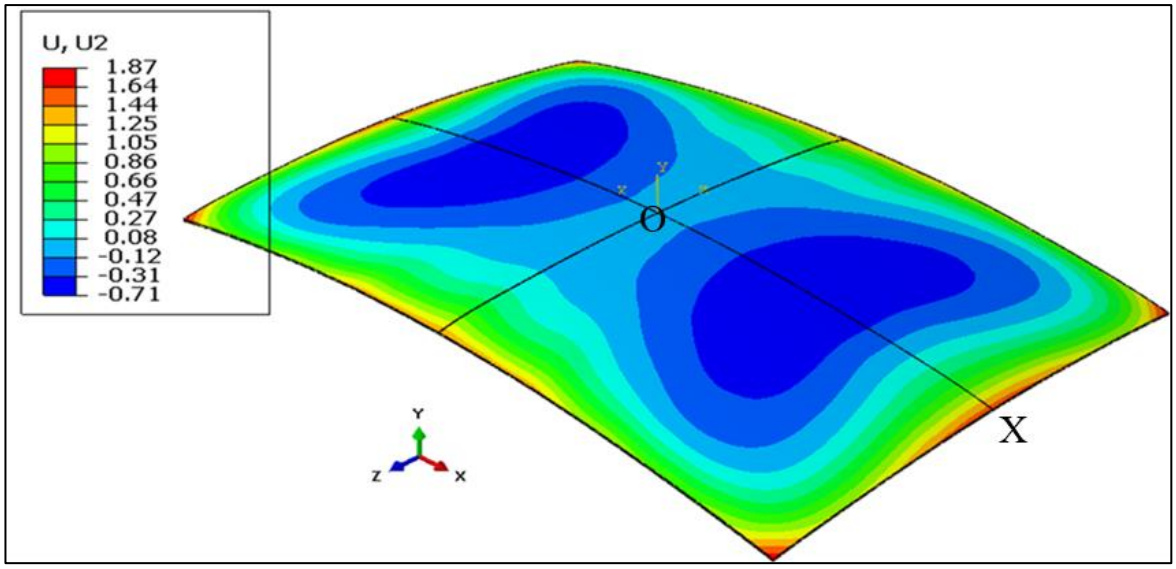


Figure 6.8 Numerical results in terms of the optimal process variables for wrinkling

Figure 6.7 was used as a guideline to determine the line O-X in order to understand the process which takes place at this position, such as wrinkling. The achieved line from the simulations was compared with the target curvature. Figure 6.8 shows the numerical results in terms of the optimal process variables for wrinkling.

The simulation results, along with the target shape of the final part are compared in Figure 6.9, a good comparison can be noticed between final results of deformed sheet (R = 400 mm) on hole-type elastic punch. The optimal values of process variables were used for the parameters. The RMSE was utilised for conniving a numerical simulation for wrinkling Figure 6.10 [65]. For the formed part, the capture points (i.e. components A-B) were related to the ideal shape. Also, the thickness deviation along the path O-B was considered to symbolise the wrinkling [93]. This is also demonstrated in Figure 6.11 and Figure 6.12.

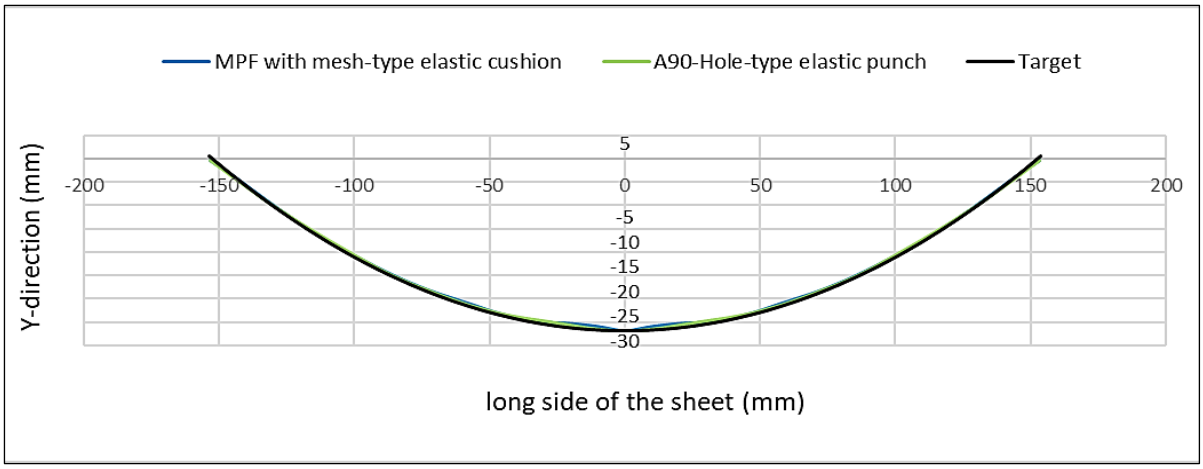


Figure 6.9 Simulation of the wrinkling for deformed part (R = 400 mm) on hole-type punch at edge

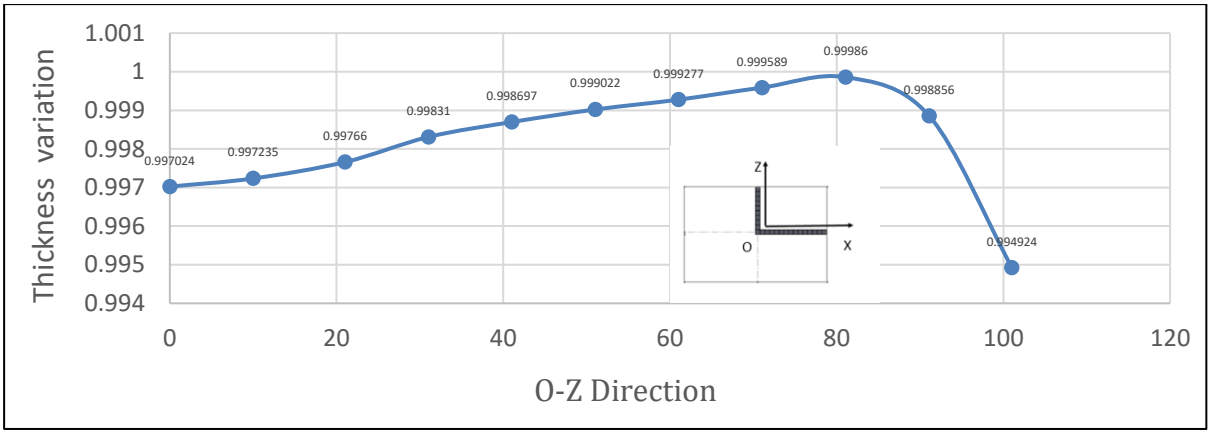


Figure 6.10 Thickness of formed part along path O-Z (R = 400mm)

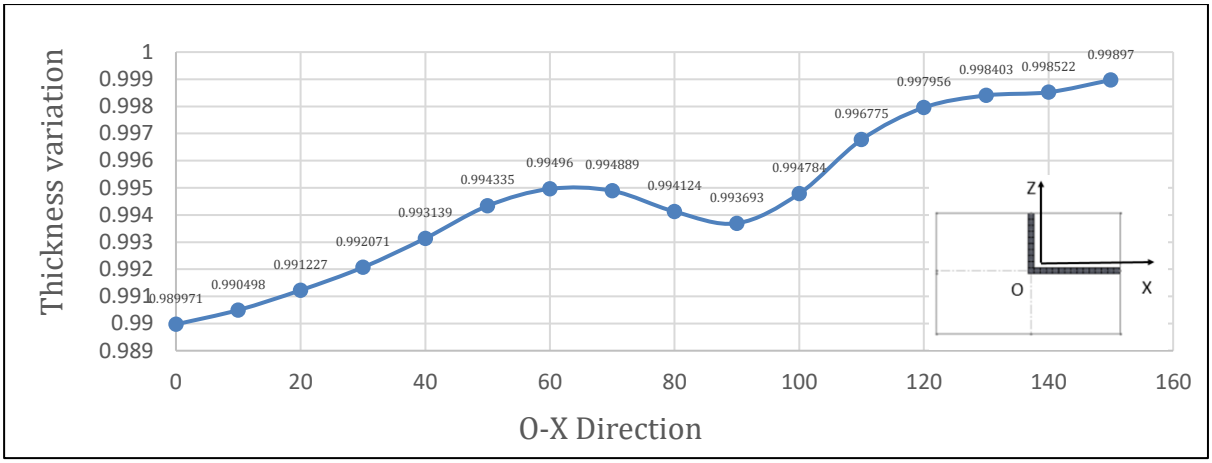


Figure 6.11 Thickness of formed part in the direction O-X (R = 400mm)

The forming technique with the use of a hole-type punch can be split in three stages. While the primary stage involves the self-deformation of the hole-type rubber, the secondary stage includes the deformation of the sheet under the application of the forming force up till the sheet shapes into the MPF die cavity. The last stage in this forming process involves the un-loading step, which is basically the load release.

With these process variables and settings, the simulations were performed for the low radius of the forming curvature.

### 6.4.3. Comparison of forming load for hole-type rubber punch on MPF die

The simulation set-up adopted in this study for the hole-type rubber punch with MPF die tools for higher compression ratio (%) is shown in figure 6.2. The radius of the formed curvature was 400 mm. In terms of the experimental results, these agreed well for the new approach with [65], which used same parts created by the MP forming process. The parts produced are illustrated in figure 6.12, using different MPF configurations.

| | | |
|---|---|---|
| 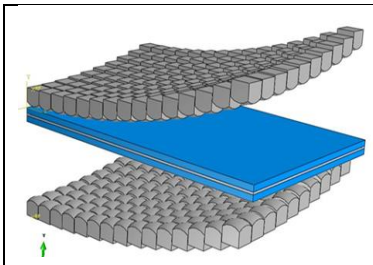 | MPF with solid elastic cushion |  |
| 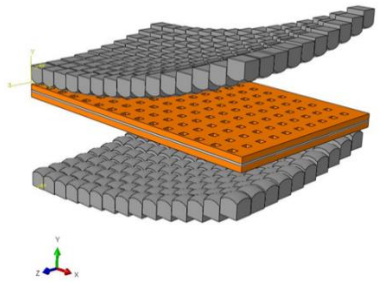 | MPF with mesh-type elastic cushion |  |
|  | MPF with solid elastic punch | 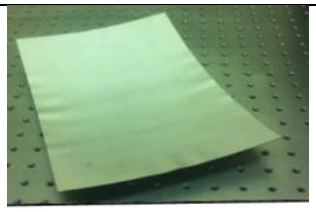 |
|  | MPF with mesh-type elastic punch | 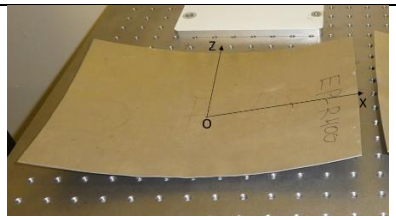 |

Figure 6.12 Parts produced used different MPF configurations

The magnitude of the applied force was achieved from an earlier experimental campaign [93]. In terms of the results, as shown in figure 6.12, there is a noteworthy difference between the results of the forming force to produce a sheet of stainless steel DC05 with a thickness of 1 mm. Figure 6.13 show two forming force-time curves using rubber punch and MP forming die technique for the formation of double curved parts with the radius of 400 mm of the curve.

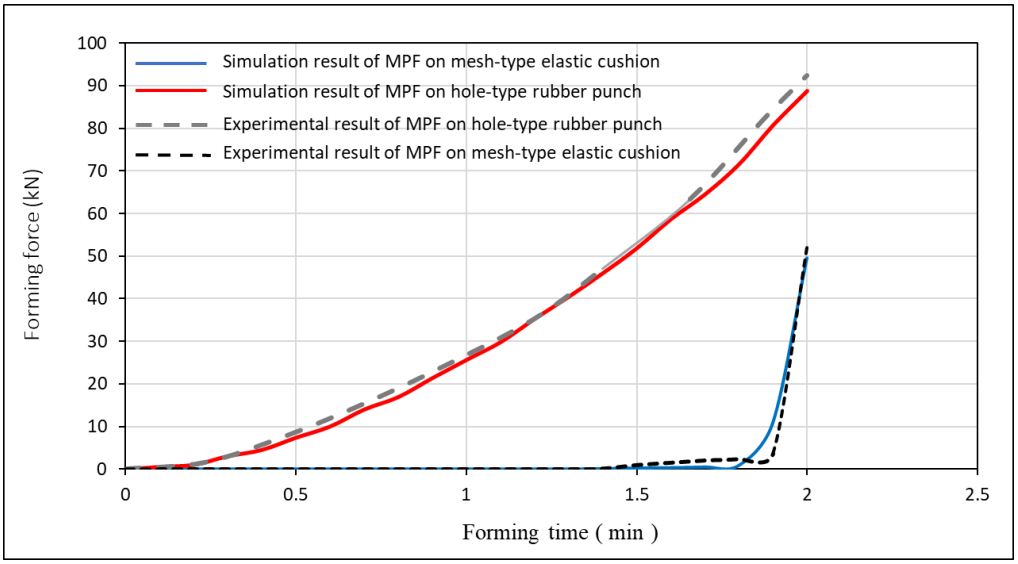


Figure 6.13 Comparing forming force time curves for radii of the forming curvature, 400 mm

The forming force used by the rubber punch MPF approach increased to 90 KN to form the part with 400 mm radii. Nonetheless, with the use of a mesh-type elastic cushion on MP forming punch, it increase to only 50 kN [95]. It can thus be stated that the forming force possesses an overall varied trend. The forming force can be split into 3 steps in the case of utilising the hole-type rubber punch. For the first stage, the hole-type rubber punch meets the sheet and the forming load is very small, about the first quarter of a minute of the process. Next, the force tends to slowly increase because of the self-deformation of the hole-type rubber punch. This also happens due to the fact that the sheet is bending as the punch moves forward into the die. The latter proceeds for about 0.25 to 1 minute. Lastly, the forming force continually increases because of the plastic deformation occurring at the sheet as it moves to replace the die cavity with an increased pressure on the rubber punch in order to cover the overall die [96]. This stage lasts for another 2 minutes. For the mesh-type elastic cushion with MP forming punch, the forming force remained minimal till the final conclusion of the procedure, where it increased all of a sudden with the sheet deformation. The same elucidations can be applied to the part with a 400mm radii of the formed curve. It is clear that for the MPF punch, the overall forming force tends to increase with a rise in the radii of formed

curve. This can be based on the fact that a greater number of pins are able to come in contact with the sheet in the initial stages of the forming procedure [65]. For the elastic punch, a reduction in the radii of the formed curve results in a rise in the forming force. The reason for this trend is due to the need for additional forming force to move the rubber in the frontward direction in order to shield the entire MP forming die.

## 6.5. FEA solution to define and optimize process parameters

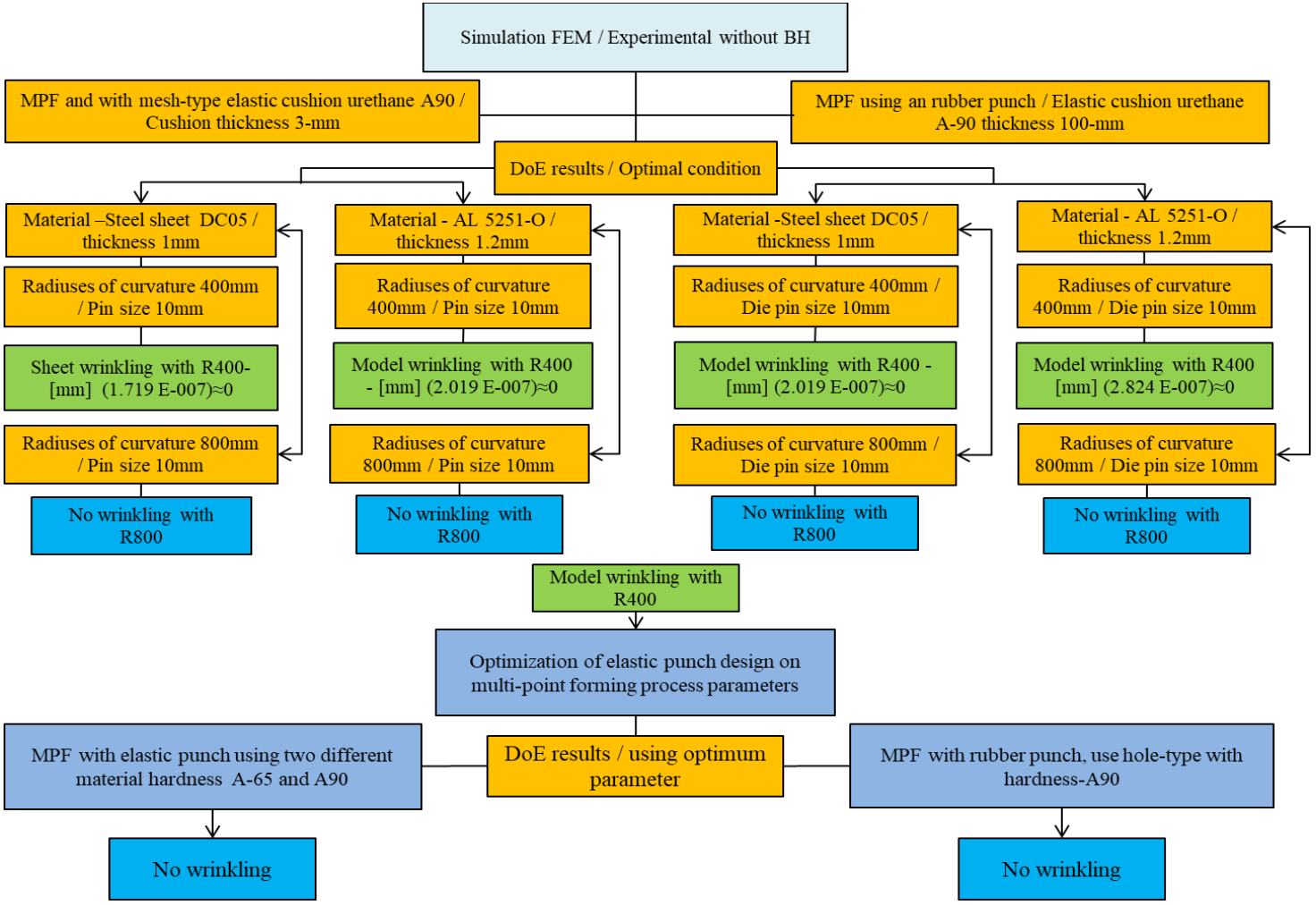


Figure 6.14 MPF process developed for mesh-type elastic punch MPF approach

## 6.6. Optimization of hole-type rubber punch on MPF die process variables

An investigation was undertaken on the effects, noticed on the quality of the formed part, caused by significant EPMPF process parameters. The optimisation of simulation and experimental process parameters the input factors (independent variables) are rubber punch hole size (mm), Compression ratio (%), and elastic punch hole-type (as the punch an elastic block and punch tools (without container and without container), as shown in Table 6.1. The compression ratio is calculated using $\frac{t_o - t_f}{t_o} \times 100$. Where $t_f$ is the punch thickness and $t_o$ is the original punch thickness at the end of loading step. Table 6.1 demonstrates how each factor was given three values. The response from the analysis determined wrinkling amplitude, thickness variation and maximum deviation as the main criteria for determining the quality of the formed part.

Table 6.1 Levels and values of the DoE variables

| Process parameters. | Units | Parameter Magnitude. | | |
|---|---|---|---|---|
| | | Low. | Intermediate. | High. |
| Elastic punch-hole size (A) | mm | 3×3 | 6×6 | 9×9 |
| Elastic punch compressor % (B) | % | 50 | 60 | 70 |
| Hole-type of elastic punch (C) | | Square | | Circular |
| Elastic punch tools (D) | | Container | | Without container |

Using DoE-Design of Expert 6.0 simulation results (listed in Table 6.2) were statistically analysed. Several design techniques such as factorial, Taguchi and Response Surface Method (RSM) are avaliable within the software. For our study RSM with central composite design (CCD) was applied. Table 6.2 [99, 100] lists the experimental factor

which was generated. To recognize the most important process prarameters and their possible influence on the overall product, ANOVA was implemented.

## 6.7. Results and discussion DoE

The numerical simulations shed light on the three response parameters wrinkling, thickness variation (mm), and maximum deviation. Table 6.2 lists these parameters for an experimental plan in accord with RSM (CCD).

Table 6.2 DoE experimental and numerical outcomes, [76]

| Exp. $N_{\bar{o}}$ | Factor 1. | Factor 2. | Factor 3. | . Factor 4. | Response 1. | . Response 2. | . Response 3. |
|---|---|---|---|---|---|---|---|
| | A: Elastic punch hole size (mm) | B: Compression Ratio (%) | C: Elastic punch hole-type | D: Punch tools | Wrinkling (mm) | Thickness variation (mm) | Maximum deviation (mm) |
| 1 | 6 | 50 | Circular | without container | 3.06 | 0.005045 | 1.323 |
| 2 | 9 | 70 | Circular | without container | 1.082 | 0.003217 | 0.32 |
| 3 | 6 | 60 | Circular | with container | 1.275 | 0.073266 | 1.34 |
| 4 | 6 | 60 | Square | with container | 1.278 | 0.072008 | 0.72 |

| | | | | | | | |
|---|---|---|---|---|---|---|---|
| 5 | 3 | 50 | Square | with container | 3.789 | 0.078435 | 1.307 |
| 6 | 9 | 50 | Square | without container | 3.801 | 0.003134 | 1.801 |
| 7 | 6 | 60 | Circular | without container | 2.004 | 0.006134 | 0.54 |
| 8 | 3 | 70 | Circular | with container | 0.789 | 0.075452 | 0.11 |
| 9 | 9 | 70 | Square | with container | 0.705 | 0.073217 | 0.31 |
| 10 | 6 | 60 | Square | with container | 1.278 | 0.070208 | 0.72 |
| 11 | 3 | 50 | Circular | without container | 2.128 | 0.005452 | 1.078 |
| 12 | 9 | 60 | Circular | without container | 2.011 | 0.005452 | 0.97 |
| 13 | 6 | 60 | Circular | without container | 2.004 | 0.006134 | 0.54 |
| 14 | 3 | 60 | Square | without container | 1.879 | 0.006626 | 0.67 |
| 15 | 3 | 70 | Circular | without container | 1.094 | 0.007003 | 0.3 |

| | | | | | | | |
|---|---|---|---|---|---|---|---|
| 16 | 6 | 70 | Circular | with container | 0.469 | 0.391401 | 0.13 |
| 17 | 3 | 50 | Square | without container | 2.277 | 0.005452 | 1.58 |
| 18 | 3 | 50 | Circular | with container | 3.189 | 0.050435 | 1.918 |
| 19 | 3 | 70 | Square | with container | 0.789 | 0.175452 | 0.11 |
| 20 | 6 | 60 | Square | without container | 2.007 | 0.005452 | 0.79 |
| 21 | 9 | 50 | Circular | without container | 3.601 | 0.003134 | 1.011 |
| 22 | 9 | 60 | Square | with container | 1.097 | 0.013841 | 0.6 |
| 23 | 6 | 70 | Circular | without container | 1.772 | 0.006545 | 0.44 |
| 24 | 9 | 50 | Circular | with container | 2.872 | 0.089974 | 1.229 |
| 25 | 6 | 60 | Square | without container | 2.007 | 0.005452 | 0.79 |
| 26 | 6 | 60 | Square | with container | 1.278 | 0.077208 | 0.72 |

| | | | | | | | |
|---|---|---|---|---|---|---|---|
| 27 | 6 | 70 | Square | with container | 0.469 | 0.371401 | 0.13 |
| 28 | 6 | 50 | Square | with container | 2.677 | 0.017817 | 1.078 |
| 29 | 3 | 60 | Circular | with container | 1.488 | 0.068817 | 0.421 |
| 30 | 6 | 60 | Circular | with container | 1.275 | 0.073266 | 1.34 |
| 31 | 9 | 60 | Square | without container | 2.044 | 0.003452 | 0.47 |
| 32 | 6 | 50 | Square | without container | 3.07 | 0.004817 | 1.067 |
| 33 | 9 | 60 | Circular | with container | 1.067 | 0.083841 | 0.6 |
| 34 | 3 | 70 | Square | without container | 1.0994 | 0.009987 | 0.4 |
| 35 | 6 | 60 | Square | without container | 2.007 | 0.005452 | 0.79 |
| 36 | 9 | 70 | Circular | with container | 0.605 | 0.009797 | 0.33 |
| 37 | 6 | 60 | Circular | without container | 2.004 | 0.006134 | 0.54 |

| | | | | | | | |
|---|---|---|---|---|---|---|---|
| 38 | 6 | 60 | Circular | with container | 1.275 | 0.073266 | 1.34 |
| 39 | 3 | 60 | Circular | without container | 2.071 | 0.003883 | 1.33 |
| 40 | 3 | 60 | Square | with container | 1.489 | 0.099071 | 0.87 |
| 41 | 6 | 50 | Circular | with container | 2.507 | 0.029817 | 0.967 |
| 42 | 6 | 70 | Square | without container | 1.171 | 0.007881 | 0.79 |
| 43 | 9 | 50 | Square | with container | 2.189 | 0.016134 | 1.4 |
| 44 | 9 | 70 | Square | without container | 1.082 | 0.009217 | 0.32 |

A double curvy sheet could be fashioned without any wrinkling possessing the correct sizes and increased thickness uniformities. ANOVA ensured the effect of every independent variable was effectively evaluated along with analysing the interactions associated to the response factors. As part of the null hypothesis it was determined that the parameter had no impact on the formed part. Hence a probability of *P*-value less than 5% reports that the independent variable had a noteworthy impact on the formed part. Only A (elastic punch hole size) had a significant impact on the wrinkling defect.

On the other hand, the three variables along with their interactions were shown to be important features for thickness variation. Hence, the forming force value was mainly

under the influence of A and C (rubber punch compression ratio). Increased wrinkling and maximum shape deviation was lead by both large and small pins although large pins reduced the thickness variation. Increased thickness variation was lead by high coefficient of friction.

Table 6.3 presents the ANOVA analysis results. It can be determined that the radius of forming curvature is the most significant process factor affecting wrinkling.

Table 6.3 Corresponding and process parameters, P-values

| Response factors / Significant factors | Wrinkling | Thickness variation (mm) | Maximum deviation (mm) |
|---|---|---|---|
| Radius of forming curvature (A) | 0.0005 | 0.0186 | <0. 0001 |
| Elastic punch compressor % (B) | 0.7574 | 0.0386 | 0.9070 |
| Hole-type of elastic punch (C) | 0.1363 | <0.0010 | <0.0001 |
| Significant interaction | - | AB=0.0094<br>AC=0.0003<br>BC=0.0027 | - |

### 6.7.1. Wrinkling

Figure 6.15 shows this influence trend. This trend was also noticed in the traditional MP forming process. A decrease in wrinkling or its exclusion was achieved by enhancing the forming curvature's radius. Wrinkling appears at the edges of the formed part when high bending deformation was generated due to small radius of forming curvature (R400). Initially the flat rubber punch maintains a surface contact with the sheet facing into a

convex MP forming die. As the punch travel starts to increase it generates increased pressures on the edges and the middle of the metal sheet causing wrinkling. Yet in this situation, wrinkling is still less when compared to conventional MP forming (see Section 6.5.3).

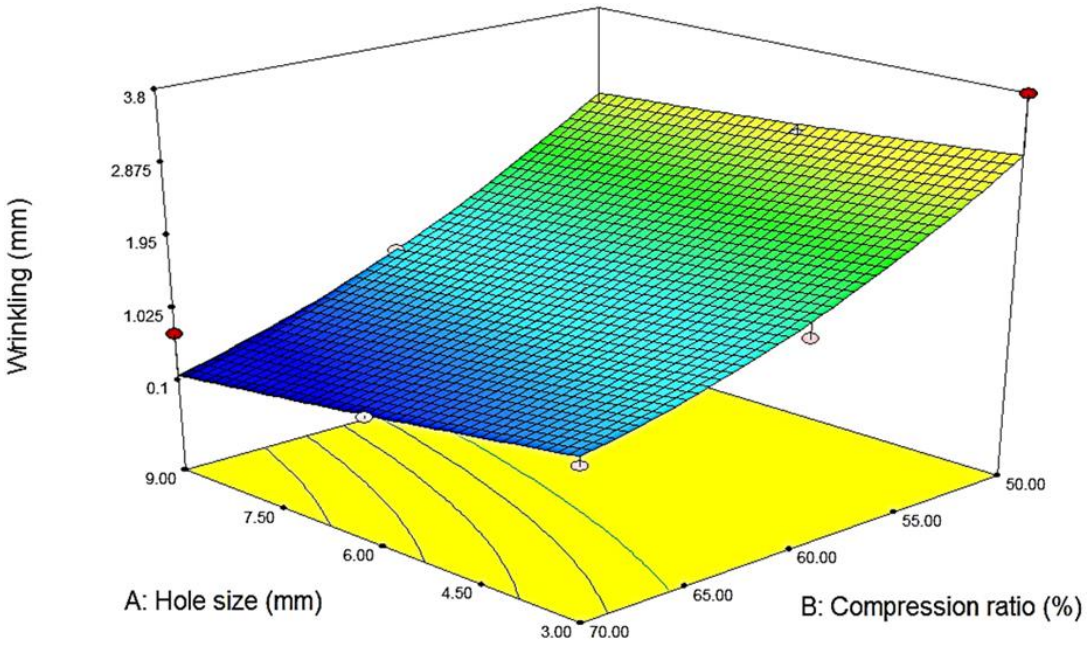


Figure 6.15 Effects of interactions between (A) Hole size (mm) and Compression ratio (%) (B) With container, the compression ratio (%) on wrinkling value

Figure 6.15 shows the (A) Hole size (mm) and Compression ratio (%) (B) effects on the container and compression ratio (%) on wrinkling value. The wrinkling value reduced to a minimum value at a compression ratio of C = 70%. The increase in compression ratio saw a decrease in the wrinkling value.

Based on the stabilities and the uniformities of the stresses in the metal sheet, a punch with thickness of 120 mm was generated. However, the resulting force needed to

complete the loading steps was large. Hence, the elastic cushion's thickness rises at the edges which further results in increased wrinkling. At the edges, large hole size cause increase in the size hole offset leading to a non-uniform stress distribution. Using medium size hole 9 mm and a large compression ratio 70% can aid in attaining minimal wrinkling.

### 6.7.2. Thickness variation

Figure 6.16 show the impact of radius of forming curvature and compression ratio of the punch on the magnitude of the forming force. These two significant working parameters. The required force for forming process increases by increasing the radius of forming curvature, this is demonstrated in the Figure 6.16. Whilst forming curvature under high pressure (outer edges) a greater number of hole-type rubber will be in contact with the sheet metal for small radius. Therefore, when generating the 400 mm radius the height difference between holes is smaller. As a consequence, an increase will incur on the thickness variation. Hence for its own self-deformation [95] the punch (A90) will need additional force.

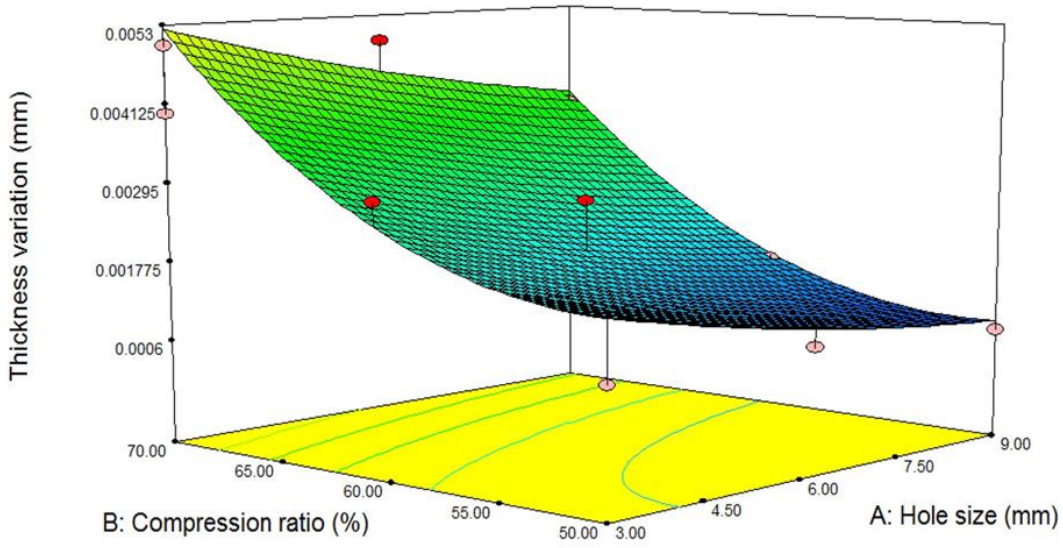


Figure 6.16 The effects of compression ratio and hole-type on thickness variation

Generally, the ratio of punch compression will lead to increased uniform stress distribution on the sheet as the radius of forming curvature increases. This can lead to a decrease in the thickness but requires an extensive exterior force to complete the loading stage, as stated in Section 6.7.2 The process will no longer be linear as the interactions on the surface of the 3D plane are more saddle shaped rather than flat.

Figure 6.16 shows the effect of the punch compression ratio on forming force. In this study, 50% was the minimum ratio of punch compression. This ensured the punch to push the metal sheet completely against the MP forming die (punch thickness 100 mm and radius of curvature 400 mm). Defects such as spring back can be reduced on the final formed part by applying more force which increased the punch compression ratio (which makes the stress distribution more uniform). This is represented in Figure 6.16. In a situation where A=400 mm and B= 125 mm the forming force is 82.8kN and 175kN at punch compression ratios of 50% and 70%, respectively.

### 6.7.3. Maximum deviation.

How radius of forming curvature and punch thickness affect maximum deviation value is shown in Figure 6.17. Smallest thickness of the punch (B=100 mm) and largest radius of forming curvature (A=400 mm) lead to maximum deviation on the formed part. This is clear from the figure 6.18.

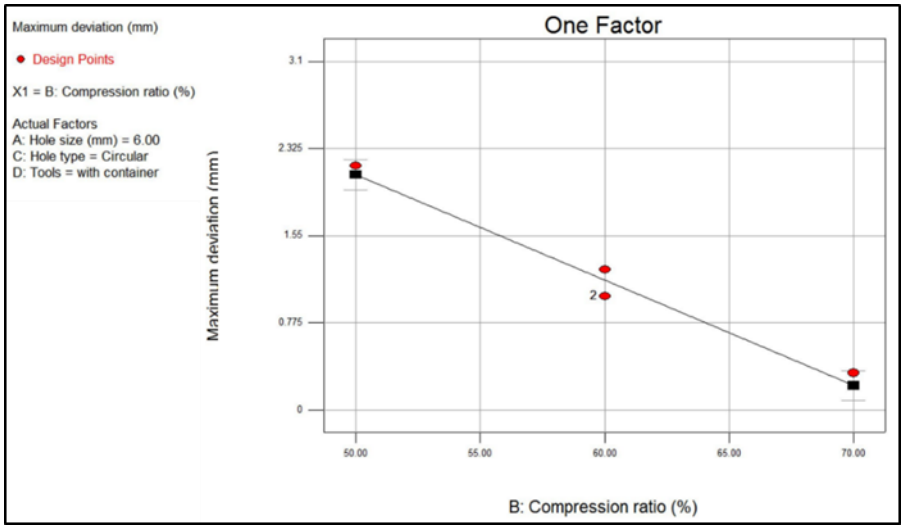


Figure 6.17 Effect of the significant parameters effecting, maximum deviation are B interaction

## 6.8. Determining the response factors.

This section describes those three independent parameters which are utilised for prediction of response factors. These can be used to generate second order quadratic polynomial, Equation 6-3 for an empirical model. For estimating the precision of the resulting part, Equation 6-3 can be utilised. Table 6.4 illustrates the prescribed values related to the process variables. Having insufficient stresses causes deformation and deviates away from the target. Minimum deviation from the target shape can be attained using a large compression ratio. Response is shown as:

$$\text{Response}=X_0+ \boldsymbol{x_1}A + \boldsymbol{x_2}B + \boldsymbol{x_3}C + \boldsymbol{x_4}\ AB + \boldsymbol{x_5}\ AC + \boldsymbol{x_6}\ BC + \boldsymbol{x_7}\ A^2 + \boldsymbol{x_8}\ B^2 + \boldsymbol{x_9}\ C^2 \quad (6.3)$$

In equation 6.3, the three variables; A, B and C refer to the independent variables. Over here, the first variable presents the forming curvature's radius, the next variable refers to the thickness of the punch and the final variable refers to the elastic punch's compression

ratio. The unknown coefficients $x_i$ ($i$ = 0, 1,……,9) are achieved with the regression analyses. This is detailed in Table 6.4.

Table 6.4 Coefficients of objective function, [102]

| Coefficients. | Wrinkling. | Thickness variation (mm) | Maximum. Deviation. (mm). |
|---|---|---|---|
| Constant - (X) | --14.33. | 6.488. | --261. 9.. |
| $-x_1$.- | --0. 011.. | -0.029. | -0.179 |
| $-x_2$.- | --0.052. | --0.089. | --0.019. |
| $-x_3$. | --0.255. | --0. 199 | -4.690 |
| $-x_4$. | --5.25E-6. | --3.90E-5. | 0 |
| $-x_5$. | -5.84E-5. | --1.71E-4 | -0. |
| $-x_6$. | -2.65E-4. | -9.10E-3 | -0. |
| $-x_7$. | -4.45E-6. | --1.07E-3 | -0. |
| $-x_8$. | -1.51E-4. | -2.52E-3 | -0. |
| $-x_9$. | -1.60E-3. | -1.41E-2. | -0. |

## 6.9. Achieving the optimum variables for operation.

The optimum variables for operation are required to form a double curved part of increased precision. As part of this study, the objective based on the low application of forming force, was to create a final part which has the least or no wrinkling. Table 6.4 presents how independent variables were chosen and set according to the limits shown in Table 6.5. This is done to minimise the forming force, spring back and wrinkling. Although, a high coefficient of friction shall resist the expansion hence leads to non-uniform deformation.  the effect of cushion thickness on workpiece thickness variation can be reduced to being negligible using a large elastic cushion (rubber). However, when large size hole wasadopted, increasing elastic cushion thickness will incur an increase in the thickness variation [78]. This is cuased by deformation of the elastic cushion which is a result of the gaps between the pins becoming smaller. Thus, it can be suggested that a large size hole and combination of a thick elastic cushion leads to the largest variation in workpiece thickness. Figure 6.18 shows the effects of the main parameters which have an influence on the hole size in terms of A interaction in DoE whereas Figure 6.19 shows the effects of the main parameters which have an influence on the compression ratio in terms of B interaction. Figure 6.20 shows the effects of the main parameters which have an influence on the tools without container in terms of D interaction.

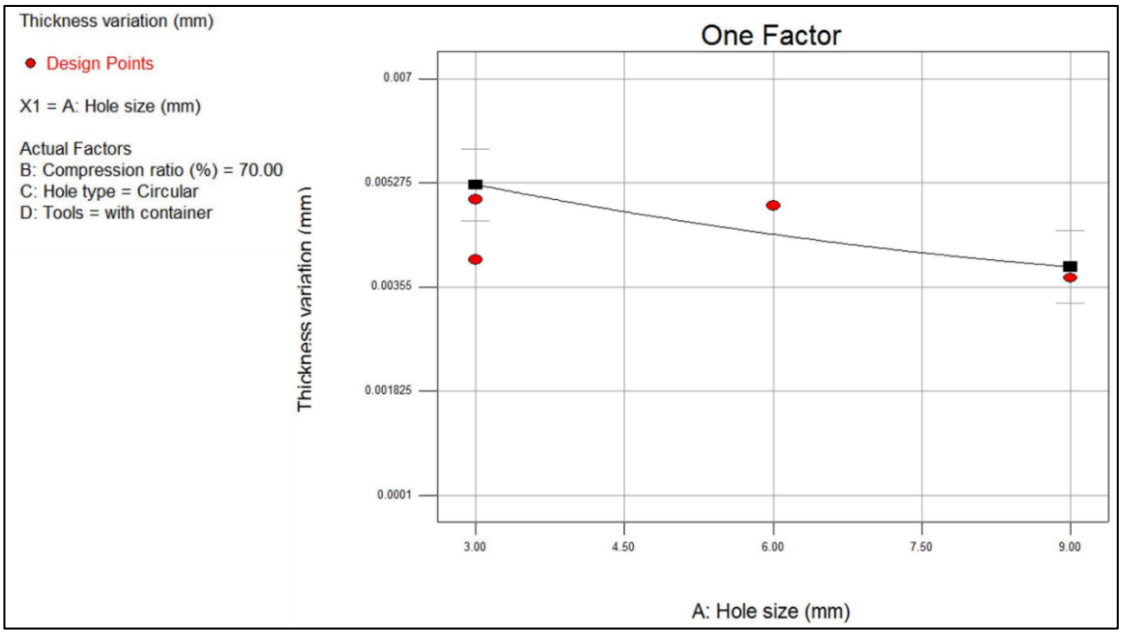


Figure 6.18 Effect of the significant parameters having an influence on the hole size in terms of A interaction.

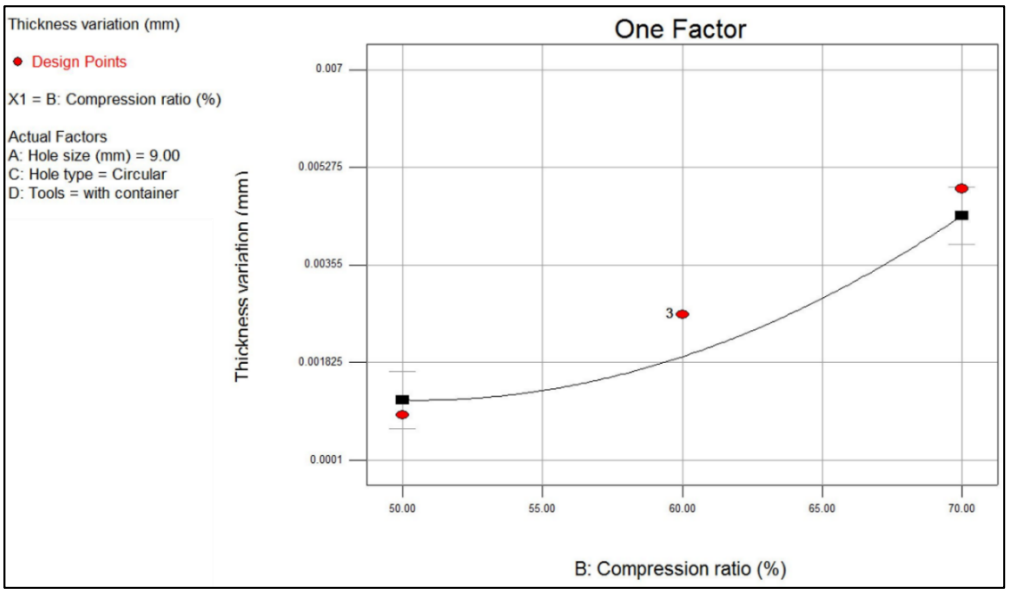


Figure 6.19 Effect of the significant parameters having an influence on the Compression ratio in terms of B interaction

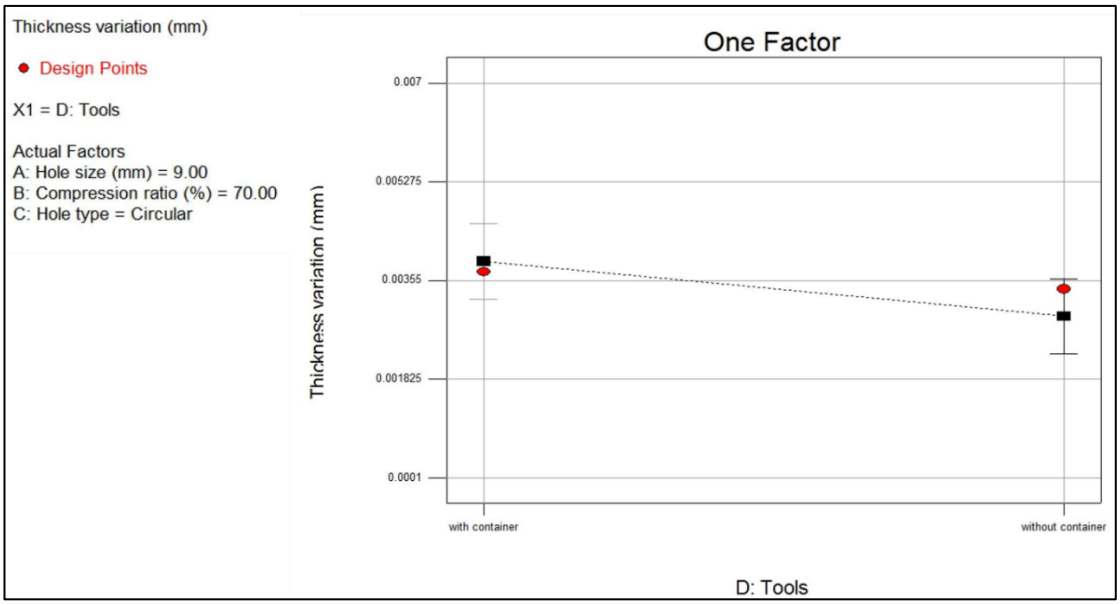


Cont.

Figure 6.20 The significant parameters having an influence on Tools without container in terms of D interaction

Table 6.5 Principles of achieving an optimum case for the independent and dependent variables

| Final Equation in Terms of Actual Factors: Thickness variation (mm) $W=X+X_1A+X_2B+X_3AB+X_4A^2+X_5B^2$ | | | | | | |
|---|---|---|---|---|---|---|
| ***Tools with container*** | | | | | | |
| Hole type | X | X1 | X2 | X3 | X4 | X5 |
| Square | +0.024582 | -4.54568E-004 | -8.38875E-004 | -3.22049E-006 | +1.57839E-005 | +8.63930E-006 |
| | | | | | | |
| Hole type | | | | | | |
| Circular | +0.023836 | -1.90670E-004 | -8.54526E-004 | -3.22049E-006 | +1.57839E-005 | +8.63930E-006 |
| | | | | | | |
| ***Tools without container*** | | | | | | |
| Hole type | | | | | | |
| Square | +0.025196 | -1.62707E-004 | -8.99904E-004 | -3.22049E-006 | +1.57839E-005 | +8.63930E-006 |
| | | | | | | |
| Hole type | | | | | | |
| Circular | +0.024522 | +1.01191E-004 | -9.15555E-004 | -3.22049E-006 | +1.57839E-005 | +8.63930E-006 |

In this study, the principles ("IN RANGE" for operating aspects and "MINIMIZE" for response variables) were applied. This was done to ensure the optimal outcome matches the objectives set. In addition, three factors in the empirical equation were solved. All this contributed to the best solution, which met the set objectives. This is further detailed in Table 6.5.

Other defects are observed on the resulting part. These include a decrease in the forming curvature's radius, increase in the punch thickness and wrinkling. This is further detailed in Section 6.7.1. However, this does reduce the wrinkling value. As mentioned earlier, it must be noted that the surface of the 3D plane, which represents the interactions is saddle-shaped and not linear. Based on the simulation results it can be deduced that the wrinkling is minimised with the use of a 9 mm circular hole-type elastic punch. The simulation was carried out on deformed part with a curvature radius of 400 mm created by hole-type rubber punch approach and MPF die process. With an increase in the curvature's radius, an increase in the uniformity of the stress distribution is visible on the sheet due to the punch compression ratio. While this results in a decrease in the value of the thickness, however, requires an increased exterior force for completing the loading step. This is mentioned in Section 6.7 where the significant parameters effecting the maximum deviation are listed. Table 6.6 shows the optimal values for minimising wrinkling, thickness variation (mm) and maximum deviation (mm).

Table 6.6 Optimal values for minimising wrinkling, thickness variation (mm) and maximum deviation (mm)

| | A: Elastic punch hole size (mm). | B: Compression Ratio (%). | C: Elastic punch hole-type. | D: Punch tools. |
|---|---|---|---|---|
| Optimum parameters setting | -9 | -70 | -Circular | Without - container |

### 6.9.1. The-results of-experimental work-to measure-a-capture-forming part

The 3D FE model was used along with the optimal process parameters listed in Table 6-6 to produce simulation results shown in Figure 6.21. At the next stop, experiments were undertaken for validating the anticipated outcomes. The steps for measurements described were repeated. Paths O-A and O-B were chosen to illustrate wrinkling measurements. Figure 6.24 represents the contrast amid the experiments and numerical work for the target shape (R=400 mm). No wrinkling is observed in the second part.

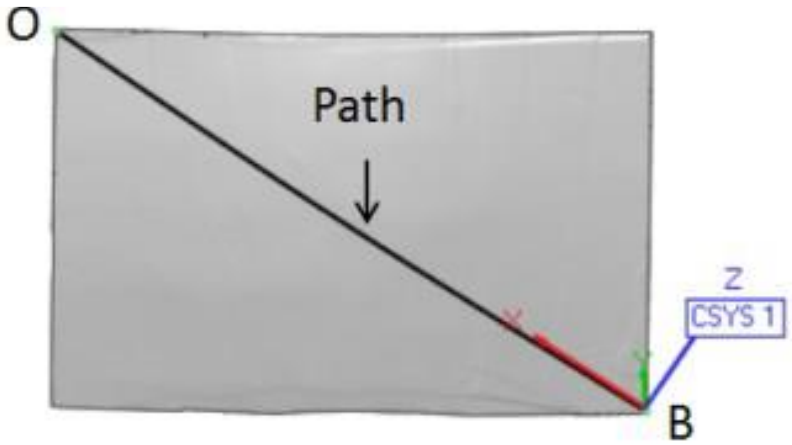


Figure 6.21 Experimental results for wrinkling

The path of wrinkling along the O-B side is shown in figure 6.21. As demonstrated in figure 6.22 and figure 6.24, a FARO Edge Arm 3D scanner equipped with Geomagic control was utilised for capturing the geometry of the produced part. This was done in order for comparisons to be made to the components and to record any errors [94]. The resulting part with a curvature of 400 mm had its wrinkling factor determined as the normal distance between the target and the formed shape for each amplitude of wrinkling along path O-B. The RMSE was utilised for conniving a numerical simulation for wrinkling [65]. For the formed part, the capture points (i.e. components O-B) were compared with the ideal shape. Also, the thickness deviation along the path O-X was considered to symbolise the wrinkling [93]. This is also demonstrated in deformed sheet Figure 6.25 and 6.27.

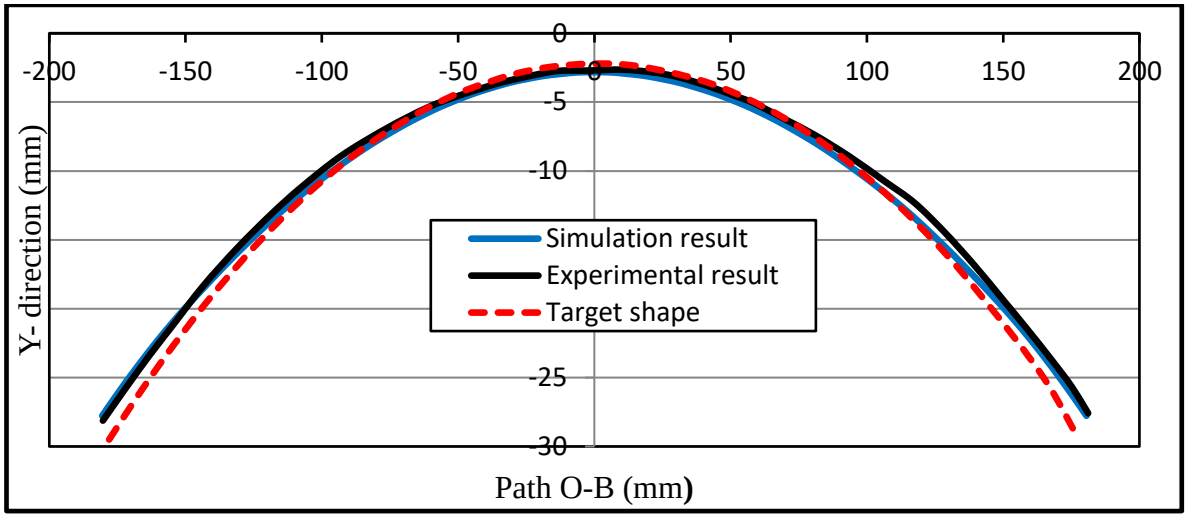


Figure 6.22 Wrinkling in path O-B (mm) of formed part

Finite Element Modeling (FEM) and design of experiments (DoE) were used to study the influence or the mesh-type elastic cushion parameters such as the hole type and hole size, and thickness variations, maximum devotion, and wrinkle of the deformed sheet.

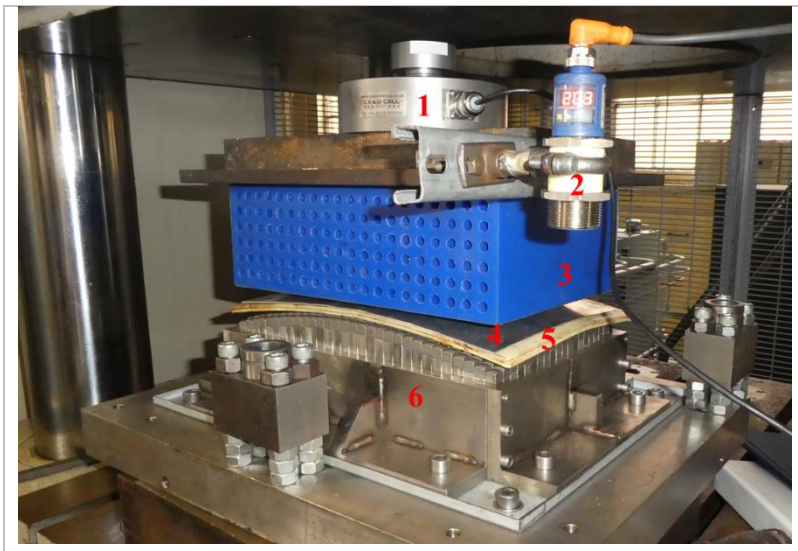


| |
|---|
| **1- Load cell** |
| 2- Distance sensor |
| 3- Mesh-type elastic punch |
| 4- Mesh type elastic cushion |
| 5- Metal sheet |
| 6-Multi-point forming die |

Figure 6.23 Set-up of the experiments for mesh-type elastic punch MPF approach

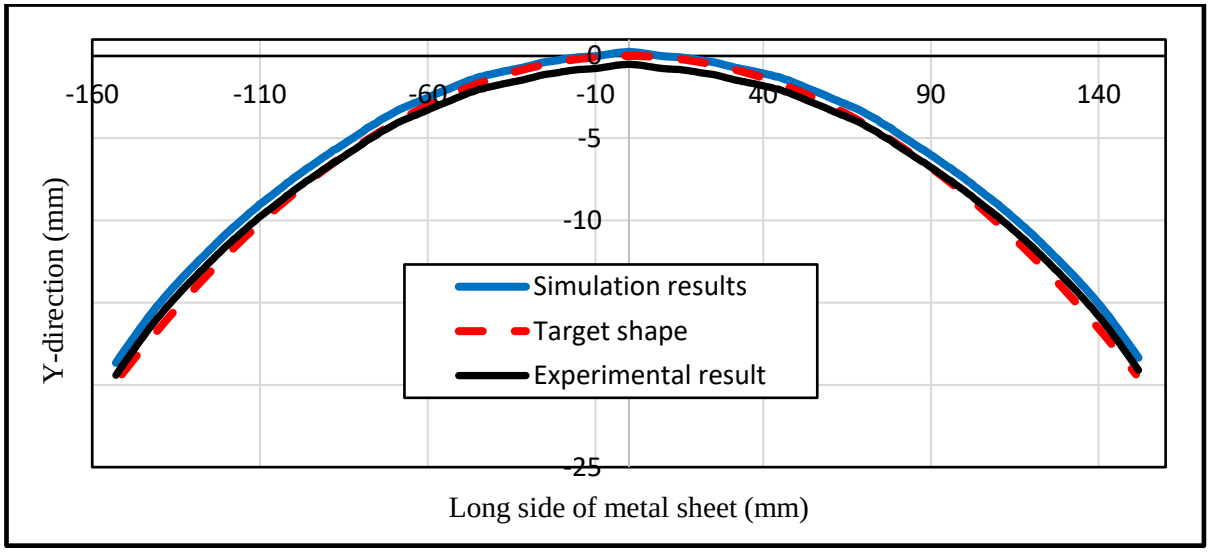


Figure 6.24 Comparisons for path O-X for the different tests

It was observed that a 2.58 mm of total wrinkling occurred on the produced component. Figure 6.24 shows numerical results of maximum deviation after the completion of forming process on the metal sheet's diameter. Figure 6.26 demonstrates the results of experimental thickness along O-X direction. Table 6.8 lists the results with optimum process variables.

Table 6.7 MPF die with optimum process parameters for rubber punch

| | Rubber punch thickness (mm) | Compression Ratio (%). | Punch hole-type | Punch hole-size | Radius of curvature MPF die(mm) |
|---|---|---|---|---|---|
| Optimal cundition | -100 | -75 | -Circular | -9 | -400 |

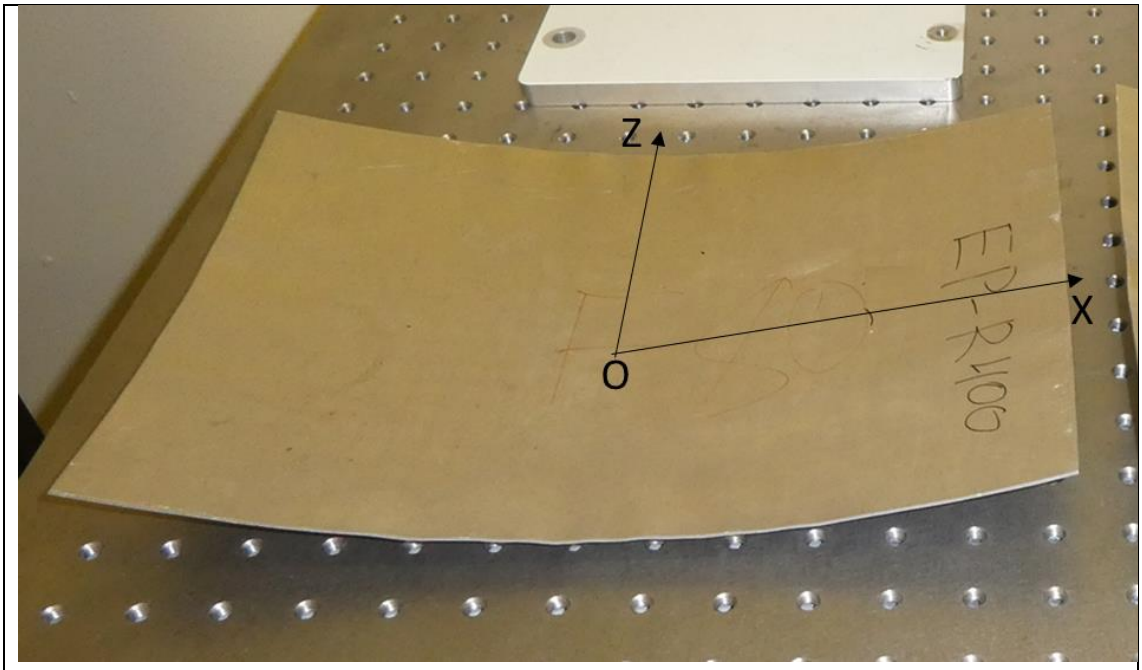


Figure 6.25 Fabricated part for R400

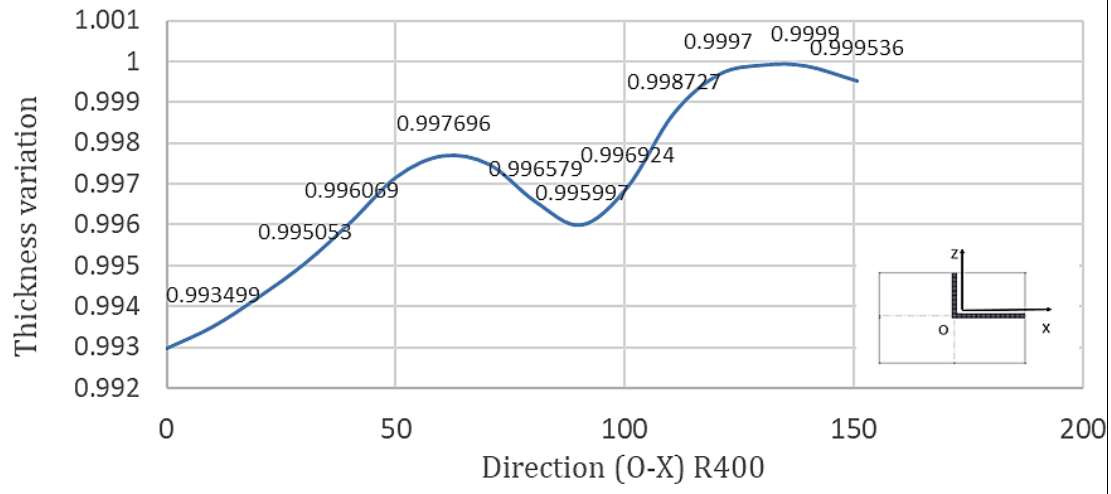


Figure 6.26 Experimental thickness along O-X direction

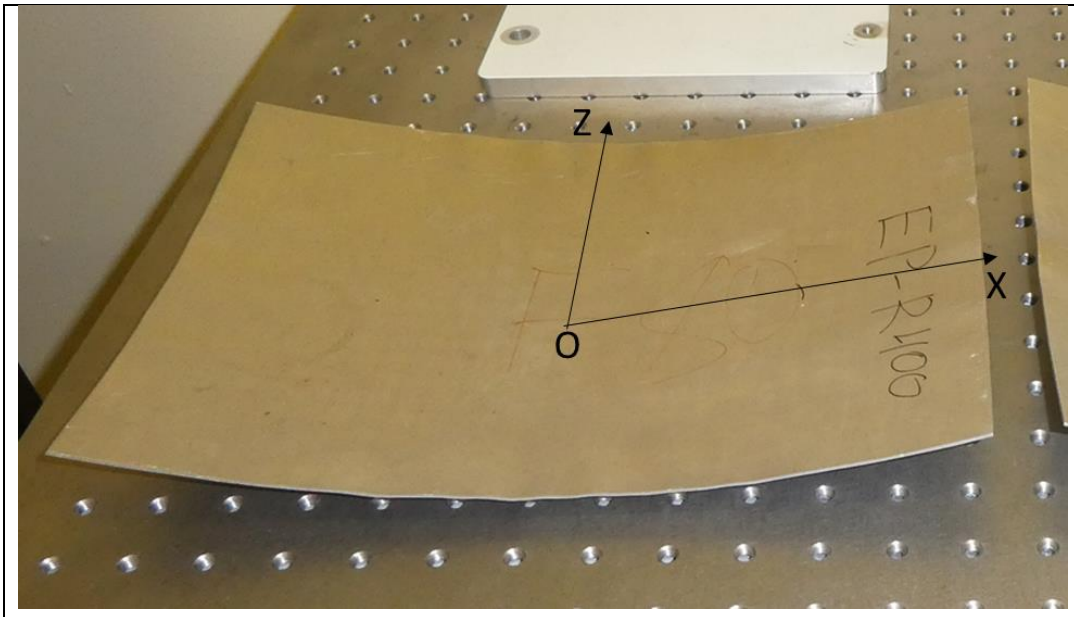


Figure 6.27 Fabricated part for R400

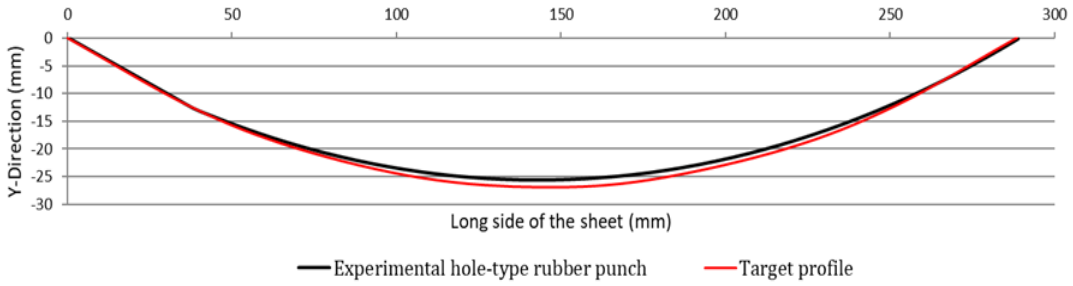


Figure 6.28 Experimental results of hole-type elastic punch alone O-X direction in the panel

Table 6.8. Results with optimum process variables

| Parameter results | Hole type | Hole size mm | Cushion thickness | Wrinkling (mm) | Max. deviation (mm) | Thickness variation (mm) |
|---|---|---|---|---|---|---|
| Solid cushion | Circular | -9 | -100 | -0.1858 | -0.0358 | -0.00499 |
| Mesh-type cushion | square | -3.5 | -3 | -1.0741 | -1.7848 | -0.09850 |

For calculating the errors between the measured and simulated results, the following correlation can be used in order to determine the precisions of the simulations:

$$\text{Numerical error} = \frac{Experimental\ result - Simulation\ result}{Simulation\ result} \times 100$$

[102]

Therefore, the resulting numerical errors are:

Wrinkling = 0.0

Maximum deviation = [(1.69 - 1.58) / 1.58] ×100 = 6.96 %

Compression ratio (%) = [(75 – 70) / 75] × 100 = -6.66 %

If the experimental outcomes were smaller than the simulated ones, a negative value for the numerical error occurs.

## 6.10. -Summary and Conclusions

Double curvy panels with varying radius of curvatures were effectively created with experiments utilising an elastic punch. These were then successfully compared with panels created through traditional MP forming approaches. Numerical simulations with FEA optimization were used for investigating the effect of process variables such as radii

of the formed curve, punch thickness along with punch compression ratio on wrinkling, thickness variation, and maximum deviation.

Wrinkling, thickness variation, and maximum deviation were used to associate the quality of final part. The results of the final experimental and simulations helped to determine the optimal process parameters. From the results of this study, it can be concluded that the tooling costs can be reduced by 70% and set-up time needed to modify the pins for a new design shape can be dramatically reduced by replacing a MP forming pin punch by a hole-type rubber punch.

Further, to produce metallic sheets with various characteristics, same tooling can be used. In comparison to the traditional mesh-type elastic cushion, MP forming punch can help in reducing wrinkling in the final part with the use of a 400 mm radius of forming curvature. This would not require the use of a blank-holder.

By applying adequate selection of process variables such as compression ratio of the 9 mm hole-size rubber punch wrinkling on the final part can be decreased.

Although it was revealed that punch thickness has less significance in this study, the hole-size and the compression ratio for the rubber punch were the parameters which had the most influence on the formed part quality. AB, AC and BC interactions were studied. Noteworthy interactions are on thickness variation and maximum deviation.

For predicting the excellence of the deformed part in terms of a mix of operational variables in specified limits, pre-selected ranges, an empirical model has been produced.

# 7. CHAPTER CONCLUSIONS-AND RECOMMENDATION FOR FUTURE WORK

## 7.1. Introduction

Sheet metal forming processes have been studied in this work in terms of complete flexible multipoint forming with mesh-type elastic cushion (MPF) and hole-type elastic rubber punch with multipoint die to reduce workpieces in the formed part. In addition, a method to enhance.the quality of the final sheet is explored. To assess the geometric. defects, for instance, the wrinkle and thickness variation produced due to elastic recovery after the final unloading stage with the Finite-Element Modeling (FEM) approach was adopted for simulating the sheet-metal forming method. This was similar to the one utilised in the manufacturing industries. Hence, fundamental knowledge of wrinkling along with the spring-back phenomena was necessary along with the understanding of material and process factors which may have an influence on the sheet panel spring-back in order to produce adequate, precise and consistent inputs for the FEM. A combination of statistical approaches with FEM were adopted for determining the procedure of sheet-metal forming. This was also done to precisely perceive and evaluate the most appropriate modeling and operating factors, which define the optimum arrangement of the variables under investigation in order to obtain a product with an overall superior quality. These variables include the elastic punch hole size, compression ratio, elastic punch hole-type, punch tools, wrinkling, thickness variation and maximum deviation.

To understand the influence of the main parameters on the excellence of the final part regarding wrinkle and variation in thickness, a verified 3D computational model of the MPF was utilised. Key factors were; the radii of the forming curvature, the thickness of the mesh-type elastic cushion along with the compression ratios and forming load (kN).

Another set of experimental work involved the investigation of a “flexible” forming procedure with the use of a hole type, (circular) rubber punch. The influence of the same abovementioned parameters was studied on the formed process quality.

Overall, this work made use of RSM for studying the performance of 44 runs, which were performed with three dependent and three independent parameters. Next, an empirical relationship was produced and utilised for estimating the qualities of the produced parts in the two processes. Also, this empirical model was eligible for use with any mix of process variables.

For a sheet of stainless steel-DC05 with a 1.0 mm thickness of spherical geometry, the following points can be concluded:

a) Use of a numerical technique incorporated with FEA was successful in determining the influence of the most important operating variables on the overall part’s quality.
b) Radii of the curvature were shown to be the most important process variables amongst the ones investigated for the mesh-type elastic cushion in the case of conventional MP forming,
c) Whereas, the compression ratio for the hole-type elastic punch was secondary with circular hole-type rubber punch on MPF die.
d) Resulting wrinkling decreases with an increase in the forming curvature’s radius till the wrinkle effect has vanished from the edges of the sheet. This results in the thickness variation decreasing.

Wrinkling and forming load rose with an increase in the forming curvature’s radius. Substituting MPF punch with a circular hole-type rubber punch, considerably enhanced the overall forming process. This was reflected by a reduction in the cost of the tools by

at least 65% while wrinkling decreased by 60% and thickness variation decreased by 70%. Optimising helped in identifying the optimum sets of process variables for producing doubly curved parts, which had minimal geometric defects in both of the flexible forming approaches. The objective of a design of experiments (DoE) is to optimise the values of response variables, i.e. “wrinkling, thickness variation and maximum deviation”, by changing the values, referred to as levels, of the factors “elastic punch hole size, compression ratio, rubber punch hole size and punch tools” that affect the response. This DoE has been used in this study and is an important element in this research.

In terms of the thesis, Chapter 1 provides a brief general introduction to the research while listing the aim and objectives of this work. Chapter 2 provides a detailed and comprehensive review of the relevant literature discussing the main works done in this field and the gap in knowledge. Chapter 3 explains the details of the experimental setup for the MPF assembly and elastic cushion. Material characterisation along with tensile testing was also discussed in this chapter. Chapter 4 discusses the optimisation of the MPF using numerical analysis and FE modelling. Chapter 5 provides a detailed discussion on the Design of Experiments (DOE), the MPF process parameters, and the mesh-type and forming processes for the numerical examination, to explore the forming force, thickness variation shear strains with radius of curvature and experimental validation of the work. Chapter 6 presents the process development and optimization using a mesh-type elastic cushion with validation, and DoE strategies to improve precision in elastic punch forming with MPF die processes.

The objectives of the work carried out in this study were:

a) To develop and construct a test machine, which can integrate the reconfigurable tooling with MPF die and vacuum-forming machineries.
b) To design and develop a tooling shape control methods for the MPF to adjust the square pins from one location to the other with the use of CAD models as the input.
c) To asses and verify the developing ABAQUS and its related support packages.
d) The multipoint sheet metal forming die process was selected circular type hole as the rubber punch needs to be examined more for advanced composite forming.

### 7.1.1. Further key findings

The mesh-type elastic cushion was optimised with a hole-type, where circular and square geometries were experimentally investigated. Three different sizes, i.e. 1.5 mm, 3 mm and 4.5 mm of the hole were studied. With the use of a design optimisation software, it was aimed to achieve the best value for the parameters. The results showed that for MPF of the sheet, the optimal size is of 3 mm. This is not only a suitable size but is one which results in less wrinkling while showing an adequate thickness variation.

In terms of elastic cushion thickness variation, once again three different sizes, i.e. 2 mm, 6 mm and 9 mm were investigated. An optimisation study showed that a size of 3 mm was the optimal size. Furthermore, forming force is another important design parameter in studies like these.

In the elastic punch study, a solid punch, with a MPF die was used under the application of pressure. Overall, it can be stated that as the applied pressure increases, the deformation also tends to increase, as expected due to an increase in the directed force. Three different hole sizes were investigated in this part of the experimental study, i.e. 5 mm, 10 mm and

15 mm. Simulating the sizes showed that the most optimal size was 9 mm, which was suitable as the applied pressure was continuous and upon completion of the pressure, the hole was to be found closed completely. With less force, there is less deformation, no occurrence of wrinkling and no thickness variation. The hole type in this part of the study was circular.

The current research was inspired by the recent requirements of modern day industries, which aim to decrease the costs and times required in tooling (hole-type rubber punch and die) development. Multipoint-forming punch and MPF die are costly approaches and are not appropriate for the existing customisation markets. Hence, this research was aimed on building a hole-type rubber punch forming system based on the MPF die in order to comprehend the overall procedures and investigate the possibility of implementing this approach at an industrialised level. Through the prediction of wrinkles, thicknesses, bridging strains (shearing and in fibers), Stresses (shearing and in fibers), fibers orientation, fiber content.

A workshop exemplar of the reconfigurable MPF forming moulding machine, which can reuse the sheet forming, is already available. However, several factors need to be investigated prior to the integration and commercialisation of this system.

## 7.2. Recommendations-for-future-work

The findings from this thesis could be used to plan further works in this field. To elaborate, the lifespan of the mesh-type elastic-punch produced from polyurethane hardness-A90 could be carefully considered. This would help in providing an understanding on the excellence of the produced part (sheet surface) over time. In addition, as Table 6-3 shows, there seems to be a noteworthy association between mesh-type rubber punch: Elastic punch hole size (A), Elastic punch compressor (B), Hole-type

of elastic punch (C) and Elastic punch tools (D) on the thickness variation of the formed sheet. This needs to be further investigated, perhaps by the creation of some suitable method to fully comprehend the influence of these interactions.

Furthermore, to ensure the precise positioning of the pins and to subsequently reduce times required in forming various shapes, the MP forming tool can be adjusted with a digital control. As the MP tools utilised were small, this can promote the programmed recompense for wrinkling. In terms of the wrinkling recompense approach, this is dependent on the composite material's characteristics. Hence, the method needs to take into consideration the force applied on the chosen pins by the formed part relaxation (wrinkling) in the last part of the formed process. Such release forces need to be converted in terms of distance in order to adjust pin heights, which can assist in compensating for wrinkling without being influenced by the metal sheet characteristics.

### 7.2.1. Address a wide range of materials

Hand lay-up is possibly the most acquainted process, which can be utilised for mechanisms of virtually any size, but usually simpler shapes. Although spray-up can help in producing similar geometries, this is a costly process. Both processes can have quality problems, which can be eliminated through vacuum bagging.

Materials and shapes: Carbon, Glass and natural fibres, Thermoplastic and thermoset resins, Including core, inserts, Woven fabrics, NCF, UD, Prepregs or dry textiles.

### 7.2.2. MPF-Composites Material-properties / characterization

Figure 7.1 Material properties / characterization

- A variant of compression moulding, called resin transfer moulding (RTM), can be used to make complex parts or where higher dimensional precision is needed.
- Dedicated to composites structural components made of continuous fibers
- For full control on costs, delays and reproducibility
- Hollow-parts-can-be-formed through-filament-winding. This can result in the production of parts with optimal-mechanical-characteristics. Pultrusion along with constant lamination can help produce prepegs as this process is also used for producing fibres and mats.

### 7.2.3. Preforming application

Fabric shearing and wrinkle prediction RTM application: Automotive floor panel. Therefore, it is important to take it into account the MPF injection/infusion process simulation. Geometric techniques are also good for approximating the fiber orientations in the preform. MPF tool composites goes one step further: it can seamlessly be used for the future.

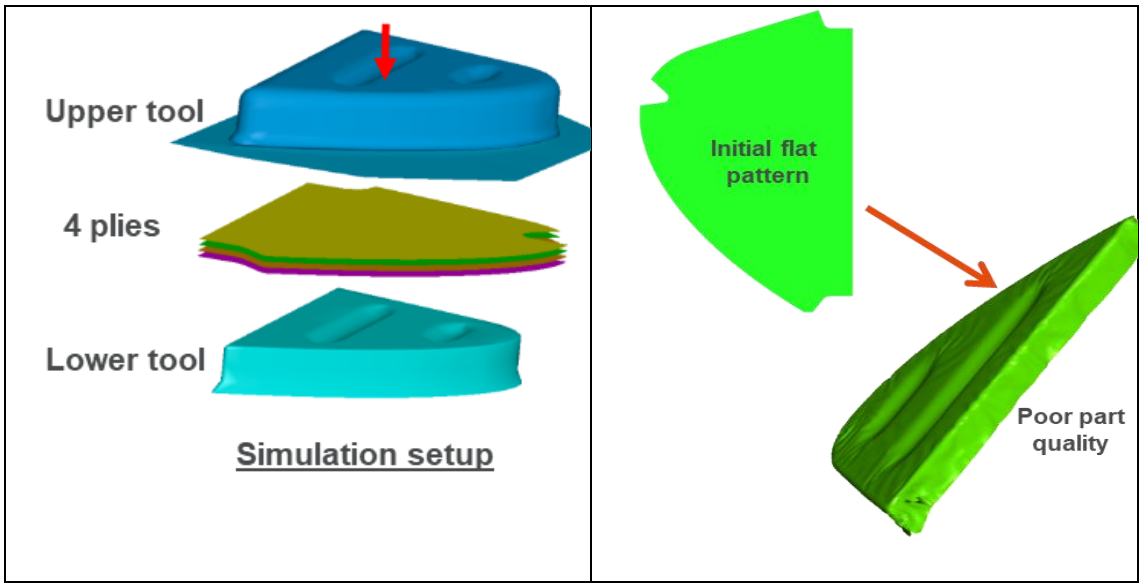


Figure 7.2 Composites forming application: Automotive floor panel

**Processes that can be modelled:**

Stamping - using two rigid moulds, Rubber pad forming, Mesh-type elastic punch MPF, Diaphragm forming.

**Typical Simulation results:**

Final fiber orientation, Thickness distribution, Optimum initial flat pattern, Bridging prediction, Wrinkling prediction, Strains and stresses, Fiber volume content, Compaction ratio.

Permeability, a key input parameter of RTM simulation, is highly dependent on fiber orientations.

# REFERENCES


1) Adamus, J., Lacki, P., Łyźniak, J. and Zawadzki, M, 2011. Analysis of spring-back during forming of the element made of AMS 5604 steel. Archives of metallurgy and materials, 56(2), pp.422-430.

2) Chung, K. and O. Richmond, Ideal forming—II. Sheet forming with optimum deformation. International Journal of Mechanical Sciences, 1992. 34(8): p. 617-633.

3) Selmi, N. and H. BelHadjSalah, Experimental implementation of the multipoint hydroforming process, in Design and Modeling of Mechanical Systems. 2013, Springer. p. 477-484.

4) Li, L., Seo, Y.H., Heo, S.C., Kang, B.S. and Kim, J, Numerical simulations on reducing the unloading springback with multi-step multi-point forming technology. The International Journal of Advanced Manufacturing Technology, 2010. 48(1-4): p. 45-61.

5) Peng, H., Li, M., Liu, C., Fu, W. and Cao, J, Numerical simulation of multi-point forming accuracy for polycarbonate sheet. Proceedings of the Institution of Mechanical Engineers, Part E: Journal of Process Mechanical Engineering, 2014. 228(2): p. 87-96.

6) Dwi Anggono, A., Combined method for die compensation in sheet metal forming. 2014, Universiti Tun Hussein Onn Malaysia.

7) Kim, J.-B. and J.W. Yoon, Necking behavior of AA 6022-T4 based on the crystal plasticity and damage models. International Journal of Plasticity, 2015. 73: p. 3-23.

8) Alghtani, A.H., Analysis and Optimization of Springback in Sheet Metal Forming. 2015, University of Leeds.

9) Tekkaya, A.E., Allwood, J.M., Bariani, P.F., Bruschi, S., Cao, J., Gramlich, S., Groche, P., Hirt, G, Metal forming beyond shaping: predicting and setting product properties. CIRP Annals, 2015. 64(2): p. 629-653.

10) Zibelnik, M., A. Petek, and K. Kuzman, FORMING WITH HYBRID TECHNOLOGY-INTEGRATION OF ELECTROMAGNETIC PROCESS INTO CONVENTIONAL FORMING. Journal for Technology of Plasticity, 2010. 35(1-2).

11) Li, M., Liu, Y., Su, S. and Li, G, Multi-point forming: a flexible manufacturing method for a 3-d surface sheet. Journal of Materials Processing Technology, 1999. 87(1-3): p. 277-280.

12) Iwasaki, Y., Shiota, H., Taura, Y., Seko, N. and Kumamoto, M, Development of a triple-row-press. Mitsubishi Tech. Rev., 1977. 14(2): p. 377-384.

13) Li, M.Z., Nakamura, K., Sima, A., Watanabe, S. and Sugawara, K, Study of the basic principles (1st report: research on multi-point forming for sheet metal). in Proc. of the Japanese Spring conf. for Technology of Plasticity. 1992.

14) Li, M.Z., Cai, Z.Y., Sui, Z. and Li, X.J, Harmful phenomena in multi-point forming (3rd report: Research on multi-point forming for sheet metal). in Proc of the 43rd Japanese Joint Conf for Technology of Plasticity. 1992.

15) Li, M.Z., Cai, Z.Y., Sui, Z. and Li, X.J, Principle and applications of multi-point matched-die forming for sheet metal. Proceedings of the Institution of Mechanical Engineers, Part B: Journal of Engineering Manufacture, 2008. 222(5): p. 581-589.

16) Abebe, M., K. Lee, and B.-S. Kang, Surrogate-based multi-point forming process optimization for dimpling and wrinkling reduction. The International Journal of Advanced Manufacturing Technology, 2016. 85(1-4): p. 391-403.

17) Hosford, W.F. and R.M. Caddell, Metal forming: mechanics and metallurgy. 2011: Cambridge University Press.

18) Elghawail, A., Essa, K., Abosaf, M., Tolipov, A., Su, S. and Pham, D., 2017, Prediction of springback in multi-point forming. Cogent Engineering, 2017. 4(1): p. 1400507.

19) NAKAJIMA, N., A newly developed technique to fabricate complicated dies and electrodes with wires. Bulletin of JSME, 1969. 12(54): p. 1546-1554.

20) GmbH., S., Metal forming handbook. 1998: Springer Science & Business Media.

21) Music, O., J. Allwood, and K. Kawai, A review of the mechanics of metal spinning. Journal of Materials Processing Technology, 2010. 210(1): p. 3-23.

22) LIU, C.-g., Z.-y. CAI, and M.-z. LI, Dimple formation and its elimination in multi-point forming for sheet metal [J]. Journal of Jilin University of Technology (Natural Science Edition), 2004. 1: p. 019.

23) Heo, S.C., Seo, Y.H., Park, J.W., Ku, T.W., Kim, J. and Kang, B.S, Application of flexible forming process to hull structure forming. Journal of Mechanical Science and Technology, 2010. 24(1): p. 137-140.

24) Li, M.-Z., Z.-Y. Cai, and C.-G. Liu, Flexible manufacturing of sheet metal parts based on digitized-die. Robotics and Computer-Integrated Manufacturing, 2007. 23(1): p. 107-115.

25) Neale, K. and P. Tuğcu, A numerical analysis of wrinkle formation tendencies in sheet metals. International Journal for numerical methods in engineering, 1990. 30(8): p. 1595-1608.

26) Nordlund, P. and B. Häggblad, Prediction of wrinkle tendencies in explicit sheet metal-forming simulations. International journal for numerical methods in engineering, 1997. 40(22): p. 4079-4095.

27) Tuğcu, P., Neale, K.W., Wu, P.D. and MacEwen, S.R, Effect of planar anisotropy on wrinkle formation tendencies in curved sheets. International journal of mechanical sciences, 2001. 43(12): p. 2883-2897.

28) Hutchinson, J.W., Plastic buckling, in Advances in applied mechanics. 1974, Elsevier. p. 67-144.

29) Cao, J. and X. Wang, An analytical model for plate wrinkling under tri-axial loading and its application. International Journal of Mechanical Sciences, 2000. 42(3): p. 617-633.

30) Correia, J.D.M. and G. Ferron, Wrinkling of anisotropic metal sheets under deep-drawing: analytical and numerical study. Journal of Materials Processing Technology, 2004. 155: p. 1604-1610.

31) Drucker, D.C., Relation of experiments to mathematical theories of plasticity. Journal of Applied Mechanics-Transactions of the Asme, 1949. 16(4): p. 349-357.

32) Hill, R., A theory of the yielding and plastic flow of anisotropic metals. Proc. R. Soc. Lond. A, 1948. 193(1033): p. 281-297.

33) Yang, X., O. Olatunbosun, and E. Bolarinwa, Materials testing for finite element tire model. SAE International Journal of Materials and Manufacturing, 2010. 3(2010-01-0418): p. 211-220.

34) Yu, T. and W. Johnson, The buckling of annular plates in relation to the deep-drawing process. International Journal of Mechanical Sciences, 1982. 24(3): p. 175-188.

35) Cao, J. and M. Boyce, Wrinkling behavior of rectangular plates under lateral constraint. International journal of solids and structures, 1997. 34(2): p. 153-176.

36) Hutchinson, J. and K. Neale, Wrinkling of curved thin sheet metal. Plastic instability, 1985: p. 71-78.

37) Triantafyllidis, N. and A. Needleman, An analysis of wrinkling in the Swift cup test. Journal of Engineering Materials and Technology, 1980. 102(3): p. 241-248.

38) Schmitt, W., Benevolenski, O., Walde, T. and Krasowsky, A., 2005. Material characterization for simulation of sheet metal forming. In Proc. VIII International Conference on Computational Plasticity, COMPLAS VIII, E. Onate and DJ Owen (Eds.) Barcelona..

39) Tolipov, A., Elghawail, A.M., Pham, D.T., Huang, J., Su, S., Kerin, M., Ji, C., Abosaf, M. and Essa, K., Experimental research and numerical optimisation of multi-point sheet metal forming implementation using a solid elastic cushion system. in Journal of Physics: Conference Series. 2017. IOP Publishing.

40) Zareh-Desari, B., B. Davoodi, and A. Vedaei-Sabegh, Investigation of deep drawing concept of multi-point forming process in terms of prevalent defects. International Journal of Material Forming, 2017. 10(2): p. 193-203.

41) Cai, Z.-Y., M.-Z. Li, and X.-D. Chen, Digitized die forming system for sheet metal and springback minimizing technique. The International Journal of Advanced Manufacturing Technology, 2006. 28(11-12): p. 1089-1096.

42) Soboyejo, W., Mechanical properties of engineered materials. 2002: CRC Press.

43) Hense, R., C. Wels, P. Kerstin, and M. Merklein, High-feed milling of tailored surfaces for sheet-bulk metal forming tools. Production Engineering, 2015. 9(2): p. 215-223.

44) Erhu, Q., M. Li., R. Li, Z. Liang and Z. Yi., , Inhibitory effects of a flexible steel pad on wrinkling in multi-point die forming. The International Journal of Advanced Manufacturing Technology, 2018. 95(5-8): p. 2413-2420.

45) Haque, M. and M. Saif, Application of MEMS force sensors for in situ mechanical characterization of nano-scale thin films in SEM and TEM. Sensors and Actuators A: Physical, 2002. 97: p. 239-245.

46) Carullo, A. and M. Parvis, An ultrasonic sensor for distance measurement in automotive applications. IEEE Sensors journal, 2001. 1(2): p. 143.

47) Kelemen, M., I. Virgala, T. Kelemenova, and M. Lorinc, Distance measurement via using of ultrasonic sensor. Journal of Automation and Control, 2015. 3(3): p. 71-74.

48) Young, K., S. Kirk, and R. Piggin, Tooling modifications using a Faro portable inspection arm and rapid prototyping. Assembly Automation, 2000. 20(4): p. 330-336.

49) Elghawail, A., K. Essa, M. Abosaf, and A. Tolipov, Low-cost metal-forming process using an elastic punch and a reconfigurable multi-pin die. International Journal of Material Forming, 2018: p. 1-11.

50) Yang, X.A. and F. Ruan, A die design method for springback compensation based on displacement adjustment. International Journal of Mechanical Sciences, 2011. 53(5): p. 399-406.

51) Reddy, R.V., T. Reddy, and G. Reddy, Optimization of blank holder force to control wrinkling and fracture of cylindrical cups in deep drawing. International Journal of Engineering Trends and Technology, 2012. 3(5): p. 669-676.

52) Menezes, L. and C. Teodosiu, Three-dimensional numerical simulation of the deep-drawing process using solid finite elements. Journal of Materials Processing Technology, 2000. 97(1-3): p. 100-106.

53) Elsayed, A., Mohamed, M., Shazly, M. and Hegazy, A, An Investigation and Prediction of Springback of Sheet Metals under Cold Forming Condition. in IOP Conference Series: Materials Science and Engineering. 2017. IOP Publishing.

54) Ma, N., Umezu, Y., Watanabe, Y. and Ogawa, T., Springback prediction by Yoshida–Uemori model and compensation of tool surface using JSTAMP. in Proceedings of the 7th International Conference and Workshop on Numerical Simulation of 3D Sheet Metal Forming Process, Interlaken, Switzerland. 2008.

55) Wahalathantri, B.L., Thambiratnam, D.P., Chan, T.H.T. and Fawzia, S, A material model for flexural crack simulation in reinforced concrete elements using ABAQUS. in Proceedings of the first international conference on engineering, designing and developing the built environment for sustainable wellbeing. 2011. Queensland University of Technology.

56) Lenard, J., Numerical Simulation of Sheet Metal Forming. Metal Forming Science and Practice: A State-of-the-Art Volume in Honour of Professor JA Schey's 80th Birthday, 2002: p. 135.

57) Wang, S., Z. Cai, and M. Li, Numerical investigation of the influence of punch element in multi-point stretch forming process. The International Journal of Advanced Manufacturing Technology, 2010. 49(5-8): p. 475-483.

58) Zhang, Q., Z. Wang, and T. Dean, Multi-point sandwich forming of a spherical sector with tool-shape compensation. Journal of Materials Processing Technology, 2007. 194(1): p. 74-80.

59) Quan, G.-Z., T.-W. Ku, and B.-S. Kang, Improvement of formability for multi-point bending process of AZ31B sheet material using elastic cushion. International Journal of Precision Engineering and Manufacturing, 2011. 12(6): p. 1023-1030.

60) Seo, Y.-H., B.-S. Kang, and J. Kim, Study on relationship between design parameters and formability in flexible stretch forming process. International Journal of Precision Engineering and Manufacturing, 2012. 13(10): p. 1797-1804.

61) Lee, S. and D.-Y. Yang, An assessment of numerical parameters influencing springback in explicit finite element analysis of sheet metal forming process. Journal of Materials Processing Technology, 1998. 80: p. 60-67.

62) Hu, J., Z. Marciniak, and J. Duncan, Mechanics of sheet metal forming. 2002: Elsevier.

63) Davoodi, B. and B. Zareh-Desari, Assessment of forming parameters influencing spring-back in multi-point forming process: a comprehensive experimental and numerical study. Materials & Design, 2014. 59: p. 103-114.

64) Heo, S.S., YH. Ku, TW. Kim, J. Kang, BS, Study on application of flexible die to sheet metal forming process. Transactions of Materials Processing, 2009. 18(7): p. 556-564.

65) Abosaf, M.E., K. Alghawail, A. Tolipov, A. Su, S. Pham, DT, Optimisation of multi-point forming process parameters. The International Journal of Advanced Manufacturing Technology, 2017: p. 1-11.

66) Sun, G., Li, M.Z., Yan, X.P., Zhong, P.P, Study of blank-holder technology on multi-point forming of thin sheet metal. Journal of materials processing technology, 2007. 187: p. 517-520.

67) Neto, D.M., Oliveira, M.C., Alves, J.L., Santos, A.D. and Menezes, L.F., 2016. Prediction of wrinkling and springback in sheet metal forming. In MATEC Web of Conferences (Vol. 80, p. 03005). EDP Sciences.

68) Venkat, R.R., R.T. Janardhan, and G. Reddy, Effect of various parameters on the wrinkling in deep drawing cylindrical cups. International Journal of Engineering Trends and Technology, 2012. 3(1): p. 2231-5381.

69) Magrinho, J.P.G., Silva, C.M.A., Silva, M.B. and Martins, P.A, Formability limits by wrinkling in sheet metal forming. Proceedings of the Institution of Mechanical Engineers, Part L: Journal of Materials: Design and Applications, 2018. 232(8): p. 681-692.

70) Di Lorenzo, R., L. Fratini, and F. Micari, Optimal blankholder force path in sheet metal forming processes: an Al based procedure. CIRP Annals-Manufacturing Technology, 1999. 48(1): p. 231-234.

71) Kim, Y. and J. Park, Effect of process parameters on formability in incremental forming of sheet metal. Journal of materials processing technology, 2002. 130: p. 42-46.

72) Doege, E. and K. Dröder, Sheet metal forming of magnesium wrought alloys—formability and process technology. Journal of materials processing technology, 2001. 115(1): p. 14-19.

73) Essa, K.H., Peter, Optimization of conventional spinning process parameters by means of numerical simulation and statistical analysis. Proceedings of the Institution of Mechanical Engineers, Part B: Journal of Engineering Manufacture, 2010. 224(11): p. 1691-1705.

74) Heo, S.-C.S., Young-Ho. Noh, Hak-Gon. Ku, Tae-Wan. Kang, Beom-Soo, Numerical study on effect of using elastic pads in flexible forming process. Transactions of the Korean Society of Mechanical Engineers A, 2010. 34(5): p. 549-556.

75) Hu, W., L.G. Yao, and Z.Z. Hua, Optimization of sheet metal forming processes by adaptive response surface based on intelligent sampling method. Journal of materials processing technology, 2008. 197(1-3): p. 77-88.

76) Cai, Z.-Y., S.-H. Wang, and M.-Z. Li, Numerical investigation of multi-point forming process for sheet metal: wrinkling, dimpling and springback. The International Journal of Advanced Manufacturing Technology, 2008. 37(9-10): p. 927-936.

77) Hassanin, H.M., Francesco. El-Sayed, Mahmoud Ahmed. Liu, Jian. Essa, Khamis, Manufacturing of Ti–6Al–4V Micro-Implantable Parts Using Hybrid Selective Laser Melting and Micro-Electrical Discharge Machining. Advanced Engineering Materials, 2016. 18(9): p. 1544-1549.

78) Abosaf, M., Optimisation of Multi-Point Forming Process Parameters. 2017.

79) Păunoiu, V.M., Catălina. Teodor, Virgil. Găvan, Eugen, Numerical analysis of multipoint forming process. International Journal of Modern Manufacturing Technologies, 2011. 3(2): p. 85-90.

80) Zheng, K., Lee, J., Politis, D. J., Li, N., Lin, J. and Dean, T. A., 2017, An analytical investigation on the wrinkling of aluminium alloys during stamping using macro-scale structural tooling surfaces. The International Journal of Advanced Manufacturing Technology: p. 1-15.

81) Cohen, M.F., Shade, J., Hiller, S. and Deussen, O., 2003. Wang tiles for image and texture generation (Vol. 22, No. 3, pp. 287-294). ACM..

82) Thiruvarudchelvan, S., 1993, Elastomers in metal forming: a review. Journal of Materials Processing Technology. 39(1): p. 55-82.

83) Sala, G., 2001, A numerical and experimental approach to optimise sheet stamping technologies: part II—aluminium alloys rubber-forming. Materials & Design. 22(4): p. 299-315.

84) Thiruvarudchelvan, S., 2002, The potential role of flexible tools in metal forming. Journal of Materials Processing Technology. 122(2): p. 293-300.

85) Irthiea, I.K., 2014, Process analysis and design in micro deep drawing utilizing a flexible die. University of Glasgow: Doctoral dissertation.

86) Ramezani, M., Ripin, Z.M. and Ahmad, R., 2010, Sheet metal forming with the aid of flexible punch, numerical approach and experimental validation. CIRP Journal of Manufacturing Science and Technology. 3(3): p. 196-203.

87) Browne, D.J. and E. Battikha, Optimisation of aluminium sheet forming using a flexible die. Journal of materials processing technology, 1995. 55(3): p. 218-223.

88) Lee, J.W., Kwon, H.C., Rhee, M.H. and Im, Y.T., 2003. Determination of forming limit of a structural aluminum tube in rubber pad bending. Journal of Materials Processing Technology, 140(1-3), pp.487-493.

89) Quadrini, F., Santo, L. and Squeo, E.A., 2010, Flexible forming of thin aluminum alloy sheets. International Journal of Modern Manufacturing Technologies. 2(1): p. 79-84.

90) Chen, L., Chen, H., Guo, W., Chen, G. and Wang, Q., 2014. Experimental and simulation studies of springback in rubber forming using aluminium sheet straight flanging process. Materials & Design (1980-2015), 54, pp.354-360.

91) Kut, S. and B. Niedziałek, Numerical and Experimental Analysis of the Process of Aviation Drawpiece Forming Using Rigid and Rubber Punch With Various Properties. Archives of Metallurgy and Materials, 2015. 60(3): p. 1923-1928.

92) Remezani, M., Ripin Z.M., and Ahmed, R., 2009, Computer aided modelling of friction in rubber-pad forming process Journal of Materials Processing Technology. 209(10): p. 4925-4934.

93) Elghawail A. Essa, K.A., M. Tolipov, A. Su, S. Pham, DT., 2017, Prediction of thickness in multi-point forming cogent-Engineering.

94) http://www.faro.com/products/metrology/faro-scanarm/overview#main., accessed on 13/01/2017.

95) Belhassen, L., Koubaa, S.,Wali, M. and Dammak, F., 2016, Numerical prediction of thickness varation and ductile damage in rubber-pad forming process of aluminum sheet metal. International Journal of Mechanical Sciences. 117: p. 218-226.

96) Liu, Y., Lin Hua, Jian Lan, and Xi Wei., 2010, Studies of the deformation styles of the rubber-pad forming process used for manufacturing metallic bipolar plates. Journal of Power Sources. 195(24): p. 8177-8184.

97) L Peng, P Hu, X Lai, J Ni, Fabrication of metallic bipolar plates for proton exchange membrane fuel cell by flexible forming process-numerical simulations and experiments. Journal of Fuel Cell Science and Technology, 2010. 7(3): p. 031009.

98) Chen, P.K., M. and Wenner, M.L., 2008, Experimental investigation of thickness variation in forming of high strength steels. Journal of manufacturing science and engineering. 130(4): p. 041006.

99) Bahloul, R., Ben-Elechi, S. and Potiron, A., 2006, Optimisation of wrinkl predicted by experimental and numerical approach by using response surface methodology. Journal of Materials Processing Technology. 173(1): p. 101-110.

100) Buang, M.S., Abdullah, S. A. and Saedon, J., 2015, Optimization of wrinkling prediction in U-channel process using response surface methodology. Optimization. 1: p. 31185.

101) Lind, D.A., Marchal, W.G. and Wathen, M., 2012, Business & Economics. USA, McGraw-Hill/Irwin.

102) Tolipov A, Elghawail A, Abosaf M, Pham D, Hassanin H, Essa K. Multipoint forming using mesh-type elastic cushion: modelling and experimentation. The International Journal of Advanced Manufacturing Technology. 2019:1-2.